Bangor University

DOCTOR OF PHILOSOPHY

Seismo-acoustic investigations of consolidated phenomena.

Mc Dermott, Ian Roy

Award date:
1992

Awarding institution:
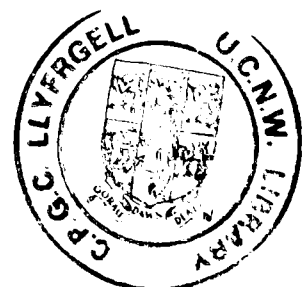Bangor University

Link to publication

SEISMO-ACOUSTIC INVESTIGATIONS OF CONSOLIDATION PHENOMENA.

IAN ROY McDERMOTT

MARCH 1992

A thesis submitted to the University of Wales
for the degree of Philosophiae Doctor

School of Ocean Sciences
University College of North Wales
Menai Bridge, Gwynedd

Text cut off in original

To my Mother and Father

SUMMARY

The understanding of the settling behaviour and subsequent consolidation of sediments deposited under water has been hampered by the difficulty of recovering high quality samples. There is a need therefore to correlate *in situ* seismo-acoustic properties of these soils to the geotechnical properties required by engineers. To this end a laboratory study was made during which an instrumented sedimentation column was developed. This apparatus allowed the successful monitoring of compressional wave velocity, shear wave velocity, electrical resistivity, pore pressure and bulk density in a number of natural marine sediments consolidating under self weight introduced into the column as a homogeneous slurry. The seismo-acoustic responses of the sediment samples were observed during primary consolidation, a period of over a thousand hours in some cases.

Shear waves were found to be small amplitude waves travelling at velocities of less than 11m/s. Shear wave velocity was subject to time dependent increase, or creep, thought to be a result of continued clay particle floc interaction during secondary consolidation. The velocity increased with decreasing porosity and increasing overburden but the effect of creep meant that no unique velocity-porosity relationship exists. Empirical relationships were established in order to determine the degree of consolidation and frame compressibility via shear wave velocity measurement.

The Biot theory was used to predict the variation of compressional wave velocity as a function of porosity, bulk density and permeability. Frame and shear modulus measurements indicated that the model is justified in assuming weak soil frame parameters and a mass coupling factor equal to unity. The continually changing velocity relationship with porosity and bulk density can be satisfactorily modelled using the Geertsma and Smit model. The full Biot model was found to predict permeability with reasonable accuracy in high porosity sediments but failed when applied to lower porosity soils. Results suggested that the soils studied exhibited anisotropy with respect to permeability.

ACKNOWLEDGEMENTS

CONTENTS

Title Page

Dedication

Declaration

Summary

Acknowledgements

Contents

List of symbols

LIST OF SYMBOLS TOGETHER WITH THE PAGE NUMBER IN WHICH THEY ARE FIRST INTRODUCED.

a	mean grain diameter	30
b	mass coupling factor	25
c	relative velocity of the soils fluid and solid phases	11
c_s	velocity of the soils solid phase	140
c_f	velocity of the soils fluid phase	140
d	characteristic pore diameter	30
d'	characteristic pore diameter calculated using Hovem and Ingram's formulae (1979)	115
d''	characteristic pore diameter calculated using formulae from Briggs (1991)	115
e	voids ratio	11
e_i	initial voids ratio for modelling purposes	88
e_0	initial voids ratio	138
f	applied frequency	26
f_c	characteristic frequency	26
f_t	transitional frequency	26
g	acceleration due to gravity	27
h_i	initial height of sediment for modelling purposes	88
h_s	height of soils solid component	88
h_t	total height of soil	88
h(0)	initial height of soil layer	15
$h(T_F)$	height of sediment at time factor T_F	15
h(∞)	final height of soil layer	15
i	hydraulic gradient	11
k	coefficient of permeability (units velocity)	11
l	wave number	146
m	mass coefficient	27
n	fractional porosity as represented in thesis diagrams	
r	radius of cylindrical tubes as used in Poiseuille's equation	11
t	time	13
u	normalized excess pore pressure	14

Q_v	volume of liquid	11
R	ratio of solid to frame compressibility	144
R-sq	coefficient of correlation	100
S	salinity	67
$S(T_F)$	degree of settlement	15
T	temperature	67
T_F	time factor	14
U	normalized excess pore pressure	14
V_p	compressional wave velocity	16
V_s	shear wave velocity	18
V_{solid}	volume of solid constituent of soil sample	88
V_{total}	total volume of soil sample	88
V_{void}	volume of the voids	88
V_0	zero frequency compressional wave velocity	27
V_∞	infinite frequency compressional wave velocity	27
W	width of bender element	50
X	elastic constant	27
Y	elastic constant	27
Z	elastic constant	27
β	constant	23
ΔG	change in rigidity modulus	102
Δt	time interval	102
ε_{xyz}	strain component due to normal stresses	143
ϕ	coefficient of permeability (units area)	30
Φ	ratio of applied seismo-acoustic frequency to the soils characteristic frequency	148
γ_{xyz}	strain component due to shear stresses	143
η	fractional porosity	11
χ	average X-ray attenuation constant	137
λ	wavelength	28
μ	viscosity	11
μ_m	total mass absorption coefficient	136
ρ	bulk density	16
ρ_s	solids density	13
ρ_w	fluid density	13
σ	vertical total stress	138

CHAPTER 1.   INTRODUCTION.

1.1 Background.

Improved knowledge of the processes of sedimentation has given an insight into the mechanism of natural consolidation of cohesive soils deposited under water. Such naturally consolidated soils are characterized by their low densities, little strength, and large strains during the primary consolidation phase of their development. Such soils have been aptly named "soft soils" by the scientific community involved in their study. These soils are compositionally and behaviourally very complex and have the ability to invalidate traditional consolidation models. This has generated much interest in such diverse fields as geotechnical engineering, sedimentology, colloid chemistry, rheology and in this present study, the field of geophysics.

The *in situ* study of soft soils has been hampered by the virtually impossible task of recovering high quality samples. As a consequence the study of such soils, with a few exceptions, has been confined to the laboratory. A need exists therefore, to correlate the *in situ* properties that can be measured with the soil properties that are required by engineers. Of the properties that can be measured, the seismo-acoustic properties have the distinct advantage in that they can be measured remotely and thereby leave the fragile soil structure intact. It is for this reason that this study strives towards relating the soils seismo-acoustic response to the fundamental properties of consolidation phenomena.

1.2 Areas of Application.

Geophysical techniques using seismo-acoustic propagation are widely used as an observational tool in the marine environment. The techniques are used in such diverse applications as geological mapping, locating sub surface and

sea bed hazards, monitoring the impact of scouring as a result of dredging and trawling, and to map the distribution of gassy sediments. More recently, seismo-acoustic methods have been used to determine the engineering properties of the soil. Seismo-acoustic measurements have been found to correlate well with soil properties such as porosity, mean grain size and bulk density. The interrelationship between the compressional and shear wave velocities, and soil porosity is of particular interest here. Since porosity changes are a natural consequence of the consolidation process in a soil, it may be reasonable to assume that the seismo-acoustic wave velocities may be used to predict the consolidation process itself. Should this be possible, is there any justification for the study of this relationship other than to satisfy academic curiosity? A number of applications can be envisaged; these are described below.

When a body of water containing suspended sediment enters the quiescent reaches of a harbour, inlet or estuary, it will allow its water borne load to settle out. On settling, the soil particles will raise the altitude of the bed, and as a consequence will decrease the depth of the free water above. In order to minimize the disruption to shipping, port authorities must maintain a navigable depth by dredging. The vast majority of port authorities use echo soundings to determine the altitude of the sea bed, a technique that sometimes proves unsatisfactory in locations where the bed consists of soft cohesive sediments. The principle of operation of echo sounders utilizes the fact that an echo will be returned when the incident acoustic beam encounters a boundary, such as the water/sediment interface at the sea bed. A weak echo would be returned from a sea bed comprising of soft cohesive sediments providing the port authorities with knowledge of the location and depth of water above the bed. A depth sounding less than the navigable depth may lead the port authorities to conclude that the bed is in an unnavigable condition requiring dredging, whereas in truth, the sea bed

may be made up of sufficiently low strength soil that it would allow the passage of a vessel virtually unimpeded.

Such a waste of resources has led a number of researchers to seek new methods of defining navigable depth. One such method, introduced by Kirby and Parker (1977), defined navigable depth in terms of a sediment density boundary layer of 1200 kg/m^3. Above this altitude a vessel was considered to be assured safe passage. Bowden (1989) pointed out that the density of the soil was not the criterion which determines the safe passage of a vessel. It was, he argued, the ability of the soil to resist shear, quoting cases of high density soils (densities above 1200 kg/m^3) having very low shear strength. Such soils, under Kirby and Parker's definition, would be regarded as a hazard to shipping and needlessly dredged. Shear strength, is indeed the quantity to be measured. However, this has proved a difficult *in situ* property to measure. Laboratory empirical density-shear strength relationships require extensive laboratory work, are restricted in use to specific localities and may even prove unreliable if the sedimentation control factors have not been modelled sufficiently accurately in the laboratory. Since the United Kingdom's annual expenditure on dredging exceeds £45 million (1985 figure), the USA spending in the order of $400 million (1989 figure), there is an urgent need to reduce dredging practices. In addition to the financial benefits gained there will also be the advantage of lessening the impact that dredging has on the marine environment.

A second application of seismo-acoustic techniques to the monitoring of consolidation behaviour is in the field of pollutant contaminated sediments. Chemical and low level radioactive wastes are dispersed in the sea and become attached to settling clay particles. There is evidence that chemical conditions change as the clay particles and associated pollutants are incorporated into the settled bed. The result is that some pollutants return into the pore fluid. Consolidation of these contaminated sediments occurs as more material arrives above, with the consequence that the

contaminated pore fluid is expelled back into the water column. Direct sampling of such soils to test for toxicity is impractical owing to the disturbance this would cause. Again the remote nature of the seismo-acoustic technique makes it a suitable method with which to monitor soil behaviour.

It is clear, therefore, that there are a number of applications to the study of the inter-relationship between the seismo-acoustic properties of a soil and consolidation phenomena. For the two examples cited above, the investigation into such inter-relationships may lead, ultimately, to the reduction of dredging costs or to the remote monitoring of contaminated soils.

1.3 Outline of Thesis.

It is useful at this point to describe the layout of this thesis. The following chapter attempts to review current and past work in the field of soft soil research. A conclusion is drawn as to the state of current research and to what is required to advance our present knowledge in terms of seismo-acoustics and consolidation behaviour.

Chapter three addresses the primary aim of the research project, that is the development of a piece of apparatus that could successfully monitor both geotechnical and geophysical parameters in a soft soil laboratory experiment.

Chapter four describes the experimental programme, including an overview of experimental procedures and conditions. This is followed by descriptions of the soil under study and how the samples are prepared prior to the experiment. Direct results are presented at the end of this chapter.

The analysis of the geotechnical and geophysical behaviour of the soil samples as they undergo self weight consolidation are documented in chapters 5 and 6 respectively. Current geotechnical (chapter 5) and geophysical (chapter 7) models

4

are used to predict consolidation behaviour and then compared to measured properties of the soil. In the final chapter the general relevance of these analyses and their implications for engineering problems are discussed. Some suggestions are made as to the future direction of this field of research and the likely problems that may be encountered.

1.4   Soil Sample Description.

The soft soils studied within this thesis were selected so as to represent soils of a broad textural range. Sampling location information and a detailed material description is presented in appendix 5.

CHAPTER 2   REVIEW OF GEOPHYSICAL AND GEOTECHNICAL BEHAVIOUR OF SOFT MARINE SOILS.

2.1   Geotechnical Behaviour of Soft Soils.

2.1.1 SOFT SOILS: SETTLING PROPERTIES.

Before considering the geotechnical characteristics of soft soils it is useful to consider the way in which the soil particles interact, and the effect this might have on the sedimentation characteristics (Grimm 1962, Partheniades 1965, Lambe and Whitman 1979, and White 1981). The solid fraction which influences the physical behaviour of a soil most decisively is the clay fraction. Clay particles are plate like in structure with a diameter of less than 2μm. This dimension is typically ten times the particle thickness. The particle surface has ionic charges such that the particles interact electrostatically. The face of each platelet normally carries a negative charge, the particle edges a positive charge, with the overall charge being negative. Clay particles coming within close proximity of each other do not act individually but have a tendency to stick together, a phenomena known as cohesion.

In the marine environment sediment is carried in suspension until the water flow velocity reduces sufficiently to allow the soil particles to settle to the sea bed. In very dilute suspensions the soil particles may exist as individual particles or discrete flocs. The particles settle, for the most part, independently of each other, such that interparticle forces have negligible effect. The forces that govern settling behaviour in this instance are gravity, buoyancy and fluid drag. The well known expression relating these forces is Stoke's law, which equates the gravitational and fluid drag forces on a spherical particle at a terminal velocity in an ideal infinitely large, quiescent suspending medium (Gartenhaus 1977).

As the soil particle concentration increases, the interparticle forces become increasingly important. Electrochemical interaction and hydrodynamic turbulence reduce the settling velocity to less than that predicted by Stoke's law. A hindered settling hypothesis is now required to describe soil particle motion, such as that developed by Kynch (1952).

Where clay minerals are deposited through sea water, the soil particle behaviour is substantially modified by the water chemistry. The free ions contained in sea water are attracted to the opposite charges on the clay particle. A closely held layer of cations forms on the face of the particle, the intensity of which decreases exponentially outwards. This charged layer is the so called "double layer", the net effect of which is to reduce the magnitude of the soils particles net negative charge. In a saline environment, the net charge of the particle is neutralized such that secondary molecular short range attractive forces (London-Van der Waals) dominate, leading to the flocculation of particles. Kranck (1973) illustrated that flocculation preferentially removes the finer particles from suspension. Einstein and Krone (1962) demonstrated that flocculation is complete once the salinity has risen to $1-3°/\circ\circ$.

In quiescent waters, the soil particles and flocs will settle to the bed. The flocs are brought closer together as additional material is deposited above. The soil subject to this self weight overburden does not assume an instantaneous deflection, but settles gradually at a variable rate. The settlement caused by a gradual transfer of the load from the fluid phase of the soil to that of a developing soil frame, with the consequential flow of fluid from the pore spaces of the soil is the process known as consolidation (Terzaghi 1925, Lambe and Whitman 1979). Partheniades (Figure 2.1) illustrated the progressive collapse of the soft soil structure as a result of self weight compression. An important feature of this behaviour is the so called pore water "piping". Here water from the sediment, instead of escaping uniformly

7

Floc aggregate

Representation of network
structure of the mud bed
at its loosest state

(A)

Aggregate structure of the
bed, with the network
structure having collapsed

(B)

Flocculate structure of the bed
with the aggregate structure
having collapsed

(C)
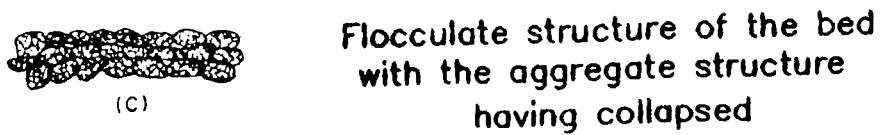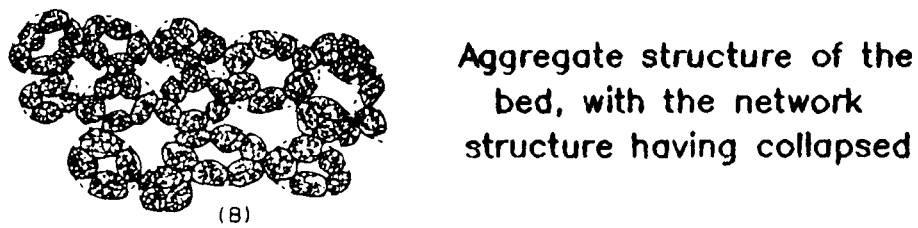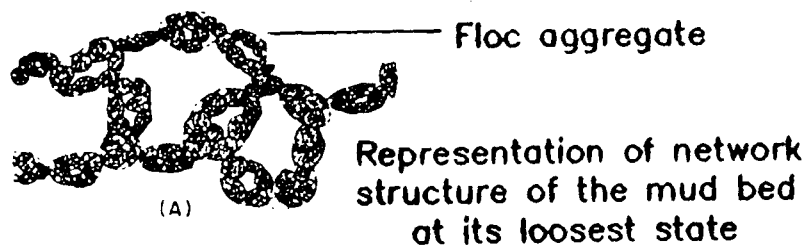
Figure 2.1   Idealised Soft Soil Consolidation Process
(after Partheniades 1965)

upwards, travels sideways to zones of higher permeability. These zones connect into thin pipes which manifest themselves at the surface as evenly spaced holes. Piping can lead to increased consolidation rates.

2.1.2 SOFT SOILS: GEOTECHNICAL PROPERTIES.

The ultimate objective of a geotechnical engineer is to model soil properties in order to make predictions of the soil behaviour. Owing to the difficulties of obtaining *in situ* test data, behavioural models have so far been based on laboratory tests which suffer from the inherent problems of sampling and core storage. (Richards and Parker, 1968; Richards, 1984). Soft soils invariably suffer from poor sampling recovery rates, and when satisfactorily sampled the soil is structurally too weak to undergo traditional soil mechanics testing. It has necessitated the abandonment of the traditional methods for more sophisticated testing procedures. In this section the current state of knowledge concerning the engineering behaviour of soft cohesive soils will be reviewed, along with current state-of-the-art testing techniques.

Gaudin and Fuerstenau (1958) report their initial attempts to study sedimentation of a 1m deep kaolin suspension in the laboratory. They used an X-ray absorption technique to determine soil bulk density non-destructively and noted density discontinuities that are now well documented by Krone 1962, Been 1980, Elder 1985, Bowden 1989. The formation of a marine sedimentary soil is reported to undergo three phases of development; from a water borne suspension a soil passes through an intermediate phase where very small effective stresses develop (Been 1980), representing the development of a soil frame work, before becoming a consolidating soil layer. Einsele et al. (1974), in artificial sedimentation studies, made pore pressure measurements within a consolidating soft soil. The work illustrated the large time span (over 200 days) required before excess pore pressures (above hydrostatic) were fully dissipated, and hence the length of time for soft soil

self weight consolidation to occur. Michaels and Bolger (1962) showed that the study of flocculated suspensions need not be limited to large tank experiments but could be carried out in columns of 4.8 cm diameter without fear of edge effects. Been (1980) initiated a study into the estuarine silty clays of Combwich, Somerset. Sediment slurries with initial densities ranging from 1040 to 1220 kg/m^3, were introduced into columns of 0.1m diameter and up to 2 m in length, as a single homogeneous input. Been made soil bulk density measurements on these consolidating slurries using X-ray absorption (Been 1980) together with pore pressure measurements. The density profiles were used to determine vertical total stress. Total stress and pore pressures were used in conjunction with the principal of effective stress to determine vertical effective stresses within the column. This method was adopted for work carried out in this thesis and is therefore more fully described in appendix 1.

Elder (1985) extended the work performed by Been (1980) and Been and Sills (1981) on Combwich silty clays, studying settlement in freshwater. Elder found that a critical density existed, of 1130 kg/m^3 (voids ratio of 12), and marked differing settling behaviour of an instantaneously dumped slurry. For an initial density below this critical value the slurry existed as a fluid supported suspension. It settled rapidly to form a consolidating layer in which effective stresses exist and large deformation occurs. Been (1980) noted that such a settled soil exhibited a unique voids ratio effective stress relationship for voids ratios below 6-7. However, above this critical density, no suspension phase occurs and surface density increases slowly with time. This was credited to the high density input creating effective stresses immediately within the soil. This resulted in quite different consolidation behaviour. For a period of up to 24 hours little strain was seen to occur despite the immediate existence of effective stresses (Elder and Sills 1984). Subsequent behaviour was marked by a large change in voids ratio for small increases in effective stress. The consolidation paths followed by different elements within the

same soil mass differed greatly. Any value of effective stress was to be associated with a wide range of voids ratio indicative of time dependent compression or creep. Elder and Sills (1984) explained this phenomenon as being a result of collapsing soil structure, that is flocs either breaking down or rearranging themselves such that a smaller rise in effective stress resulted. At this stage creep behaviour had previously been documented for stiffer, *in situ*, normally consolidated marine clays by Bjerrum (1967), and the conventional view was that creep was effectively negligible until primary consolidation was nearly complete. However, in Elder's (1985) experiments the creep component was comparable if not larger than the primary compression. The magnitude of this creep phenomenon decreased with decreasing initial voids ratio whilst the onset of creep was delayed. The factors affecting the stress history of a soft soil were summarized by Sills and Elder (1984), these being initial density, initial height, initial rate of deposition, the effect the afore mentioned have on the drainage conditions, and of course time. This time dependent creep behaviour is believed to provide an explanation for the apparent over consolidation reported for sediments taken from near the sea bed surface (Elder and Sills, 1984).

Einsele et al.(1974) were amongst the first to notice that the rate of sedimentation affected the geotechnical behaviour of the soil. That is, the slower the rate of deposition the less compressible the soil is on loading as compared to the same soil consolidated from a slurry. Sills and Thomas (1984) studied the settlement and consolidation of a steadily deposited sediment using rates of 4 to 400 mm of solids per day. They argued that at slow rates of sedimentation, there was an increased isolation of the flocs before reaching the settled bed. As a consequence a much more open soil frame work is produced, and as a result a much thicker bed is produced.

At this point it is convenient to consider the mechanism of flow through the soil. It is known that a soil's pore spaces are generally interconnected via small irregular diameter

conduits (Lambe and Whitman, 1979). On a microscopic level, providing fluid movement is slow, the flow of fluid through these pore spaces may be considered laminar, equivalent to the flow of a volume of fluid down a cylindrical tube, as described by Poiseuille's equation,

$$Q = \frac{\pi r^4}{8 \mu} \frac{dp}{dl}$$

where Q is the volume of liquid, of viscosity μ, flowing through a cylindrical tube, radius r, in unit time whilst subject to a pressure drop per unit length of dp/dl along the axis of the tube. As the fluid increases its flow rate it spontaneously initiates turbulent flow at which point Poiseuille's flow breaks down. On a macroscopic level any flow quantities calculated by the theory of "pipe flow" through it must be in error owing to the complexity of the soil matrix. It is useful to think in terms of an average flow rate through a given soil area, in the form of Darcy's law (Lambe and Whitman 1979).

$$c = k \, i$$

where c is the relative velocity of the fluid to the solid phase, k is the coefficient of permeability (units of velocity) and i is the hydraulic gradient. Figure 2.2 shows that in a column of saturated soil, in this example sand, water is considered to flow from point A to point B. Actually the water does not flow in a straight line with constant velocity as assumed by Darcy's law, but instead follows a tortuous path from pore to pore as shown in figure 2.2. The permeability (k) of a marine soil is invariably linked to the porosity (η) or voids ratio (e) of the soil. It has been the concern of a number of researchers to establish a relationship between these two quantities for the case of soft soils. Bryant et al. (1974) fitted an empirical equation of the form $k=10^{-11}e^5$ for a wide range of marine silts and clays ranging in voids ratio from 5 to 0.4. Been and Sills (1981), and Tan et al. (1988) saw a similar approximately linear e versus log k relationship in voids ratios ranging from 12 to 1. Permeability was seen to increase with increasing voids ratio. The work of Elder (1985) and Bowden (1989) cast some doubt
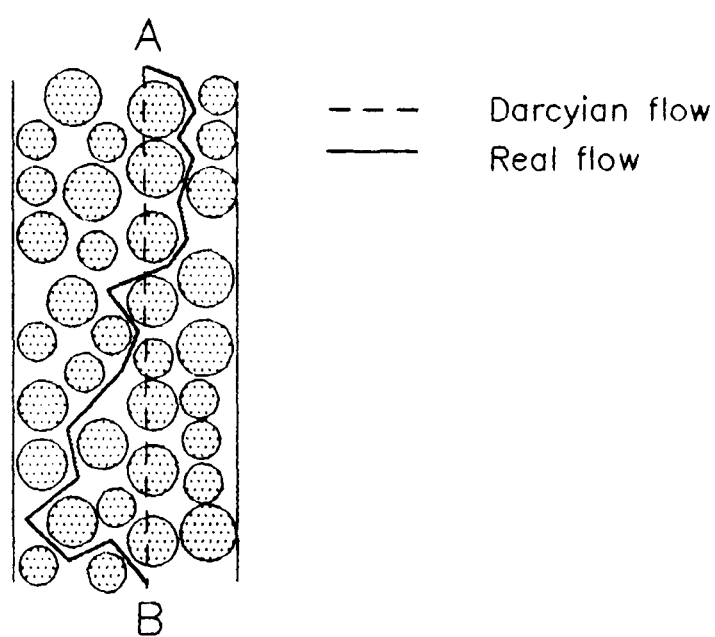
Figure 2.2 Showing the real pore fluid flow
as compared to the idealized Darcyian flow.

upon the validity of Darcy's law in its application to soft soils when they showed that permeability-void ratio behaviour was in fact non linear for voids ratio greater than between 4 and 6 depending on the mode of sedimentation.

The shear strength of soft soils has been investigated by both Elder (1985) and Bowden (1989). Using peak shear vane measurements, Elder (1985) calculated a range of secant shear moduli (0.01 to 10.0 kPa) for soft soils. Bowden showed that shear strength increased linearly with decreasing voids ratio, also increased linearly with effective stress, and increased with salinity. Initial density was shown to have negligible effect on the soil shear strength.

2.1.3 MODELLING AND PREDICTION OF SELF WEIGHT CONSOLIDATION.

A simple mechanism to explain consolidation in soils was first proposed by Terzaghi (1925). Terzaghi's theory is based upon the assumption that the permeability and the compressibility remain constant during the consolidation process. As a consequence the theory is not valid for the consolidation of soft soils, where compressibilities and permeabilities are reported to change by the order of 10^{-3} to 10^{-4} during consolidation (Mikasa 1964). In addition, a soft soils sole loading agent is its self weight which in turn induces large strains. Neither of these factors are incorporated into the Terzaghi theory.

The large strain analysis most often used in soft soil engineering problems is that based upon the one dimensional finite strain consolidation theory of Gibson et al. (1967). This theory invokes the following assumptions:
(1) Negligible compressibility of soil grains and soil water.
(2) Complete saturation exists.
(3) The principle of effective stress is taken to be valid, that is intrinsic or electrochemical forces are negligible.
(4) Secondary compression is negligible.

(5) The water flows through the soil skeleton according to Darcy's law.

(6) Behaviour is independent of strain/loading rates or intrinsic time effects.

(7) Unique compression-voids ratio and permeability-voids ratio relationships exists.

The Terzaghian restrictions to small strains, constant compression and permeability of the clay under a particular increment in load have been removed in this theory. The self weight of the consolidating soil is also included. Removed also is the traditional Eulerian coordinate system in which soil elements are defined in space relative to a fixed point in space. The soil is thus viewed in terms of a Lagrangian coordinate system in which a point is labelled in terms of the solid material between that point and an origin fixed in the material. In this particular application the reference point is the soil surface such that a normalized material co-ordinate, y, is defined by (figure 2.3)

$$y = \frac{\text{mass of solids above the element}}{\text{total mass of solids present}}$$

The soil is now viewed as a two phase medium in which it is the relative velocities of the soil skeleton to that of the pore fluid in a changing hydraulic gradient that is of interest. The theory produces a differential equation governing the voids ratio for one dimensional consolidation

$$\frac{\partial e}{\partial t} = \frac{\partial e}{\partial z} \left(\frac{k}{\rho_w(1+e)} \frac{d\sigma'}{de} \frac{\partial e}{\partial z} \right) - (\rho_s - \rho_w) \frac{d}{de} \left(\frac{k}{\rho_w(1+e)} \right) \quad (2.1)$$

where t is time, z is soil thickness co-ordinate, k is the permeability, e is voids ratio, σ' is the vertical effective stress, ρ_s and ρ_w are the solid and fluid density respectively (a similar theory was proposed by Mikasa, 1964). The solution of equation 2.1 for e(z,t) requires knowledge of the compression (e versus σ') and permeability (k versus e) relationships in addition to initial boundary conditions. To solve this equation analytically, Lee and Sills (1981)

Initial position of soil element
time t=0

Current position of
soil element at
time t
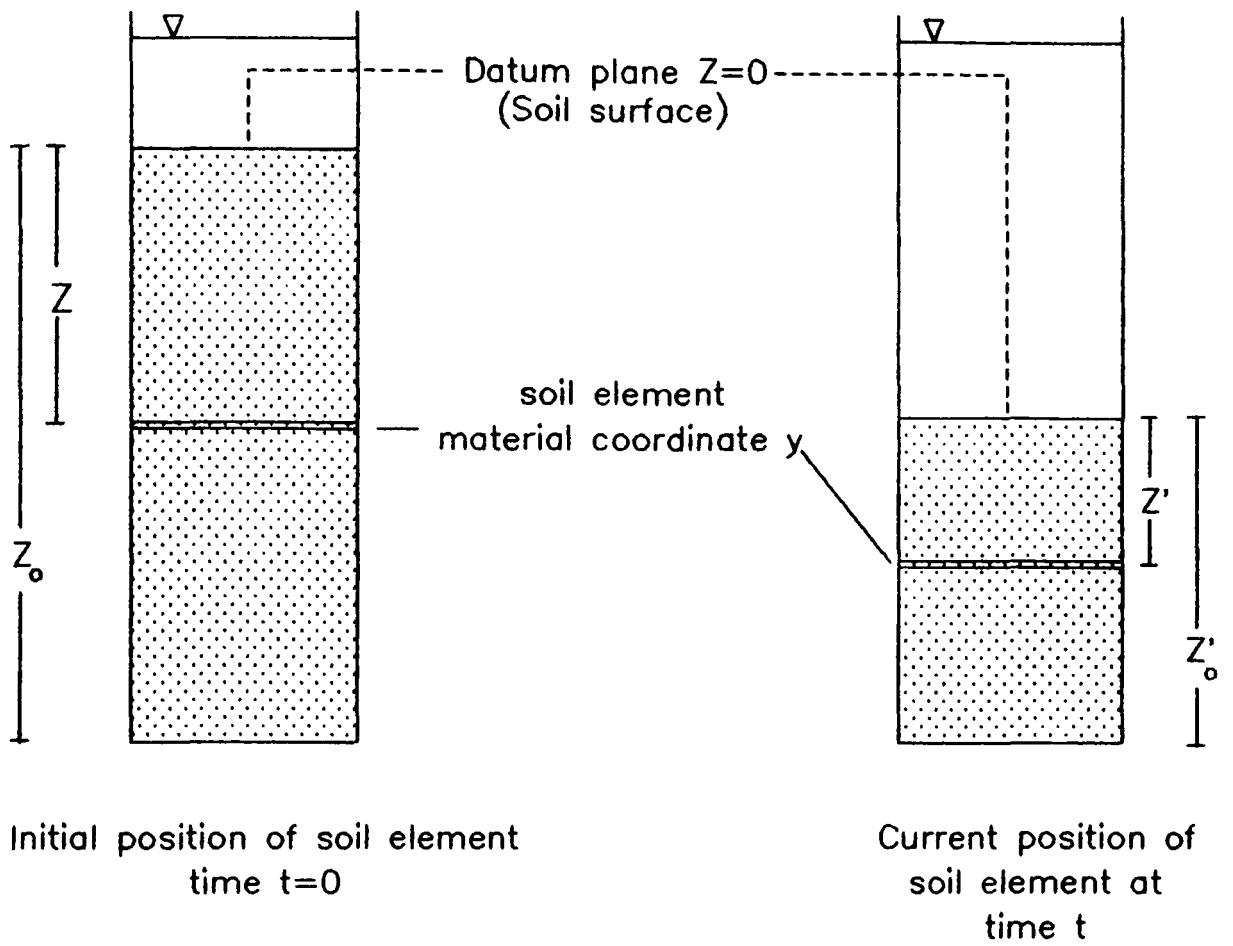
where $Z_0 =$ total soil thickness
$Z =$ soil thickness between element
and soil surface

Figure 2.3   Lagrangian co-ordinate system.

required that the voids ratio versus effective stress and the permeability versus voids ratio relationship be linear, and that the coefficient of consolidation be constant. In their solution effective stress was given by the form

$$\sigma' = A - Ce \qquad (2.2)$$

where σ' is the effective stress, e the voids ratio and A and C are constants. Permeability k was given by

$$k = \rho_w K(1 + e) \qquad (2.3)$$

where k is the permeability, ρ_w is the pore fluid density and K is a constant. The coefficient of consolidation, C_c, was defined by Gibson et al. (1967) as

$$C_c = \frac{-k}{\rho_w (1 + e)} \frac{d\sigma'}{de} \qquad (2.4)$$

where C_c is the coefficient of consolidation. In practice Been and Sills (1981) showed that the stress-strain and permeability relationships were non-linear although their effects tend to cancel out such that C_c remains reasonably constant. Equation (2.1) then becomes

$$\frac{\partial e}{\partial t} = C_c \, \partial^2 e/\partial z^2 \qquad (2.5)$$

Lee and Sills (1981) solution to this equation for a dredged fill of initial uniform density is applicable to this study. For an impervious base (i.e. drainage from the surface only) and boundary conditions $e(z,0) = e_0$ and $0 \leq z \geq z_0$ the normalized excess pore water pressure U was shown to be:

$$U = 2 \sum \frac{(-1)^N \sin (M\pi (1-y))}{M^2 \pi^2} \exp (-M^2 \pi^2 T_F) \qquad (2.6)$$

where

M = 0.5 (2N + 1)

N = 0,1,2,...,

y = the normalized material co-ordinate (z/z_0)

z_0 = the total thickness of the soil (see figure 2.3)

z = the soil thickness between a point in the soil and the surface

14

T_F = the Time factor given by

$$T_F = \frac{C_c t}{z_0^2}$$

(2.7)

The settlement behaviour of the fill can be investigated in terms of degree of settlement defined as

$$S(T_F) = \frac{h(0) - h(T_F)}{h(0) - h(\infty)}$$

(2.8)

where $h(0)$ is the initial thickness of the sediment layer, $h(T_F)$ = thickness of sediment layer at T_F, $h(\infty)$ = final thickness of sediment layer. Assuming the same boundary conditions as above and allowing surface drainage only, the settlement at any time is given by

$$S(T_F) = 1 - 4 \sum \frac{(-1)^N}{M^3 \pi^3} \exp(-M^2 \pi^2 T_F)$$

(2.9)

where $M = 0.5(2N + 1)$ and $N = 0,1,2,\ldots$.

Been (1980) and Been and Sills (1981) have shown that assumption 7 of Gibson et al. (1967) theory was not valid, since at very low effective stresses there was no corresponding unique voids ratio. The predictions based on Lee and Sills (1981) analytical solution were shown to be at variance with that of observed soil behaviour (Been 1980). However Been found that by introducing an imaginary overburden, and thereby redefining the model's boundary conditions, the behaviour of the soil could be predicted with a high degree of accuracy. Been's results are summarized in Table 2.1 together with other geotechnical data for soft soils.

Investigators	Sediment Description	Voids Ratio Range	Coefficient Consolidation $\times 10^{-8} m^2/s$	Permeability m/s	Shear Modulus kPa	Comments
Bryant et al. (1974)	wide range of clays − silts	0.4 − 5		$k = 10^{-11} e^5$		best fit line to data set from numerous authors
Herrmann (1974)	fine grained sediment	2 − 5	5.7 to 240			Consolidometer
Been (1980)	mud	4 − 12	0.4 − 6.0▲ 0.5 − 4.0● 8.0 *	1.7 − 30		Self weight experiments ▲ Calculated ● Pore Pressure Model * Settlement Curve Model (see text for details)
Silva & Jordan (1984)	silty clays Inorganic Pelagic clays	2.1 − 3.4 2.6 − 3.3	23 − 55 3.2			Consolidometer
Elder (1985)	mud	3 − 12			10.0 − 0.01	Self weight experiments Secant modulus derived shear vane measurements
Tan et al. (1988)	silty clay	6.7 − 5.8		△		Large strain consolidation cell. △ $k=\exp(-22.4+1.47e -0.09e^2)$

Table 2.1. Summary of Soft Soil Geotechnical Data.

2.2 GEOPHYSICAL PROPERTIES OF SOFT SOILS.

2.2.1 INTRODUCTION.

This section reviews the background knowledge of geophysical measurement as applied to soft soils. Compressional wave, shear wave and soil electrical resistivity measurements are discussed as a precursor to the review of the Biot model which follows in section 2.3.

2.2.2 COMPRESSIONAL WAVE MEASUREMENTS IN SOFT SOILS.

The fundamental equation for compressional wave velocity V_P originates from the solution of the wave equation (Telford et al. 1978)

$$V_P = \left(\frac{B + {}^4/_3 \, G}{\rho} \right)^{0.5} \tag{2.10}$$

The equation indicates that V_P is governed by B, the bulk modulus (resistance to change in volume); G, the rigidity modulus (resistance to change in shape); and ρ the bulk density. Many attempts have been made to use this equation to explain how a soils solid and fluid phases might combine, to carry the impinging pressure wave. One of the earliest of these is the Wood's equation. The Wood's equation for suspensions, applicable to soils with no rigidity (Hamilton 1971) represents the lower limit for P-wave velocity in water saturated soils. Wood's equation is given by

$$V_P = \left(\frac{1}{(\eta C_w + (1-\eta)C_s) \, (\eta \rho_w + (1-\eta)\rho_s)} \right)^{0.5} \tag{2.11}$$

where C_w and C_s are the fluid and solid compressibilities, ρ_w and ρ_s are the fluid and solid densities and η is the soil porosity. The gradual development of a soil frame, and hence developing rigidity, would serve to increase V_P to a value

greater than that predicted by Wood's equation (Hamilton 1971). The inability to predict bulk modulus from measurements of V_p led Gassman (from Hamilton 1971) to propose the existence of a frame bulk modulus. The bulk modulus B was considered to be made up of solid phase, fluid phase and frame bulk modulus components (Hamilton 1971). Continued failure of such models to predict compressional wave behaviour was partly attributed to the dispersive nature of marine soils towards compressional waves (Biot 1956(a)(b), Stoll 1977, Hovem 1980). The most successful model to date, for the prediction of P-wave propagation in saturated porous media, including dispersion, is Biot's model. The Biot theory is discussed in detail in section 2.3 and appendix A2.

The measurement of sediment compressional wave velocity in the laboratory is straight forward. It has been well documented (McCann 1968, Dewes and McCann 1972, Clay and Medwin 1977, Paul and Jobson 1987), and will be considered further in Chapter 3 of this thesis . The majority of such studies have been devoted to the interrelationships between the seismo-acoustic properties of the soils and a large number of engineering parameters. Scattergrams indicate that correlations exist between V_p and such quantities as mean grain size, porosity, bulk density and acoustic impedance (Nafe and Drake 1963, Hamilton 1971, McCann 1968, Akal 1972, Hamilton and Backman 1982). The majority of sediments studied in the above analyses belong to the sand and silt groupings of soils. Little data has been published for the clay and clay-silt soils that are amongst those studied in this thesis. Urick (1947) and Hampton (1967) made V_p measurements in kaolinite suspensions ranging in porosity from 98% to 65% (figure 2.4). The V_p versus η plots are characterized by a distinct minimum at 75%-80% porosity. At this minimum, V_p was found to be 3% to 3.5% lower than the velocity observed in the pore fluid alone. Wood's equation (Hamilton 1971) applied to suspensions, was able to predict a lower limit to the velocity-porosity relationship. Ogushwitz (1985) reported that the Biot model, fitted using a largely empirical technique, closely matched the overall behaviour of V_p as a function of

17
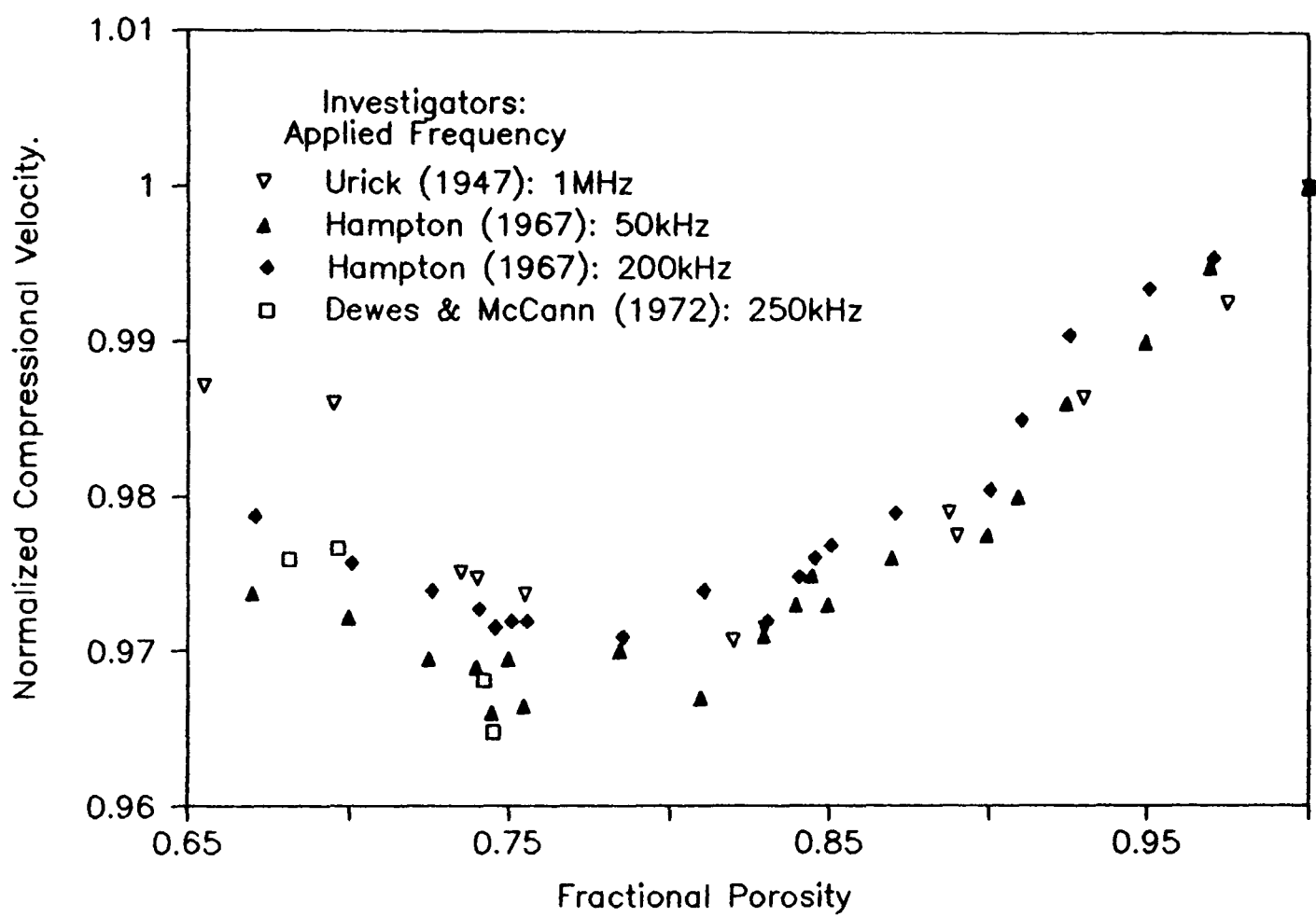
Figure 2.4   Summary diagram of P—wave behaviour
in soft cohesive sediments.

porosity, and that the approximate porosity at which the minimum occurs could be predicted. The sharpness of the V_p versus η minimum was said to be a function of increasing density contrast between the solid and fluid phases of the soil.

2.2.3 SHEAR WAVE MEASUREMENT IN SOFT SOILS.

The fundamental difference in behaviour between compressional waves and shear waves (V_s) is realized on comparison of the elastic equations. For shear waves

$$V_s = \left(\frac{G}{\rho} \right)^{0.5} \qquad (2.12)$$

it is noted that there is just one component of elasticity, that is the rigidity "G". A glance at table 2.1 reminds us that soft soils have little rigidity, G=10.0-0.01 kPa (Elder 1985). It might be expected therefore that V_s may be a relatively small value in such soils, if not zero. This view is probably substantiated by the lack of data for soft soils appearing in the literature.

The difficulty of detecting shear waves in soft soils proved so unremitting that Laughton (1957) pronounced that he was unable to measure shear waves in a sample of calcareous ooze until the material was compacted to a porosity of 32% under a pressure of 512 kg/cm^2. Difficulties of obtaining shear wave velocity measurements prompted Hamilton (1971) to pose the question "*do natural surficial marine sediments have enough rigidity to allow the transmission of shear waves, and if so, what are the reasonable magnitude of these waves?*" The difficulties experienced by experimentalists in attempting to achieve low pressure measurements of shear wave velocity in high porosity soft soils appeared unsurmountable.

It was not until Shirley and Hampton (1978) developed a composite shear wave transducer composed of a stack of four piezoelectric bender elements, 2.54 cm long by 1.27 cm wide,

18

that Hamilton's question was finally answered. Shirley and Hampton (1978) measured shear waves over a transducer separation of just under 6cm, in artificially sedimented kaolinite displaying velocities as low as 2 m/s for bulk densities of 1380 kg/m^3. Admittedly the signals were of extremely low amplitude, barely discernible above background noise, but the technological breakthrough had come. Large shear wave attenuation was observed which increased rapidly with increasing frequency. It was apparent that low frequency signals were demanded in order to to maintain a tolerable signal to noise ratio in such soft material, the frequency of the transmitted shear wave being dependent upon the dimensions of the bender element and upon the transducers compliance.

The effect of consolidation upon shear wave propagation was clearly seen in Shirley and Hampton's experiments (1978). Over a 50 hour settlement period a change in voids ratio from 3.0 to 2.1 was accompanied by an increase in shear wave speed from an initial 2m/s to 24m/s. Shirley and Hampton successfully monitored shear waves in a natural black carbonate soil, having a voids ratio of 3.9, finding a shear wave velocity of 3.6m/s and a soil rigidity modulus of 16.7 kPa.

Further studies by Shirley and Bell (1978), into the variation of shear wave speed in a variety of sea bed soils, produced a general trend of decreasing shear wave speed from coarse, low porosity sand to the finer, high porosity clay. Summarising literature values for shear wave velocity for broad sediment types: sands have velocities typically ranging from 40 to 100 m/s (Schultheiss 1983, Shirley and Bell 1978); soft soil silts typically have velocities in the range 10 to 40 m/s (Shirley and Bell 1978, Briggs 1991); soft soil clays have velocities ranging from 2 to 40 m/s (Shirley and Hampton 1978). Shirley and Bell's data also indicated for the first time the dispersive nature of saturated soils upon the shear waves, a view which conflicted with that previously held by Hamilton (1976). In the frequency band 0.8 to 4.0kHz there now existed evidence of dispersion in silt. Little evidence of dispersion was observed in clays for a frequencies range of 0.7 Khz to 1

kHz. Bell and Shirley(1980) demonstrated that shear wave velocity had negligible temperature dependence.

At the time of publishing the results of these studies, Shirley and colleagues were dedicating their efforts to the development of an *in situ* shear wave probe (Shirley and Bell 1978, Shirley 1980). Schultheiss (1983) made a comprehensive assessment of the state of bender element technology and looked to the incorporation of these types of shear wave transducer in standard soil mechanics apparatus, such as consolidometers and triaxial cells. The bender elements were subsequently also incorporated in other newly developed apparatus at the University College of North Wales, such as the porosity cell (Jackson 1975, Schultheiss 1981). Since in the laboratory environment, the rigidity of the bender element was of less importance, it became possible to modify the transducer such that it consisted of two piezoelectric transverse expander plates bonded together face-to-face (Chapter 3). This had the effect of improving the transducers compliance thereby improving its propagating capabilities. Following this development by Schultheiss (1981), shear wave velocity could be measured and compared to a wide variety of soil properties in the laboratory. In terms of soil properties, Hardin and Black (1968) summarize the various quantities which exert an influence on the shear wave propagation (derived mainly from resonant column experiments). These are shown in the functional relation

$$V_s = F\ (\sigma, e, q, \alpha, f, s, \tau, \gamma, t, \theta, T) \qquad (2.13)$$

σ = overburden pressure

e = voids ratio

q = grain characteristics,mineralogy,grading,grain shape and size.

α = ambient stress history and vibration history

f = frequency of vibrations

s = degree of saturation

τ = shear stress

γ = amplitude of strain

.

t = secondary time effects, and magnitudes of load increment

θ = soil structure

T = temperature

The major control on V_s is exerted by σ, q and θ ,voids ratio being a manifestation of these properties (Akal 1991). In the context of the present study the parameters s, γ, and T are essentially constant and therefore their influence on V_s variability is negligible.

Hamdi and Taylor Smith (1982), using a modified oedometer cell, analysed the seismo-acoustic properties of consolidating Irish Sea silty-clays. Though a little denser ($1.37 \leq e \leq 1.92$) than the soils to be studied here, it is worthy of note that Taylor Smith (1986) found that soil frame compressibility (C_f) was related to shear wave speed by the following empirical relationship

$$C_f^{-1} = 0.001 \, V_s^2 \qquad (2.14)$$

A number of researchers made the logical step of comparing the rigidity modulus derived from bender element measurements to the recognized ASTM experimental standard for obtaining the dynamic shear modulus, namely the resonant column apparatus (Bennell et al. 1984, Dyvik & Madshus 1985). Results showed that there was close agreement between small strain amplitude measurements for G in soft marine clays. Hardin and Black's (1968) equation for clays with low surface activity shows the correlation thought to exist between shear wave velocity and effective stress

$$V_s = (18.4 - 6.20e)(\sigma')^{0.25} \qquad (2.15)$$

The expression was also shown to be valid for turbidites with voids ratios greater than 2. (Davis and Bennell 1986).

James et al. (1989), and Williams and Williams (1989a,b) used a pulse shearometer to investigate shear wave propagation in suspensions. This apparatus incorporates shear wave torsional

transducers, propagating over a maximum 5cm transducer separation. This apparatus enabled small amplitude, high frequency shear wave measurements to be made in mud suspensions. The results indicated that a critical voids ratio (for effective propagation) of e=13.3 existed, representing they believed, the transition between flocs in suspension and a cohesive sediment. This critical value was reported to vary for different sediments, rising to e=50.6 for the clay mineral k-illite. Williiams and Williams (1989) reported non-linear and dispersive behaviour with regards to shear wave propagation in k-illite at an operating frequency of 220Hz. These data are viewed with some scepticism since these measurements were recorded over a transducer separation of 0.3mm. It is questionable whether sufficient material is sampled in this instance for a true measurement of the soil matrix to be made. It is possible that over such small distances, it is some function of the individual soil grains, rather than the matrix that is being measured. It is also questionable as to whether the soil sample is not being detrimentally affected by the transducer movement, strains possibly being sufficiently large to induce decoupling and/or liquefaction around the transducer element. The data discussed here are also presented in table 2.2, this serving as a summary of present day knowledge of shear wave propagation in soft soils.

Investigators	Sediment Description	Voids Ratio Range	S–Wave Velocity (m/s)	Shear Modulus (kPa)	Applied Frequency (Hz)	Method Used
Shirley & Hampton (1978)	Kaolinite	2.1–3.0	32–2		338	Bender Element
	Black Carbonate	3.9	3.6	16.7		
James et al. (1989)	mud	4.5–13.3		1.50–0.05		Pulse Shearometer
Williams & Williams (1989a)	K–illite	13.3–50.6	2.6–0.3	7.31–0.087	220	Pulse Shearometer

Table 2.2. Summary of Soft Soil Shear Wave Data.

2.2.4 ELECTRICAL RESISTIVITY MEASUREMENTS IN SOFT SOILS.

The analogy between electrical conductivity and hydraulic conductivity has been utilized by geophysicists to investigate many properties of marine sediments. It was argued that since both phenomena were affected by the proportion of pore spaces within the soil, and of the shape of the interconnecting pore spaces, it was logical to look for a correlation between the electrical resistivity of the marine sediment and its porosity and permeability (Boyce 1968, Taylor Smith 1971, Jackson 1975, Lovell 1984, and Mirza 1991). This section describes how the measurement of soil resistance may be utilized to experimentally determine the mass coupling factor as defined by Biot (1962). This factor accounts for the tortuosity, or complex geometry of the connecting pores that are found within a soil. Readers who are unfamiliar with the concept are referred to appendix 2 where a brief review of the subject will be found.

Tortuosity is a function of the soil matrix and not of the pore fluid. It is essential therefore that the influence of the interstitial fluid is eliminated from the measured soil resistance. This is achieved by defining a quantity known as the Formation Factor (F). Providing the geometry of the measuring apparatus remains fixed, the Formation Factor is related to electrical resistance by the following relationship (Archie 1942):

$$F = \frac{\text{resistance of the porous medium}}{\text{resistance of pore fluid}} \qquad (2.16)$$

The empirical relationship between Formation Factor and soil porosity is well known having the general form

$$F = A \, \eta^{-\beta} \qquad \text{Winsauer et al (1952)} \qquad (2.17)$$

where A and β are constants dependent upon the shape and cementation of the soil particles. For marine sediments most researchers have found A $\simeq$ 1 (Mirza 1991). A summary of typical values of β for soft cohesive soils are shown in table 2.3. Figures A3.6 and A3.7 in appendix 3 show the effect of

particle size, particle shape and cohesion upon the measured formation factor.

Table 2.3. Empirical Relations Between Formation Factor and Porosity in Cohesive Marine Sediments.

Soil Classification	Equation	Source
Bering Sea samples (silty clays/clayey silts)	$F= 1.2\rho^{-1.72}$	Boyce 1968
Irish Sea clay	$F = 1 \eta^{-2}$	Taylor Smith 1971
North East Atlantic clay	$F = A \eta^{-\beta}$ $A = 0.95 - 1.25$ $\beta = 1.36 - 3.50$	Lovell 1984
Kaolinite	$F = 1 \eta^{-1.8}$	Lovell (personal communication)

Despite the relative success of fitting equation 2.18 to cohesive soil data, a number of researchers (amongst them Boyce 1980 and Urish 1981) have debated the validity of the Winsauer equation in cases where the composition of the sediments contains a high percentage of conductive solids and clay minerals (section 2.1). They argue that, owing to the presence of such conductive solids, the additional problem of ion mobility, both on the soil matrix and into the pore fluid, has to be considered. They consider that the True Formation Factor is impossible to determine in such soils and it is an Apparent Formation Factor that is measured, which is generally lower than the "True" value. Such researchers have attempted to establish matrix conduction corrections to correct Apparent to True Formation Factors. These correction factors are simply empirically derived constants applicable to local conditions only. Boyce (1968) identified a further problem, recognizing that Formation Factor was affected by the temperature sensitivity of a variety of clay minerals. He noted that Formation Factor increased by up to 1% per $^{\circ}$C temperature decrease.

The mass coupling factor (b) is a parameter, introduced by the Biot theory (1956a,b; 1960 and section 2.3 below), which attempts to take account of the complex tortuous nature of a soils connecting pores. It takes on the theoretical values of

$$1 \leq b \leq 3 \qquad \text{(Stoll 1974)}$$

The lower limit, b = 1, represents uniform pores with axes parallel to the seismo-acoustic pressure gradient, while the upper limit, b = 3, represents a random system of uniform pores with all possible orientations. In a real soil however, the distribution of the pores is far more complex and it is impossible to calculate theoretically. Therefore the mass coupling factor must be determined experimentally. Brown (1980), making use of the analogy of hydraulic and electrical tortuosity suggested "b" could be determined using the expression below

$$b = F \, \eta \qquad\qquad\qquad (2.18)$$

Critics of Brown (including Dullien, 1979) objected to the over simplification of soil structure in terms of a single pore geometry. However, Hamdi and Taylor Smith (1982) have used Brown's relationship for "b" to predict permeability in cohesive soils with apparent success. To establish whether Brown's relationship may be valid for lower density cohesive soils a diagram from Partheniades (1965) (figure 2.1) was studied. This idealized diagram depicting soil formation shows how originally the developing soil takes on a honeycombed structure consisting of large voids. Gradually this structure collapses with a subsequent decrease in voids ratio and increase in strength. Elder (1985) and Bowden (1989) (section 2.1.2), have demonstrated how little strength soft soils have. The implications are that the soil structure is in a relatively loose state (figure 2.1,B). Perhaps there is some justification, therefore, to say that soft soils may approximate to uniform pores with random orientation. The Brown equation will therefore be used in this study to provide an estimate of mass coupling factor.

2.3 Modelling and Prediction of Seismo-acoustic Propagation.

2.3.1 INTRODUCTION: BIOT THEORY

The widely used theory for the propagation of seismo-acoustic waves in fluid saturated porous media is the model based on the classic work of Maurice Biot. The theory is documented in a number of papers spanning the time period 1941 to 1973. Biot's initial work (1941) covered the quasi-static consolidation of a porous, linearly elastic medium and then extended the theory to cover the dynamic response for a number of different cases which included considering the solid to be visco-elastic (1956a,b).

The Biot theory considers the soil to be a two phase system consisting of an elastic solid phase, comprised of the soil matrix, and a viscous pore fluid phase. An elastic wave incident upon a soil element will cause relative movement of the fluid in the soil pore spaces. The theory assumes that the soil is made up of parallel or circular ducts, with a degree of tortuosity, allowing the motion of the fluid to be modelled in terms of Poiseuille and non-Poiseuille flow. The theory considers the case of both low and high frequency applied seismo-acoustic waves. Within the low frequency range, that is between zero and some transitional frequency (f_t), the pore fluid flow is considered to be of the Poiseuille type (section 2.1.2) whilst above the transitional frequency Poiseuille flow breaks down. The theory's wide acceptance is mainly based upon the successful prediction of two compressional waves and a single transverse wave (experimentally verified by Plona 1980 and 1982) and also its ability to predict the occurrence of seismo-acoustic wave dispersion in many marine sediments.

The Biot theory is mathematically unyielding, requiring information of the sediment which is difficult to determine. It is for this reason that numerous authors have worked towards simplifying the theory in order to provide a working model to describe seismo-acoustic propagation in

unconsolidated marine sediments. After the classic papers of Biot in 1956a,b perhaps the biggest contribution to the development of the theory was made by Geertsma and Smit (1961) and Geertsma (1961), who unraveled the deformation constants of the Biot theory in terms of compressibility and porosity. The Geertsma and Smit model simplifies the Biot theory by assuming that an incident seismo-acoustic wave will cause fluid in the soil pore spaces to undergo linear flow (defined in terms of Darcy's law of fluid flow) no matter what frequency of vibration is applied. The model is regarded as an "approximation" to the "full" Biot model since linear flow only practically exists if the applied frequency (f) is within the low frequency range (i.e. $0 \leq f \leq f_t$).

The Geertsma and Smit approximate solution makes use of two velocities: the "zero frequency velocity" (Vo) for applied frequencies very much lower than the characteristic angular frequency (ω_c) of the soil and the "infinite frequency velocity" (V∞) for applied frequencies very much higher than the characteristic angular frequency. A resume of this approximate treatment of the Biot model is outlined in appendix 2 and forms the basis of the following discussions.

$$V_P^2 = \frac{V\infty^4 + Vo^4 (\omega_c/\omega)^2}{V\infty^2 + Vo^2 (\omega_c/\omega)^2} \qquad (2.19)$$

where

$$Vo^2 = X/\rho \qquad (2.20)$$

$$V\infty^2 = \frac{Z\rho + Xm - 2Y\rho_w}{m\rho - \rho_w^2} \qquad (2.21)$$

and the characteristic angular frequency of the sediment, ω_c,

$$\omega_c = \frac{g\eta\rho}{(b\rho - \eta\rho_w)} \cdot \frac{1}{k} \qquad (2.22)$$

where X, Y and Z are elastic constants, η is porosity, g is the

acceleration due to gravity, b is a mass coupling factor, k is the permeability in units of velocity, ρ_w and ρ are bulk and fluid densities respectively. (For a detailed description of these parameters refer to appendix 2).

For an applied frequency above the transitional value linear flow breaks down and the full Biot theory (Biot 1956b, Stoll 1989) is required in order to model seismo-acoustic propagation in the porous media. Biot allows for non-laminar flow by introducing a complex viscosity correction factor $F(\Phi)$ through the dimensionless ratio f/f_c (where f is the applied frequency and f_c is the characteristic frequency of the soil). The transitional frequency, between laminar and non-laminar flow, depends upon the size of the soil pore spaces and upon the kinematic viscosity of the fluid as shown by the equation below:

$$f_t \quad = \quad \frac{\pi\mu}{4\,\rho_w d^2} \quad \approx \quad 0.15\ f_c \qquad (2.23)$$

where d represents the characteristic pore diameter, μ and ρ_w are the fluid viscosity and density respectively.

Figure 2.5 illustrates the relationship between the approximate and full model in terms of the compressional wave dispersion curve, the relevant details of which will now be described. Allowing the viscosity correction factor to assume the value of unity (f=1) introduces the laminar flow condition for all frequencies with the subsequent generation of the approximate solution curve. Allowing $f\neq1$, the V_P dispersion curve becomes dependent upon the pore radius parameter (d). In figure 2.5, "d" is varied with respect to the applied compressional wavelength (λ) keeping all other model parameters, including permeability, constant. The dispersion curve becomes smeared out over several decades as the magnitude of pore radius is increased. As the average pore radius parameter becomes small the full model curve tends towards the approximate solution. Therefore with decreasing pore radius linear flow is maintained for an increasing range

28
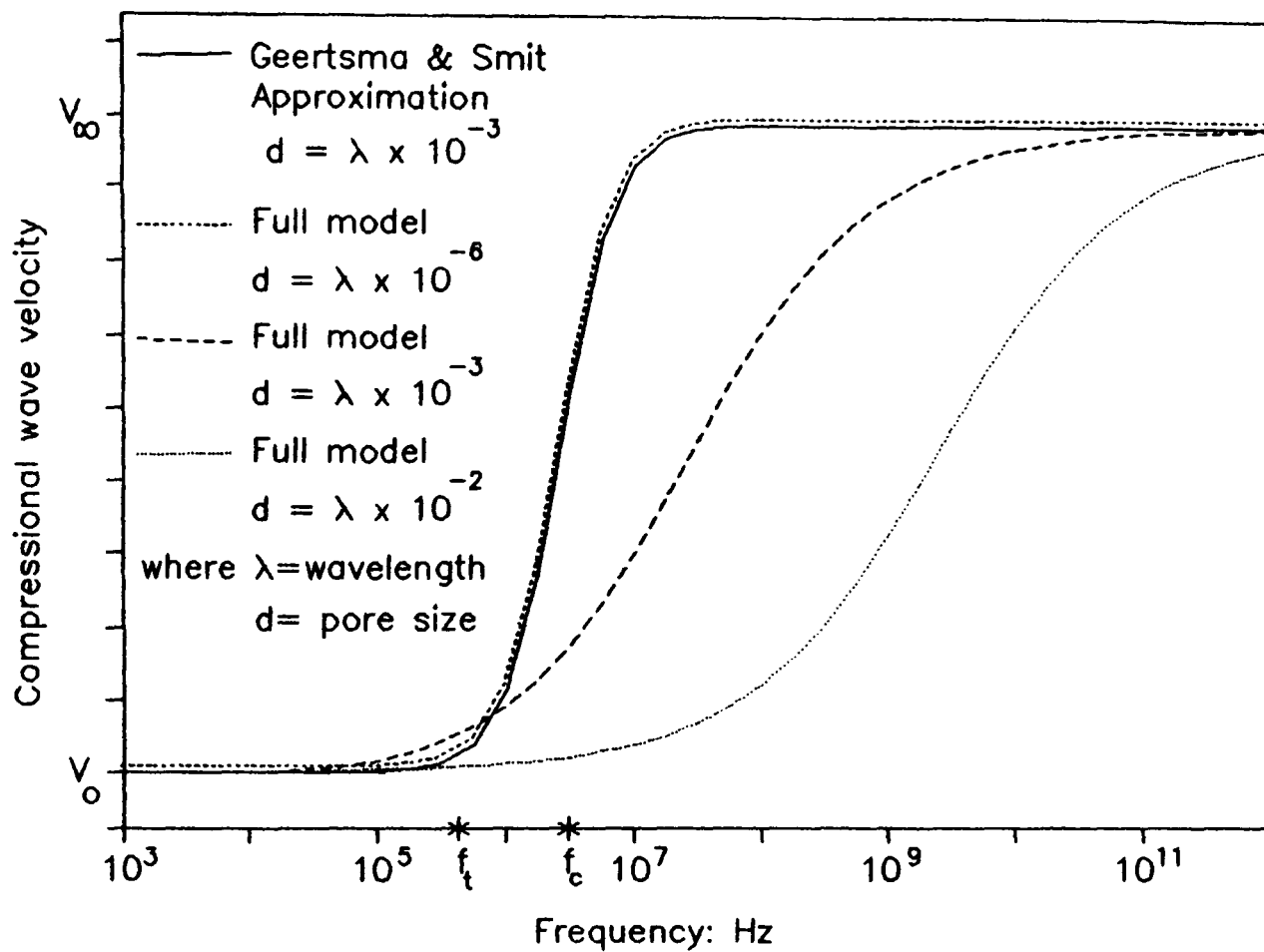
Figure 2.5 Comparison of the full Biot model and the Geertsma and Smit approximation for varying pore size.

Figure 2.6 Changing compressional wave dispersion curves as a function of permeability (after Stoll 1986).
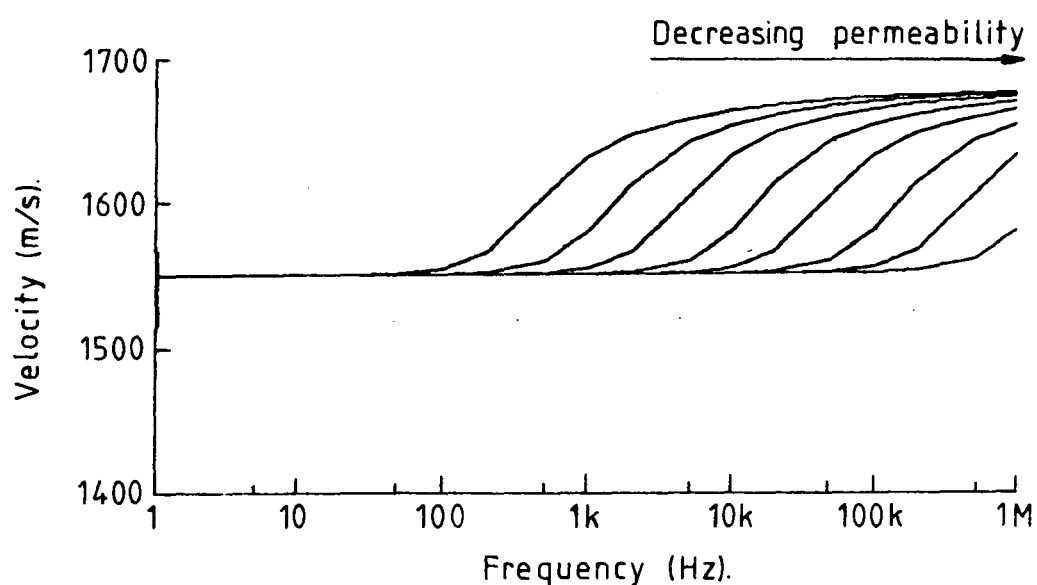
of frequencies and as a consequence the approximate solution becomes increasingly valid for that range of frequencies.

2.3.2 THE BIOT THEORY AND CONSOLIDATION PHENOMENA.

Following Geertsma and Smit's (1961) approximate solution, the Biot theory gradually gained acceptance in the geophysical community as a workable model. The Biot model was utilized by numerous authors to predict compressional wave velocity and attenuation by manipulating various soil parameters, or conversely, using compressional wave velocities and attenuation to predict properties of the soil (e.g. Stoll & Bryan 1969, Stoll 1974,1977,1986, Hovem & Ingram 1979, Hovem 1980, Hamdi & Taylor Smith 1981,1982, Taylor Smith 1986). In these studies permeability received a great deal of attention, and is considered here to be of considerable importance as the controlling mechanism of consolidation.

Ishihara (1968) related the mode of propagation of the two types of compressional wave to the dissipation of the pore water pressure at a microscopic level. As a result of the repeated loading by a seismo-acoustic wave propagating at low frequencies, the solid and fluid phases of the soil move in phase. Theory predicts therefore that the velocity of the wave of the first kind is identified as being a wave that travels in an undrained propagation state. On the other hand, a wave propagating at very high frequencies (f ∞), causes the solid and fluid phases to move out of phase, evidenced by viscous attenuation. Such a wave is predicted to travel in a drained propagation state. This, Ishihara argued, would imply that in order to successfully measure the permeability of a soil using the seismo-acoustic means, the applied frequency must be much larger than that frequency used to measure V_0. In somewhat contradictory style, Ishihara (1968) continues by suggesting that at very high frequencies the motion becomes so fast that the soil matrix and pore fluid move freely without any interaction between the two phases. The flow therefore does not correspond to Darcy's flow at higher frequencies.

Since the usefulness of the approximate model to predict consolidation behaviour can only be judged on the basis of comparison with the laboratory measurement it is essential that only those predicted permeability values (from the Geertsma and Smit model) are used for comparison when Darcy's flow is obeyed. Some consideration must be given as to when Darcy's flow no longer exists. Swartzendruber (1961) showed that Darcy's flow was only realized in coarse grained soils and that the law was not truly applicable to cohesive soils. However, Darcyian flow has been found to exist to a first approximation in high voids ratio cohesive soils (Lambe and Whitman 1979, Been and Sills 1981, Edge 1985, Bowden 1989).

Based on Ishihara's observations it is at first unclear whether the measurement of "high frequency" seismo-acoustic waves is a viable technique for measuring permeability. It must be remembered however that the Biot model calculates "high frequency" velocities by allowing for the breakdown of Poiseuille flow. Thus although at high frequencies Darcy's law may not be obeyed it should not affect the prediction which is after all a constant input parameter required to calculate compressional wave velocity as a function of frequency.

As seen earlier in figure 2.5 the correct value of the pore size parameter "d" is crucially important to the successful application of the full Biot model. However there are considerable practical difficulties in measuring the quantity "d" for natural sediments. It is for this reason that several authors (e.g. Hovem and Ingram (1979), Stoll (1980), Yamamoto and Turgut (1988) and Briggs (1991)) have suggested the following approximations:

$$d = \left(\frac{a}{3} \right) \cdot \left(\frac{\eta}{1-\eta} \right) \qquad \text{Hovem \& Ingram (1979)} \qquad (2.24)$$

$$d \approx \frac{a}{6} \text{ or } \frac{a}{7} \qquad \text{Stoll (1980)} \qquad (2.25)$$

$$d = \left(\frac{8 \, \phi}{\eta} \right) \qquad \text{from Briggs (1991)} \qquad (2.26)$$

where "η" is the soil porosity, "a" is the mean grain diameter and ϕ is the coefficient of permeability (units of area). Equations 2.24 and 2.25 are estimations of "d" for coarse grained soils where as the equation from Briggs is suitable for cohesive sediments. The Hovem and Ingram formula and that from Briggs will be used in this thesis as they allow the pore size parameter to vary with changing porosity.

2.3.3 THE PRACTICALITIES OF USING SEISMO-ACOUSTIC MEASUREMENT TO PREDICT PERMEABILITY.

The theoretical possibility of using seismo-acoustic measurement to predict permeability was considered in the above section. The practicalities of performing such measurements are now reviewed.

It is apparent from equation 2.22 that the characteristic angular frequency (ω_c) is a function of permeability. If the approximate solution velocity given by equation 2.19 is solved for k (Taylor Smith 1986) the following equation is obtained.

$$k = \frac{\eta \, g}{\omega} \left(\frac{\rho}{(b\rho - \eta\rho_w)} \right) \left(\frac{V_0}{V_\infty} \right)^2 \left(\frac{(V_P/V_0)^2 - 1}{1 - (V_P/V_\infty)^2} \right)^{0.5} \qquad (2.23)$$

Evidence of the importance of permeability with respect to compressional wave velocity was provided by Stoll (1986) and Hurley (1989). Compressional wave dispersion curves were reproduced expounding the effect of changing permeability. The dispersion effect is confined to a narrow band of frequencies, this band of frequencies shifting to higher and higher frequencies (figure 2.6) as the fluid mobility decreases, because of lower permeability. V_0 and V_∞ are shown to be independent of permeability. Theoretically therefore by sweeping through several decades of applied frequency, at the same mapping the changing compressional wave velocity dispersion curve, the characteristic permeability of the soil could be determined from the dispersion curves position relative to the y-axis. Such measurements are practically

difficult to accomplish owing to the limitations of present transducer technology.

Another approach would be to use a single applied frequency on the dispersive portion of the curve, and observe the change in compressional wave velocity relative to fixed values of V_o and V_∞ (figure 2.6). Just such an approach was used by Hamdi and Taylor Smith (1981,1982) using a modified oedometer cell in which seismic velocities, of applied compressional wave frequency 1MHz and applied shear wave frequency 5kHz, were monitored during the consolidation process for normally consolidated marine sediments of initial voids ratio ranging from 2.2 to 1.4. According to Hurley (1989) the characteristic and transitional frequencies for this Irish Sea silt, having a porosity of 0.6 would be:

$f_c=3.1$ Mhz

$f_t=1.3$ MHz

Hurley (1989) went on to show that the applied frequency used in Hamdi and Taylor Smith's experiment would fall on the dispersive portion of the compressional wave velocity-frequency curve below the transitional frequency. The characteristic frequency is known to vary from one soil to another, and will vary in the same soil depending, to a major extent, on the permeability of the soil. The larger the permeability is, the less the value of ω_c becomes. The characteristic frequency of a soil ranges between 100 kHz for sands to over 100 MHz for clays (Ishihara 1968, Taylor Smith 1986, Stoll 1986 , Hurley 1989).

In the same experiments described above Hamdi and Taylor Smith (1982) demonstrated that the divergence of the measured velocity (V_P) from the calculated velocity at zero frequency (V_o) correlated well with low values of permeability measured in the oedometer. Taylor Smith (1985) showed that an improved correlation was obtained if the mass coupling factor (appendix 2) was determined using the electrical analogous quantities of apparent formation factor and porosity (Brown 1980). Mirza (1991) reworked the data of Hamdi (1981) and Hamdi and Taylor Smith (1982), and found that the measured permeabilities
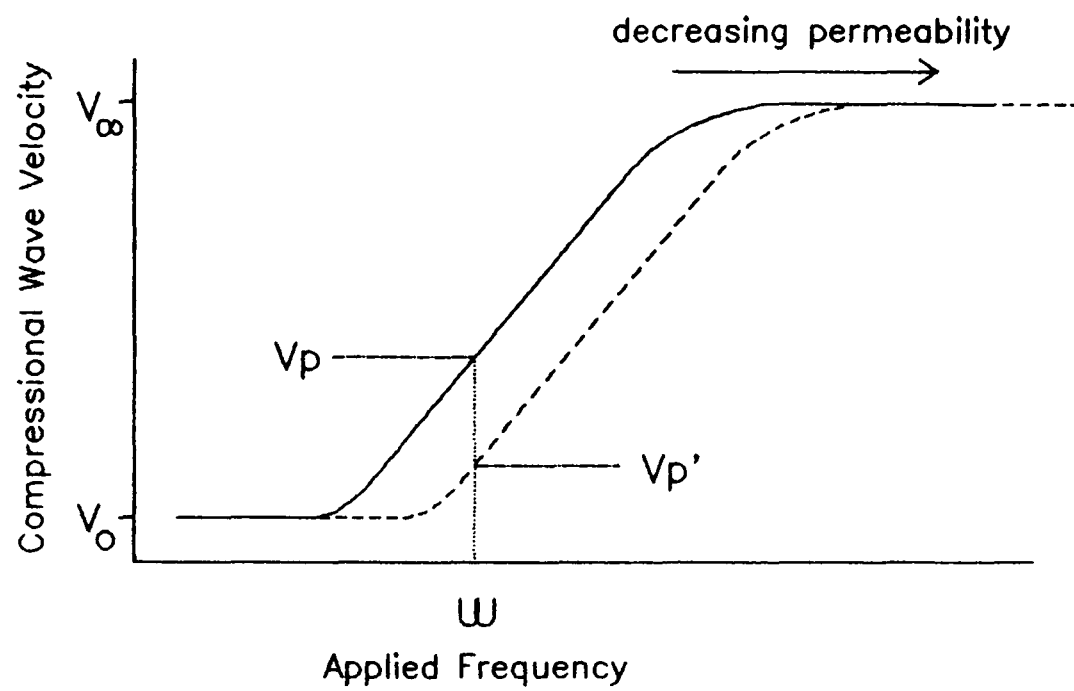
Figure 2.7   Determining permeability using a single applied seismo—acoustic frequency.

(derived from oedometer measurements) were consistently of two
to three orders of magnitude less than those predicted by the
Biot model. Mirza believed that this disparity in results was
due to the break down of Darcyian flow at the applied seismic
frequency which conflicts with Hurley's findings. If Mirza was
correct then the data need to be re-analysed using the full
Biot model which would require an estimation of the pore size
parameter as described earlier.

Hurley (1989) compared the permeability results from various
in situ and laboratory techniques. He observed that measured
permeabilities spanned 6 orders of magnitude for the same
soil. Hurley gives numerous possible explanations for the
diversity of the results ranging from non-representative
sub-sampling, coring disturbance, and apparatus design
problems, but also questions the fundamental mechanism under
study. Studying Hurley's data, it is observed that the Biot
prediction most closely agrees with low stress tests such as
permeability from direct flow and the tidal piezometer method.
Large stress techniques, such as the oedometer test, are in
disagreement with Biot's predictions.

2.3.4 PREDICTION SUCCESSES OF THE BIOT MODEL.

Hovem (1980) applied the Biot model to sediment suspensions
and showed that although the model predicted consistently
higher compressional wave velocities than those observed, it
did represent a large improvement upon existing suspension
theory. Johnston and Plona (1982) stated that according to
Biot theory a "weak frame" soil was expected to act as a
suspension as far as seismo-acoustic waves were concerned.

Ogushwitz (1985) used the data from Hampton (1967) and Urick
(1948), to demonstrate that the Biot model could be
successfully applied to artificial suspensions of kaolinite,
ranging in porosity from 95% to 65%. He was able to show that
the Biot model could predict compressional wave speeds at
least as well as other suspension models. The model used a

number of estimated parameters making the fitting technique largely empirical. Permeability was computed from the Kozeny-Carman relationship, and the frame moduli were estimated from the self-consistent theory of composites (Ogushwitz 1985). In terms of this study the research aimed to experimentally measure most of the model input parameters thereby reducing the empirical nature of Ogushwitz's method.

Here then is the difficulty faced by any researcher in this field. In order to use the Geertsma and Smit approximate solution an applied frequency is required that falls upon the dispersive part of the velocity-frequency curve but must also be within the region of Darcyian flow which exists below the transition frequency. The measured velocity must at the same time be significantly larger than V_o in order to make meaningful permeability predictions. Should the applied frequency fall above the transitional frequency, the full Biot model would need to be used, with its inherent difficulty of predicting a representative pore size parameter.

2.4 Implications of the Literature Review on Research Requirements.

An attempt has been made in this chapter to collate known geotechnical and geophysical behaviour of soft soils. The reported behaviour of such soils is at times unclear as a result of conflicting evidence. This is due in part to the difficulty of obtaining accurate results and partly due to the application of assumptions that have not yet been validated at very low density states. Models have been reported that may best explain behaviour of these sediments, the validity of which will be reviewed in this thesis. The research has the following important questions to answer:

(1) Do seismo-acoustic waves behave in a predictable manner in soft soils? Can the Biot theory be used to predict this behaviour?

34

(2) Can the Biot theory be used to predict consolidation properties of the soil using the geophysical measurements?

(3) Have the input parameters of earlier suspension and soft soil researchers been valid?

(4) With respect to shear waves:

    (a) At what density do shear waves first propagate?

    (b) Does this limit agree with previous findings?

    (c) Can anything be learnt of the mechanism of shear wave propagation from these results?

    (d) Will shear waves be affected by creep phenomena?

    (e) What is the relationship of shear wave velocity to that of effective stress and frame compressibility at very low density?

(5) What practical measurements should be made in order to investigate the questions posed above?

(6) What apparatus should be developed for these measurements?

(7) Can recommendations be made as to the improvement of measurement apparatus developed in this research programme.

These questions will be addressed in the following chapters of this thesis.

CHAPTER 3.   EXPERIMENTAL APPARATUS:
The Development of an Instrumented Settling Column.

3.1 Research Objectives.

The research programme consisted of five main objectives. The main aim was to expand the general knowledge of soft soils by making comprehensive geotechnical and geophysical measurements in the laboratory, during the self weight consolidation of a soil from a homogeneous low density slurry.

In order to perform such measurements, an instrumented settling column was required. The main aim of the research programme therefore was to produce a laboratory apparatus which would be capable of measuring compressional wave and shear wave velocities, soil electrical resistivity, and soil pore pressure. The apparatus was to be designed such that it was compatible with the density logging X-ray facility housed at the Department of Engineering Science, Oxford.

During the course of the research programme it would be necessary to establish whether the weak soil frame, characteristic of a soft soil, would be capable of supporting the transmission of shear waves. This would enable the soils rigidity to be studied during the initial stages of development of the soil frame.

The research aimed to establish the suitability of the Biot model (chapter 2) to predict the consolidation behaviour of soft soils. Should the model fail to predict consolidation behaviour, evidence would be sought as to why this should be.

Finally, since the self weight consolidation process is by nature, of extremely long duration, of the order of several months, a loading system would be developed, the idea being that the consolidation process might be accelerated. An

investigation would be made to establish the effect of using such a system upon the soil.

The remainder of this chapter will be devoted to the details of development of the instrumented settling column. Decisions as to the column design will be substantiated with supporting evidence where necessary. Supporting experimental work regarding the column design is documented in this chapter and in chapter 6.

3.2 Preliminary Study: The Prototype Column.

The conclusions drawn after reviewing the literature indicated a need for considerable instrument design and testing before any experimental data could be collected. In order to gain familiarity with the nature of soft soil behaviour, both geotechnically and geophysically, a prototype column was built. This column was constructed of acrylic having dimensions of 1m height, 9.9cm diameter, and walls 0.5cm thick. This column (shown in appendix 3, figure A3.1) contained fourteen self sealing "subba seal" ports through which sediment samples could be extracted using a 1.5mm bore hypodermic syringe. It was intended that such samples would be analyzed for particle size, or, for bulk density analysis using a hand held PAAR Density Meter (for details refer to appendix 3). Eight pairs of transducer mounts were also incorporated into this prototype column. These mounts were to be used in testing various designs of compressional and shear wave transducers, and to establish suitable drive/receive instrumentation for these transducers. A single Druck pressure transducer, type PDCR 810, 1 bar pressure range, was used in conjunction with a digital voltmeter to investigate pore pressure dissipation and to test the efficiency of various piston designs.

It was intended that the findings from the preliminary investigations using the prototype column would be used in the subsequent design of an instrumented sedimentation column.

3.3 The Compressional Wave Transducer.

3.3.1 INTRODUCTION.

One of the input parameters required for the Biot model is the compressional wave velocity of the soil. Within the prototype column this was to be obtained by measuring the transit time of a high frequency compressional wave pulse as it traversed the diameter of the column. The high frequency pulse was to be generated and received by pairs of thickness expander piezoelectric ceramic crystals. The dimension and construction of these compressional wave transducers would be governed by the various experimental constraints together with the type of logging system to be adopted. These factors will be discussed in the following sections of this chapter.

3.3.2 COMPRESSIONAL WAVE LOGGING SYSTEM: POINT MEASUREMENT VERSUS CONTINUAL MEASUREMENT SYSTEMS.

An early decision has to be made as to whether to monitor the variation in velocity down the column using either:
(a) a pair of transducers mounted exterior to the column thereby enabling a continual velocity gradient to be measured.
or
(b) a number of transducers in fixed positions in the column wall thereby allowing point measurements to be taken.
Both methods have advantages and disadvantages which are summarized below.

Advantages of the Continual Logging Method.

(1) This is potentially, a very versatile system. The logging step distance can be varied such that the apparatus can home in on areas of interest within the soil. The versatility of this system could enable individual soil elements to be monitored during the consolidation process in a Lagrangian measurement manner.

(2) It requires only one pair of transducers.
(3) The drive mechanism can be controlled by microcomputer.

Disadvantages of the Continual Logging Method.

(1) It is necessary to develop some form of logging mechanism, a potentially expensive and technically complex development.
(2) Such a logging system can have inherent coupling problems since the transducers are mounted exterior to the column.
(3) There are often calibration complications. Because the transducers are mounted externally they are affected by varying column wall thickness and ovalling of the column diameter.

Advantages of Point Measurement Method.

(1) No coupling problems are likely to occur since the transducers are in direct contact with the sediment.
(2) Calibration of the transducers is straight forward.
(3) Transducers can be fitted into simple port construction.
(4) The measurement system can easily be controlled and data logged by a microcomputer.

Disadvantages of Point Measurement Method.

(1) A large number of transducers are required depending on the vertical spatial resolution specification.
(2) The consolidating soil must pass the seismo-acoustic sampling points in a Eulerian method of measurement. This can complicate any detailed study of the seismo-acoustic response of individual soil elements.

For the current study the measurement technique to be adopted had to be capable of monitoring small variations in compressional wave velocity within the sediment. It was therefore decided that the primary concern would be the

precision of measurement. Hence a simple experiment was devised to compare the precision of the two methods.

Initially, a comparison was made of the signal quality of two transducers transmitting through a column filled with water. One pair of transducers was mounted in the column such that the transmitting and receiving faces were in contact with the water. A second, identical set of transducers was clamped against the column walls. The transducers in contact with the water gave received signals that were significantly larger in amplitude and displayed clearer onsets than the signals received from the externally mounted transducers. Extreme care was taken to ensure that the clamped transducers were in alignment, and coupling was made good by the use of petroleum jelly. The picking of the compressional wave onset was considerably more precise in the signals produced by the transducer pair in direct contact with the water.

It is likely that the major source of error in the external logging system would be due to incorrect knowledge of the column wall thickness, estimated at 5mm ± 5%, and to the effect of column diameter ovalling, estimated at 9.9cm ± 6%. It became clear that with a moving logging system coupling could prove a major problem. Based upon these facts it was decided that, despite the advantages of the continuous logging system, the experimental conditions in this particular application demanded the spot sampling technique.

3.3.3 APPLIED FREQUENCY DESIGN CONSIDERATIONS.

Chapter 2 illustrated the crucial importance of the correct selection of the applied compressional wave frequency in the measurement of permeability using the Biot theory. In order to determine what applied frequency would be suitable for wave

velocity measurements in soft soils, a series of calculations were made utilizing equation 2.22.

$$\omega_c = \frac{g \, \eta}{k} \left(\frac{\rho}{b\eta - \eta\rho} \right) \qquad (2.22)$$

Since the term in brackets is close to unity a good estimate of ω_c can be obtained from the following expression

$$\omega_c = \frac{g \, \eta}{k}$$

Given this relationship, the porosity and permeability data from Been and Sill's (1981) experiments on an estuarine mud could then be used to calculate estimates of the characteristic frequencies expected in soft soil. Making use of the approximation (Biot 1956a,b)

$$\omega_t = 0.15 \, \omega_c$$

meant that the transitional frequency could also be estimated. The results of these calculations are shown in table 3.1.

Table 3.1 Approximation of transitional and characteristic frequency ranges for a soft estuarine mud.

Fractional Porosity	Permeability (x10^{-6} m/s)	Critical Frequency (MHz)	Transitional Frequency (MHz)
0.90	7	0.2	0.03
0.85	5	2.7	0.4
0.80	2	6.2	0.9
0.75	1.5	7.8	1.2
0.70	1.0	11.0	1.6

The range of transitional frequencies expected in an estuarine mud consolidating under self weight ranges from approximately 0.03MHz to 1.6MHz. Below these frequencies laminar flow is believed to exist in the soil, and the Geertsma and Smit approximation can be applied. Increasing clay content would cause the characteristic and transitional frequencies to increase. Hurley's (1989) dispersion curves indicate that

compressional wave dispersion occurs over two decades of frequency. A transducer transmitting a frequency of 500kHz would satisfy the criterion for all but the highest porosities. By way of substantiating this selection of transducer one need look no further than to Hurley (1989) who predicted that for silt of initial voids ratio of 1.5, frame compressibility of $1.5 \times 10^{-7} Pa^{-1}$, and a rigidity modulus of $1.2 \times 10^7 Pa$ would have a characteristic frequency of 3.1 MHz. Hamdi and Taylor Smith (1982) had used an applied frequency of 1MHz in their measurements in such soil, and were thus able to use the low frequency approximation to the Biot theory (appendix 2). It seems reasonable therefore to propose a 500 kHz applied frequency for soils of higher voids ratio (i.e. voids ratio>2), larger frame compressibility, and lower rigidity modulus.

3.3.4 COMPRESSIONAL WAVE TRANSDUCER CONSTRUCTION.

Schultheiss (1983) has shown that a PZT piezoelectric crystal potted in a manner similar to that shown in figure 3.1 can be used in a wide variety of standard geotechnical apparatus. This type of piezoelectric transducer was therefore tested in the prototype column, and found to be satisfactory. A typical received signal from a pulsed 500kHz transducer (having traversed the diameter of the column, propagating through a clayey silt of density 1474 kg/m^3) is shown in figure 3.2. The transducer assembly is shown in appendix 3, figure A3.3. The supporting electronics of the compressional wave system is described in section 3.8.
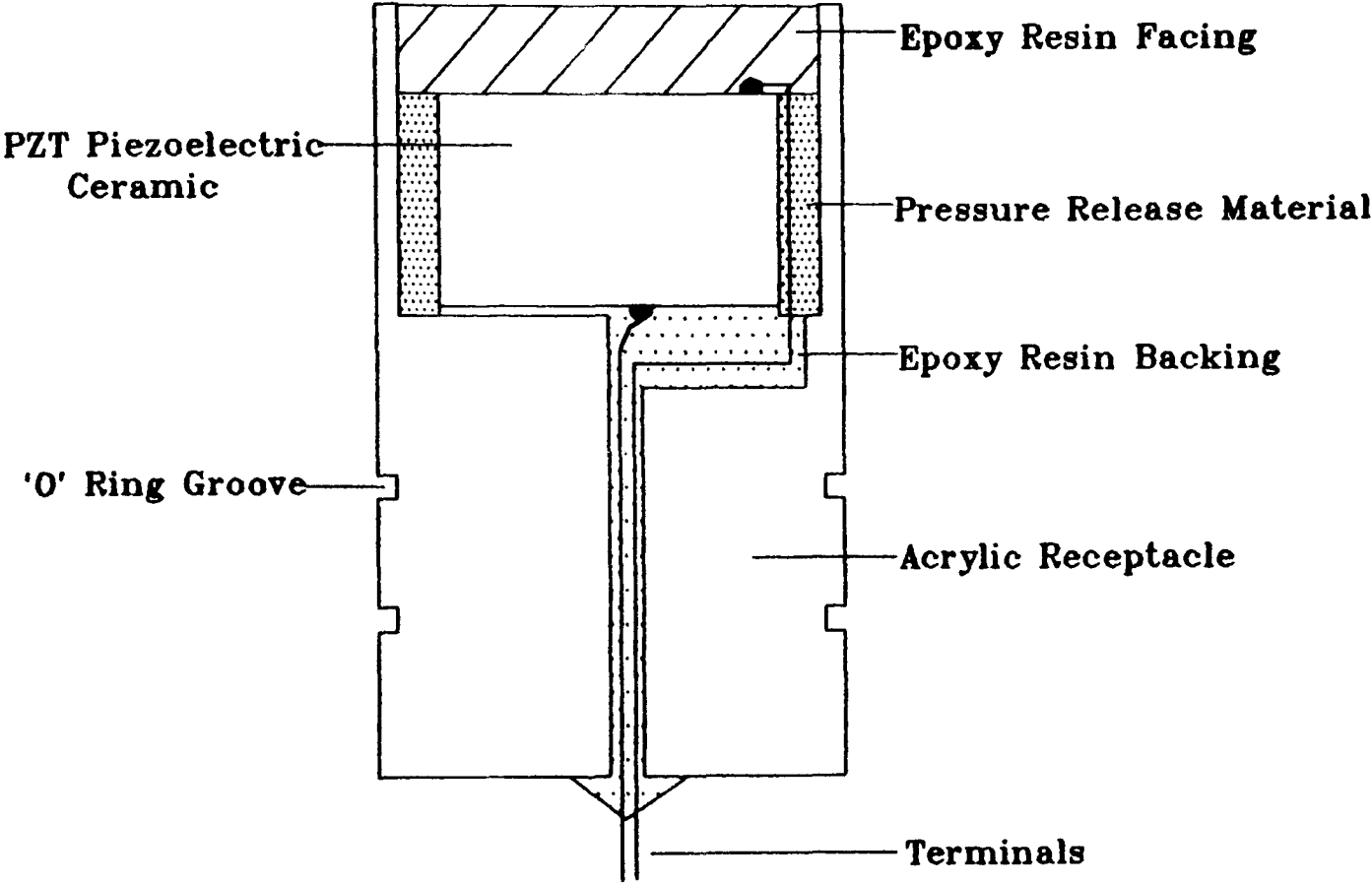
Figure 3.1   Compressional wave transducer construction.

Epoxy Resin Facing

PZT Piezoelectric Ceramic

Pressure Release Material

Epoxy Resin Backing

'O' Ring Groove

Acrylic Receptacle

Terminals

Graph [1]   250 mV/div   0.00 V   9.36 μs/div   48.00 μs

1:

Cursor X

V_x -16.1 mV
T_x 122.0 μs

V_0 0.00 V
T_0 69.40 μs

ΔV 16.1 mV
ΔT -52.60 μs
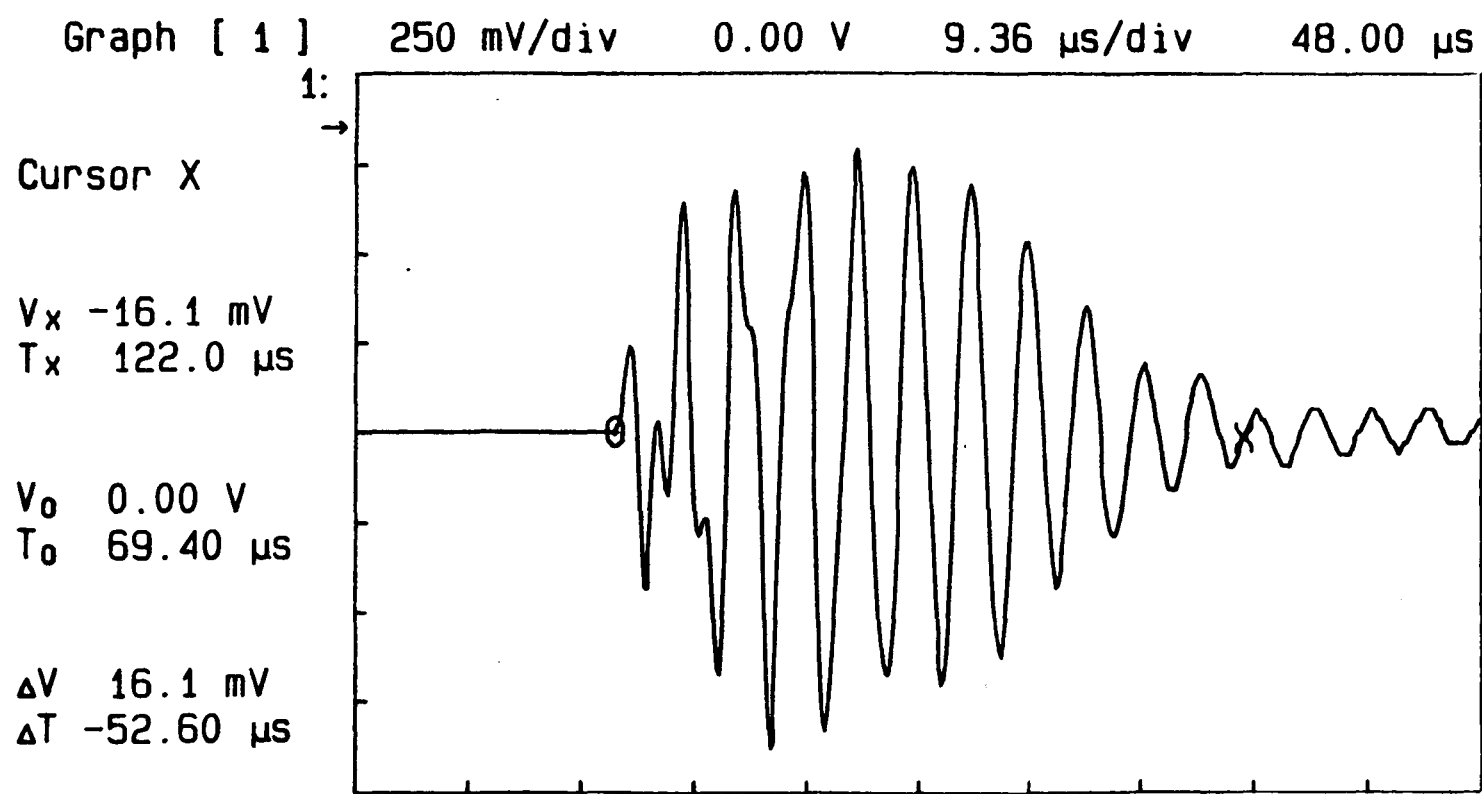
Figure 3.2   Typical signal from compressional wave transducer.

3.3.5 DETERMINATION OF THE COMPRESSIONAL WAVE TRANSDUCERS PERFORMANCE CRITERION.

In developing a new piece of geophysical laboratory apparatus it is important that some understanding of the performance criterion of those transducers incorporated in the apparatus be established. This holds considerable significance not only for the present studies but also for future design development. The performance of the basic piezoelectric element is greatly affected by its incorporation into the transducer housing. The extent of this effect must be measured if it is to be used as an analytical tool. To do this, electrical impedance (or its reciprocal, admittance) has to be measured. Although it is measured electrically, the impedance is a function of the mechanical and radiation characteristics of the transducer. The mechanical mass, compliance, and resistance, all appear as electrical impedances through the electromechanical coupling characteristic of the transducer. The density characteristic of the medium also appear as electrical impedances because of the effect on the vibrating component. Readers unfamiliar with the technique are referred to the standard texts of Kinsler and Frey (1962) and Bobber (1970).

An HP4192A LF Impedance Analyser was used in a series of experiments to determine the performance characteristics of the compressional wave logging transducers used in the settling column. The cabling between transducer and analyser was kept to an absolute minimum to reduce any stray capacitance. The transducers under test were type PZT/BMF/10P-4 (Vernitron catalogue reference), with the nominal frequency of the transducers quoted by the manufacturer being 500 kHz ± 7%. Having soldered the electrode wires onto the piezoelectric crystal the resonant frequency was found to be 468kHz. This is a difficult measurement to make owing to the number of spurious resonances created by transducer clamping difficulties and background noise, and is presented here purely as a qualitative illustration of effects on resonance, and not as a definitive result.

The analyser was swept through 300kHz to 700kHz at 1kHz steps giving 400 data points for each of the data sets. A typical data set from the suite of experiments is shown in figures 3.3 to 3.5. The transducer was made first to radiate in air and then into a load, in this case distilled water. Figure 3.3(a) shows how conductance of the transducer is affected by loading. Clearly loading affects the conductance of the transducer decreasing the amplitude and shifting the resonant frequency towards zero. A less marked shift in frequency was observed in the susceptance versus frequency data (figure 3.3(b)). However the peak-to-peak value of susceptance is again affected by the loading. The value of "blocked conductance" and "blocked susceptance" was determined above resonance at frequencies between 800 kHz and 3 MHz, see table 3.2 for results. It is the departure of conductance /susceptance from these blocked values that provides a measure of the motional admittance component of the transducer, and enables the investigator to determine the efficiency of the transducer.

In order to visualize the motional admittance of the transducer more clearly, the same data are presented as motional admittance circles, applying a correction for static capacitance before plotting (figure 3.4). The resonant efficiency of this transducer can be computed from the values of D_a, D_w and G_e measured from the figure. Using the relationship

$$\eta = \frac{D_w(D_a - D_w)}{D_a(D_w + G_e)} = \frac{0.424(0.469 - 0.424)}{0.469(0.424 + 0.050)} = 8.6\%$$

where from figure 3.4
$D_a = 0.469$ mS
$D_w = 0.424$ mS
$G_e = 0.050$ mS

All transducer efficiencies were found to be within 10% of this value. Such a low efficiency is due to the transducer design. A limited development budget meant that the transducer lacked any backing material, but was instead fixed to the acrylic back wall of the transducer mount. This, together with

Figure 3.3 The variation of (a) Conductance and (b) Susceptance with frequency as the transducer radiates in air and water.
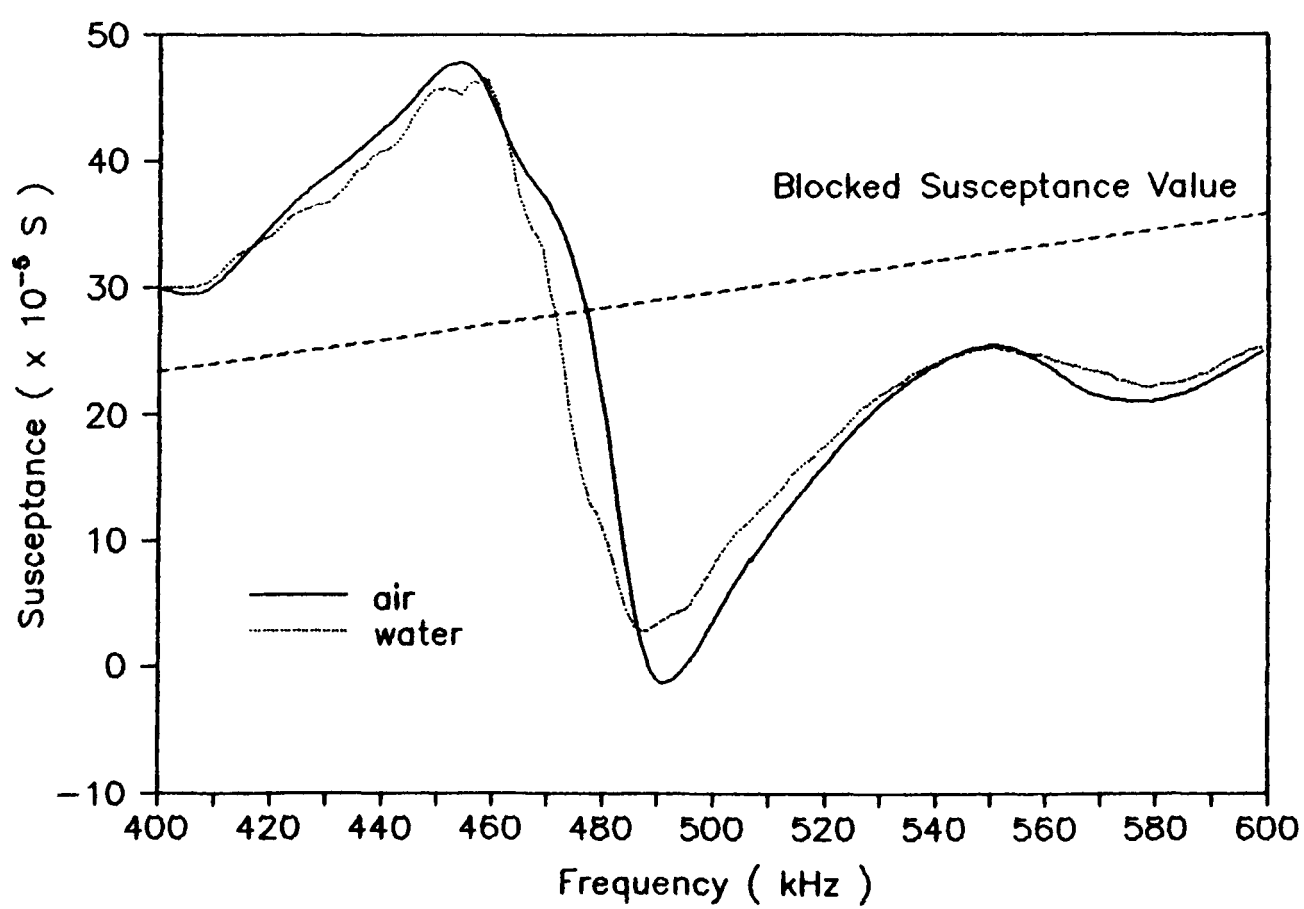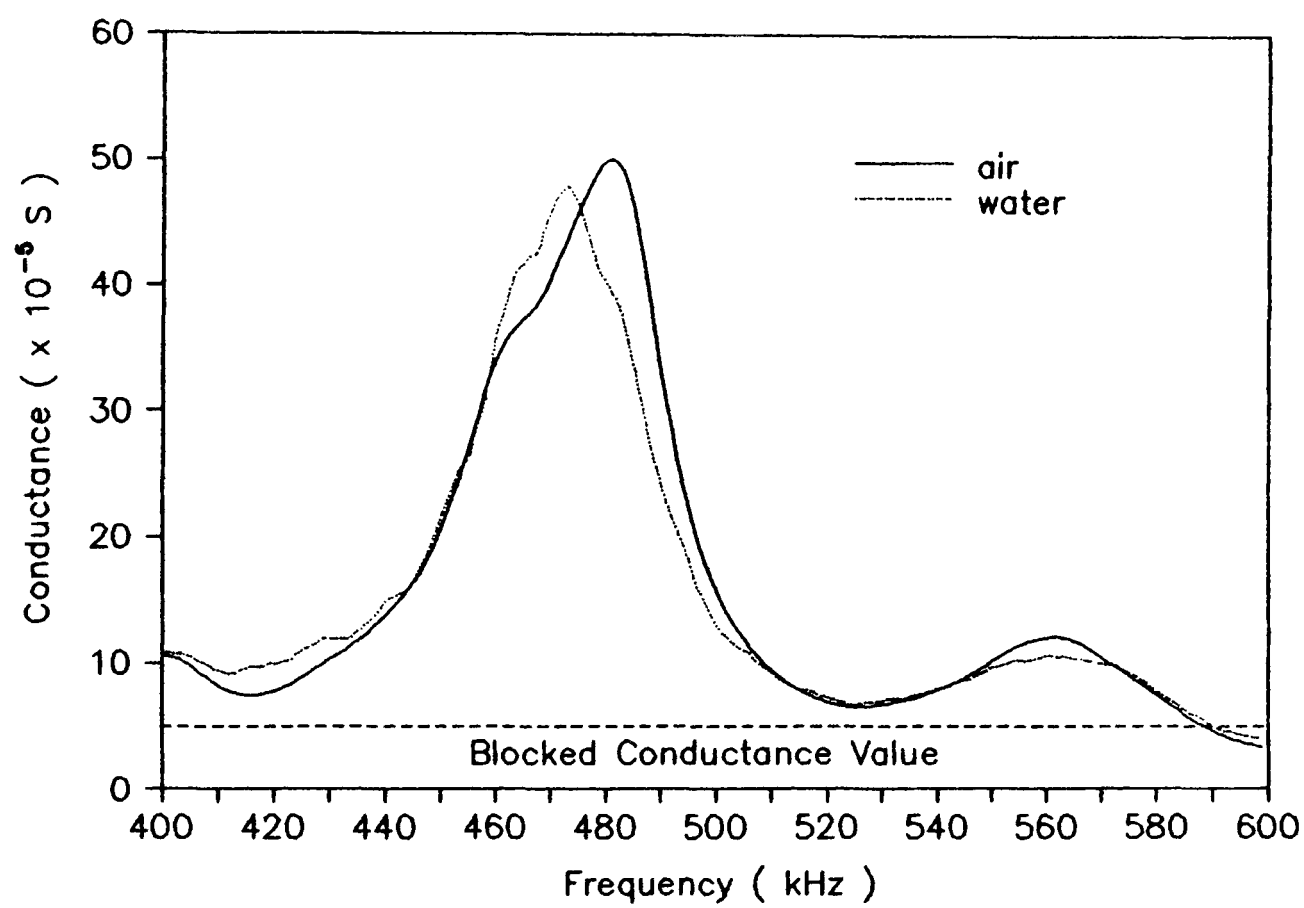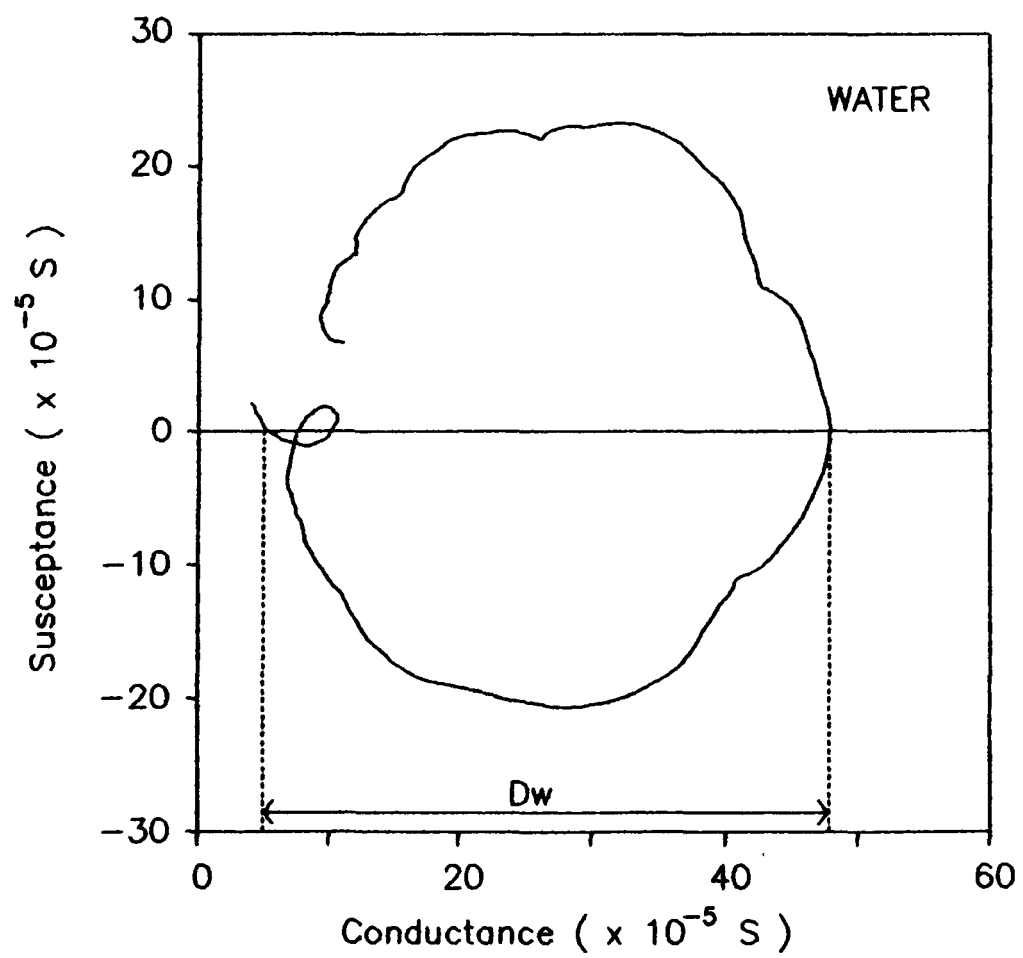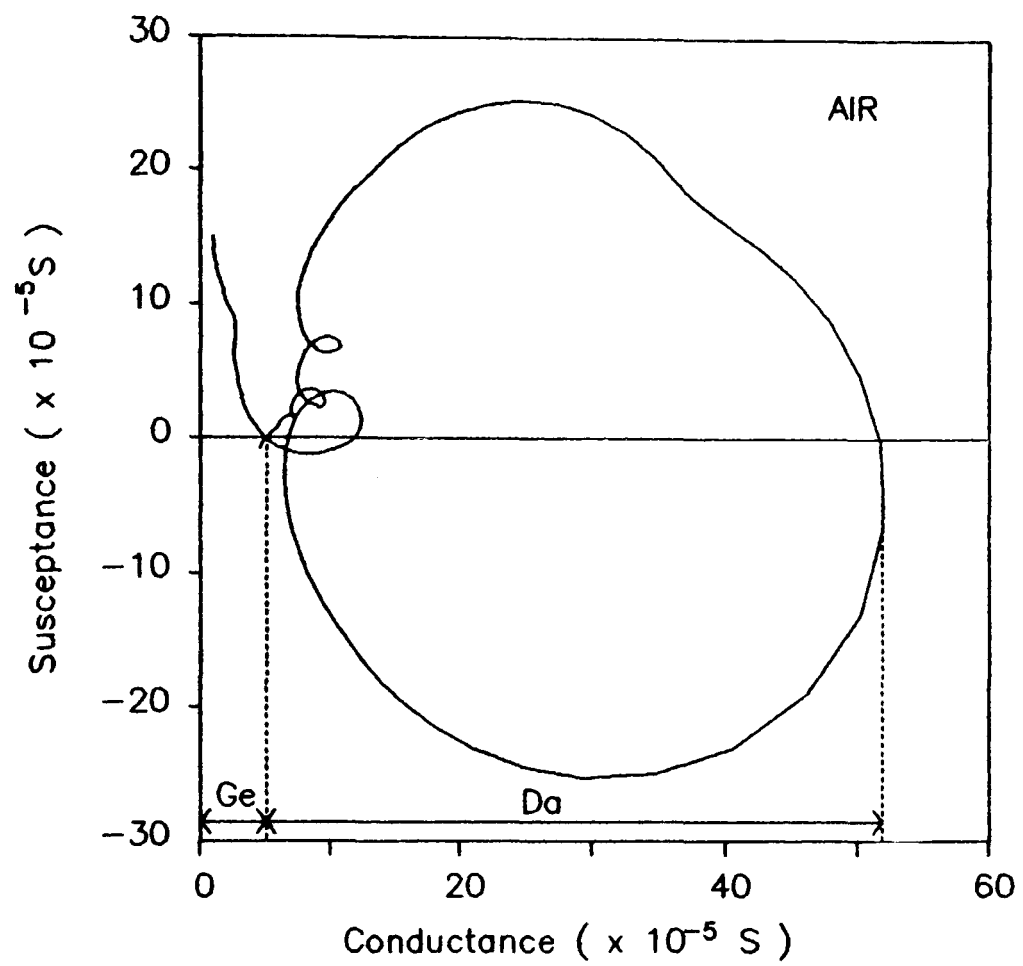
Figure 3.4 Motional admittance circles of a compressional
wave transducer in air and water.

Figure 3.5 Admittance versus frequency curve of the compressional wave transducer resonating in air.
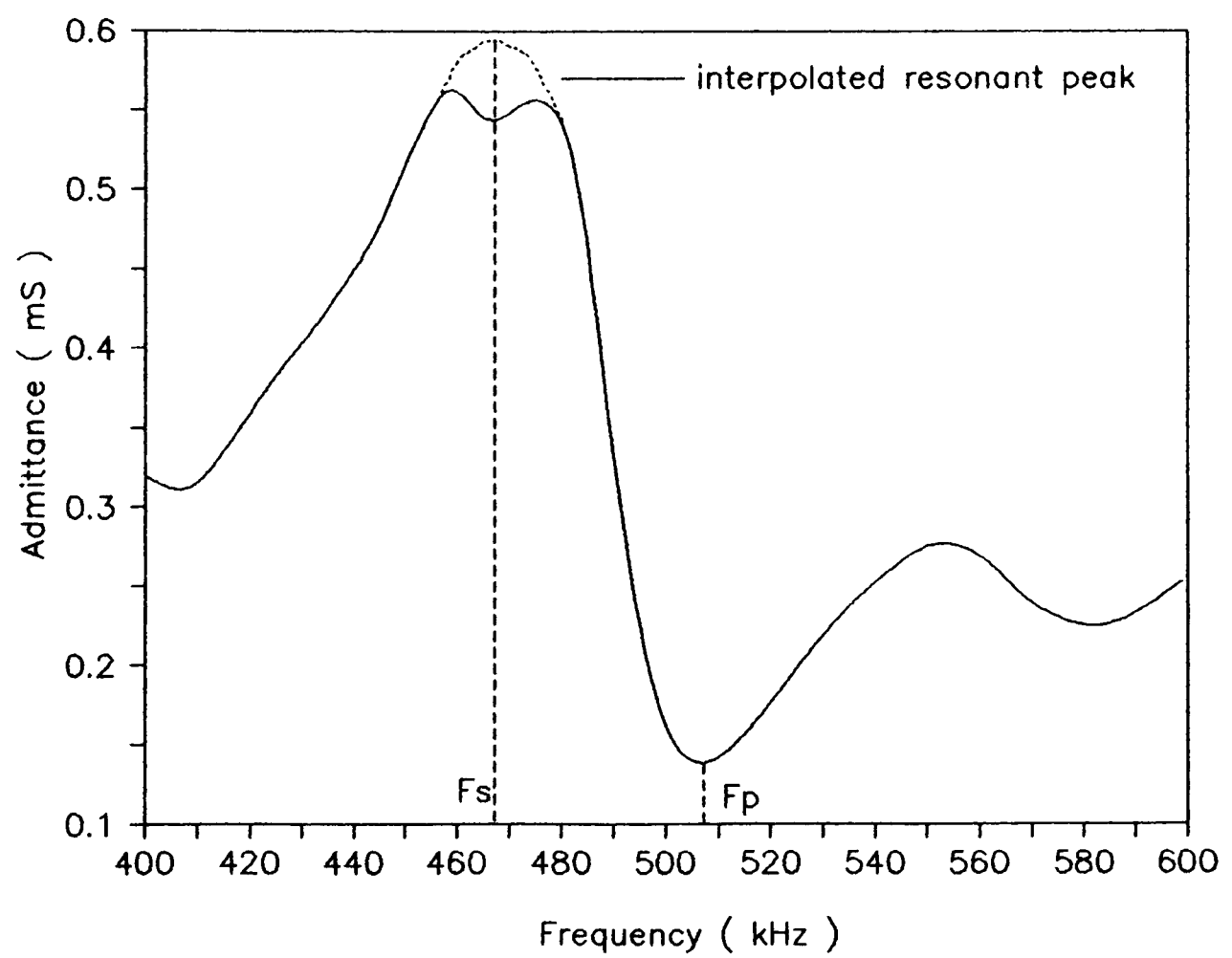
the epoxy resin front face made a somewhat less compliant transducer than had been desirable. In defence of the design itself, the transducer housing was based upon the tried and tested short travel path compressional wave transducers described by Schultheiss (1981). They do provide a cheap and effective transducer suitable for laboratory measurement.

Presenting the data in yet another format a study can be made of the resonance and anti-resonant behaviour of the transducer. The admittance versus frequency response of the transducer resonating in air (figure 3.5) shows that the maximum acoustic output for constant voltage is at a frequency of 467KHz, and anti-resonance occurs at 507kHz. These values can be used in turn to determine the coefficient of electromechanical coupling found here to be 0.180.

In addition to these standard tests, one of the transducers was made to resonate in a variety of sediments from clay/silt slurries to saturated sands. These materials did not, within the boundaries of experimental error, appreciably alter the resonant frequency of the transducer from that monitored in distilled water. A summary of the essential transducer characteristics is shown in table 3.2 illustrating the effect of potting upon the transducers performance characteristics.

Table 3.2 Compressional Wave Logging Transducers Performance
Characteristic Summary Table.

QUANTITY	VALUE	COMMENTS
Series Resonance(F_s)	500 kHz	manufacturers literature
	468 kHz	unpotted/resonating in air electrodes attached
	467 kHz	potted/resonating in air
	460 kHz	potted/resonating in water
Parallel Resonance(F_P)	484kHz	unpotted/resonating in air electrodes attached
	507 kHz	potted/resonating in air
	501 kHz	potted/resonating in water
Capacitance Ratio	0.179	
Coefficient of electromechanical coupling	0.180	
Efficiency	8.6 %	
Quality Factor	47	unpotted/resonating in air electrodes attached
	13	potted/resonating in air
	13	potted resonating in water

3.4 The Shear Wave Transducer.

3.4.1 INTRODUCTION.

For this study, shear wave velocity was to be measured and used as an important input parameter to the Biot model. In addition shear wave velocity, together with soil bulk density measurements, would be used to calculate the rigidity modulus of the soil, which is indicative of the development of the soil frame. At this point of the study scant evidence existed as to whether shear waves would propagate in such soft soils at all. It was realized that the shear wave transducer design would be of considerable importance in the tests to establish if such soils could sustain transverse wave motion. The considerations and investigations made into a suitable transducer design are addressed in the following sections.

3.4.2 DESIGN CONSIDERATIONS.

Three design criteria had to be fulfilled by the shear wave transducers:

(1) The shear wave transducers should be capable of generating and detecting a shearing motion within the soft soil medium.

(2) The received signal should be of such quality that either its signature and, preferably, the initial onset could be clearly identified in order that the travel time measurements could be performed.

(3) The shear wave transducers should not interfere, as far as practically possible, with the settling process occurring within the column.

The characteristics of the soft soil with respect to shear wave propagation would make these requirements difficult to

achieve because of the following:

(1) The propagation of shear waves is dependent upon the existence of a rigid soil frame. The weak frame that is likely to exist in such a newly developed soil will highly attenuate the propagating wave (Shirley and Hampton 1978). Any effort to increase the shear wave transducer output is likely to destroy this weak structure. In order to observe and successfully interpret the received wave, to obtain a representative shear wave velocity, it is likely that some degree of signal enhancement or processing would be required.

(2) Additional complications arise by virtue of the fact that a shear wave transducer invariably generates a compressional wave in both the sediment and the transducers supporting structure, i.e. in this case the column. As these compressional waves form a significant contribution to the received signal an effort must be made by the designer to clearly separate these compressional components from the required shear wave.

(3) Attenuation of the shear wave energy increases rapidly with increasing frequency though a higher frequency signal is more desirable since it can be more often easily identified as a high frequency wavelet on low frequency background noise. The frequency of a shear wave transducer is a function of its geometry and its stiffness and a compromise of these design propagation characteristics must be reached. While the attenuation of the shear wave signal may be minimized by reducing the travel path, reducing the travel path may result in compressional frame wave interference, or interference with the soil settlement process, or even interference with the X-rays used to determine soil bulk density. Attention must therefore be given to these matters during the design stage of the instrumented settling column.

(4) A soft soil has a very high compliance. Shirley and Hampton's data (1978) indicate a shear modulus as low as 5.5×10^3 Pa may be expected in soft soils. The transducer output can be optimized by matching the transducer stiffness to that of the sediments.

3.4.3 SHEAR WAVE TRANSDUCERS.

A suitable shear wave transducer for use in soft soils appeared to be the bender element. Developed and described by Shirley and Hampton (1978), these transducers comprise of two lead zirconate titanate (PZT4) transverse expander plates bonded together such that when a driving voltage is applied to the element, one plate elongates and the other contracts. The net result is a bending displacement which far exceeds the length change in either plate (figure 3.6). By operating the bender element in cantilever mode (that is clamped at one end whilst the other end is free to vibrate) one end of the transducer can be inserted into the sediment sample causing minimum of disturbance to the soil fabric. In this mode of operation the radiating area of the transducer is increased which improves the coupling of the transducer and hence amplitude of the shear waves generated into the sediment.

The bender element may be energized by using the leading edge of a low voltage square wave in a pulse excitation fashion. On energizing the bender element a small strain amplitude shear wave is generated in the soil and propagates at right angles to the soil particle motion (figure 3.6). The transit time for these shear waves to travel a known path length yields the shear wave velocity in the sediment.

The bender element characteristics come close to the shear wave transducer requirements outlined in the previous section. Such transducers are used in a number of geotechnical laboratories for the investigation of shear wave propagation in marine sediments. Typically, these sediments are much stiffer than the soft soils to be investigated in this

Direction of element tip and
soil particle movement

Direction of
shear wave
propagation

Soil specimen
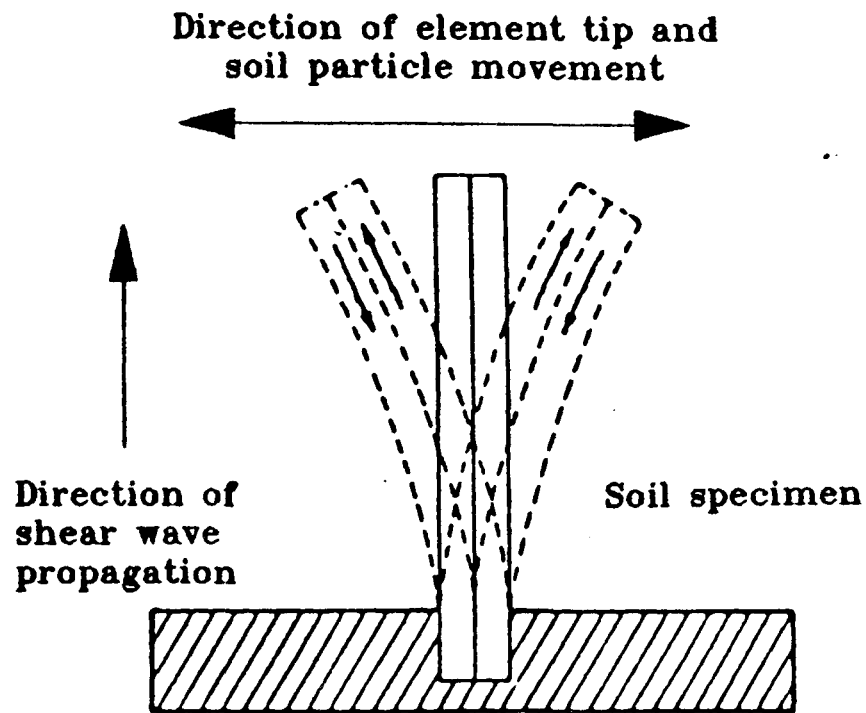
Figure 3.6 A bender element in use as a
shear wave transducer.

1 55 1

Bender
Element

Epoxy Resin
Encapsulation

1

200

60

Epoxy Resin
&
Acrylic Mount

0.75
0.48
0.75

155
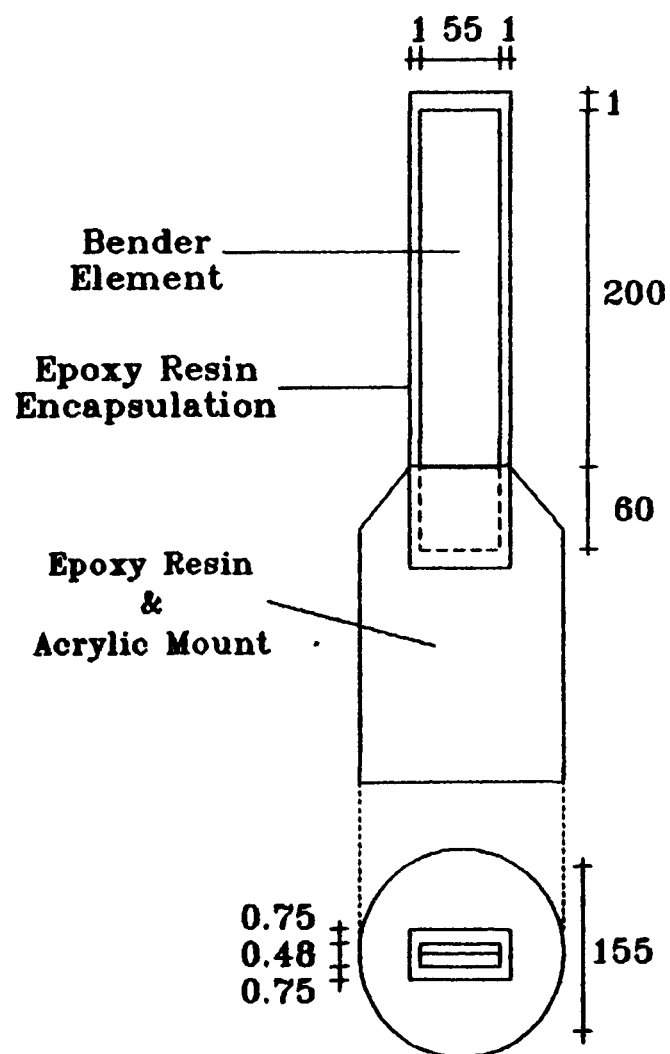
(All dimensions in millimetres).

Figure 3.7 Transducer encapsulation.

research. Thus, to fully understand the propagation
characteristics in soft soils some information would be
required on the performance characteristics of the bender
element in such a medium.

3.4.4 SHEAR WAVE TRANSDUCER PERFORMANCE CHARACTERISTICS.

Theoretical Prediction of the Bender Elements Frequency
 Response.

Using the equations and specifications quoted for PZT(4), type
5BN series bender element materials (Vernitron Bulletin
66012/D) a number of preliminary calculations were performed
to establish the suitable dimensions of an element for use in
soft soils. To determine the resonant frequency of an element
vibrating in cantilever mode, the following equation was used

$$\text{Resonant Frequency} = \frac{1}{2\pi\sqrt{(M_e \ C_m)}}$$

where
M_e= Effective Mass = $3.0 \times 10^{-2} \times L \times W \times D$ (kg)
C_m= Mechanical Compliance = $(3.2 \times 10^{-9} \times L^3)/(W \times D^3)$ (m/N)

     L = Bender elements length in inches.
     W = Bender elements width in inches.
     D = Bender elements thickness in inches.

For a bender element of dimensions 2.00cm x 0.55cm x 0.048cm,
a resonant frequency of 477 Hz is predicted.

By encapsulating the bender element in a material to improve
the transducers robustness and insulation qualities, one
expects the compliance of the transducer to be lowered and as
a consequence the resonant frequency to be increased.
Schultheiss (1983), in an attempt to quantify the increase in
frequency due to encapsulation, used a "self monitoring"
technique (Section 3.4.5). His results indicated that the
resonant frequency was likely to increase by 85%. Thus by

encapsulating the above bender element (resonant frequency 477Hz) in epoxy resin in the manner of Schultheiss (1983), the process would have the effect of increasing the resonant frequency of the transducer to nearly 900 Hz. As Shirley and Bell (1978) showed that at frequencies between 600 Hz and 1.5 KHz there was no evidence of dispersion in shear waves propagating in clays and silts, it was concluded that such a transducer would be suitable for applications in soft soil research.

3.4.5 BENDER ELEMENT FREQUENCY RESPONSE: EXPERIMENTAL WORK.

In order to physically measure the effect of encapsulation (or potting) upon frequency response of a bender element, a number of identical elements were cut from a sheet of PZT 5BN type piezoelectric material, to the dimensions of 2.60cm x 0.55cm x 0.048cm using a diamond edge cutting wheel. Having soldered terminal connection wires to the bender elements, half were mounted as unencapsulated elements, the other half were potted and then mounted as shown in figure 3.7.

(a) Impedance Analysis Experiment.

A Hewlett Packard HP4192A LF Impedance Analyser was used to investigate the frequency response of the above bender elements. The analyser was swept through a frequency range of 100Hz to 3kHz and the response of the benders monitored. The results of this experiment proved disappointing. Instead of a single clear resonant response frequency, as had been expected, the response showed a multitude of low amplitude resonances. Repeating the experiment with different clamping arrangements failed to change the response significantly. The reason for the failure of this procedure to yield satisfactory results still remains unclear.

(b) Self Monitoring Technique.

The self monitoring technique of investigating the frequency response of a bender element is described by Schultheiss

PLAN VIEW   CROSS SECTION

Active
Electrodes

1.6 mm

Piezoelectric
plates cut to
isolate central
section

Bottom plate
electrode

Top plate
electrode

Insulation between
Piezoelectric plates

Monitoring
Electrode
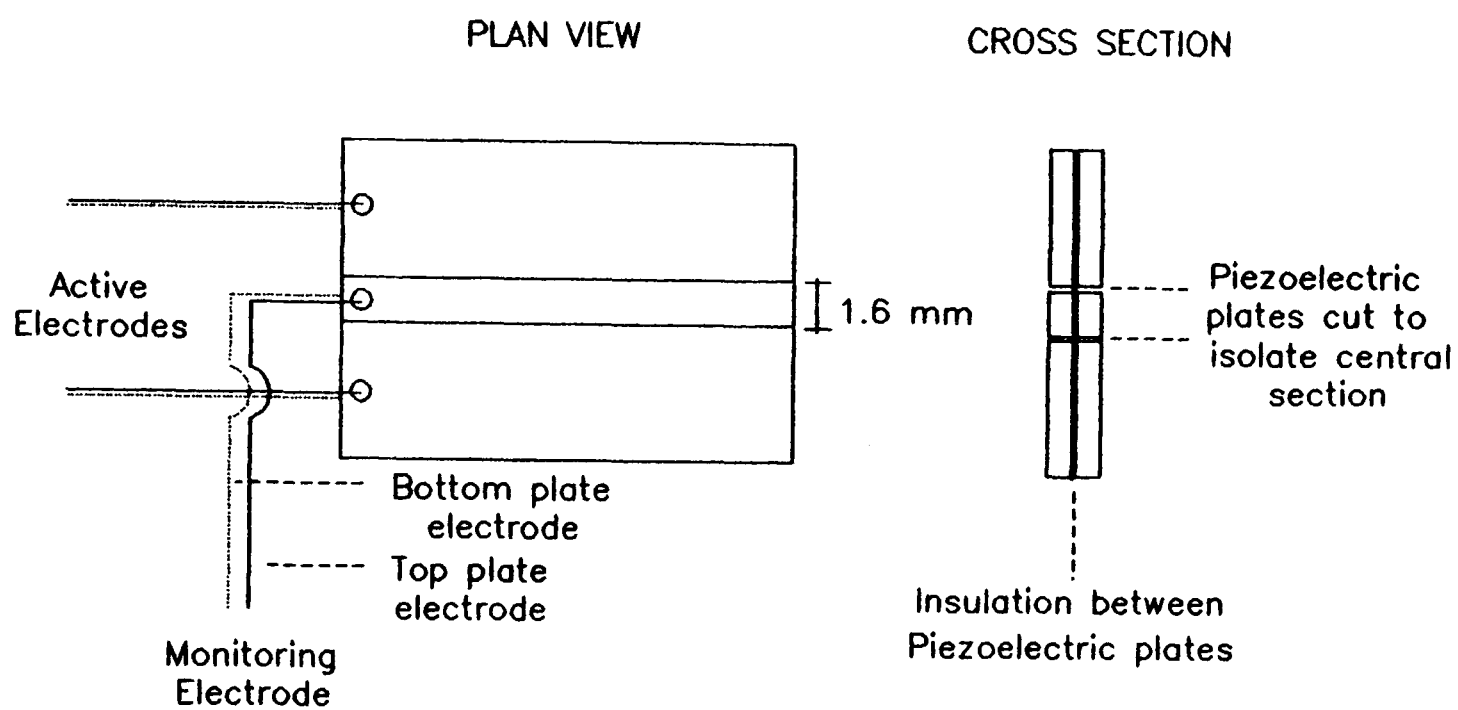
Figure 3.8 The self monitoring bender element.

Figure 3.9 The self monitoring bender element response
to pulse excitation.

GRAPH 1:

GRAPH 2:

Time (microseconds)
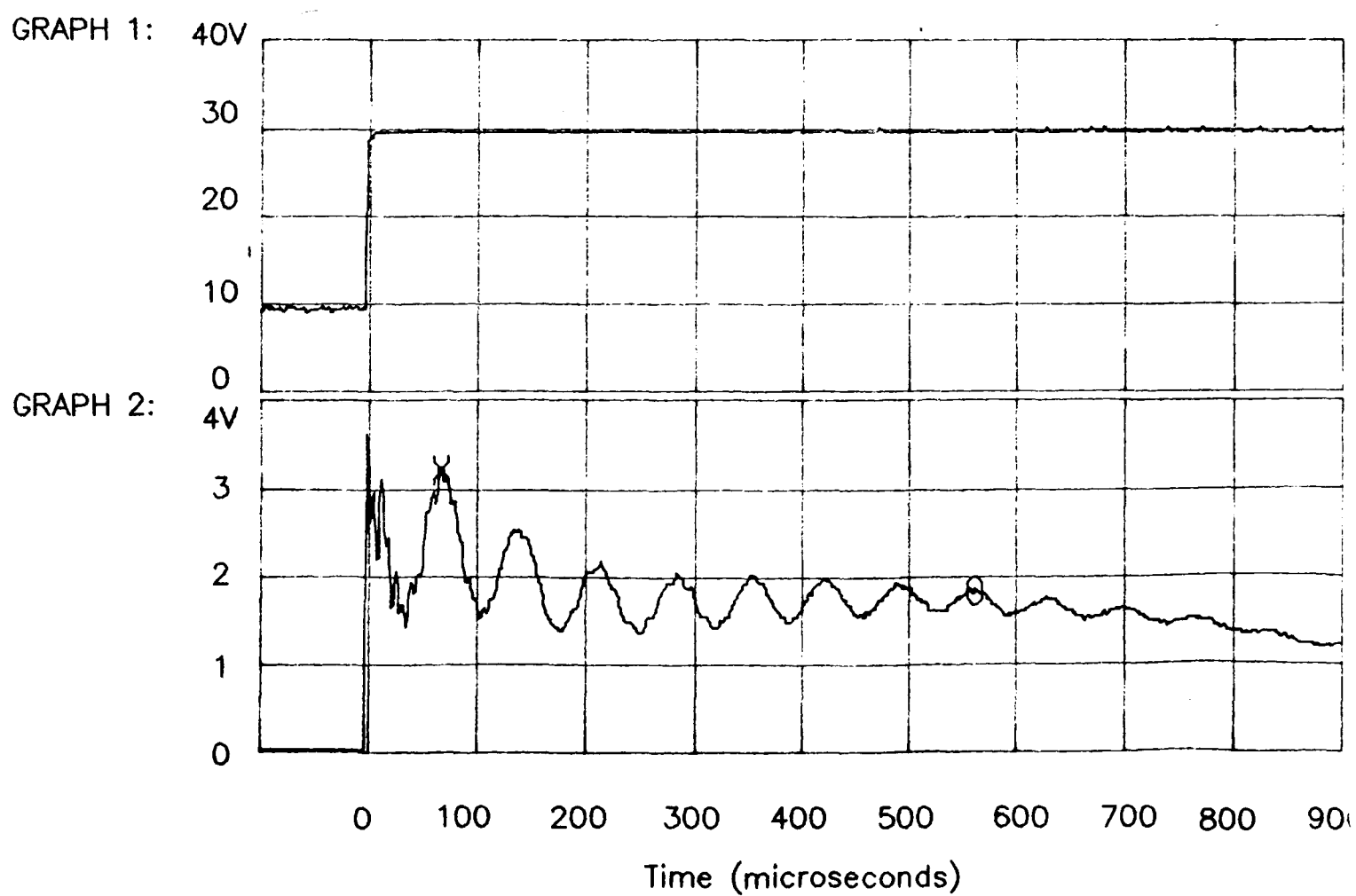
(1983). In brief, the technique requires that a central
sector of the bender element be electrically isolated from the
main element such that it is able to act as a passive monitor
of the transducers frequency response (figure 3.8). Having
completed the "self monitoring" modifications to the bender
element it has to be mounted in an acrylic housing such that
when clamped the element resonates in cantilever mode.

Figure 3.9 shows the response of an unpotted transducer. The
upper figure (graph 1) shows the 20 Volt square wave which was
used to drive the active electrodes in a pulsed fashion. The
lower figure (graph 2) shows the output from the monitoring
electrode, demonstrating that the element resonates at
14.1kHz. Clearly this resonance is at a far higher frequency
than the 477Hz that had been predicted. It is thought that the
modifications made to the bender element, induce a highly
complex resonant behaviour and therefore this self monitoring
technique is not suitable for studying the frequency response
of such small bender elements.

(c) Measurement of the Bender Elements Frequency Response
    using a displacement Sensor.

Two identical bender elements of dimensions 2.00cm x 0.55cm x
0.048cm, were set up to resonate in cantilever mode as shown
in figure 3.10. A Kaman type KD2310 displacement transducer
(utilizing the eddy current sensing principle) was used to
sense the vibration response of the bender elements as they
were driven through a range of frequencies from 100Hz to
1.4kHz. The displacement sensor was calibrated using a Kaman
micrometer gauge. The frequency responses of both the unpotted
and potted bender elements are shown in figure 3.11 (a) and
(b).

The following observations can be made from figure 3.11. The
unpotted transducer has a resonant frequency of 494Hz ± 1Hz
(figure 3.11(a)) which agrees well with the predicted
frequency of 477Hz (section 3.4.4). The result of potting the
bender element in epoxy resin causes the resonant frequency to

52

Figure 3.10 Apparatus for measuring the frequency
response of a bender element.

FUNCTION
GENERATOR

10V pk-pk

POWER
AMPLIFIER

FREQUENCY
COUNTER

DISPLACEMENT
SENSOR

BENDER
ELEMENT

CLAMP

ATTENUATOR

SCOPE

DVM
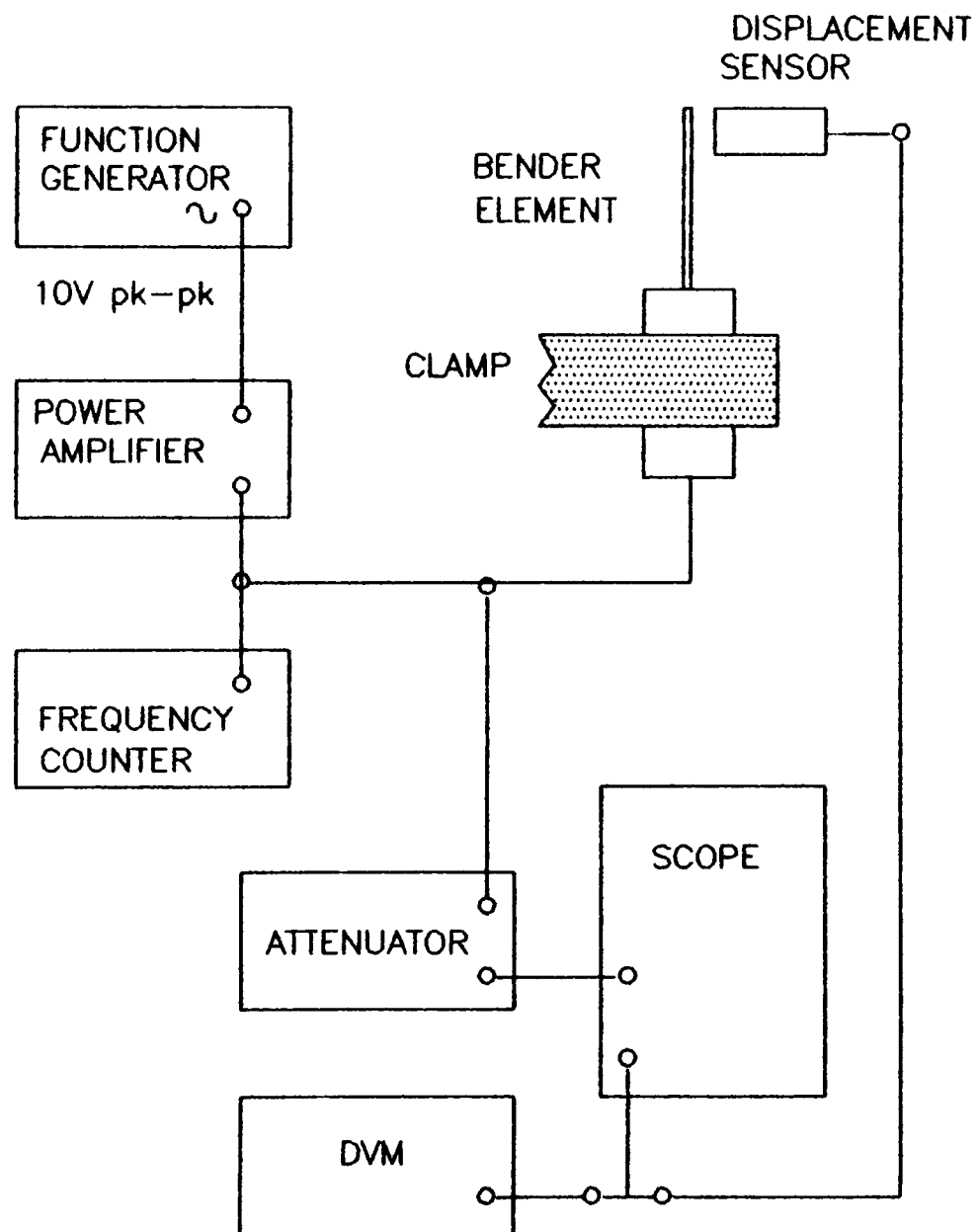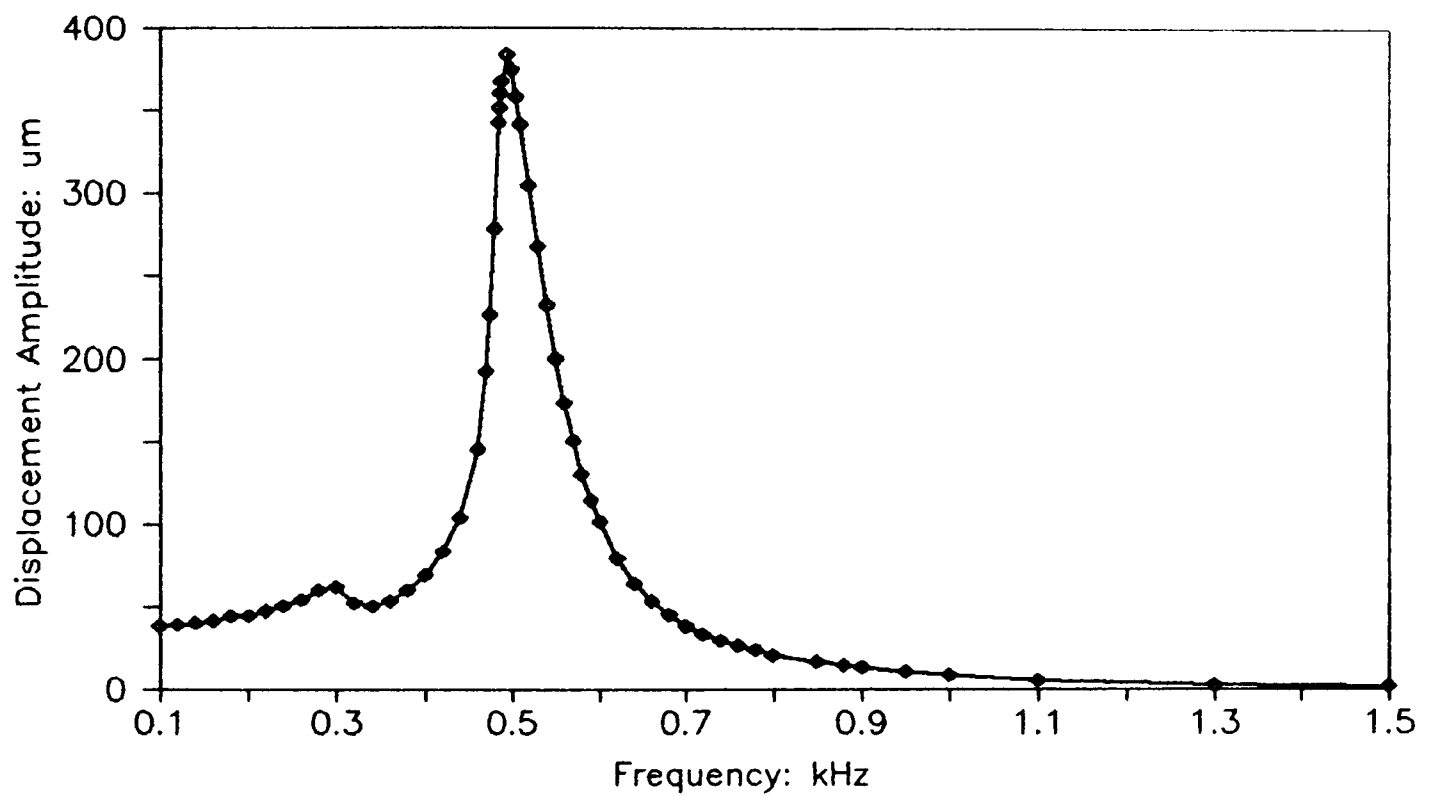
Figure 3.11(a) Frequency response of an unpotted bender element resonating in cantilever mode.
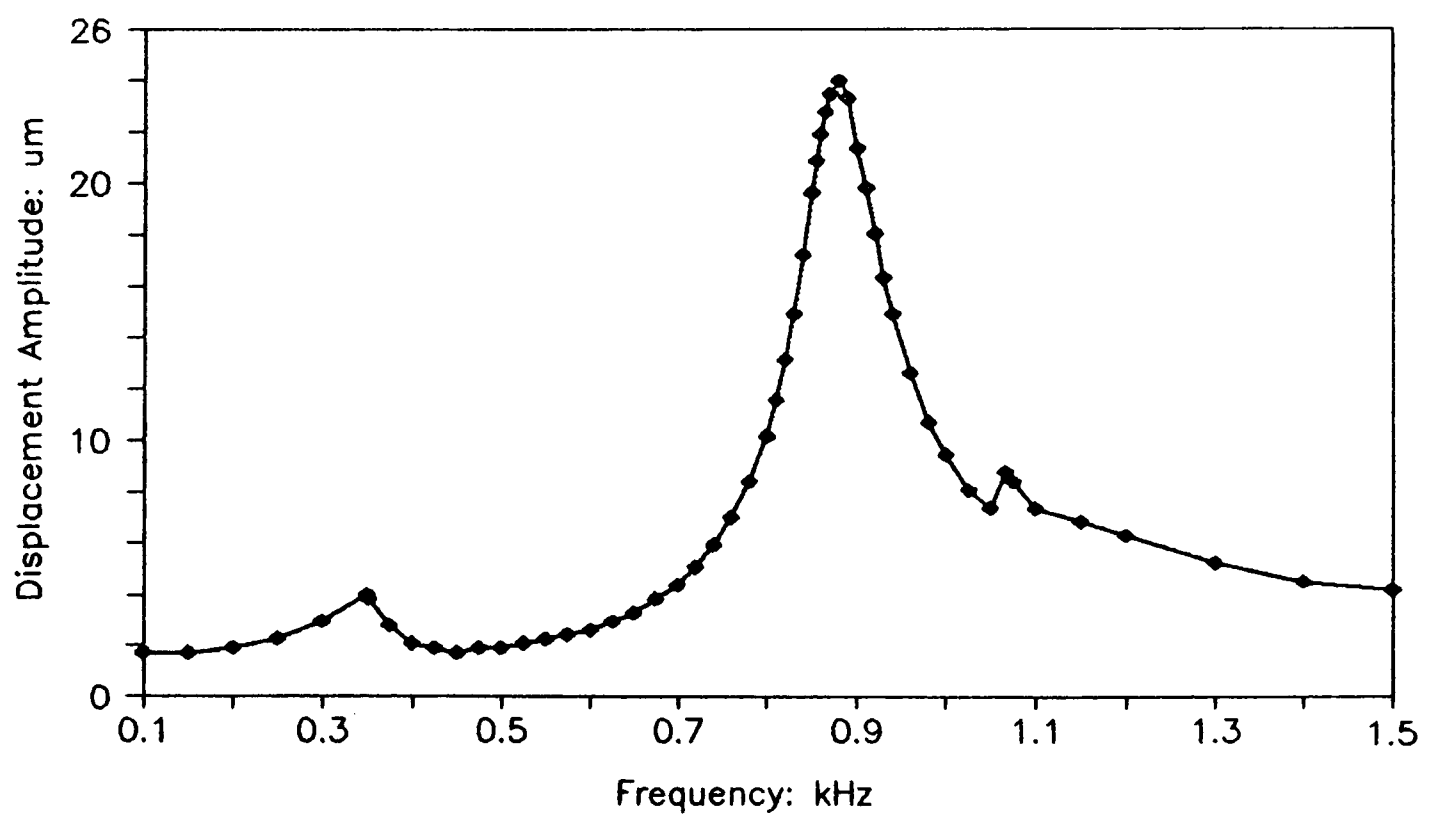
Figure 3.11(b) Frequency response of a potted bender element resonating in cantilever mode.

increase to 880Hz ± 3Hz (figure 3.11(b)). The effect of potting upon the amplitude of vibration is quite drastic; reducing an unpotted element's amplitude of vibration at resonance of 384μm to 24μm in the encapsulated transducer. This does not pose a problem within the experiment at hand, since a low amplitude of vibration is desirable in order to meet the criterion of the Biot model (Stoll 1980). The subsidiary peaks observed in the figure 3.11 are believed to be due to resonances in the clamping structure rather than modes of vibration in the bender element.

3.4.6 THE PROBLEM OF THE FRAME GENERATED WAVE.

As stated in section 3.4.2, shear wave transducers invariably generate compressional waves in both the sediment and the supporting structure in this case the perspex column). The likelihood of these "frame waves" travelling around the column walls and interfering with the shear wave signal had to be assessed before an interpretation of soil properties could be attempted. This was done by measuring the P and S-wave velocities in the perspex material. This allowed the travel times of the frame waves around the column to be calculated:

Table 3.3 Frame Wave Travel Times.

Compressional wave velocity in perspex	= 2456 m/s
Shear wave velocity in perspex	= 1440 m/s
Column circumference	= 0.314m
Compressional Frame Wave travel time	= 0.13ms
Shear Frame Wave travel time	= 0.22ms

Table 3.4. Predicted Shear Wave Travel Time

Shear wave velocity in kaolinite[*]	= 30 m/s
Travel path between bimorphs	= 0.07m
Bimorph generated Compressional Wave travel time	= 2.1ms

* maximum shear wave value in kaolinite Shirley and Hampton 1978.

From the above it is clear that, providing the shear wave transducer is suitably damped to prevent "ringing", the interference of frame and direct waves should not prove a problem.

3.4.7 BENDER ELEMENT INSULATION QUALITY CONTROL TESTS.

During preliminary experimentation upon bender shear wave transducers a practical problem was identified. In the literature a similar problem referred to as "electronic pickup" was described by Hurley (1989) and was characterized by a voltage spike at time zero which decays slowly with time. This pickup was found to be caused by poor electrical insulation surrounding the bender element, probably originating from poor potting procedures. The potting procedure requires the use of a mould into which deaired liquid epoxy resin is poured. The bender element is subsequently placed into the mould. The element often has a tendency to twist or fall during solidification of the epoxy resin thereby causing resin insulation thinning on parts of the transducer. Thus a simple continuity test was devised to examine the insulation qualities of the transducer. Using the arrangement shown in figure 3.12 the continuity between electrode and electrolyte can be examined. A resistance of >20MΩ between electrode and electrolyte was found to be desirable. For resistances lower than this value a transducer should be discarded or else have its epoxy resin insulator patched before retesting.

In order to meet this criterion a new mould was designed, (see figure 3.13). The small "spacers" at the side of the mould are designed to prevent the bender element from twisting or falling during the potting process, thereby preventing the bender from breaking through the insulation. The holes left in the insulation by the spacers are filled at a later stage with epoxy resin. Performing the potting procedure in this manner
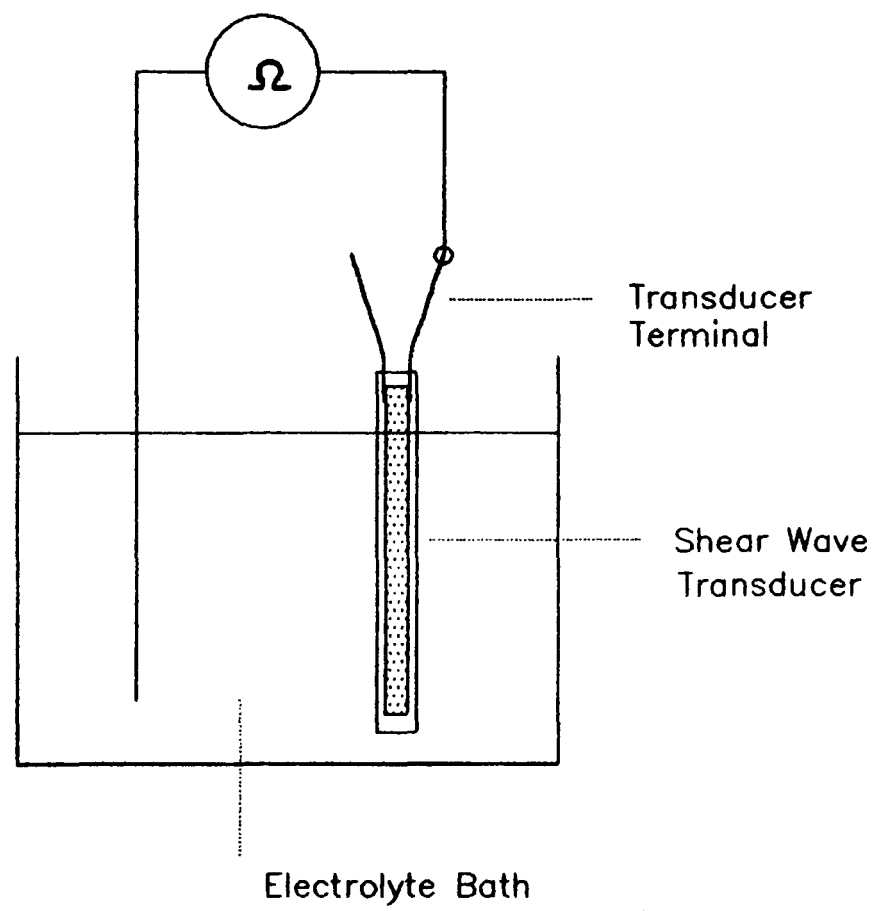
Figure 3.12 Shear wave transducer insulation test setup.

Figure 3.13 Showing design of bender element mould.

SIDE VIEW

SECTION THROUGH A-A

72 mm

A

A

<- 28 mm->

A.B.S. spacers

screw holes

A

A

perspex central divider

PLAN VIEW

<----- 110 mm ----->
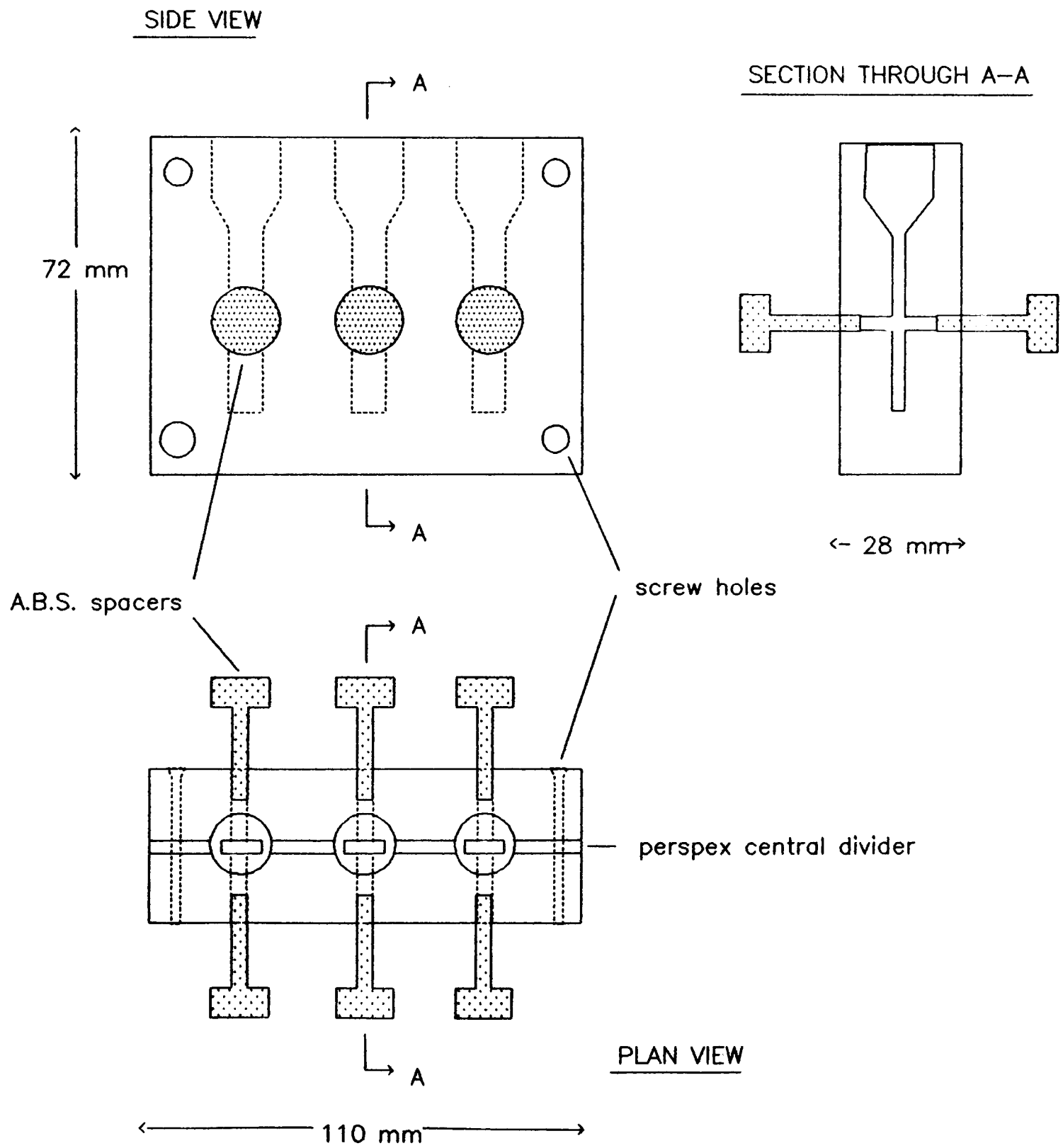
ensured an almost 100% pass rate of the insulation test, and ensured that no "electronic pickup" corrupted the shear wave signal.

3.4.8 SHEAR WAVE TRANSDUCER CONSTRUCTION.

Having established suitable dimensions of the bender element based on frequency requirements, it became evident that the transducers, owing to their length, would influence the settling behaviour of the sediment and possibly also interfere with the X-ray bulk density measurements. The bender elements clearly could not therefore remain permanently mounted in the column wall but instead would need to be mobile i.e. be able to be pushed into the soil during shear wave velocity measurement and extracted for the remainder of the time. Considerable experimentation was performed in order to arrive at the final deign shown in figure 3.14. The bender elements dimensions are 20.4mm x 5.5mm x 0.5mm encapsulated in epoxy resin, before being mounted in an acrylic housing. The element housing makes a sliding "O" ring sealed fit with the transducer port walls. When in position, the bender element protrudes 1.5cm into the sediment and vibrates in the horizontal shear mode. The transducer remains isolated from the sediment by means of a strong flexible membrane. Tests showed that this membrane reduces the shear wave amplitude by as much as 7%, while not affecting the shear wave velocity in anyway. A typical shear waveform using these transducers transmitting into soft soil is shown in figure (3.15). The supporting shear wave instrumentation is described in section 3.8.
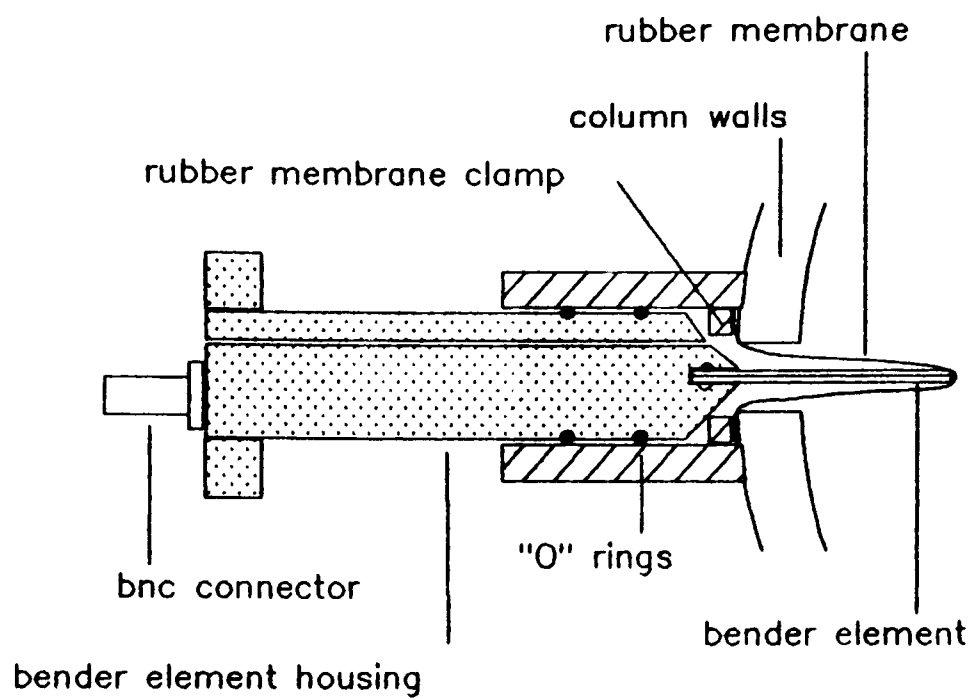
Figure 3.14 Shear wave transducer construction.

Figure 3.15 Typical shear wave signal from the seismo—acoustic logger.
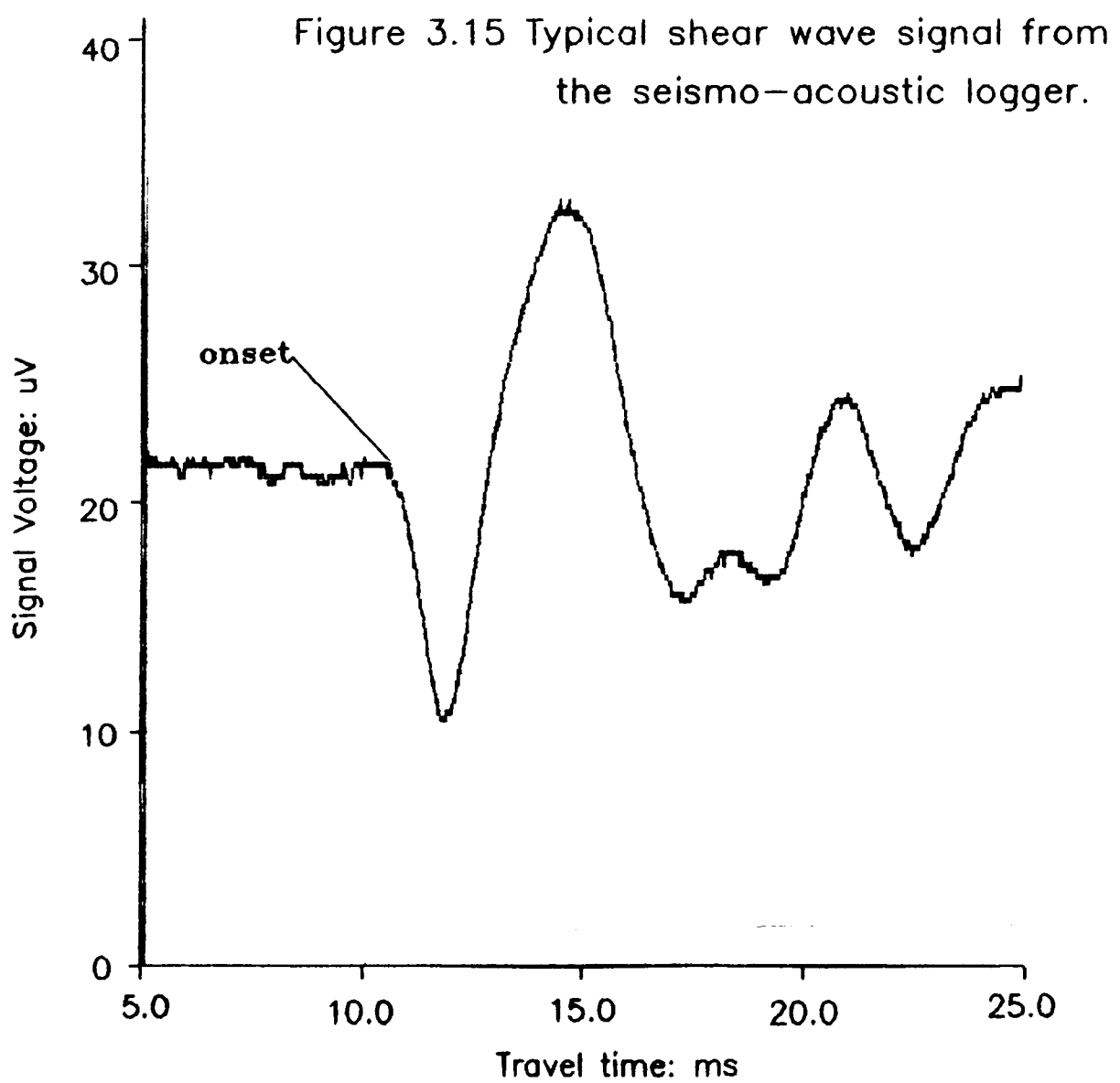
3.5 The Instrumented Settling Column.

Having completed the instrumentation development experiments using the prototype column the fully instrumented sedimentation column was designed and built according to the specifications outlined in figure 3.16. The column comprises two sections. The upper section is machined from a single piece of acrylic to the dimensions of 0.99m in length, 0.1m inner diameter and 10mm wall thickness, to an accuracy of ±0.1mm. The flanges at the ends of the column are understood to reduce curvature of the acrylic column during the engineering process.

Set in the walls are portals in which the seismo-acoustic transducers, pore pressure outlets and soil resistance electrodes were finally installed. Sections A-A and B-B of figure 3.16 show the relative positions of the compressional wave transducers, (P-port) and shear wave transducer, (S-port). In all there are 15 pairs of P-ports and 15 pairs of S-ports having, alternate orientation up the column as shown, and a vertical separation of 5cm. The 20mm diameter holes positioned at $45°$ to the P and S ports represent the location of the pore pressure outlet ports. These number 15 in total, spaced at 5cm intervals up the column wall. An additional pore pressure outlet is located in the column base. The cross section C-C shows the 0.5mm recesses spaced at 5cm vertical intervals up the column and into which 5 stainless steel electrode rings are placed. The upper 4 electrodes are for soil resistance measurements, the lower electrode being used for grounding purposes only.

The column base consists of a 200mm diameter acrylic disc which is screwed up against an "O" ring making a water tight seal. The base plate central recess was for the incorporation of a large 500 kHz compressional wave transducer which was intended to be used to monitor P-wave velocity vertically through the sediment. In such experiments a matching transducer was clamped at the top of the column. The entire
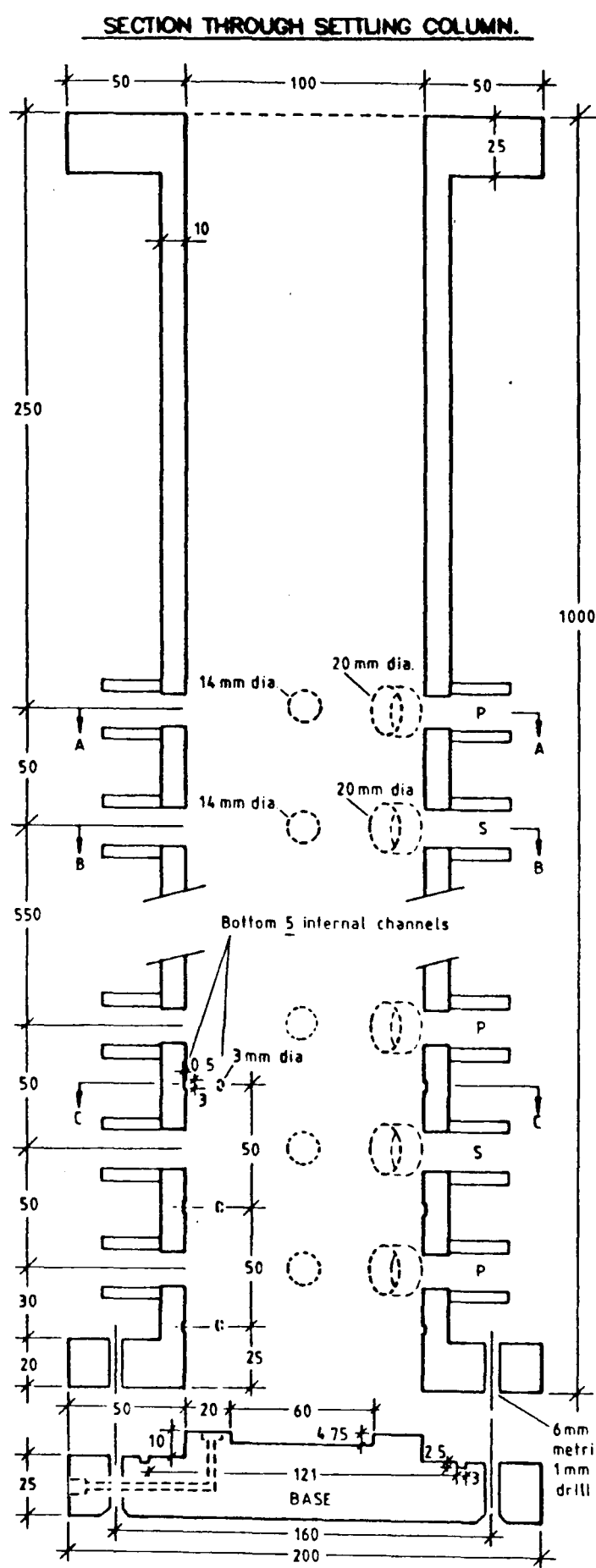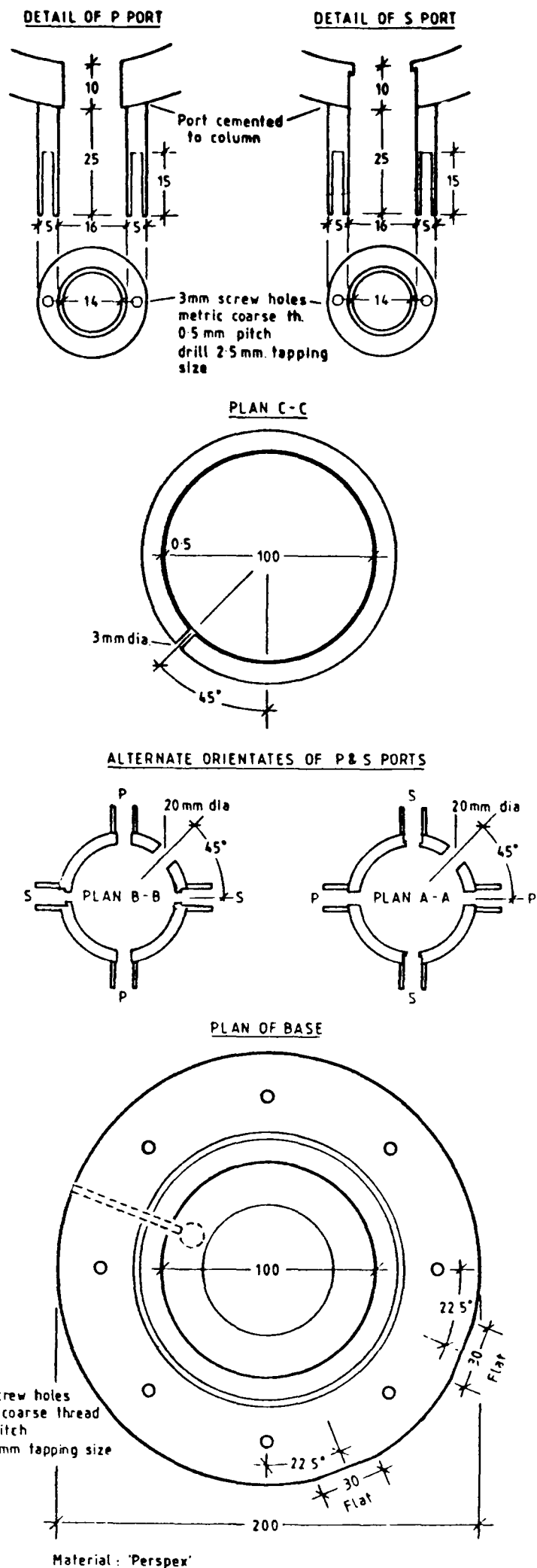
Figure 3.16 The Instrumented Settling Column.

column was placed on a rotating base which could be fixed to the vertical stanchions at the Oxford X-ray laboratory.

The instrumented sedimentation column enabled the measurement of compressional and shear wave velocities, soil electrical resistivity, pore pressure and, when used in conjunction with the Oxford laboratory X-ray apparatus, soil bulk density.

3.6   Soil Bulk Density Measurement: The X-Ray Apparatus.

Soil Bulk density was determined non-destructively by measuring the degree of X-ray attenuation in the soil sample. The X-ray apparatus used in the experiments documented here was that of the Department of Engineering, University of Oxford. The apparatus was developed by Been (1980) and modified by Elder (1985). Apart from modification to the data logging capabilities, the system used here was as described by Elder. The essential features of the system are shown in the schematic, (figure 3.17).

The X-ray tube, collimator and detector were mounted on a fixed horizontal arm which will hence forth be referred to as the X-ray rig. The sedimentation column was placed midway between the source and detector. The rig was driven vertically via a lead screw using a stepper motor, this providing a position of the rig to a digital display and to the data logger. The detector count rate output was displayed simultaneously on an X-Y chart recorder, a digital counter display and to the data logger. The addition of the data logging system to the X-ray apparatus was designed to circumvent the time consuming manual digitisation of the count rate-height chart records which were to be used to determine bulk density. The logging system consisted of a DAS-8PGA A-D conversion board used in conjunction with an IBM microcomputer. Time of sampling, rig position and X-ray count rate were logged at a sample rate ranging from 2Hz to 10Hz. The data logging software "XLOG2", shown in appendix 4, was written by the author (subsequently updated by G.Sills) such

Figure 3.17 Plan view schematic of the X—ray system.

1.8mm Lead Screen
(Low Energy Filter)

Beam Collimator

Collimator

X—Ray
Detector

Column

X—Ray
Source

160kV
Power
Source

X—Ray Rig
Drive
Mechanism

X—Ray Rig

Rig Height
Digital
Display

X—Y Chart
Recorder

Harwell
6000
Digital
Counter
System

DAS8
Interface
Board

IBM
Micro.
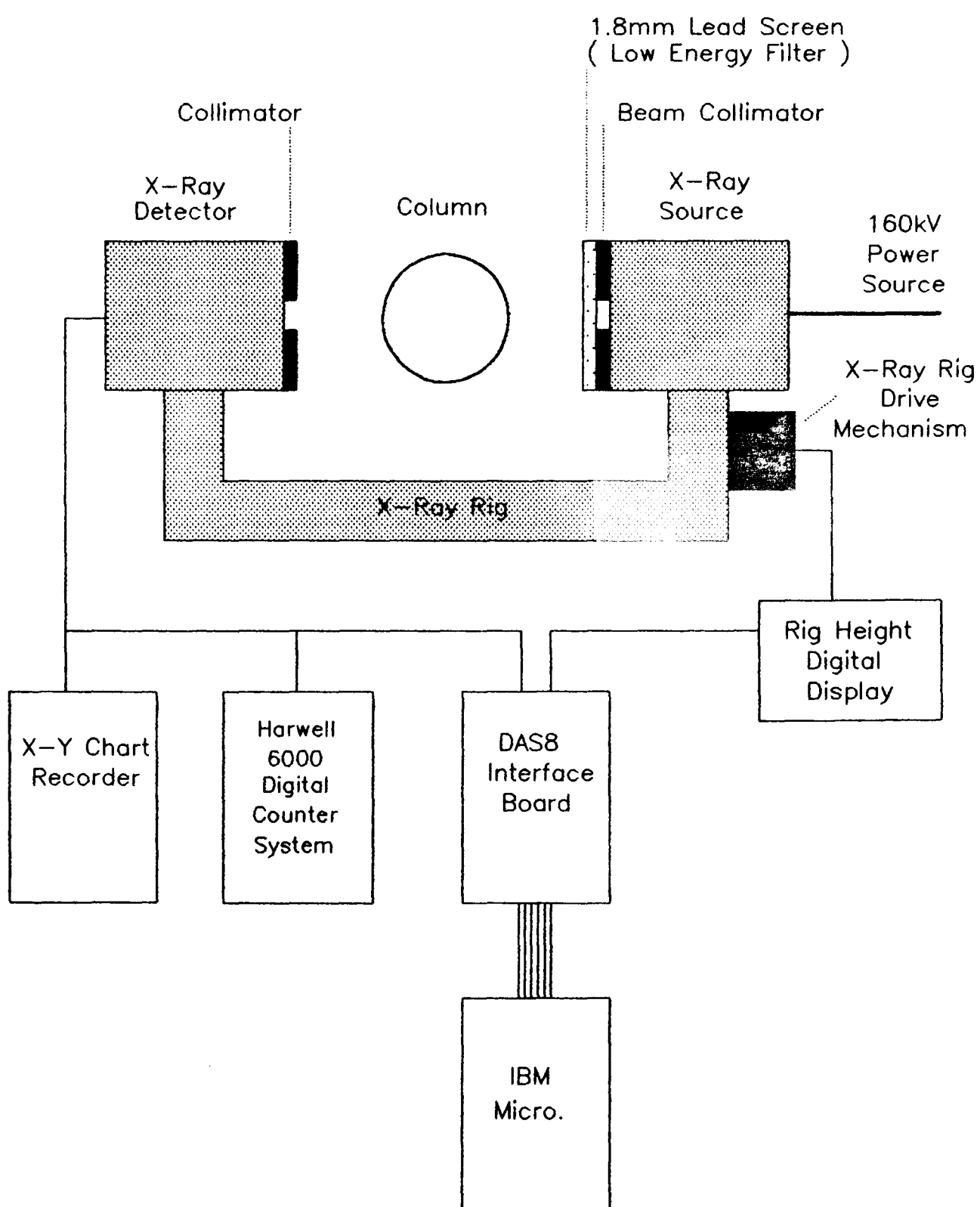
that the logged data could be directly incorporated into a LOTUS SOFTWARE spread sheet. The data was then processed using the empirical treatment described in appendix 1 in which the X-ray count rate is converted to a bulk density measurement of the soil.

A number of problems described by Elder (1985) were addressed in this study in the following manner. Firstly, the dimensional and geometrical inhomogeneity caused by column curvature, column cross sectional ovalling and wall thickness variations were very much reduced by having the instrumented column engineered from a single piece of acrylic. Secondly, prior to any experiment the X-ray current was adjusted, at a constant X-ray voltage of 160kV, to give a steady count rate of 95000 counts per second (cps) through a calibration sample of sea water. This procedure standardized the experiments thereby improving the accuracy and repeatability of the measurement. When static conditions were reached in the calibration sample the rig would be set up to undergo both upward and downward traverses of the column (a single traverse of 1m would take in the region of 10 minutes to complete). If the chart recorder traces from both logs indicated no variation from the steady state then the data logging process would be completed by transferring the data to disc. The one remaining source of error relates to misalignment of the column relative to the X-ray rig. While the current alignment procedure is time consuming and prone to error, it does have the potential of becoming automated sometime in the future. Overall, the bulk density of the soils could be measured to an accuracy of $\pm 7 kg/m^3$ with the X-ray system, with a positional accuracy of $\pm 1mm$.

3.7 Pore Pressure Measurement.

Pore pressure was measured using a 1 bar DRUCK pressure transducer (type PDCR 810). The pore pressure measuring system made use of a "Central Pressure Unit" (CPU) (see figure 3.18) and is described by Bowden (1989). This enabled a single pore pressure transducer to be switched, in a multiplexing fashion, between pore pressure sampling ports (figure 3.19) located at various heights up the column. The sampling ports consisted of acrylic receptacles into which fitted a Vyon porous disc. A single "O" ring seal made a push fit into the side of the column. The porous disc, made of a flexible material, was easily replaced in the event of sediment clogging. Connection between the port and the CPU was made using AVS fittings (type 6510-6-1/8) into which nylon flexible tubing (4mm inner diameter) could be inserted. The CPU system described by Bowden was modified to incorporate more sampling ports for the current study. The CPU consisted of two acrylic disc, the upper disc being mobile with a single screw fitting suitable for the pore pressure transducer. The lower disc consisted of 15 AVS fittings, made up of 14 connections to the pore pressure ports and one connection to the calibration reservoir. The pressure transducer on the upper disc could be rotated into any of the 15 positions.

A digital voltmeter (DVM) was used to display the output voltage of the pore pressure transducer (figure 3.18). Experimental procedure would require the recording of steady state voltages from each port position. These voltages were then converted to pressure above hydrostatic by use of calibration equations. Pore pressure transducer calibrations were performed after every set of readings. Pore pressure dissipation was measured as a function of both column height and time to an estimated accuracy of ±0.02kPa.

Figure 3.18 Schematic of the Central Pore Pressure Unit.

Calibration
Reservoir

CPU Axis

DVM

Pore Pressure
Transducer

CPU Rotating
Top Disc

CPU Fixed
Bottom Disc

"O" Ring Seals

AVS Fitting
(15 in total)

Port 1

Port 2   Port 3   Port 5

Port 4

To the Column

(column contains 15 pore pressure)
(sampling positions   )

Column Walls

Silicon Sealant

'O' Ring

AVS Fitting

Porous Disc

Tubbing

OUTSIDE
COLUMN

INSIDE
COLUMN
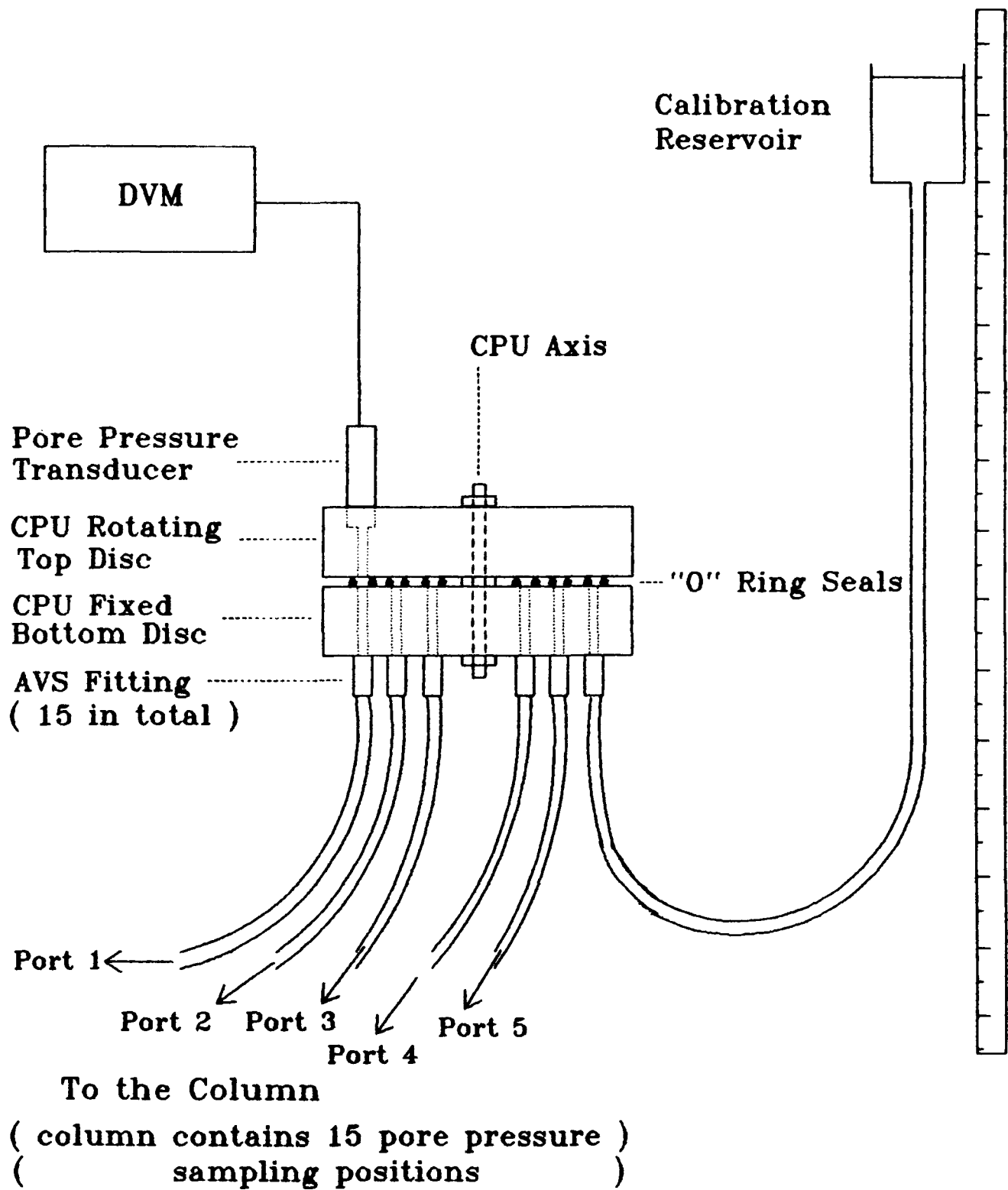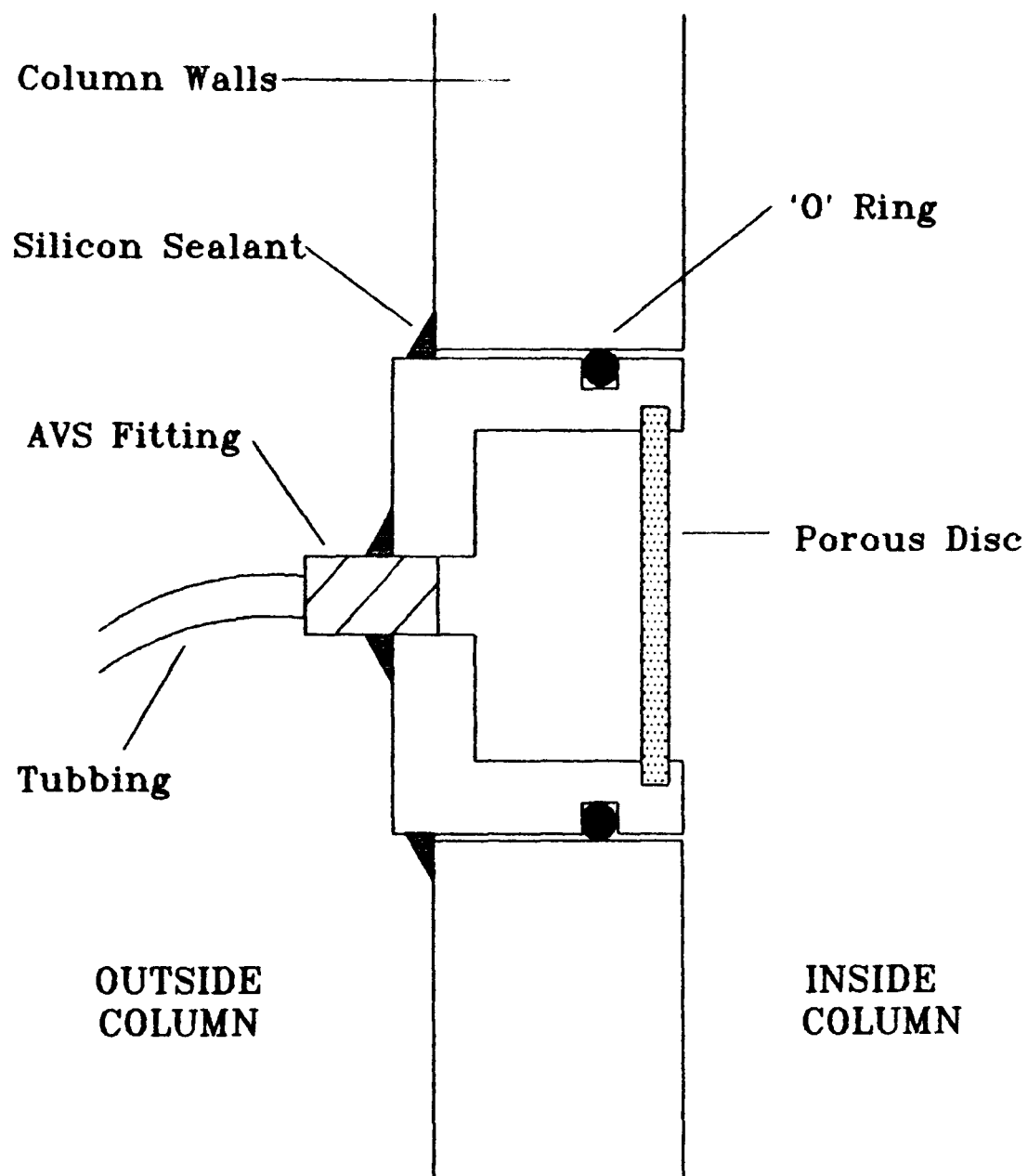
Figure 3.19   Schematic of the pore pressure port.

3.8 The Seismo-acoustic Data Logging System.

Figure 3.20 shows a schematic of the seismo-acoustic data logging system. This comprises two sub-systems, a compressional wave (or P-wave) sub-system and a shear wave (or S-Wave) sub-system. The logging system for both wave types is essentially controlled by a BBC Master computer in conjunction with a Hewlett Packard 54200A programmable/digital oscilloscope.

The P-wave sub-system consists of a pulse generator providing a 240 volt excitation spike to a piezoelectric transducer (described in section 3.3.4). A compressional wave consequently propagates through the soil sample, and is received by a second transducer, opposite the transmitting transducer and of known distance from it. In order to improve the quality of the received signals, particularly necessary in the electrically noisy environment of the X-ray laboratory, some form of signal enhancement is required. In this case 16 waveforms were signal averaged prior to being stored on disc by the BBC microcomputer. The instrumented settling column was constructed with 15 pairs of compressional wave transducers such that P-wave velocity could be monitored with both depth and with time to an accuracy of ±0.4%. In order to standardize the compressional wave velocity measurements, temperature and salinity were monitored during the logging procedure using a digital thermometer and refractometer respectively.

The S-wave sub-system is shown in figure 3.20. A d.c. step from a 20 volt square wave was used to drive the transducer (section 3.4.8). As described earlier, the transmission of the shear wave through the soft soil causes the received signal to be severely attenuated. In addition because the laboratory was an electrically noisy environment, this meant that the signal to noise ratio was very poor. Thus the received waveform was band pass filtered between 100Hz and 10kHz and amplified by as much as 60dB. The received shear waveforms were signal averaged 64 times prior to downloading to the microcomputer. The signals were stored onto disc for analysis at a later
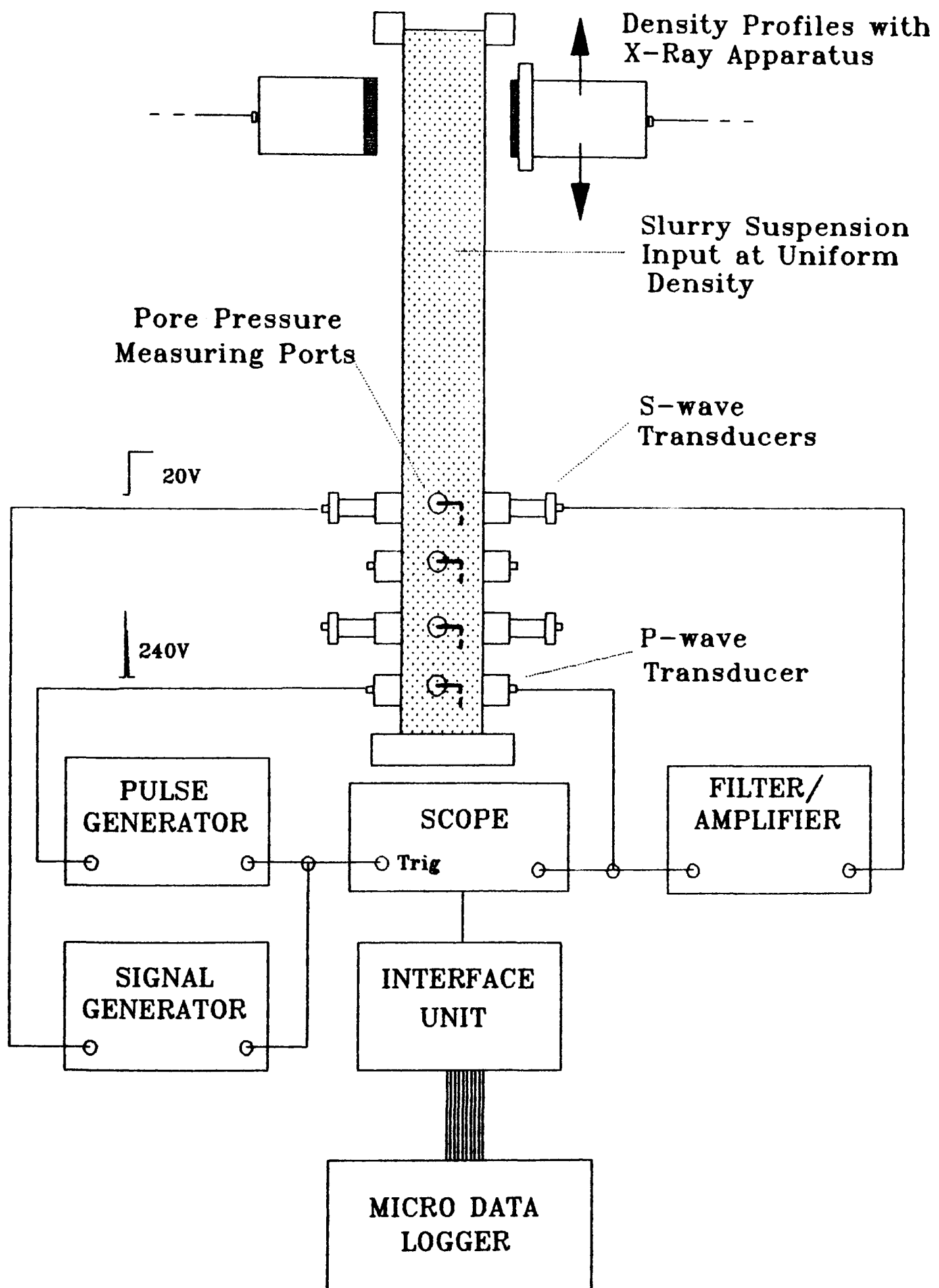
Figure 3.20 The seismo-acoustic data logging system.

stage. A typical signal averaged shear wave trace is shown in figure 3.15 (This signal may be compared to the signals shown later in the thesis, namely figure 4.7, which did not undergo such a filtering and signal averaging process). The shear wave transducer separation was measured using the travel time of the compressional wave generated by the tip of the bender element. Utilizing the compressional wave velocity data from the P-wave sub-system, at the same height, but perpendicular to the shear wave transducers, the bender element separation could be determined to an accuracy of ±8.7%. In order to calculate bender element separation in this manner horizontal anisotropy in terms of P-wave propagation has been assumed to be negligible.

A suite of software entitled "COLSOFT" (Appendix 4) was written for use with the instrumented settling column. The software comprises of a series of compressional wave and shear wave logging, display and processing programs. The logging software was written such that the oscilloscopes display parameters could all be pre-programmed. This makes the system operation particularly "user friendly" such that a non-specialist operator, e.g. a laboratory technician, could operate the system with only a little preparatory instruction.

3.9 Soil Electrical Resistivity Measurement.

The electrical resistivity of the soil was required in order to establish changes in the apparent formation factor (F) during consolidation, which in turn could be used to derive an estimate of Biot's mass coupling factor (b) using Brown's relationship

$$b = F.\eta \qquad \text{where } \eta = \text{fractional porosity}$$

A system previously used by Lovell (1984) to measure soil resistance in an instrumented permeameter appeared suitable for the present application. Thus, four stainless steel electrode rings were incorporated into the instrumented

settling column. The electrodes were fixed towards the base of the column in a Wenner configuration (figure 3.16) with an electrode spacing of 5cm. The electric field generated by such an arrangement was described by Lovell as being a toroid. A signal averaging Terrameter resistivity meter was used in conjunction with the electrode array to record variation in soil resistance during the consolidation process. This enabled resistance to measured to an accuracy of $\pm 0.005\Omega$.

Since a cross coupling effect between temperature and resistance exists, a correction curve was drawn up (figure A3.4) so that all resistance measurements could be corrected for temperature variation. The temperature was measured using a digital thermometer placed at the soil/water interface.

3.10 Soft Soil Loading System.

One of the research aims was to develop a loading system suitable for use with soft soils that would be capable of accelerating the consolidation process. The problems associated with the development of such a loading system are two fold:
(1) Very small applied stresses can cause the soil to return into suspension.
(2) Perspex columns are notoriously subject to ovalling during the process of annealing, that is the column tends to loose its circular cross section. Any piston loading system design must therefore be able to adapt to a variety of cross sections.

A number of designs using "O" ring seals and "rolling diaphragms" were tested but failed either to successfully seal the sediment, or suffered from too much side wall friction. An adjustable seal was therefore called for, and a suitable design was ultimately found.

An adjustable molded rubber "torous" seal was used in conjunction with a "tommy bar" (see figure 3.21). By screwing
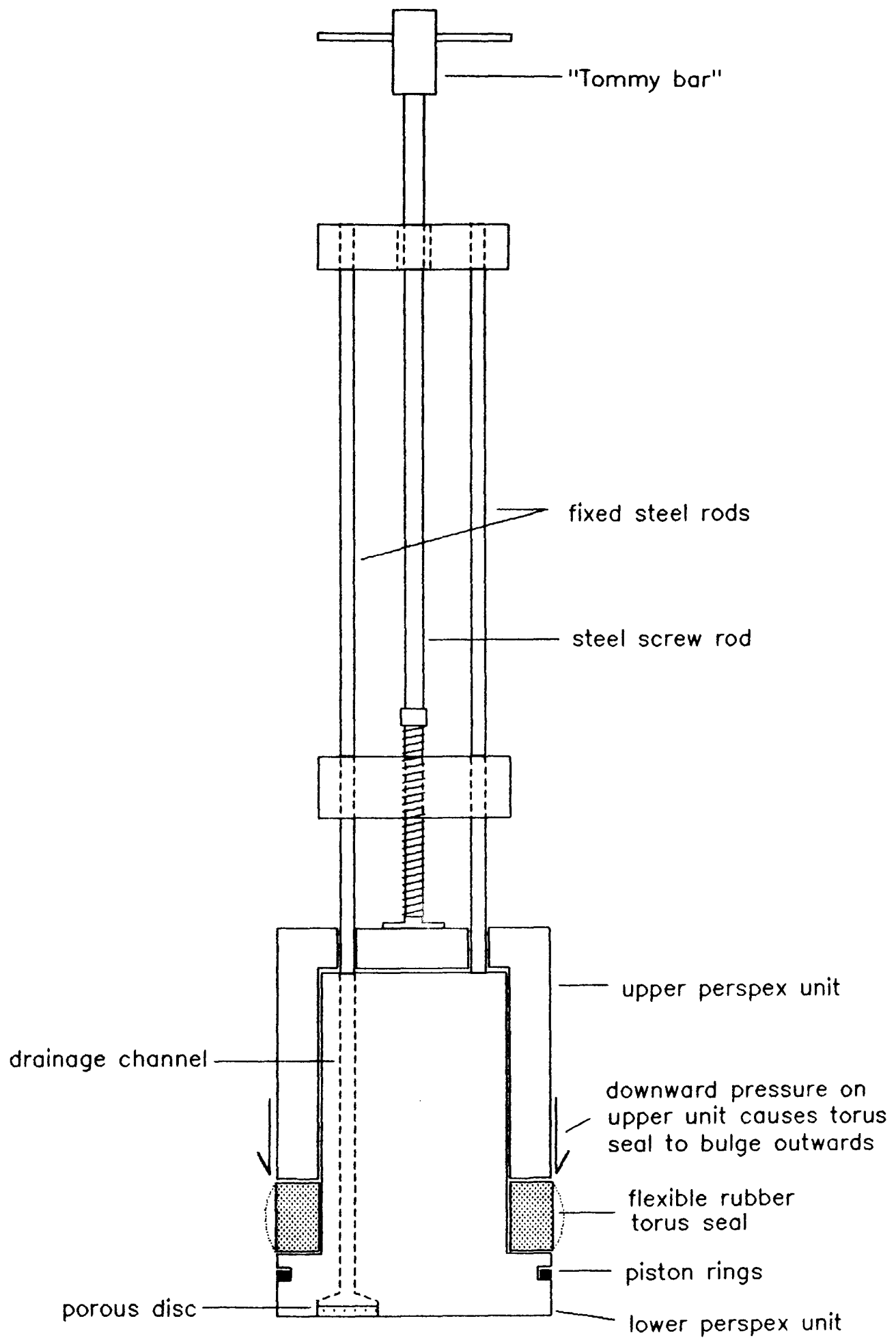
Figure 3.21   Soft soil loading system.
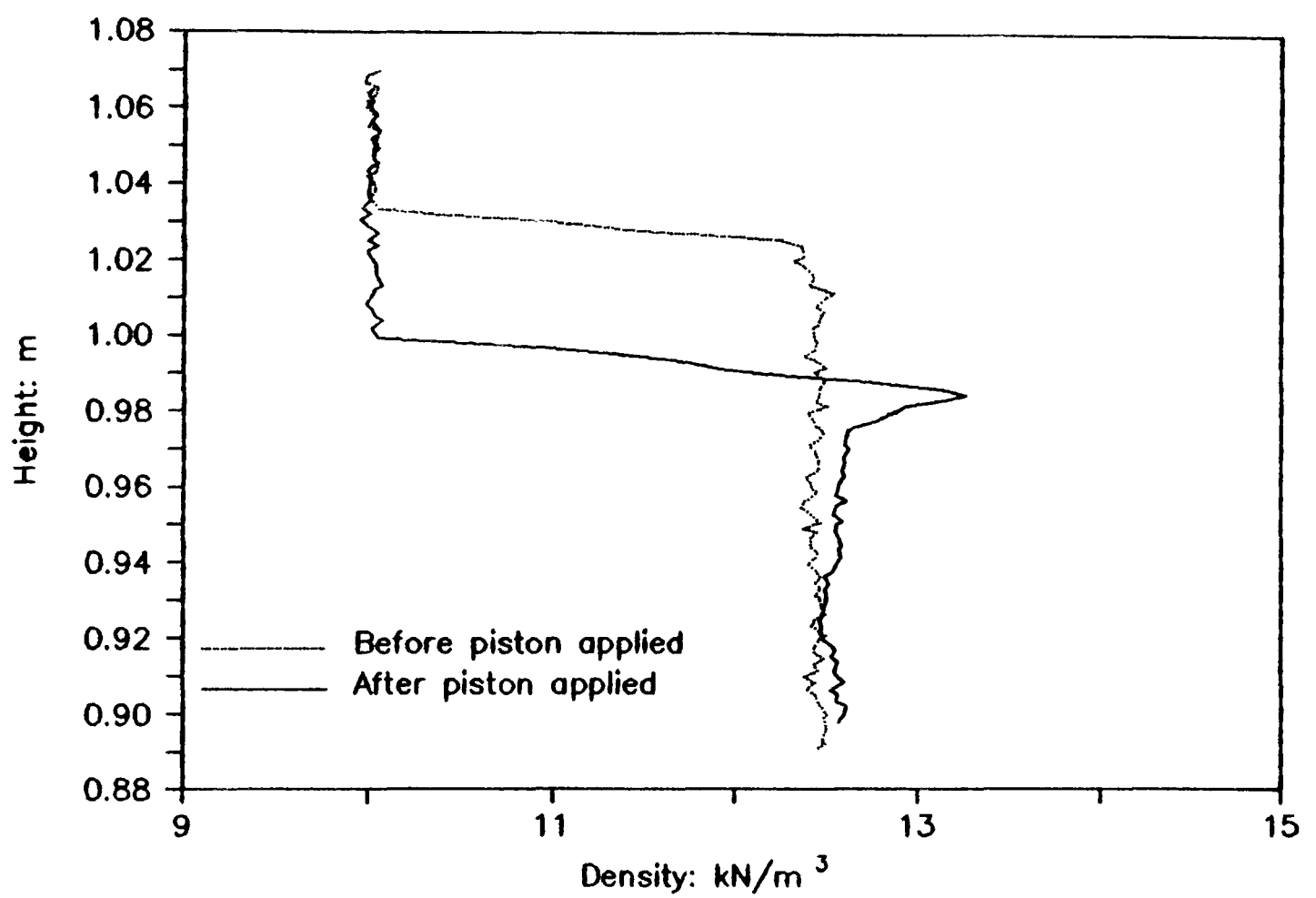
Figure 3.22 The effect of applying a piston to a soft soil.

down the tommy bar the rubber seal flattens and pushes outwards against the column wall. In use, the piston is gently lowered onto the sediment surface. The piston ring, near the base of the loading system, provides a suitable seal to stop the sediment returning to suspension until the "torous" seal is made good. With careful adjustment the "torous" seal can be made to make a sliding fit such that pressure can be applied to the soil without any loss of sediment to suspension. By observing the variation of the pore pressure reading at the base of the column a suitable load can be applied and then held in place by a further tightening of the seal. Using this procedure drainage at the sediment surface is allowed throughout the loading process via a porous disc situated in the piston (as shown in figure 3.21).

While such a system can successfully seal and load a soft soil it was not considered suitable for the present study. During experimentation, as a load of 2.02kPa was applied, a thin layer of high density material developed at the top of the sediment (as indicated by the density log in figure 3.22). This effect was considered to be detrimental to the present consolidation studies as it is likely that this dense layer could adversely alter the free drainage of a soil. The loading system was therefore not used further in this research project and has been presented here for fellow researchers who may find a suitable application.

3.11 Apparatus Validation Experiment.

In order to validate the instrumented sedimentation column as a practical geotechnical-geophysical apparatus, a set of geophysical measurements were made on a saturated sand sample. P-wave, S-wave and soil resistance measurements were made on the sample as it was compacted from a high porosity structure. The porosity of the sample was measured using the X-ray apparatus and applying the calibration curve shown in figure A3.5 (appendix 3) to determine bulk density and then porosity. The results obtained from this validation experiment were

compared to similar measurements previously made in the Jackson Porosity Cell (Schultheiss 1983). These results together with an analysis of the data will be presented in section 6.2.

3.12 Summary.

An instrumented settling column was designed and built which enabled the measurement of compressional and shear wave velocities, soil electrical resistivity, and pore pressures in soft soils characterized by low density, low strength and large strains. The apparatus was designed such that it could be used in conjunction with the Department of Engineering, Oxford University, X-ray apparatus for determining soil bulk density.

The loading system designed to accelerate the consolidation process was found to create a high density soil layer at the loading system/soil interface. This was considered to be detrimental to the consolidation studies in this particular case and was not used in subsequent research.

CHAPTER 4:   EXPERIMENTAL PROCEDURES AND PRELIMINARY RESULTS.

4.1   Introduction.

In this chapter the experimental technique used in this research programme will be described. The procedures for setting up the X-ray, pore pressure, seismo-acoustic and soil electrical resistivity apparatus will be outlined in section 4.2. The importance of the standardization of soil preparation will be discussed, and the technique used outlined (section 4.3). Section 4.4 describes the soil sample's input into the instrumented settling column and the geotechnical and geophysical measurements made as the soil consolidates under self weight. A summary table will be presented towards the end of the chapter, giving details of all the experiments carried out in the programme.

The concluding part of the chapter will be devoted to a presentation of the preliminary experimental results, these being divided into two parts: geotechnical and geophysical. A detailed analyses of the results will be given in chapters 5 to 7.

4.2   Experimental Set Up Procedures.

4.2.1   COLUMN SET UP PROCEDURES.

After cleaning, the instrumented settling column was fixed to vertical support stanchions (in the X-ray laboratory). The column was vertically aligned using a plumb bob and spirit level. Precision at this stage was of crucial importance not only to prevent differential settlement of sediment within the column, but more importantly to prevent differential absorption of X-rays through the column walls. The column was then filled with a deaired laboratory standard sea water, of

$34°/°°$ salinity, 24 to 48 hours prior to commencing the experiment.

4.2.2 X-RAY APPARATUS: SET UP PROCEDURES.

The X-ray rig was set for vertical alignment around the column, the X-ray source and detector being positioned equidistant from the centre of the column. The standard sea water within the column was used as one of the calibration samples, the second calibration sample being a homogeneous slurry of known density (see appendix 1 for further details). Initially the X-ray apparatus was allowed to warm up, this being achieved once a steady count rate was observed. With an operating voltage of 160 kVolts, the X-ray generators current was adjusted until the digital display registered a count rate of 95000 ± 200 counts per second. The X-ray rig calibration height, fixed near the top of the column, was noted. This position was repeatedly used in the set up of the X-ray so as to avoid variation in the calibration count rate due to variation in column wall thickness. (Since, in the early stages of the experiment, the calibration position was unlikely to be clear of suspended sediment, a second container filled with the standard sea water, referenced to the original calibration sample, was used for calibration. On such occasions, a reading of surface density was also recorded with the PAAR density meter by way of a check).

4.2.3 PORE PRESSURE APPARATUS: SET UP PROCEDURES.

Filling the column with sea water 24 to 48 hours prior to the beginning of the experiment enabled the porous discs of the pore pressure ports to become fully saturated. It also allowed the temperature of the entire column apparatus to stabilize. An hour prior to the start of the experiment, air bubbles from the inside of the column were removed using a long handled brush. The pore pressure system was then carefully de-aired. The pore pressure measuring electronics, comprising of a pore

pressure transducer and digital voltmeter, remained switched on throughout the course of the experiment in order to avoid any thermal fluctuations.

4.2.4 SEISMO-ACOUSTIC SYSTEM: SET UP PROCEDURES.

Prior to the column set up, the shear wave transducers were subject to an insulation test as described in section 3.4.7. Transducers passing this test were divided into transmitter and receiver pairs and were then inserted into the column. The compressional wave transducers remained fixed in position at all times.

Prior to the beginning of the experiment, any air bubbles that had accumulated on the submerged transducer faces were removed. The seismo-acoustic logging system was then switched on and both compressional and shear wave transducers were pulsed in order to cause compressional waves to propagate through the sea water. At this stage any transducers failing to generate compressional waves were deemed faulty and replaced before the main experiment commenced. The compressional wave travel time between the P-wave transducers pairs was noted. The water temperature was also measured using a digital thermometer accurate to $0.1\ ^\circ C$, and salinity was measured using a refractometer accurate $0.5\ ^\circ/\circ\circ$. Using a standard velocity equation given by Clay and Medwin (1977);

$$V_w = 1449.2 + 4.6T - 0.055T^2 + 0.00029T^3 + (1.34 - 0.01T)(S - 35)$$

where V_w = velocity of sound in water (m/s)
       T = temperature ($^\circ C$)
       S = salinity (parts per thousand: $^\circ/\circ\circ$)

the fixed delays of the compressional wave measuring system could then be calculated and subsequently subtracted from the observed onset times during data analysis. The fixed delays of the shear wave measuring system were considered negligible compared to the overall travel time. The pre-experimental set

up now complete, the shear wave transducers were retracted to the stand by position ready for the input of the slurry.

4.2.5   ELECTRICAL RESISTIVITY APPARATUS: SET UP PROCEDURES.

During the course of the pre-experiment set up procedures the electrical resistivity, temperature and salinity of the sea water in the column was measured. This resistivity measurement was compared to that of the calibration curve value, (figure A3.4 in appendix A3). Any deviation from the expected value was presumed to be a result of trapped air or dirt on the electrodes which required removal before commencing the experiment.

4.3   Soil Description and Preparation.

4.3.1   SOIL DESCRIPTION.

The sediment samples used in the experiments originated from areas of current geophysical interest at the time of this research programme. These areas were Traeth Lligwy (Anglesey), the Irish Sea to the west and south-west of the Isle of Man (Yuan 1992) and the Irvine Bay (Huws et al. 1991 and Huws 1992) area of the Firth of Clyde (exact location coordinates are given in table A5.1 and figures A5.1 to A5.3). The sea bed in these areas had undergone extensive geophysical and geotechnical testing, using both *in situ* and laboratory techniques. It was hoped ultimately to compare the results presented in this thesis with the work of Yuan, Huws and co-workers.

A detailed description of the sediment samples properties including liquid limit, plastic limit, specific gravity, calcium carbonate content and organic content is given in appendix 5 (table A5.1). The probable clay mineralogy of the sediment samples are also summarized in appendix 5 (tables A5.2 to A5.4). Each core sample was sub-sampled and subjected

to British Standard hydrometer particle size analysis in order to categories the sediment in terms of texture.

4.3.2   SOIL PREPARATION.

Since flocculation in a suspension can be greatly influenced by the sediments initial state, a set procedure for soil preparation was deemed necessary. Approximately 10kg of sediment was removed from the soil sample and was placed into a 5 litre capacity mechanical soil mixer. Laboratory standard sea water was stirred into the soil until an homogeneous slurry of required density was produced. The slurry density was ascertained by using a hand held PAAR density meter accurate to ± 1.0 kg/m^3 (see appendix 3 for details). This entire procedure took about 20 minutes after which the sediment was left undisturbed overnight.

4.4   Experimental Method.

The following day, having completed all the set up procedures outlined above, the slurry was again mixed for a further 15 minutes prior to its introduction into the column. In the meantime a predetermined volume of sea water was siphoned from the column. (Prior studies had shown that completely emptying the column of sea water tended to introduce air into the pore pressure piping and also allow air bubbles to develop on the seismo-acoustic transducer faces). The height of the water left in the column was noted using a steel rule.

At the end of the fifteen minute period, the homogeneous slurry was removed from the mechanical stirrer and the bulk density recorded using the hand held PAAR density meter. The slurry was then promptly siphoned into the column making sure that the siphon tube always remained just below the surface of the rising water/slurry mixture. The height and density of the final mixture was noted such that the initial density could be

calculated. As a check, the mixture density at the top of the column was also measured using the density meter. The input of the slurry into the column marked the beginning of the experiment proper, the time was carefully noted. The main data acquisition programme thereby commenced, consisting of 5 measurement steps described below. These measurements were repeated at suitable time intervals up to and beyond the conclusion of primary consolidation. Throughout the data acquisition programme a careful note of time, temperature and salinity was made.

1. Up and down scans of the slurry/sediment were made using the X-ray apparatus. Providing the scans produced coincident plots, the data was stored onto disc. (Note that the X-ray apparatus was always set to give a count rate of 95000 ± 200 cps in the calibration sample prior to this measurement).

2. The slurry/sediment electrical resistivity was measured using a ABEM Terrameter.

3. The output voltage of the pore pressure transducer from different heights within the slurry/sediment column were recorded. A calibration of the pore pressure transducer was then performed. A calibration equation would be determined at a latter stage so as to convert the output voltages into pressure above hydrostatic.

4. Compressional wave propagation through the slurry/sediment were logged as a function of height and time.

5. Shear wave propagation through the sediment was logged as a function of height and time.
NOTE: This step was only performed 50 hours after the input of the slurry.

Table 4.1 summarizes the experiments carried out in this research programme. Experiments referenced as IM05, IM06 and IM10 were carried out as part of the instrumentation

development and apparatus verification programme. Experiments IM03 and IM04 were performed in the prototype column as part of the investigation into compressional wave behaviour during consolidation. Experiments IM07, IM08, IM09 and IM11 represent the main seismo-acoustic/consolidation behaviour studies performed with the newly developed instrumented sedimentation column.

4.5 Geotechnical Experimental Results.

4.5.1 PARTICLE SIZE ANALYSIS.

The British Standard hydrometer method of particle size analysis for fine grained soils was performed on sub-samples of the sediment cores. The results are shown in figure (4.1). A triangular classification diagram (Krumbein and Pettijohn 1938) was used to give a descriptive classification of the sediments, based on the percentage sand/silt/clay components of the soil. For details of the soil types studied in these experiments reference should be made to table 4.1.

The soils solid component density (ρ_s) was determined using the British Standard Specific gravity test, BS1377 1975 test 6a, 6b. The test was performed in triplicate, the results are shown in table 4.1.

4.5.2 SURFACE SETTLEMENT RESULTS.

The changing height of the surface of the slurry with the logarithm of time is one way of characterizing the behaviour of the soil. Figure 4.2 shows the degree of settlement against time. It can be seen from figure 4.2, that experiments IM07,IM08, and IM11, had initial slurry densities below the critical value described by Elder (1985) for freshwater settlement. Although these sediments were in fact settling in sea water the characteristic settlement curves appear to be

71
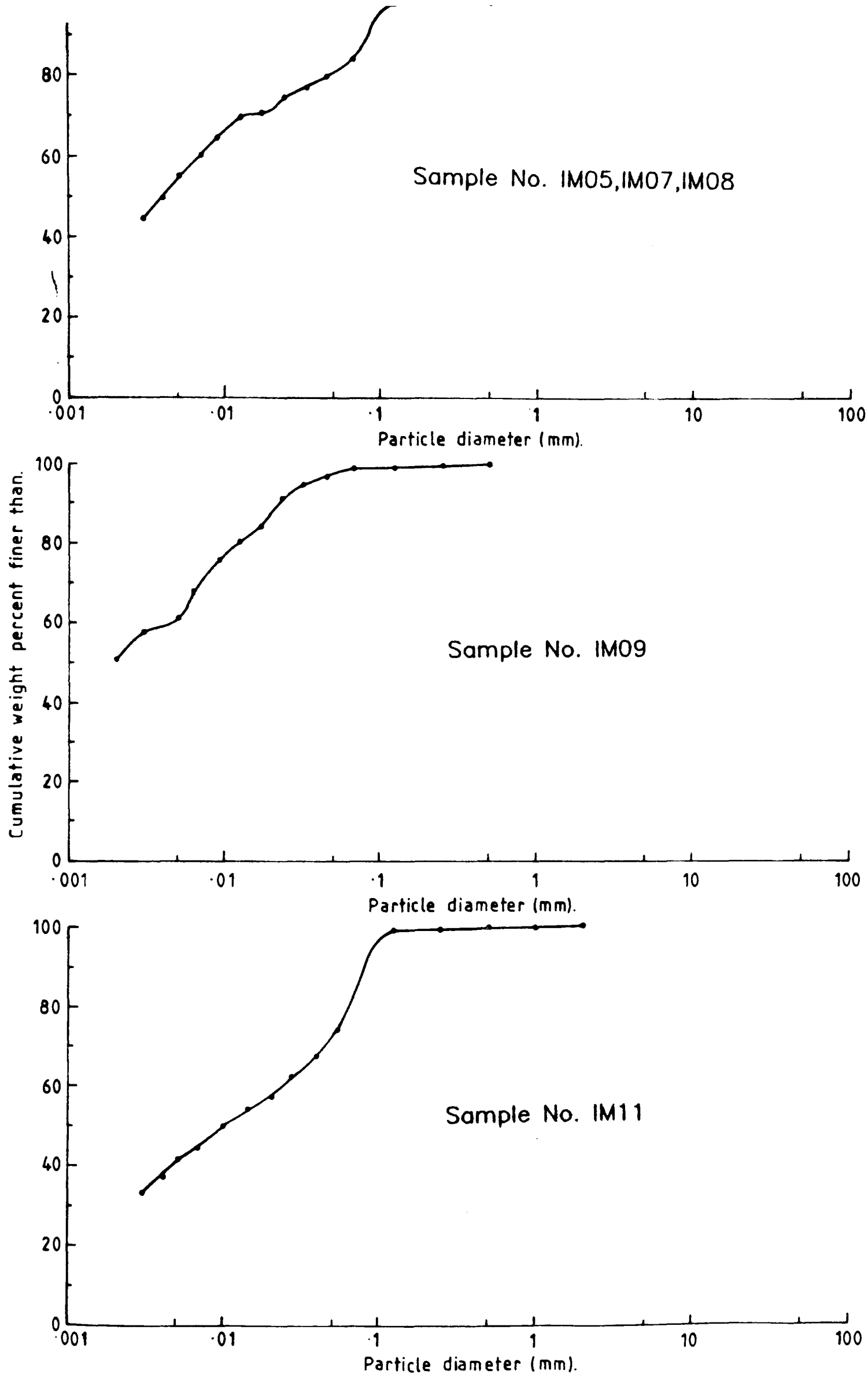
Figure 4.1 Sediment size analysis of Irish Sea samples.
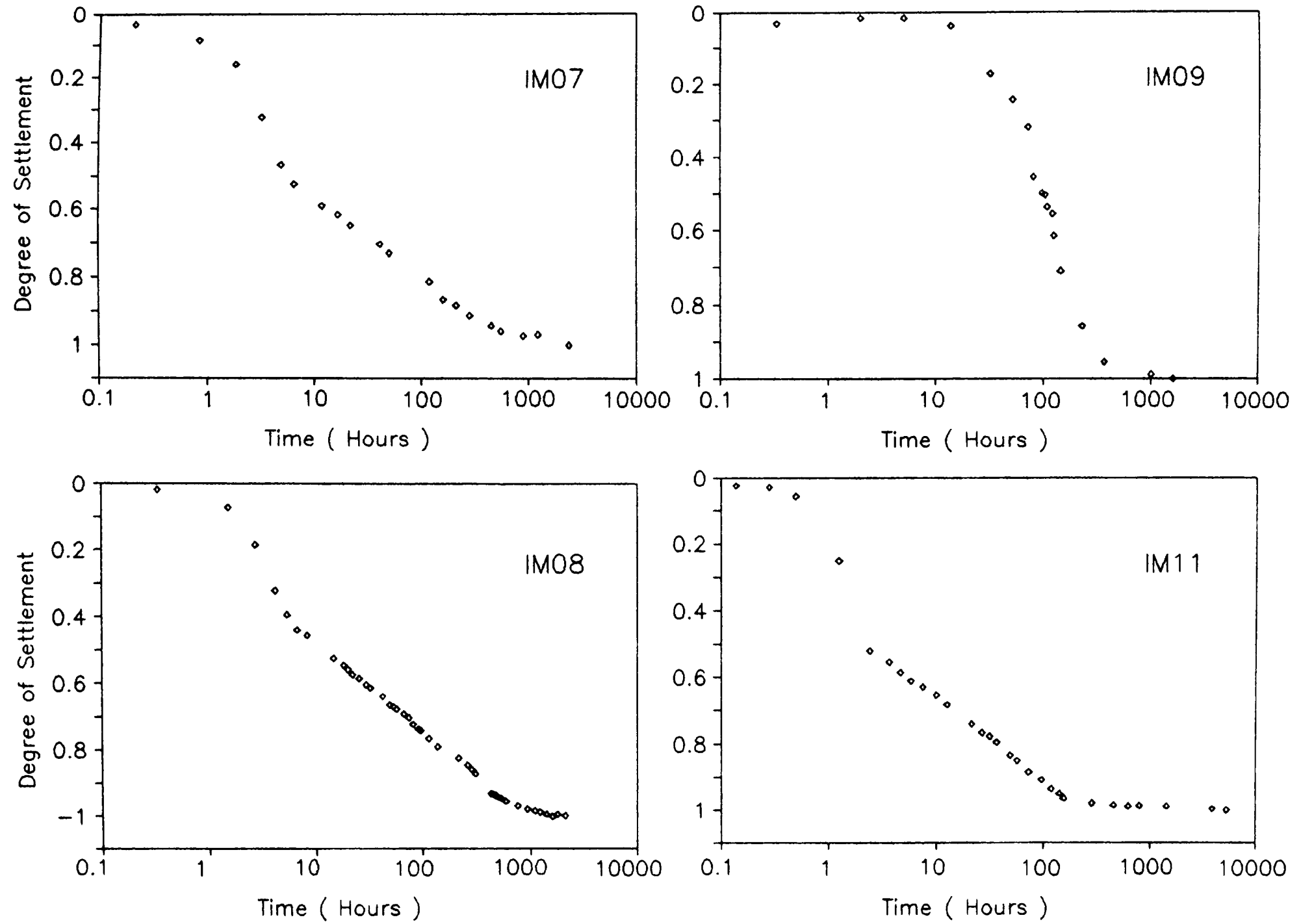
Figure 4.2 Surface settlement curves.

maintained. The curves consist of a primary phase representing a period of fluid supported suspension, a linear gradient representing the primary consolidation virgin compression curve, and a flattening of this gradient marking where secondary consolidation is dominant.

Experiment IM09 represents an initial slurry density that is greater than the critical value. Again the characteristic surface settlement curve can be observed. However no suspension phase exists for this sample. The curve shows little settlement within the first 10 to 20 hours of the beginning of the experiment. This is believed to represent the period of soil structure development described by Elder and Sills (1984). Permeability must clearly be reduced during this initial period such that the settlement is retarded. Rapid surface settlement follows until the gradient flattens indicating the onset of secondary consolidation.

4.5.3 BULK DENSITY PROFILES.

The surface settlement curves, described above, may be used to characterize the initial conditions of the settling slurry and may also be used to determine some averaged properties of the sediment, e.g. a bulk voids ratio and bulk compressibility. Previous researchers (Been 1980, Been and Sills 1981 and Elder 1985) have shown subtle variations within the soil, which may be greatly at variance with the averaged properties of the sediment. One method of revealing such local variations in distribution of mass within the soil bed is by the use of X-ray apparatus as described earlier, in chapter 2. The apparatus measures X-ray count rate through the sediment sample which can be converted to bulk density using the empirical method described in appendix 1.

The bulk density profiles were recorded as soon after the slurry was introduced into the column as possible. This enabled the degree of homogeneity of the slurry to be established. Subsequent profiles were made at suitable time

intervals depending upon the rate of settlement of the sediment. During the course of the four experiments i.e. IM07, IM08, IM09, IM11, 110 profiles were recorded. Representative profiles have been selected for presentation and are shown in figures 4.3 to 4.6. (each density profile is represented by over 500 data points). A discussion of typical density profile characteristics will be presented below.

Figures 4.3 to 4.6 show successive density profiles taken during experiments IM07, IM08, IM09 and IM11 respectively. Initially the slurry density is almost uniform except for a narrow region of high density material, comprising coarse particles, at the base of the column. A single layer exists above this dense region, comprising finer silt and clay particles. It is this layer that is under study in these experiments. The homogeneity of the slurry is lost shortly after input. In the case of experiments IM07, IM08, and IM11 the surface density decreases to less than the original input density, indicative of differential settling, and represented by the settling phases of figure 4.2. As the developing soil consolidates, the height of the soil layer decreases whilst its density gradually increases with time as indicated by a broadening of successive profiles. Experiment IM11 shows the development of a density inversion. It will be noted that such an inversion persists for several hundred hours.

While all the phenomena described above have been observed and reported by earlier researchers (Been 1980, Been and Sills 1981, Elder 1985), using the newly modified data acquisition system it is possible to document the subtle variations in bulk density. Previous authors (Been 1980, Been and Sills 1981, Elder 1985) have had to smooth the density curves owing to drafting and acquisition limitations. The finite variations in density witnessed in these experiments were observed to remain individual and separate for considerable periods of time. This gives rise to the concept of soil element tracking, a concept introduced by Been (1980) and which will be utilized in this study.
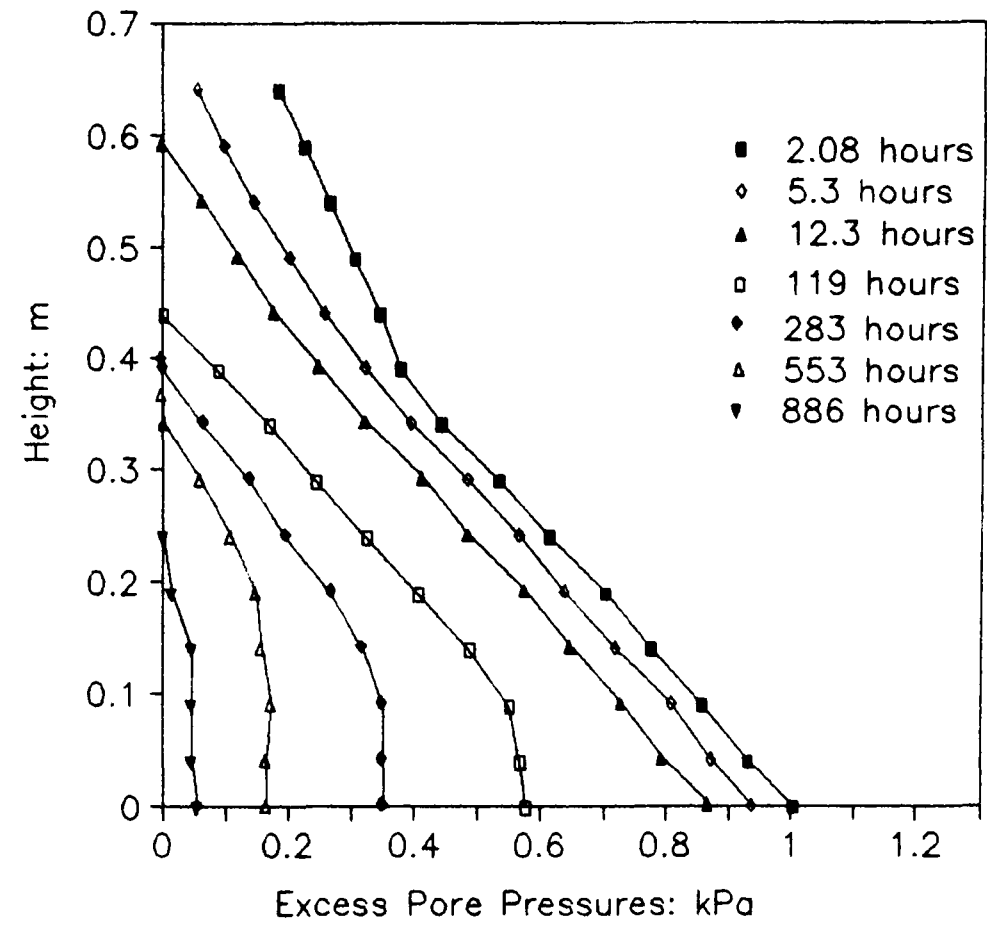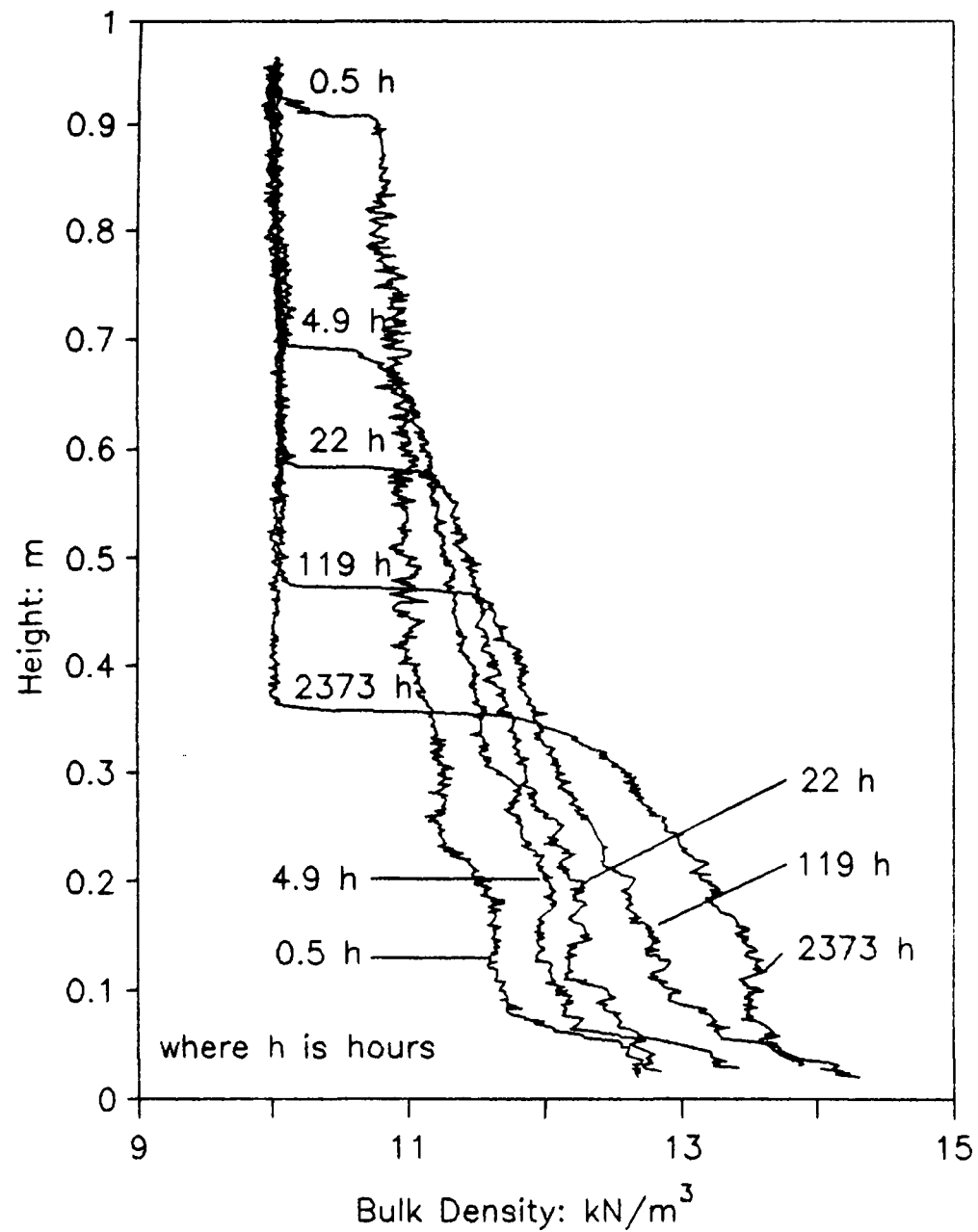
Figure 4.3   Bulk Density and Excess Pore Pressure Profiles: Experiment IM07.
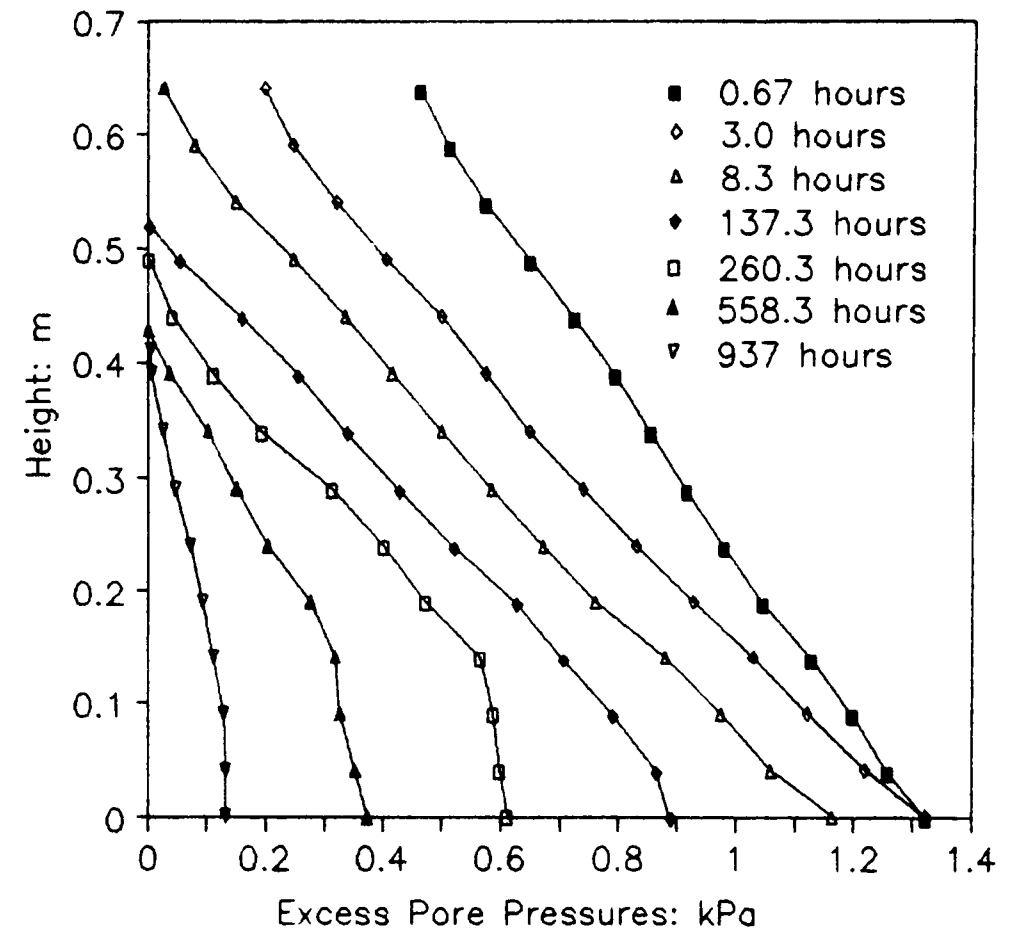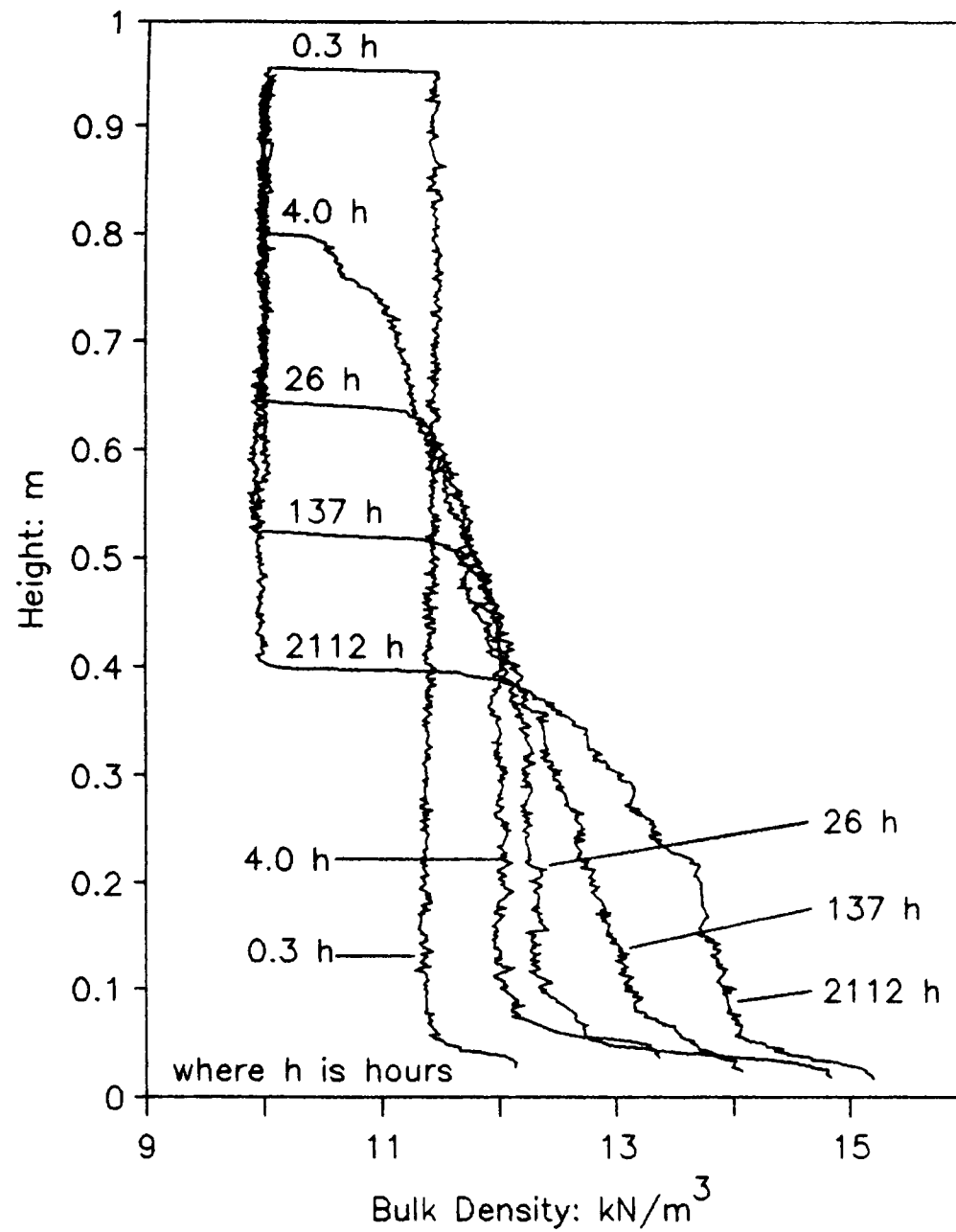
Figure 4.4   Bulk Density and Excess Pore Pressure Profiles: Experiment IM08.
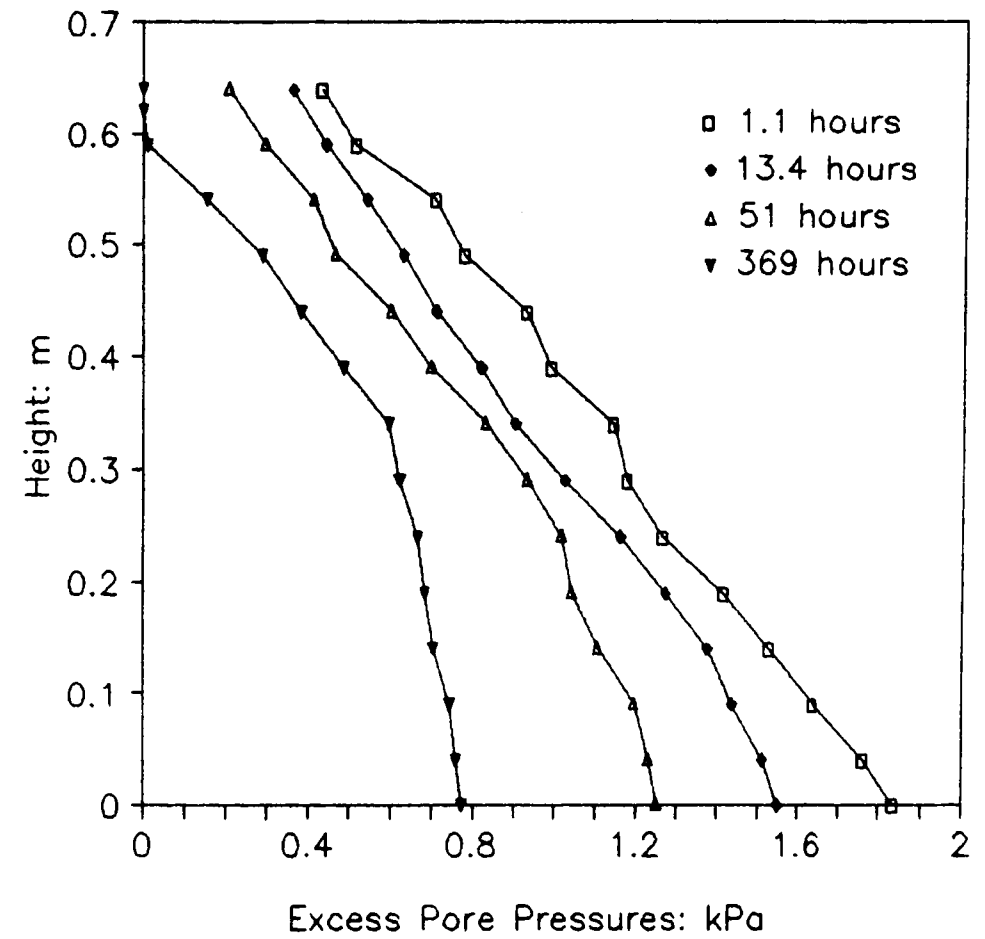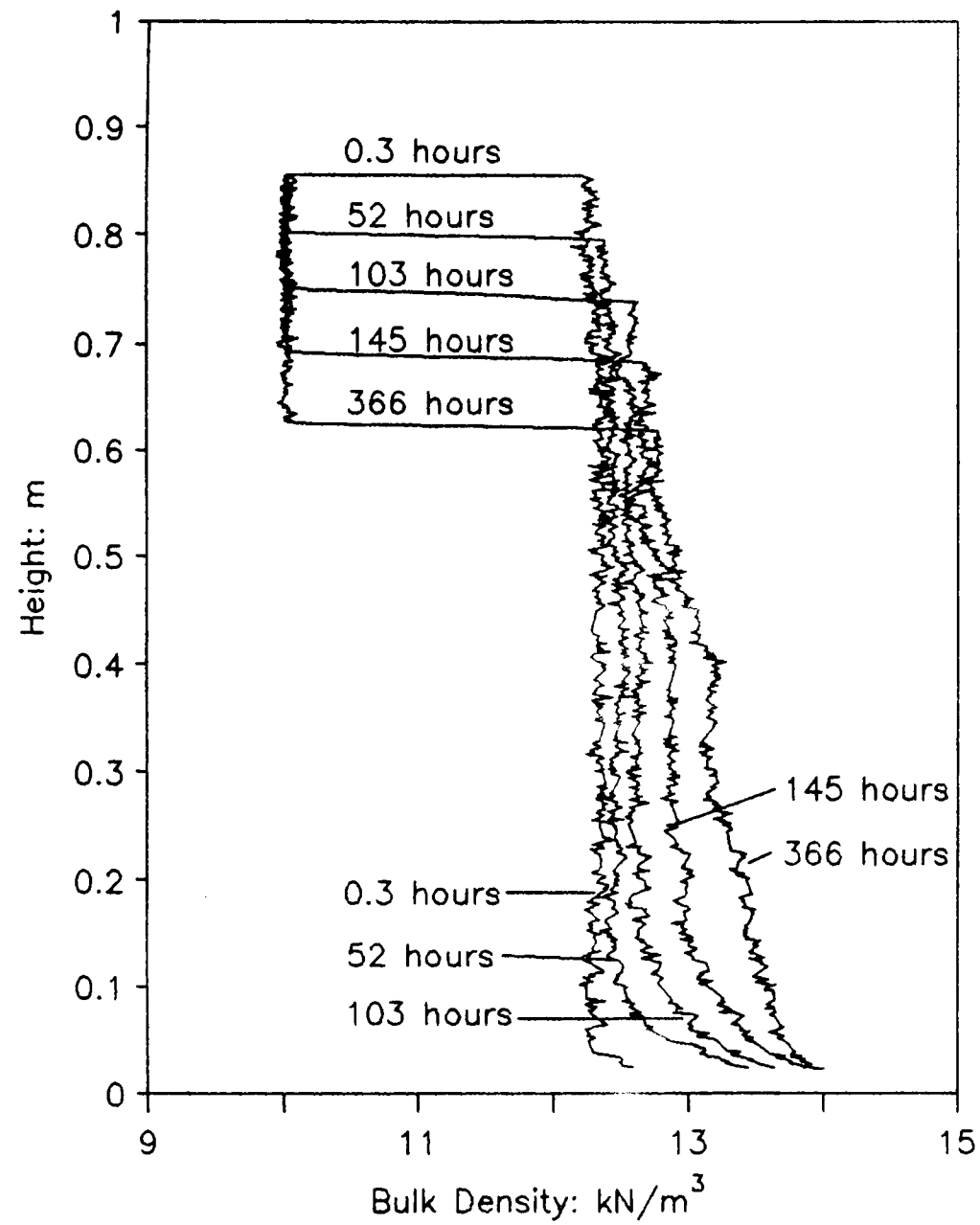
Figure 4.5 Bulk Density and Excess Pore Pressure Profiles: Experiment IM09.
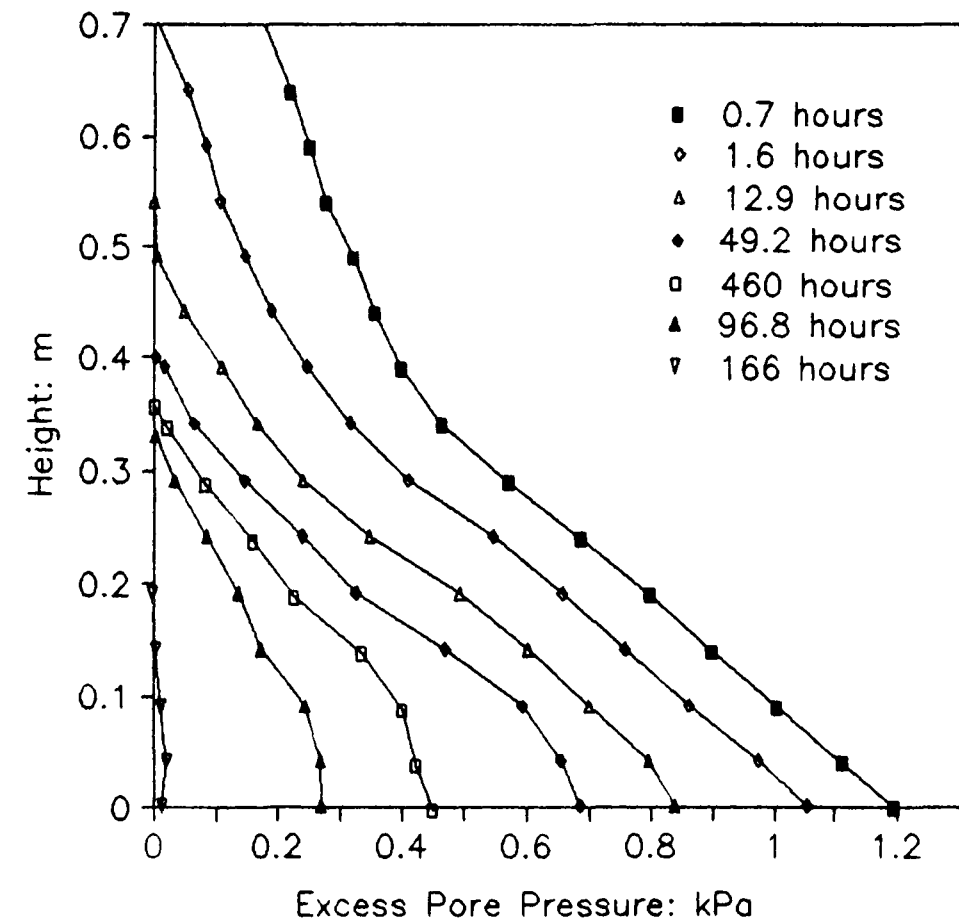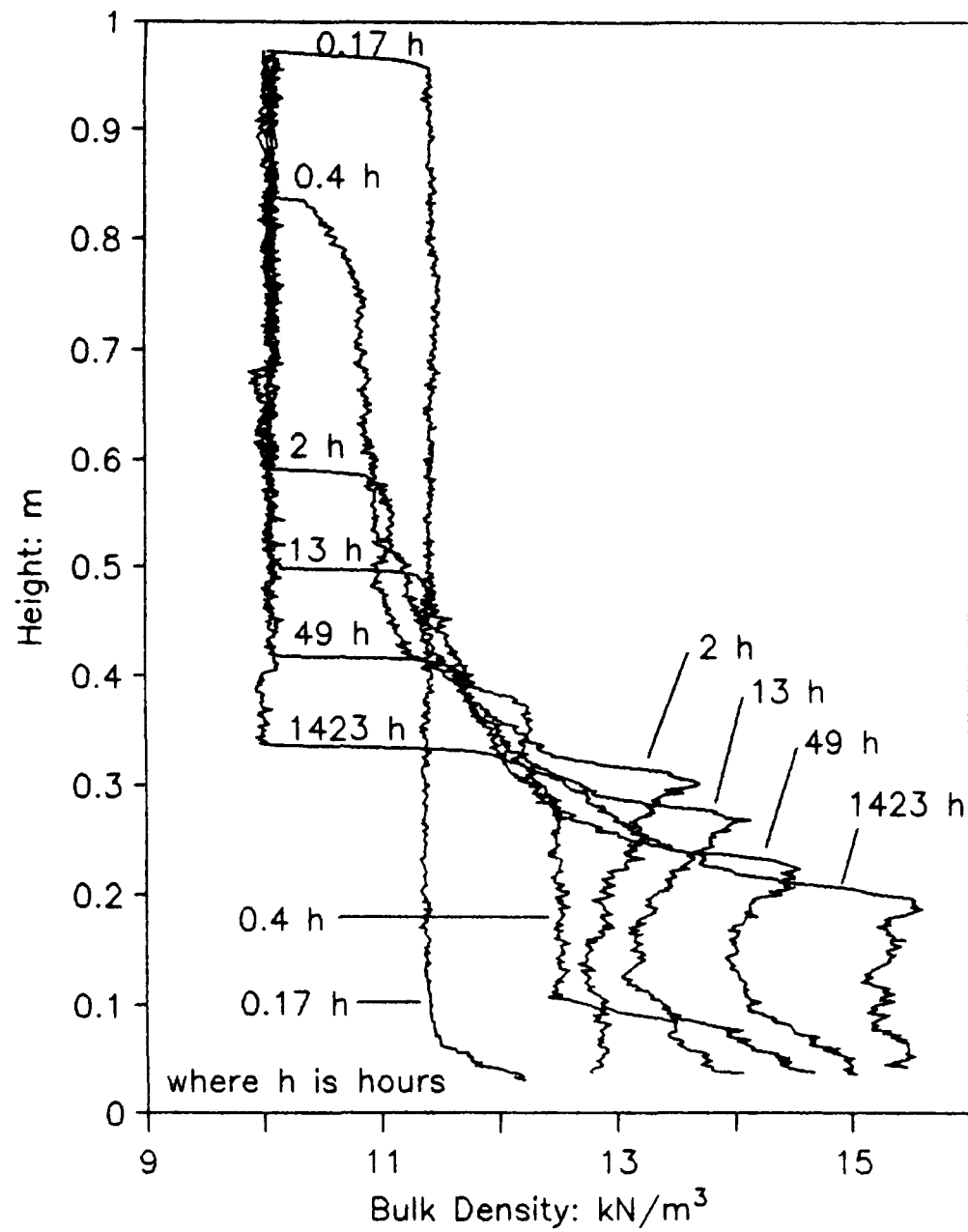
Figure 4.6 Bulk Density and Excess Pore Pressure Profiles: Experiment IM11

4.5.4 PORE PRESSURE PROFILES.

Pore pressures were recorded in order to ascertain the degree of consolidation of the settling soil. They will be used in conjunction with the density data to calculate the effective stresses within the soil. The pore pressure measurements will also be used to determine the hydraulic gradients set up within the soil, which ultimately lead to the derivation of soil permeability. In each case the pore pressure profiles were recorded until the end of primary consolidation identified by zero excess pore pressures being measured throughout the soil sample.

Figures 4.3 to 4.6 indicate the dissipation of pore pressure as a function of height and time. Initially the pore pressure profile appears to comprise of two gradients, one for the settling suspension, the other for the settled soil below, (as shown in experiments IM07 and IM11). The maximum value of excess pore water pressure, observed at the base of the column, at the moment of sediment input, is equal to the total stress above hydrostatic pressure, and that of the effective stress when the soil is fully consolidated.

With time the pore pressure versus height gradient becomes linear and gradually, as the pore pressure dissipation becomes more rapid toward the base of the column due to increased loading, the gradient begins to curve at the base of the column. In the majority of cases, the point of zero excess pore pressure is coincident with the settling surface. However, there were occasions when this point preceded the settling surface. The absence of pore pressure data after 369 hours during experiment IM09 was due to an electronic fault in the pore pressure measuring apparatus.

4.6 Geophysical Experimental Results.

4.6.1 INTRODUCTION.

The geophysical data presented below represent cursory coverage of that actually recorded. Geophysical data presented as a function of time and height, as it stands, are of limited use. In order to fully appreciate the relationship of geophysical behaviour as a function of soil properties, this invariably requires an element of data analysis. As a consequence, the data will be presented in a much more comprehensive form later in the thesis (chapter 6).

Experiment IM06 compared the results of the instrumented settling column with those of the Jackson porosity cell (Schultheiss 1983) in an effort to validate the column apparatus as a geophysical tool. These data will also be presented in chapter 6.

4.6.2 SHEAR-WAVE RESULTS.

In an experiment to investigate shear wave propagation in soft soils (Experiment IM05), a sediment slurry of initial bulk density 1168 kg/m^3, was instantaneously dumped into the instrumented sedimentation column. Shear waves were propagated into the sediment at roughly 5 hourly intervals. Unlike Shirley and Hampton's (1978) experiments in kaolinite, shear waves could not be observed immediately; it was not until 50 hours had elapsed that the first shear waves were observed, initially at the very base of the column. In agreement with Shirley and Hampton's (1978) observations, the waves were of very low amplitude (figure 4.7), having velocities between 1-2 m/s which corresponded to a density of 1244 kg/m^3 and voids ratio 5.5.

The problems associated with measuring small amplitude shear waves are illustrated by figure 4.7. In this case while the shear wave transducers initially had approximately 20cm of
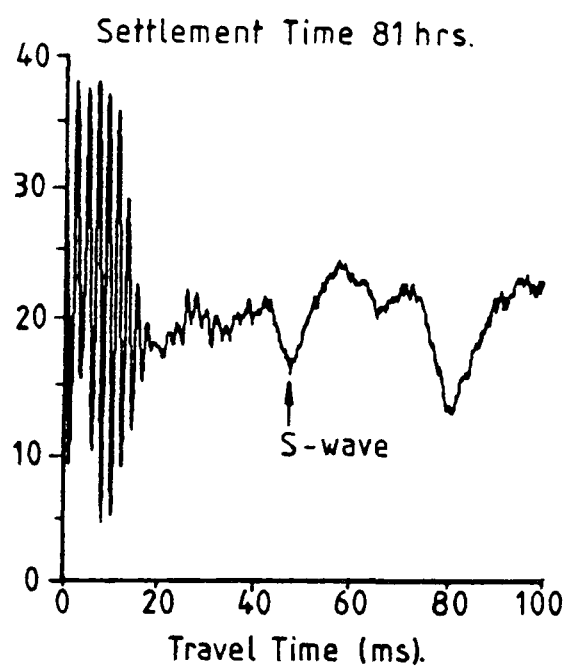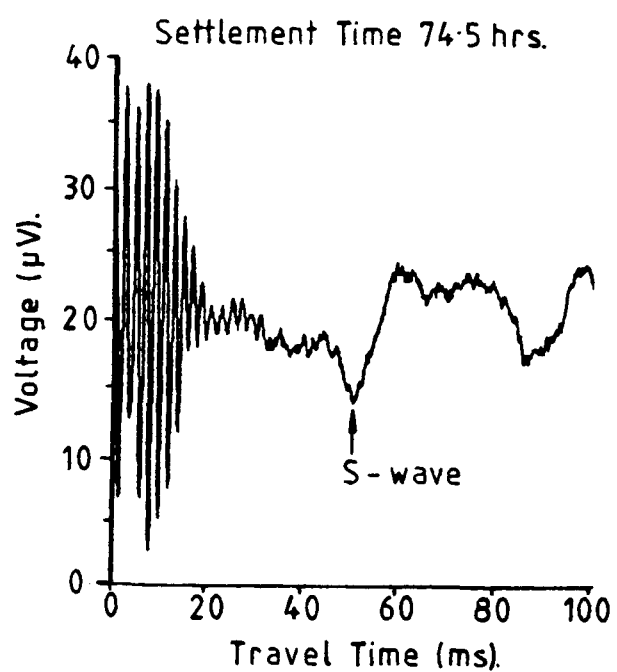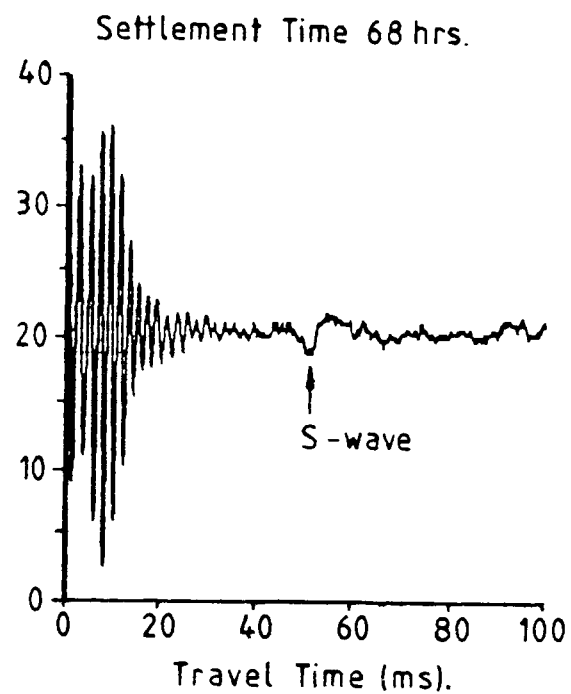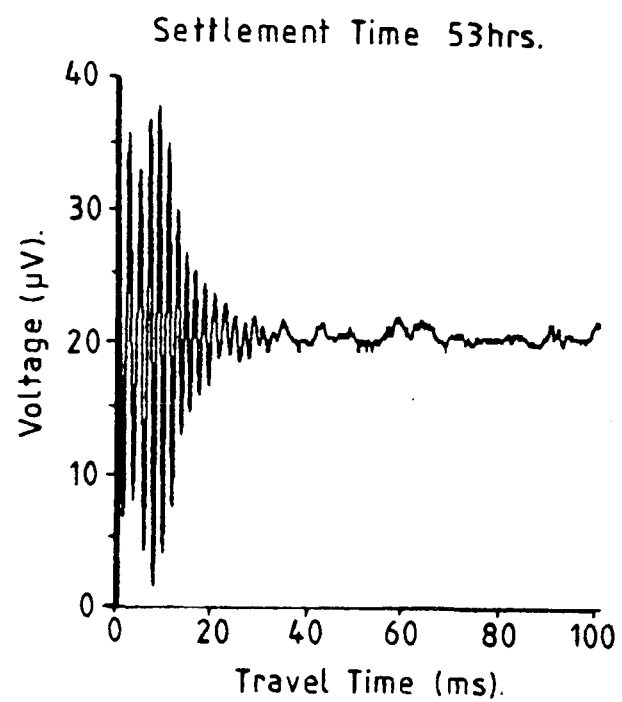
Figure 4.7   Shear wave evolution showing the development
of the soil matrix.

overburden above them, this overburden decreased slowly with time as the sediment consolidated. For the signatures presented in figure 4.7, the signals have been filtered through a 100Hz to 1MHz bandpass filter and subsequently amplified by 60dB. No signal averaging was performed in this series of measurements. The negative going trough was believed to represent the shear wave. It is argued that the wave propagates at a depth that would discount it being a surface wave, and is too slow to represent a wave propagating in the column frame. In addition the wave is not visible on the 53 hour record only appearing after 68 hours of sediment consolidation. The wave is seen to increase in amplitude and travel time across the column. This is coincident with increasing soil bulk density as would be expected in the case of a shear wave. The high frequency signal recorded in the initial part of each trace was believed to be the compressional wave generated by the shear wave transducer, and travelling both in the sediment and in the column frame itself.

Occasionally, in the early phase of settlement the shear wave propagating through the sediment, appeared suddenly to deteriorate and vanish giving rise to the suspicion that either the transducer motion or the propagating shear wave itself was destroying the fragile soil matrix. The decision therefore of whether or not to make a shear wave measurement during the early stages of an experiment was always a tantalizing one and it is recommended here that shear wave measurements be avoided until a period of 50 hours has passed. Additionally, it is advised that observations should commence at the bottom transducer gradually working up the column.

A set of shear wave velocity versus height and time measurements are shown in figures 4.8 and 4.9. Figure 4.8 demonstrates the changing V_s gradient as consolidation progresses. At the initial, measurement time of 53.4 hours shear waves are recorded only at the base of the column. After 91.5 hours, the velocity appears to be approximately uniform
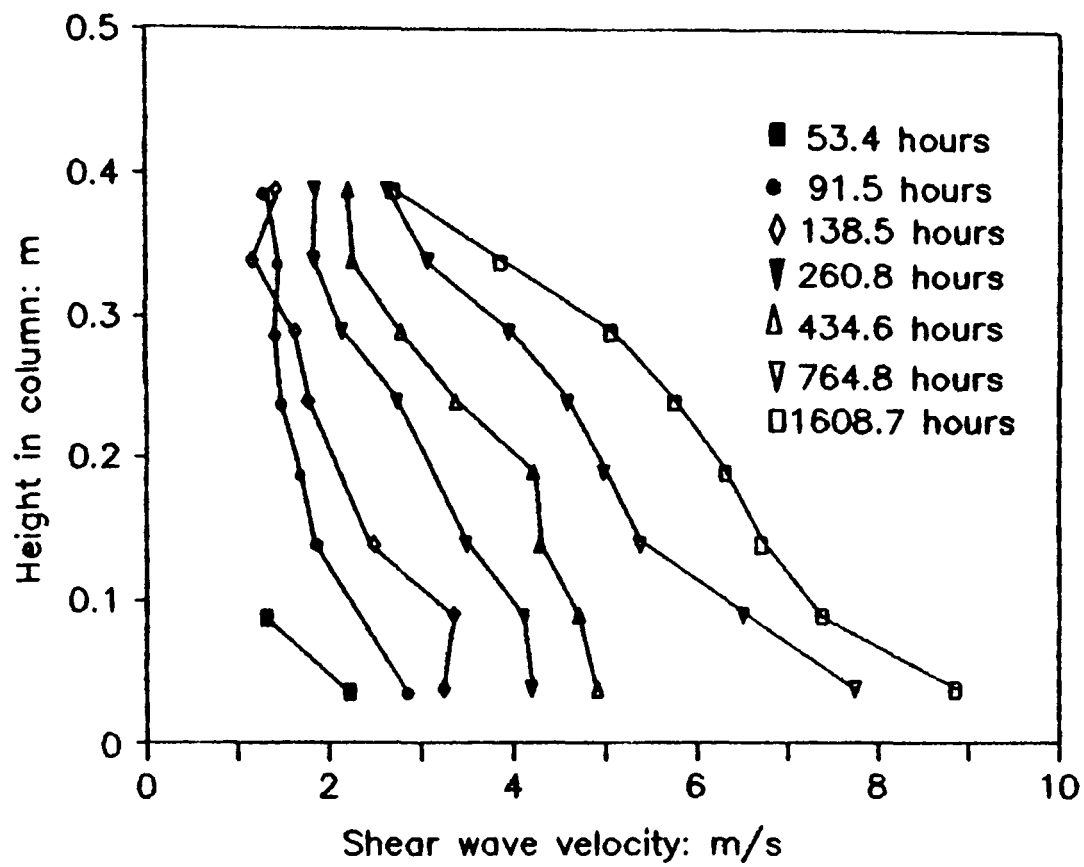
Figure 4.8   Shear wave velocity versus column height.
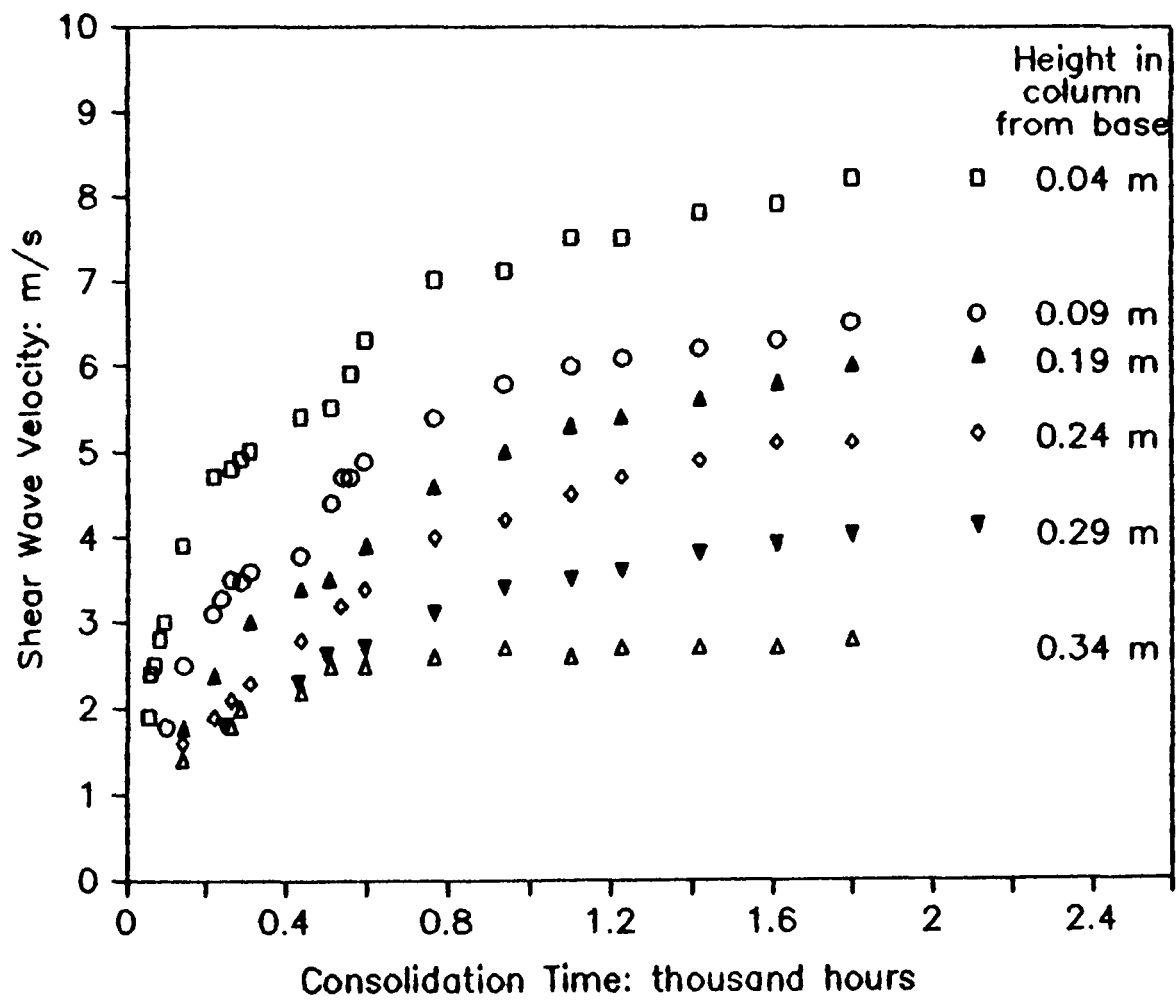
Figure 4.9   Variation of shear wave velocity with consolidation time.

throughout the sediment column. V_s appears to increase more rapidly in the lower part of the column giving rise to a distinct velocity gradient develops.

The development of a V_s gradient with consolidation time is illustrated by figure 4.9. The initial shear wave velocity was always found to be between 0.6 and 2 m/s, the waves themselves were of low amplitude. With time and increasing overburden pressure, the S-waves rapidly increased in both velocity and amplitude. These gradients remain distinct and separate illustrating V_s dependence upon overburden. The sharp gradient gradually levels off as the shear wave velocity tends towards some equilibrium value.

4.6.3   COMPRESSIONAL WAVE VELOCITY.

Compressional wave velocity was recorded as a function of sediment height and time. A typical velocity profile is shown in figure 4.10. Here the velocity is compared to the coincident bulk density profile. From this figure it can be seen that the velocity inversion correlates well with the density inversion between 0.2m and the base of the column. The compressional wave velocity falls below the expected V_P for water in the low density region of the soil i.e. between the sediment/water interface and 0.25m. This is due to the nature of the V_P-porosity relationship in high porosity soils, shown in figure 2.2 and discussed in more detail in chapters 6 and 7.

4.7 Summary

A laboratory experimental technique has been described which has been successful in monitoring P-wave and S-wave velocities, soil electrical resistivity, pore pressure dissipation and bulk density. This was carried out in a number soft soil samples consolidating under self weight. The soil samples used in the experiments originated from the Irish Sea and include a variety of sediment types ranging from clays to mud.
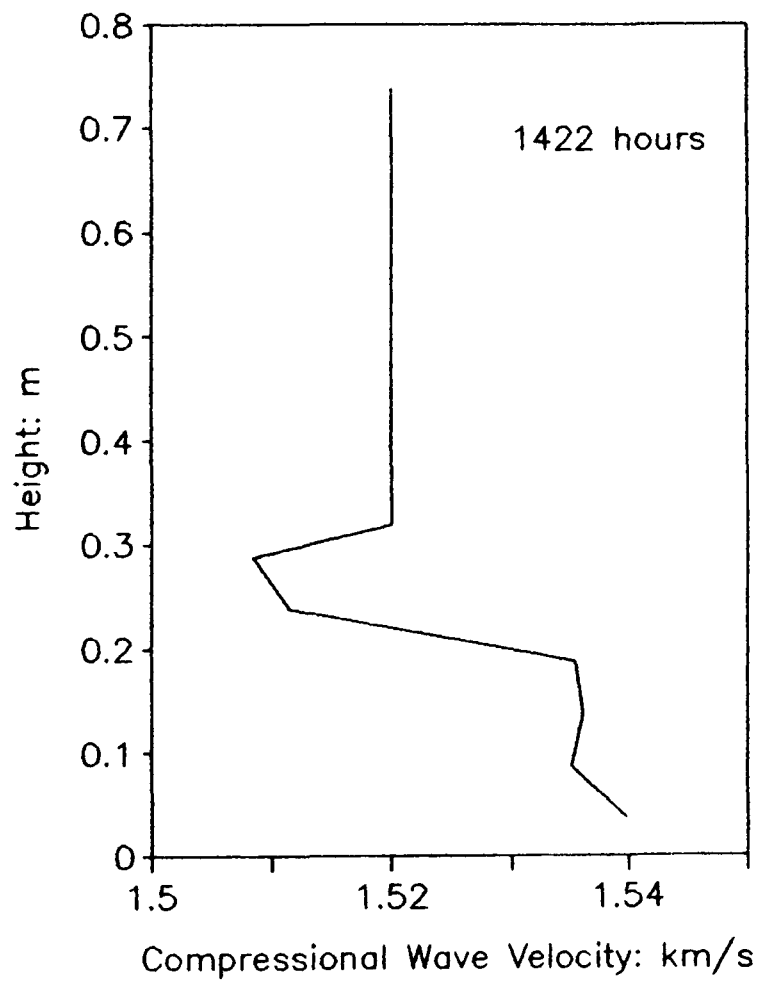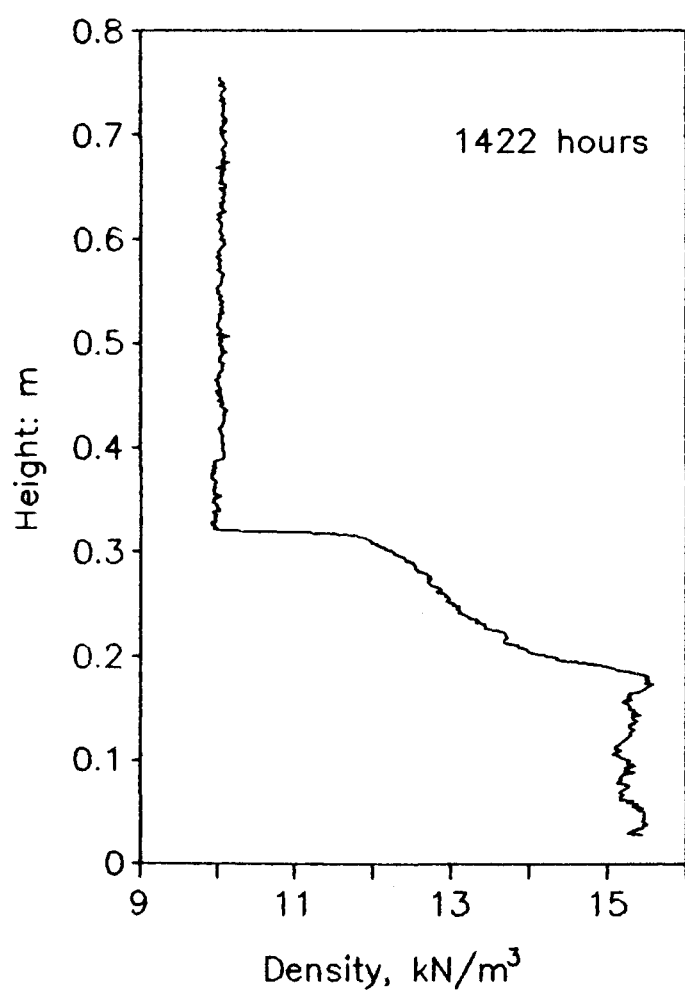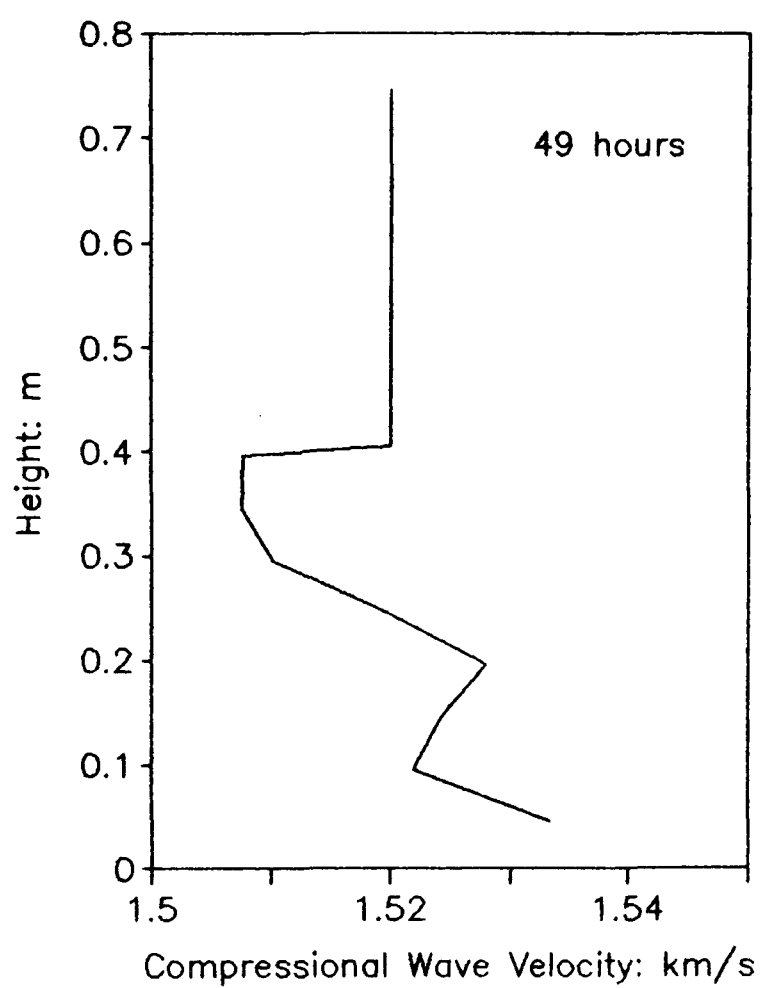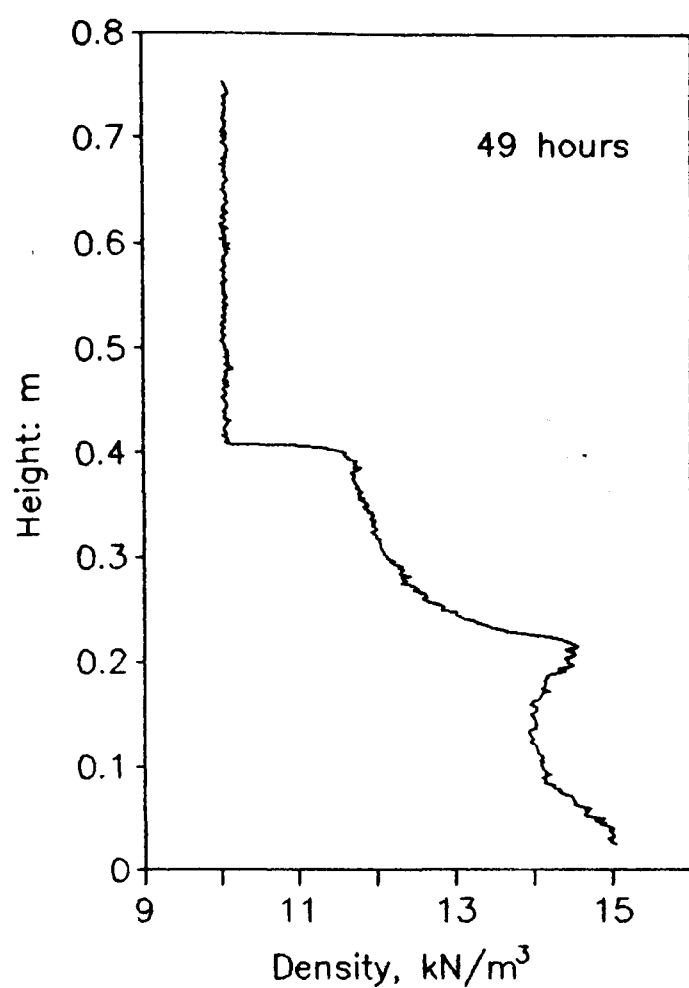
Figure 4.10 Comparison of Velocity and Density Profiles.

Expt. Ref.	Slurry initial conditions				Expt. Duration (hours)	Soil Type	Sp. Gravity	Fluid Density kg/m³	Comments Tests: D=density, U=pore press. P=P-wave, S=S-wave, R=resistance
	Initial Height (m)	Initial Density kg/m³	Initial Voids Ratio	Total Stress (kPa)					
IM03	0.990	1135	11.64		23	Clay	2.706	1000	Prototype column (D,P)
IM04	0.990	1168	10.61		1244	Clay	2.718	1000	Prototype column (D,P)
IM05	0.990	1168		1.389	283	Silty clay		1.025	Experiment to investigate shear (P,S,R) propagation in soft soil
IM06						Sand	2.65	1.025	Apparatus verification expt. (D,P,S,R)
IM07	0.990	1130	14.94	1.034	2373	Clayey silt	2.665	1.024	(D,U,P,S,R)
IM08	0.990	1160	11.54	1.321	2113	Clayey silt	2.665	1.024	(D,U,P,S,R)
IM09	0.861	1248	6.615	1.909	1596	Silty clay	2.684	1.025	(D,U,P,S,R)
IM10						Silty clay			piston experiment (D,U,P)
IM11	0.956	1158	11.758	1.238	5427	Mud	2.643	1.025	(D,U,P,S,R)

TABLE 4.1 Details of Column Experiments.

Preliminary geotechnical results indicate that the soils investigated behave in much the manner described by previous authors (Gaudin and Fuerstenau 1958, Krone 1962, Einsele et al. 1974, Been 1980, Been and Sills 1981, Elder 1985, Bowden 1989). Complete dissipation of excess pore pressures within the soils occurs over a time scale of hundreds of hours as documented by Einsele et al. (1974) and Been (1980). The time taken for the completion of primary consolidation appears to be governed by sediment type but does not seem to be affected by the slurry's initial density. The settling behaviour however, is greatly influenced by the initial density as reported by Elder 1985. The bulk density discontinuities first reported by Gaudin and Fuerstenau (1958) were observed in these samples and included a notable density inversion in the mud sample experiment, a phenomena observed by Elder (1985).

Preliminary geophysical results indicate that the soils under study here are capable of supporting shear wave propagation. The fact that shear wave propagation was not recorded immediately in the initial sediment slurry suggests that the soil particles and flocs undergo a period of soil fabric development before shear wave propagation can occur (a period of approximately 50 hours in this series of experiments). Initially the shear waves are of very low amplitude having velocities of between 1-2m/s, velocity increasing as the soil develops (in agreement with Shirley and Hampton's (1978) observations). Observed compressional wave velocities were typical of high porosity sediments as previously described by Urick (1947) and Hampton (1967), and are found to correlate well with the bulk density measurements.

The implications of the geotechnical and geophysical results with respect to soft soil behaviour are now analysed in the remaining chapters.

CHAPTER 5   ANALYSIS OF CONSOLIDATION BEHAVIOUR

5.1 Introduction.

The soils geotechnical behaviour will now be analysed as it consolidates under its self weight. Analytical techniques previously used by Been (1980) and Elder (1985), enabling individual elements of the soil to be tracked with time, will be utilized here to determine the compression behaviour, and the permeability characteristics of the soil samples. A one dimensional finite-element consolidation program based upon the Lee-Sills model (1981) will be used to make predictions on the settlement curves and excess pore pressure dissipation profiles. Values of permeability and coefficient of consolidation obtained from the soft soil modelling will be used in the following chapter for comparison with those derived from the Biot model.

5.2 Surface settlement analysis.

The changing height of the surface of the slurry with the logarithm of time has already been shown in figure 4.2. It was noted then that the original density of the slurry appeared to control the form of settlement curve observed. Elder (1985) made similar observations and consequently carried out a detailed study of surface settlement in fresh water of a Combwich silty clay. Elder identified a critical slurry input voids ratio (e=12) above which a rapidly deposited soil would exist initially as a fluid supported suspension (as seen in experiments IM07, IM08 and IM11). For an initial voids ratio below the critical value, no such suspension phase exists and the sediment behaves immediately as a consolidating soil (as in experiment IM09). All but one of Elder's data sets involved fresh water settlement. Based on this single settling experiment in saline water Elder predicted that the critical voids ratio would increase for settlement in salt water. Within this thesis therefore, a study will be undertaken to obtain more data on settlement in salt water and to see if

Elder's prediction is correct.

The variation of surface void ratio with time for the current experiments are presented together with Elder's single data set (SW2), in figure 5.1. The behaviour of the surface sediments is very similar to that reported by Elder (1985) in fresh water. In sediment slurries deposited above the critical voids ratio (experiments IM07, IM08 and IM11), a suspension phase was observed in which the voids ratio increased with time. This is believed to be due to coarser soil particles settling out of suspension towards the base of the column. On reaching a peak, the surface suspensions voids ratio falls rapidly until the suspension surface reaches the consolidating layer beneath. The voids ratio at which this occurs was found to be 14.5 to 15. Following this a gradual decrease in surface voids ratio occurs over a much longer time scale. Sediment slurries introduced below the critical value experience no suspension phase and the surface voids ratio decreases slowly with time.

The results appear to show that settlement in salt water of the soils tested have a critical voids ratio of 11.54. Elder suggested that the settlement mechanism would be accelerated by increased floc interaction due to the salt water. However, comparing actual settling in a clayey silt sample (experiment IM08) to that predicted by Stoke's law for two particle radii (figure 5.2) little floc development is seen to occur in the surface suspension. To be sure of the effect of salt and fresh water, a comparative test would need to have been performed on the same batch of sediment.

Figure 5.1 Surface Voids Ratio changes in a settling soil.

Initial
Voids Ratio

▲ IM07: e = 14.88
◇ IM08: e = 11.03
▽ IM09: e = 6.61
□ IM11: e = 11.76
---- SW2 : e = 13

Voids Ratio

Time: hours
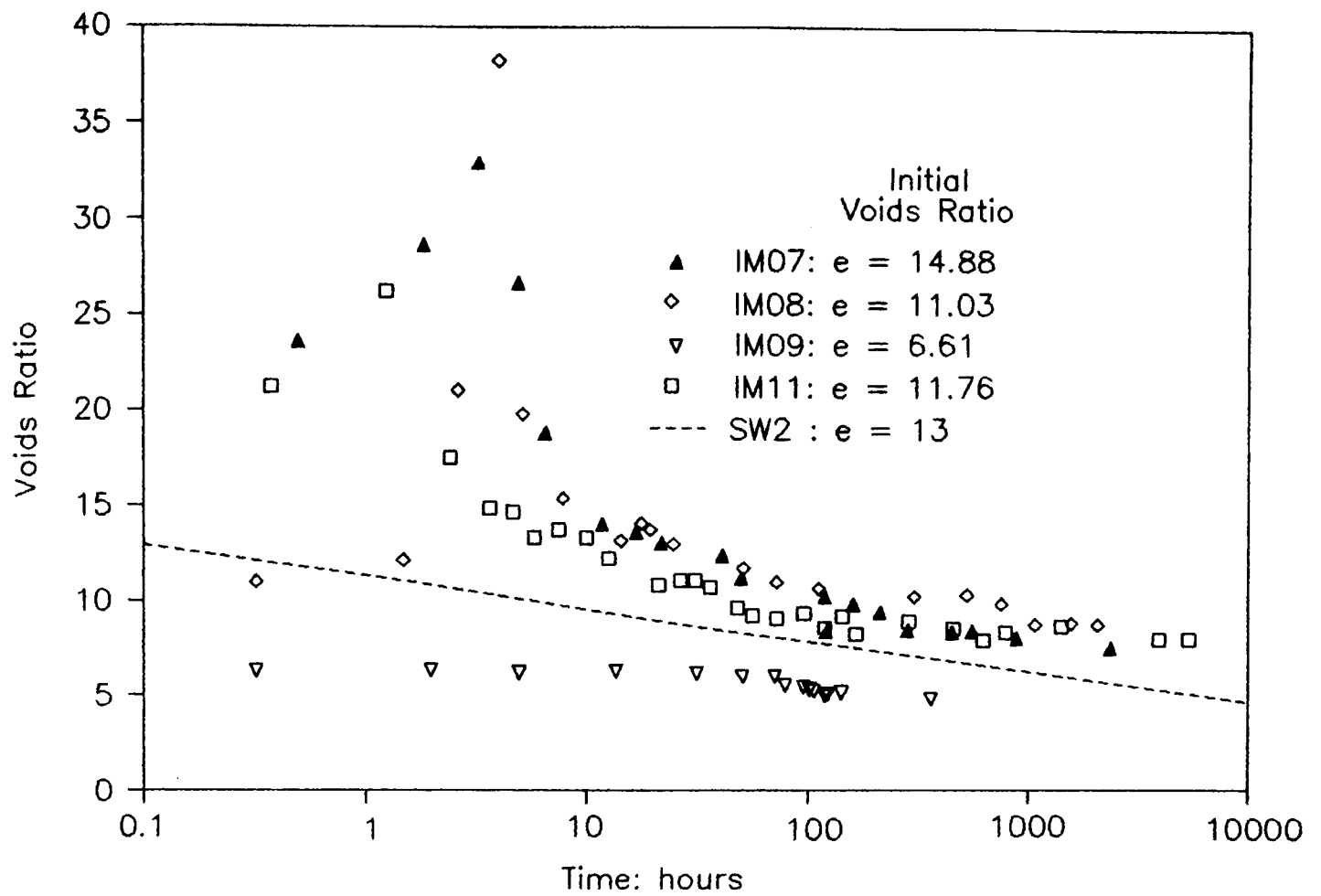
Figure 5.2 Stokes Settling in Experiment IM08.

particle radius
2.0um

particle radius
2.5um

Degree of Settlement

Time: hours
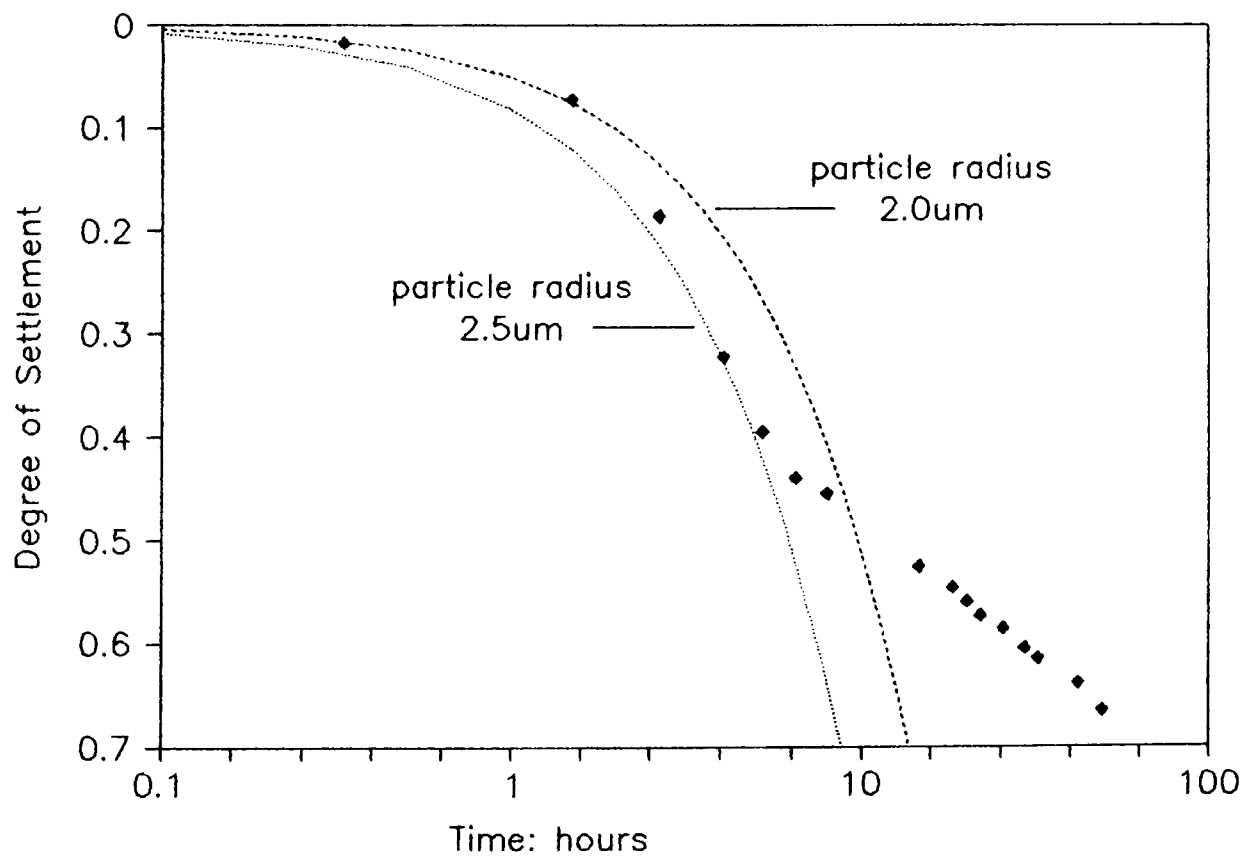
5.3 Compressibility.

In stiffer marine sediments (ie voids ratio's ≤ 2.2) the compressibility of the soil frame can be determined by analysing the decompression curve made during a standard oedometer test (Hamdi and Taylor Smith 1981). The lack of strength exhibited by soft marine soils (ie voids ratio's > 3) limits the use of such a test in order to determine frame compressibility. The frame compressibility (C_f') of soft soil was investigated using the surface settling curves discussed earlier using the relationship below (Smith 1978).

$$C_f' = \frac{\text{Total settlement}}{dp \times Z_0} \qquad\qquad (5.1)$$

where C_f' = Soil frame compressibility determined from surface settlement curves

dp = Change in loading pressure

= Total vertical effective stress

Z_0 = Total soil thickness

The results of these calculations are shown in table 5.2 at the end of this section.

Been (1980) and Elder (1985) showed that the compressibility of the surface sediments need not necessarily represent the frame compressibility of elements at different elevations within the soil. Surface settlement is easily measured and can be used to quantify soil compressibility. It was important to establish in what way the surface settlement derived compressibility represented the compressibility of the soil as a whole.

The soils compressibility may be determined from the differentiation of the voids ratio-vertical effective stress (e versus σ') relationship as described in appendix 1, the e versus σ' relationship being obtained from the experimental measurement of pore pressure and bulk density as described earlier. Making use of the analysis technique described by Been (1980) and Elder (1985), in which individual elements within the soil can be tracked, it is necessary to define a

normalized material co-ordinate, y, using the soil surface as a datum (figure 2.2 shown previously).

$$y = \frac{\text{mass of solids above the element}}{\text{total mass of solids present}} \qquad (5.2)$$

This may be re-written in terms of density and volume in the form:

$$y = \frac{\int_0^Z (\rho - \rho_w)\ dz}{\int_0^{Zo} (\rho - \rho_w)\ dz} \qquad (5.3)$$

The following diagrams show the voids ratio versus vertical effective stress relationship for this set of experiments. Within these figures the lines join elements of constant normalized material co-ordinate, y. The different symbols depict differing soil elements consolidation state at the same instant of time. Soils deposited above the critical density, namely experiments IM07, IM08 and IM11, are shown in figures 5.3 to 5.5. It appears the relationship between voids ratio and vertical effective stress observed by Been (1980) for Combwich soil similarly applies for the Irish sea soils studied here. A unique compression relationship exists for soils deposited above the critical voids ratio. It can be seen that at effective stresses close to zero, the soil can have a large range of void ratios (ranging from over 14 to a voids ratio of approximately 6). A transition is observed in the e versus σ' curve at a voids ratio between 6 and 7 in experiments IM07 and IM08 (figures 5.3 and 5.4), and between 5 and 6 in experiment IM11 (figure 5.5). Within this band of voids ratios the gradient of the e versus σ' curve becomes less steep and effective stresses begin to rapidly increase. This transition is believed to represent the development of a soil frame and which may prove of considerable interest in the shear wave propagation study described later.

Applying the limit $e \leq 6.5$ to the e versus σ' data and plotting a series of e versus Ln σ' plots in the manner of Tan et al. 1988 (shown in figures 5.6 to 5.8) the compressibility of the soil frame can be determined by differentiating the regression

Figure 5.3 Voids Ratio versus Vertical Effective Stress Relationship.
Experiment IM07;

y = 0.05

y = 0.2

y = 0.4

y = 0.6

y = 0.8

y = 0.95

Time
□   5 hours
◆   12 hours
△   42 hours
▽   119 hours
■   283 hours
◇   553 hours
▲   886 hours

Voids Ratio

Vertical Effective Stress: kPa
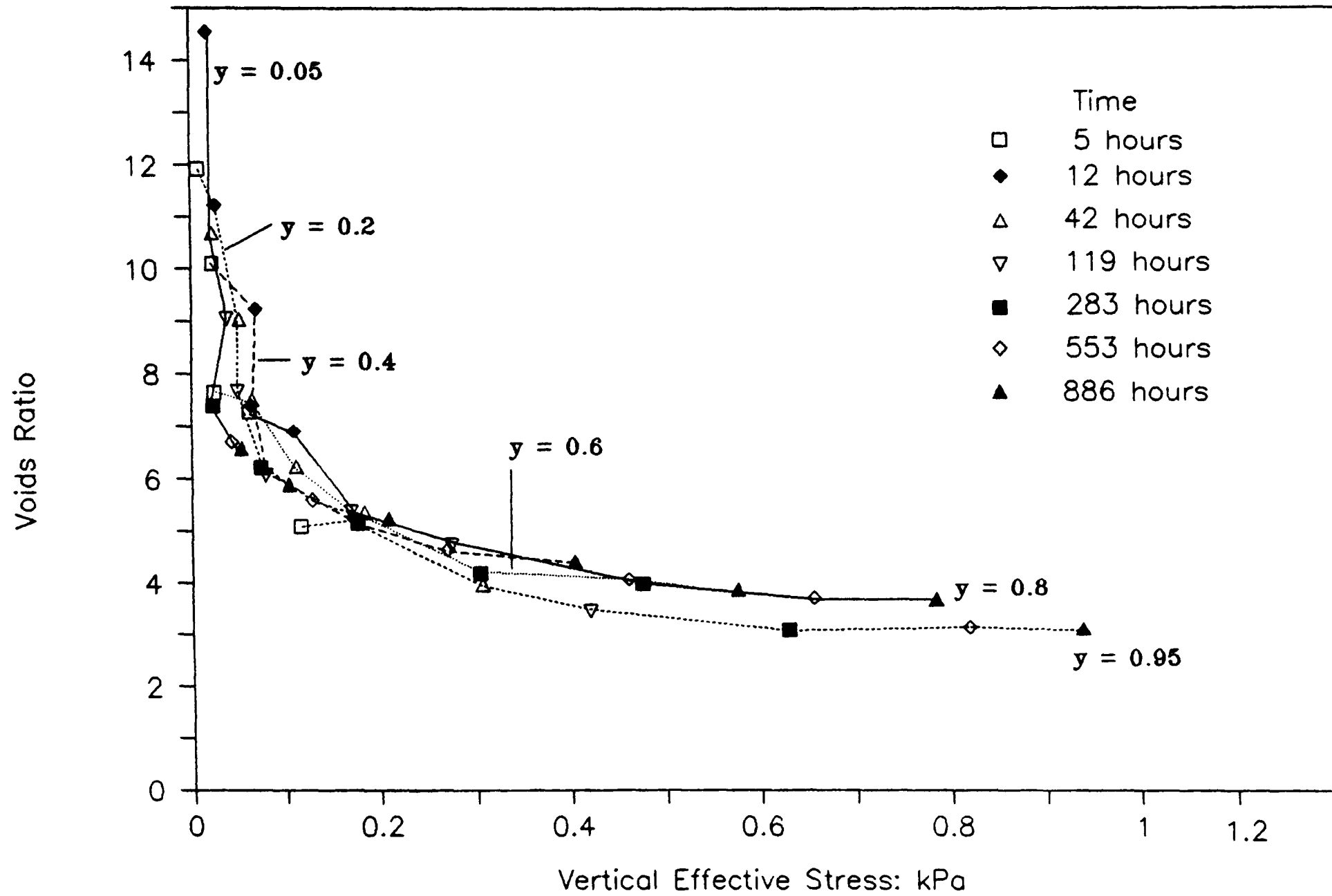
Figure 5.4   Voids Ratio versus Vertical Effective Stress Relationship. Experiment IM08.
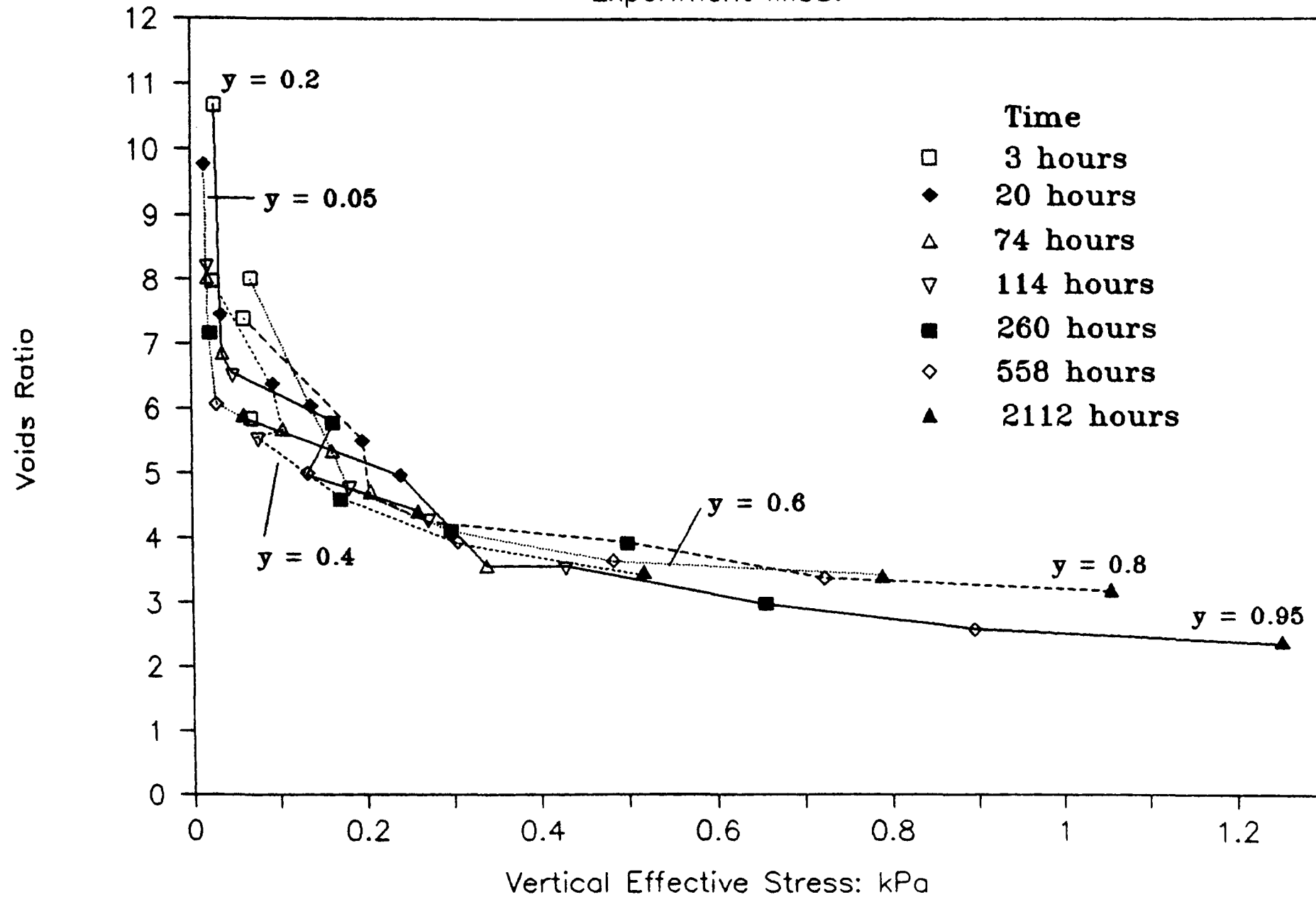
Figure 5.5   Voids Ratio versus Vertical Effective Stress Relationship.
Experiment IM11.
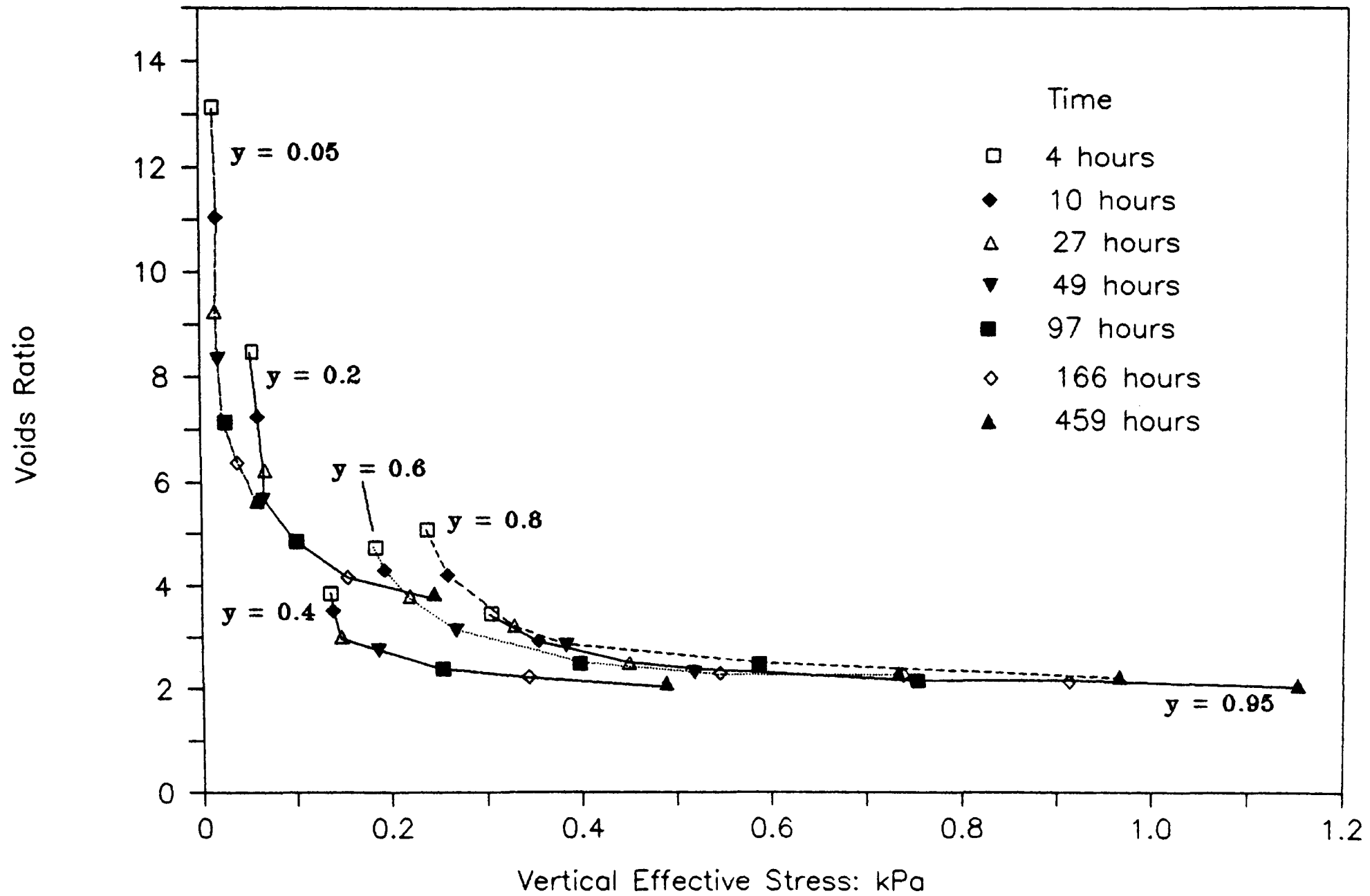
equations that best fit these data (shown in table 5.1). The frame compressibilities derived in this manner are compared to those derived from the surface settlement curves in table 5.2.

It will be seen from table 5.2 that the frame compressibility decreases with decreasing voids ratio. The compressibility range over two orders of magnitude from 10^{-3} to 10^{-5} Pa^{-1} for voids ratios ranging from 6 to 2. Hamdi and Taylor Smith's (1982), investigation of natural Irish Sea clay/silts recorded compressibilities of the order of 10^{-7} to 10^{-9} Pa^{-1} for voids ratios ranging between 2.0 and 0.6. The discrepancy in the value of C_f for comparative voids ratios is believed to be a result of ageing. The frame compressibility calculated from the surface settling curves do not represent an arithmetic mean value but rather some integrated value of the individual compressibilities of the soil elements.

The consolidation curves for soil elements in experiment IM09, an Irish Sea silty clay, are shown in figure 5.9. This soil, introduced at a voids ratio below the critical value (section 5.2), shows no unique compression relationship. The consolidation curves take on a completely different character to those discussed above. Initially effective stresses develop within the soil without any corresponding increase in voids ratio. Elder (1985) describes this period as one of floc and interfloc contact development. Following this initial phase of soil frame development, rapid compression occurs, each element within the soil following a separate but parallel compression line. A wide range of effective stress values may be associated with any value of void ratio which is indicative of time dependent compression or creep. This sample therefore gives an opportunity to study the effect of creep upon seismo-acoustic velocities, a subject to be treated in the following chapter.

Figure 5.6 Relationship between Voids Ratio and Vertical Effective Stress for an Irish Sea clayey silt: Experiment IM07.

$$e = 11.671 - 1.258 \, \text{Ln} \, \sigma'$$
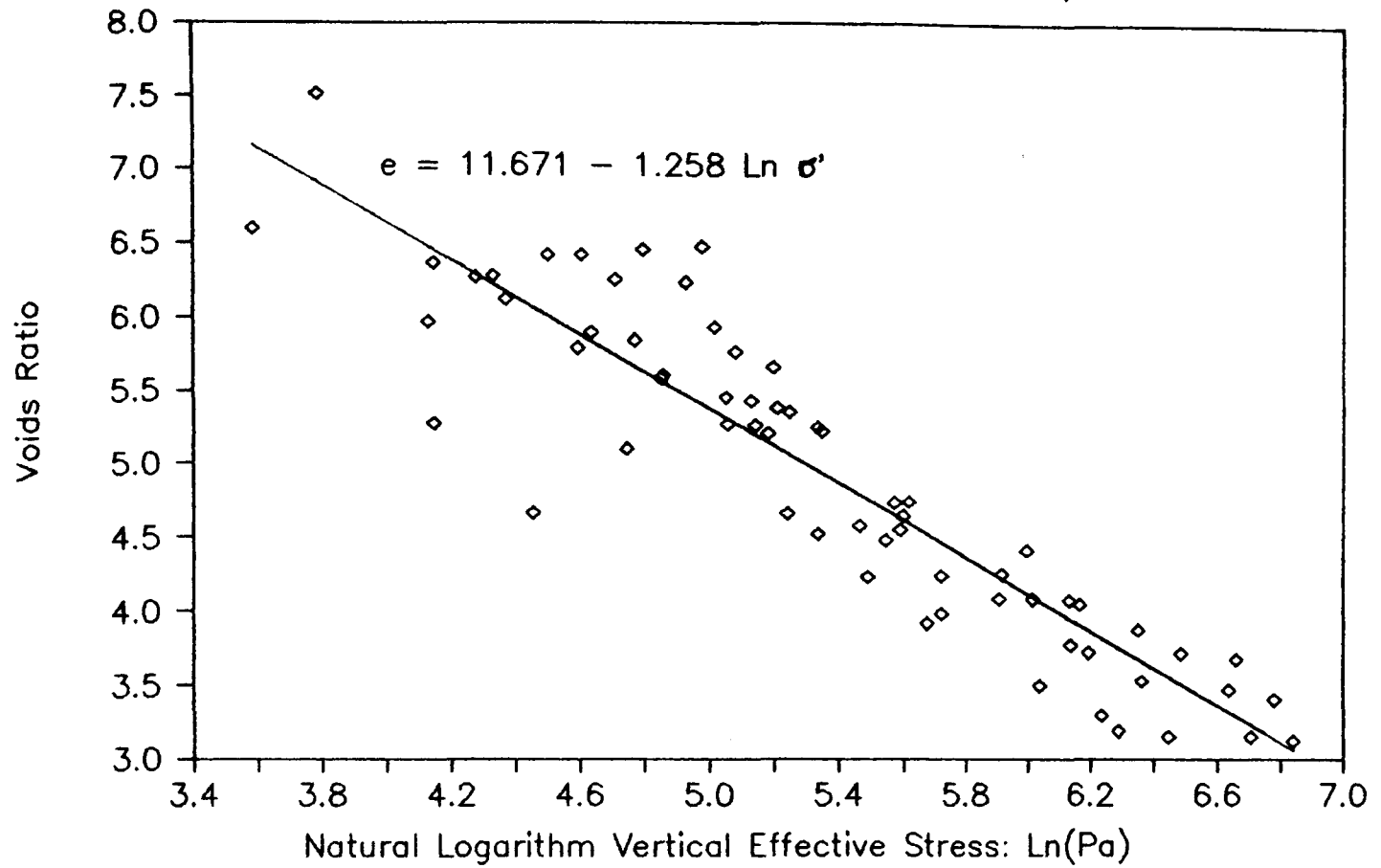
Figure 5.7 Relationship between Voids Ratio and Vertical Effective Stress for an Irish Sea clayey silt: Experiment IM08.

$$e = 10.340 - 1.089 \, \text{Ln} \, \sigma'$$
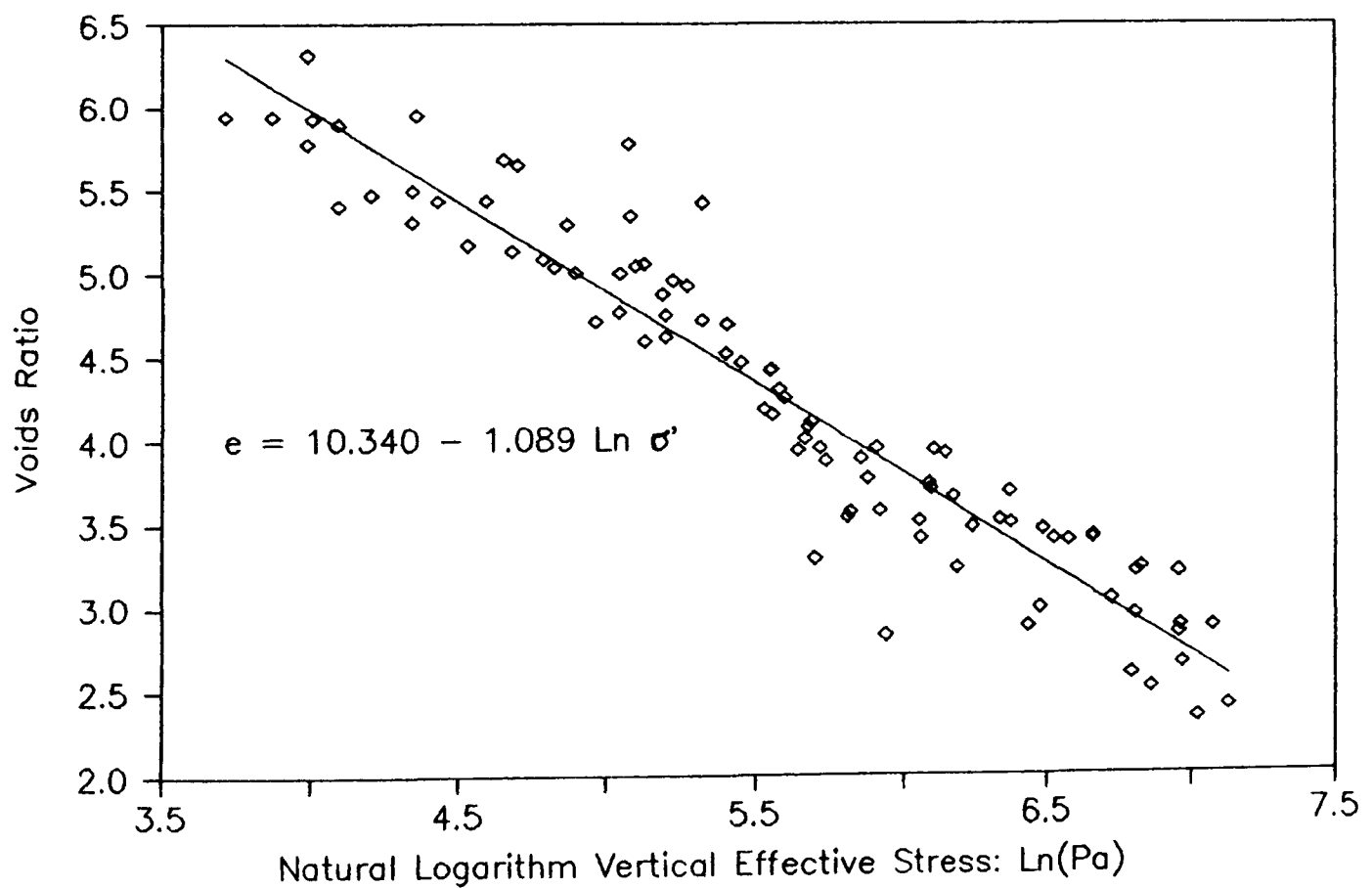
Figure 5.8 Relationship between voids ratio and effective stress.
for an Irvine Bay mud: Experiment IM11.

$$e = 26.0 - 6.89 \ln \sigma' + 0.497 \ln \sigma'^2$$

Voids Ratio

Natural Logarithm Vertical Effective Stress: Ln (Pa)
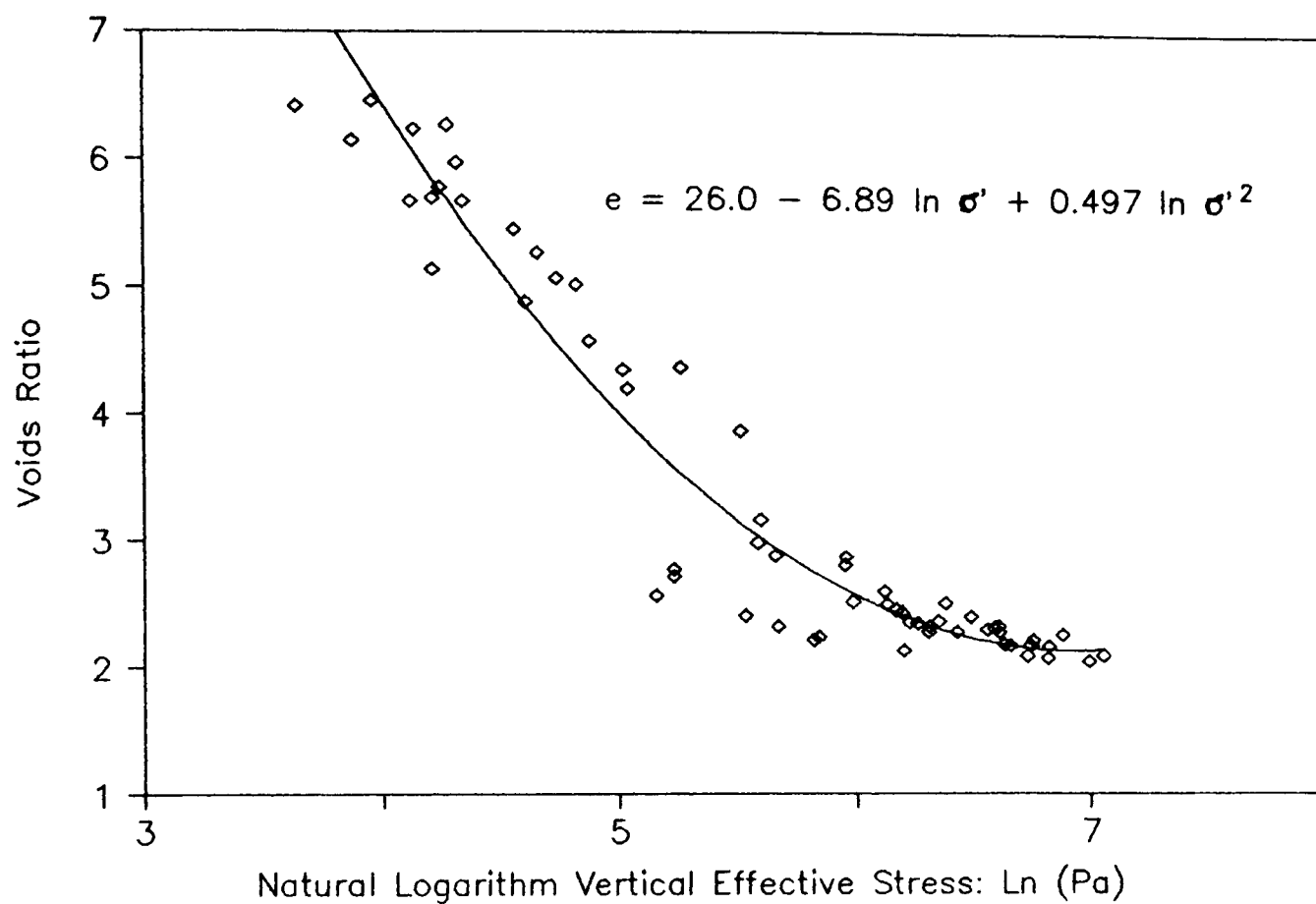
Figure 5.9 Consolidation Curves for Soil Elements in Experiment IM09.

Time

□ 1 hour
◇ 12.5 hours
△ 53 hours
▽ 369 hours

y=0.2
y=0.4
y=0.6
y=0.8
y=0.9

Voids Ratio

Vertical Effective Stress: kPa
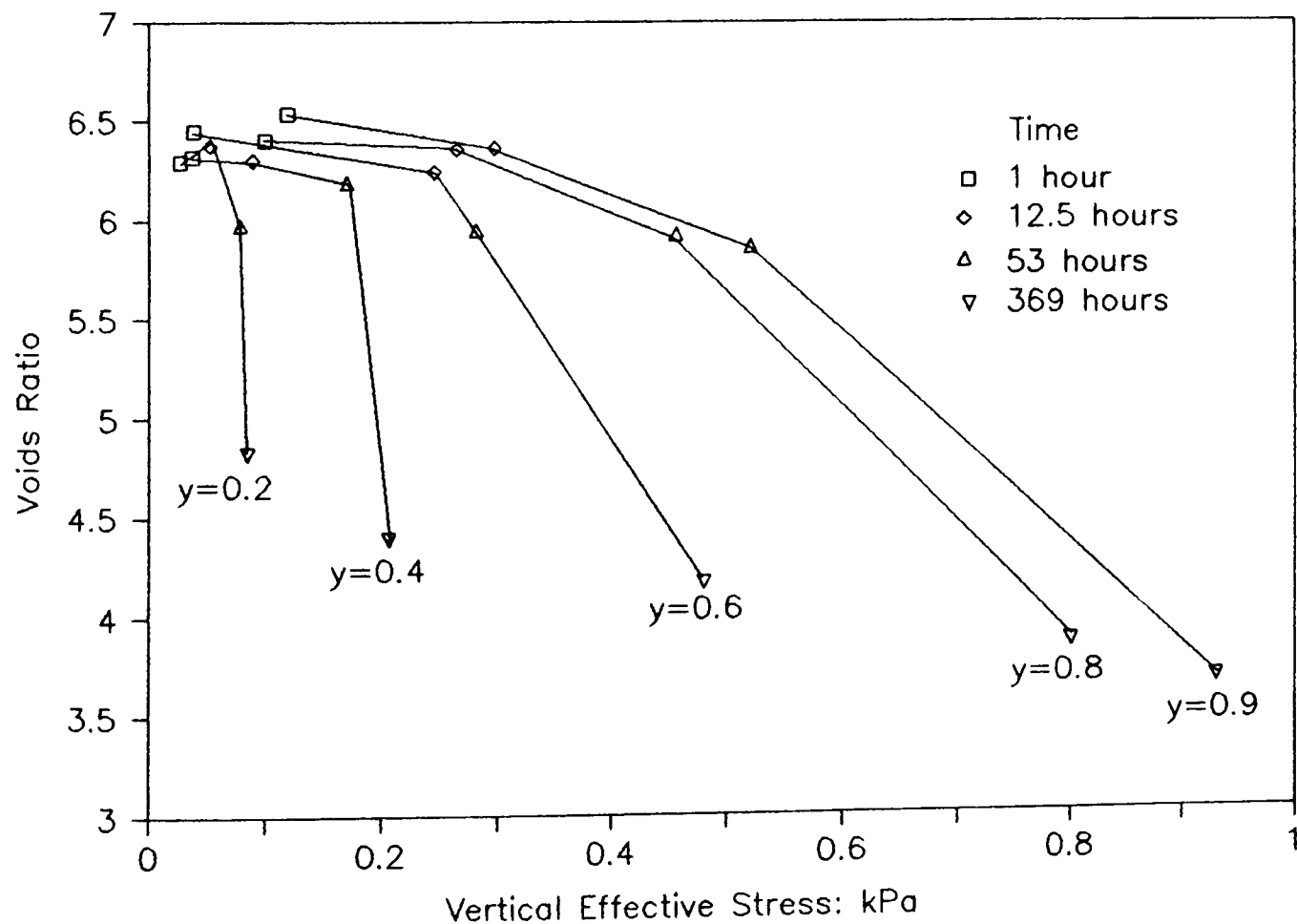
Table 5.1 Showing Voids Ratio versus Vertical Effective Stress
Empirical Relationships.

Expt. Ref.	Regression Line	Limit	R-sq	N
IM07	$e = 11.67 - 1.26 \ Ln \ \sigma'$	$6.5 \geq e \leq 3$	83.9%	65
IM08	$e = 10.34 - 1.09 \ Ln \ \sigma'$	$6.5 \geq e \leq 3$	90.7%	90
IM11	$e = 26.0 - 6.89 \ Ln \ \sigma' + 0.50 \ Ln \ \sigma'^2$	$6.5 \geq e \leq 1.9$	92.9%	59

where e = voids ratio

σ' = vertical effective stress

R-sq = coefficient of correlation

N_N = Number of observations

Table 5.2   Calculated Frame Compressibility.

Expt. Ref.	Voids Ratio	Frame Compressibility C_f	Error in C_f	Settlement Curve Estimate
IM07	6	$8.70 \times 10^{-4} \ Pa^{-1}$	±4.5%	$5.56 \times 10^{-4} \ Pa^{-1}$
	3	$8.02 \times 10^{-5} \ Pa^{-1}$	±4.5%	
IM08	6	$1.61 \times 10^{-3} \ Pa^{-1}$	±1.2%	$4.37 \times 10^{-4} \ Pa^{-1}$
	3	$1.02 \times 10^{-4} \ Pa^{-1}$	±1.2%	
IM11	6	$4.73 \times 10^{-3} \ Pa^{-1}$	±1.0%	$3.81 \times 10^{-4} \ Pa^{-1}$
	4	$8.31 \times 10^{-4} \ Pa^{-1}$	±1.0%	
	2	$1.10 \times 10^{-4} \ Pa^{-1}$	±1.0%	

5.4 Permeability.

The permeability, k, of the consolidating soft soil can be determined using the experimentally derived bulk density and pore pressure data (obtaining k from bulk density and pore pressure measurements is described in appendix 1). Figures 5.10 to 5.13 show permeability plotted against voids ratio. The plots demonstrate that an approximately linear relationship exists between the logarithm of permeability and voids ratio of the soil. the apparent trend is for permeability to decrease with decreasing voids ratio but any single value of voids ratio may have a range of permeabilities associated with it. It can also be seen that elements within the same soil mass may have quite different permeability histories. Such observations may be explained by the differential settlement of the soil particles, coarser grains appearing towards the column base, finer grains remaining closest to the sediment surface. Figure 5.12 relating to experiment IM11, an Irvine Bay mud, shows this effect quite distinctly. Here an upper layer comprising of less dense finer particles ($y=0.1$ and $y=0.2$) lies above a more dense basal layer. The end result is that the two layers demonstrate quite distinct k versus e characteristics.

The non-uniqueness of the permeability-voids ratio relationship poses a number of problems within the present application. Permeability has been measured in terms of moving soil elements, while the seismo-acoustic measurements are made at stationary points. The soil elements migrate past the seismo-acoustic measurement points, and as a result individual measured velocities represent different soil elements, which in turn exhibit quite different permeabilities. The simplest course to take at this juncture is to fit a best line to the permeability-voids ratio data, thereby introducing a unique, albeit artificial, k versus e relationship. The problem with this approach is that large error bands have now been induced in the empirical equation, as can be seen from the data below (table 5.3).

Figure 5.10   Permeability versus Voids Ratio: Experiment IM07.
Irish Sea clayey silt sample
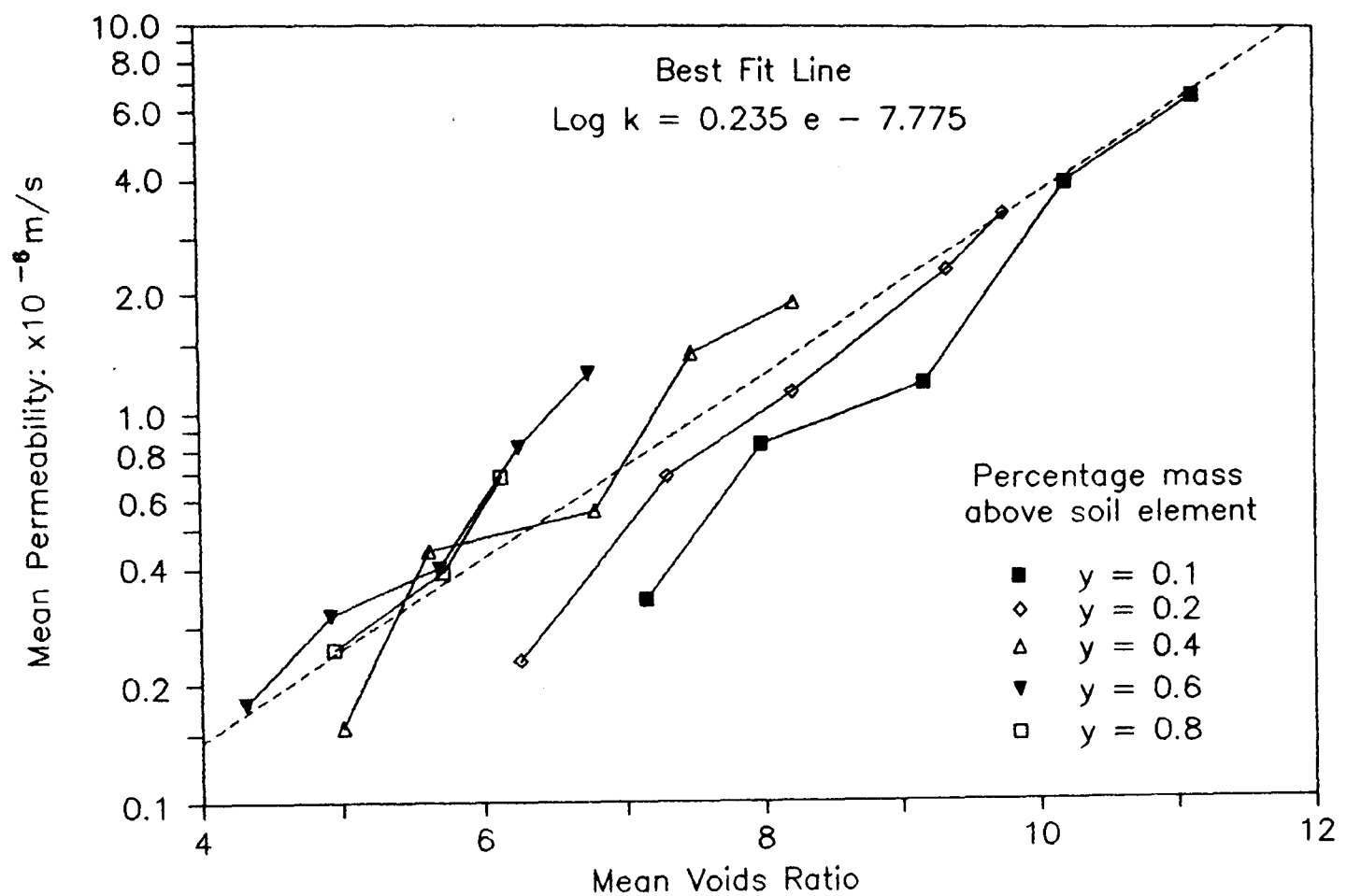
Figure 5.11   Permeability versus Voids Ratio: Experiment IM08.
Irish Sea clayey silt sample
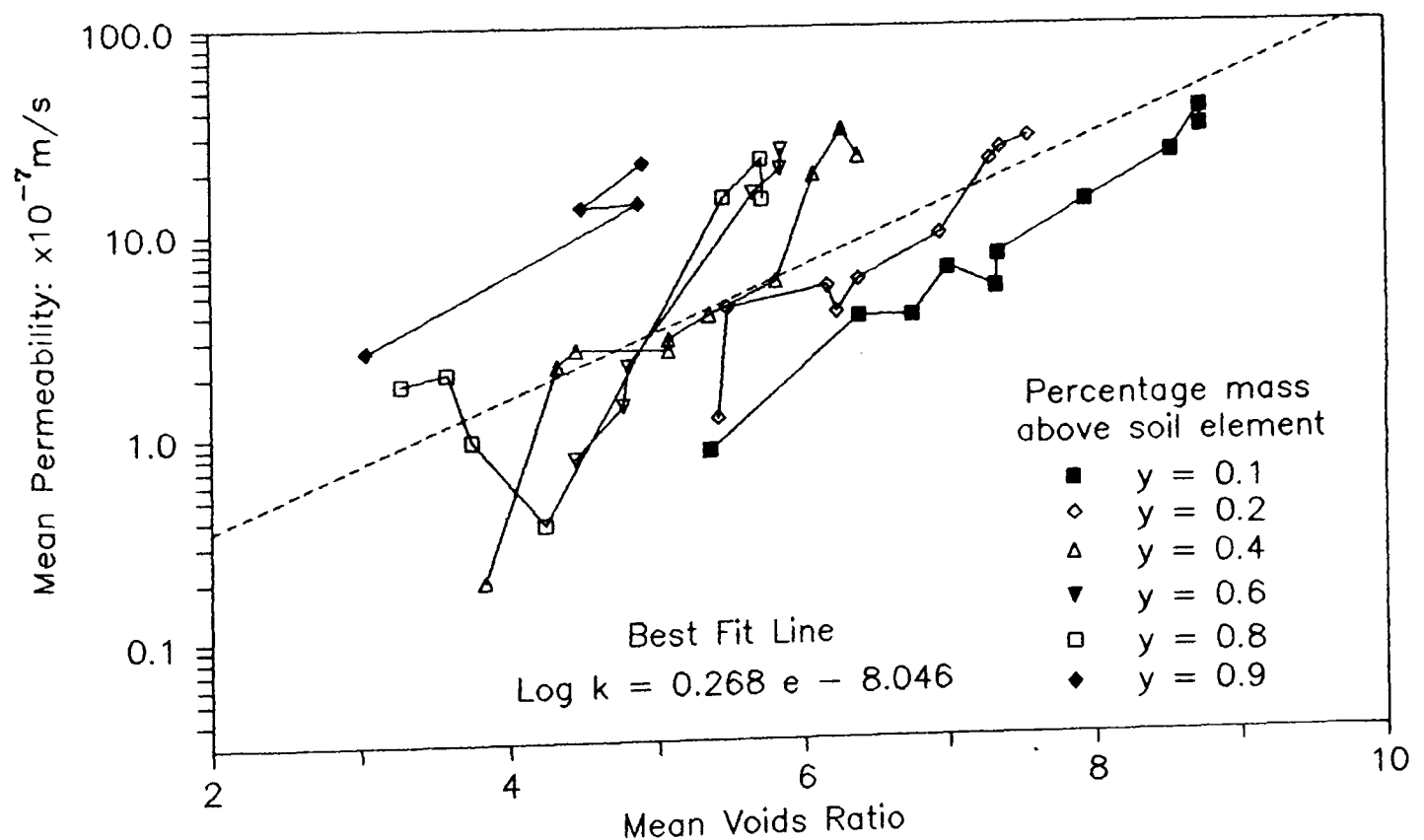
Figure 5.12 Permeability versus Voids Ratio: Experiment IM11.

Irvine Bay mud sample

Percentage mass
above soil element

■ y = 0.1
◇ y = 0.2
△ y = 0.4
▼ y = 0.6
□ y = 0.8
◆ y = 0.9

Mean Permeability: x10^{-6} m/s
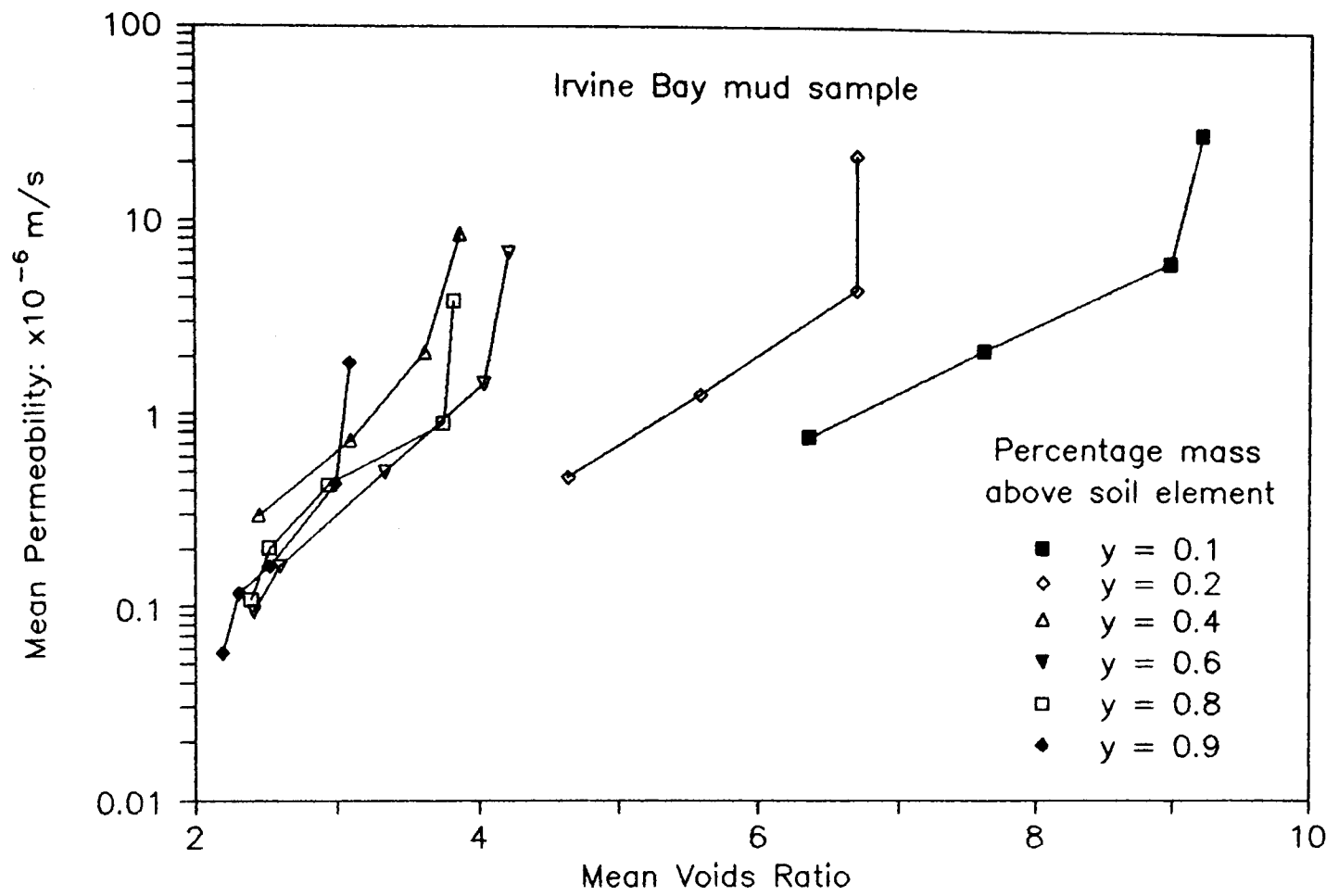
Mean Voids Ratio

Figure 5.13 Detail of Figure 5.12: Experiment IM11.

Irvine Bay mud sample

Best Fit Line
log k = 0.849 e − 8.950

Mean Permeability: x10^{-6} m/s
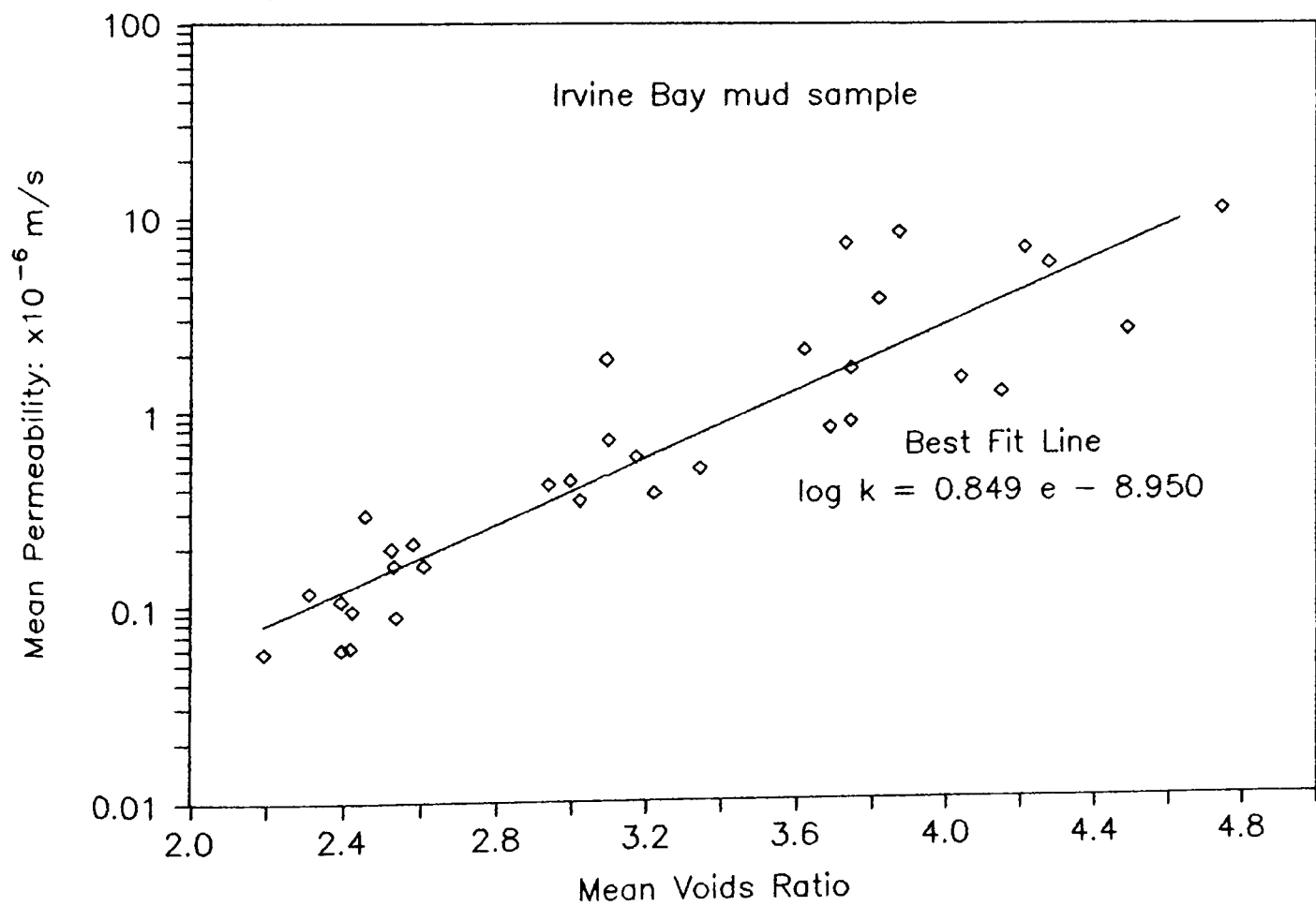
Mean Voids Ratio

Table 5.3   Permeability   versus   Voids   Ratio   Empirical
Relationship.

Expt. Ref.	Regression Line	Limit	R-sq	N_N	Error in log k
IM07	Log k = 0.235 e - 7.775	$11 \geq e \leq 4$	80.3%	39	±0.205
IM08	Log k = 0.268 e - 8.046	$9 \geq e \leq 3$	58.7%	37	±0.262
IM11	Log k = 0.849 e - 8.950*	$5 \geq e \leq 2$	83.1%	33	±0.292

where   e = mean voids ratio

k = mean permeability

R-sq = coefficient of correlation

N_N = Number of observations

* indicates that this equation is the best fit to data with normalized material co-ordinate $0.3 \geq y \leq 1.0$ as shown in figure 5.13.

5.5 The Coefficient of Consolidation.

5.5.1 INTRODUCTION.

The coefficient of consolidation C_c, has been determined using three different methods:

(a) By comparing the observed settlement to that predicted by the Lee-Sills model (1981).

(b) By comparing the excess pore pressure profiles to those predicted by the Lee-Sills model (1981).

(c) By direct calculation using Gibson et al. (1967) definition of the coefficient of consolidation:

$$C_c = \frac{-k}{\rho_w (1 + e)} \frac{d\sigma'}{de} \qquad (2.4)$$

5.5.2 SURFACE SETTLEMENT MODELLING.

The Lee and Sills consolidation model (1981) was used to make predictions of the degree of settlement of the soils under investigation. For an impervious base the settlement at any time is given by

$$S(T_F) = 1 - 4 \sum \frac{(-1)^N}{M^3 \pi^3} \exp(-M^2 \pi^2 T_F) \qquad (2.9)$$

where $\quad M \quad = \quad 0.5(2N + 1)$

$\qquad\qquad N \quad = \quad 0,1,2,\ldots\ldots$

where $\quad S(T_F) \quad$ = degree of settlement = $\dfrac{h(0) - h(T_F)}{h(0) - h(\infty)}$

$\qquad\quad h(0) \quad$ = initial thickness of sediment layer

$\qquad\quad h(T_F) \quad$ = thickness of sediment layer at T_F

$\qquad\quad h(\infty) \quad$ = final thickness of sediment layer

$$T_F \quad = \quad \frac{C_c \, t}{z^2_0} \qquad\qquad \text{= Time Factor} \qquad (2.7)$$

A major problem arises in defining $h(0)$ since there is no clear transition point between the settling and consolidating soil masses in experiments IM07, IM08 and IM11. The time taken for the settling phase, lasting up to 10 hours, means that effective stresses begin to develop and a density gradient created before the whole bed is deposited. The model, however, has no capacity to deal with a slowly deposited load, as occurs here, but rather demands an instantaneously dumped slurry of uniform density in a stress free state. The duration of the suspension phase is short however, compared to the consolidation process, therefore it is reasonable to assume that the state of the soil at the end of the settling phase can be used to model the initial conditions of the consolidation process, to a close approximation. The analytical solution (equation 2.9) requires the initial thickness $(h(0))$ and final thickness $(h(\infty))$ of the consolidating soil. It is possible that these values can be obtained from the surface settlement curves (figure 4.2) although the persistence of finer sediments in suspension may give an anomalous initial sediment thickness $(h(0))$. Another method, believed to be a superior approach, is based upon the

identification of a voids ratio at which the soil begins to exhibit effective stresses. Such a method requires the e versus σ' curves, shown in figures 5.3 to 5.5, to be studied and a value of voids ratio coinciding with the onset of rapid effective stress increase to be selected. In these experiments these values are taken to be:

> e=7   Experiment IM07
>
> e=6   Experiment IM08
>
> e=5.5   Experiment IM11

This value of voids ratio can now be used to estimate the height of the consolidating layer in the following manner:

By definition the voids ratio e

$$ e = \frac{V_{void}}{V_{solid}} = \frac{V_{total}}{V_{solid}} - 1 \qquad (5.4) $$

where V_{void} = volume of the voids

V_{solid} = volume of the solids

V_{total} = volume of the total

assuming the cross sectional area of the soil mass remains constant it is possible to re-write equation 5.4 as

$$ h_s = \frac{h_t}{(e + 1)} \qquad (5.5) $$

where h_s = height of solids

h_t = height of sediment

Within the column the height of the solids will remain constant and can be derived by using the initial conditions of the slurry, i.e. time zero of the experiment. Estimating the voids ratio e_i from the e–σ' curves for the onset of primary consolidation, the equivalent sediment height h_i can be calculated. This is the initial sediment height to be input into the model.

$$ h_i = h_s (e_i + 1) \qquad (5.6) $$

By way of illustrating this method, the model initial height h_i will be determined for experiment IM08 shown below.

88

Initial slurry conditions as given in table 4.1:

initial voids ratio $e = 11.54$

initial height $h_t = 0.990$ m

The height of the solids is given by equation 5.5

$$h_s = \frac{h_t}{(e + 1)} = \frac{0.990}{(11.54 + 1)} = 0.079 \text{ m}$$

The voids ratio at which the vertical effective stresses take effect is estimated from equation 5.6 to be

$e_i = 6.5 \pm 0.5$

from figure 5.4, and therefore

$h_i = h_s (e_i + 1) = 0.079 (6.5 + 1)$

$= 0.592 \pm 0.040$ metres

Having arrived at the input parameters (shown on figures 5.14 and 5.16) the Lee-Sills consolidation model can be used to solve for surface settlement for changing time factor T_F in equation (2.9). Although this analytical solution now takes on an empirical nature, the agreement between the model and the observed settlement is reasonably good as can be seen in figures 5.14 to 5.16.

Although the Lee-Sills model does not take into account the effects of creep behaviour, it was felt appropriate to compare the model to the data set of experiment IM09. The model agrees well with observed settlement as shown in figure 5.17. An average coefficient of consolidation was determined for the experiment using equation 2.7, and was found to be $6.5 \times 10^{-7} \text{m}^2/\text{s}$. In order to show that this was not a unique result, results from Elder's (1985) experiment 10, were also modelled (figure 5.18).

The results of this section is shown in table 5.5 (section 5.5.5) where the computed coefficients of consolidation are compared to other methods of derivation.

Figure 5.14 The Lee and Sills Model for Surface Settlement.

Experiment IM07.
(Irish Sea clayey silt)

Model Parameters

$h(0) = 0.527m$
$h(\infty) = 0.360m$
$C_c = 1.1 \times 10^{-7} m^2/s$
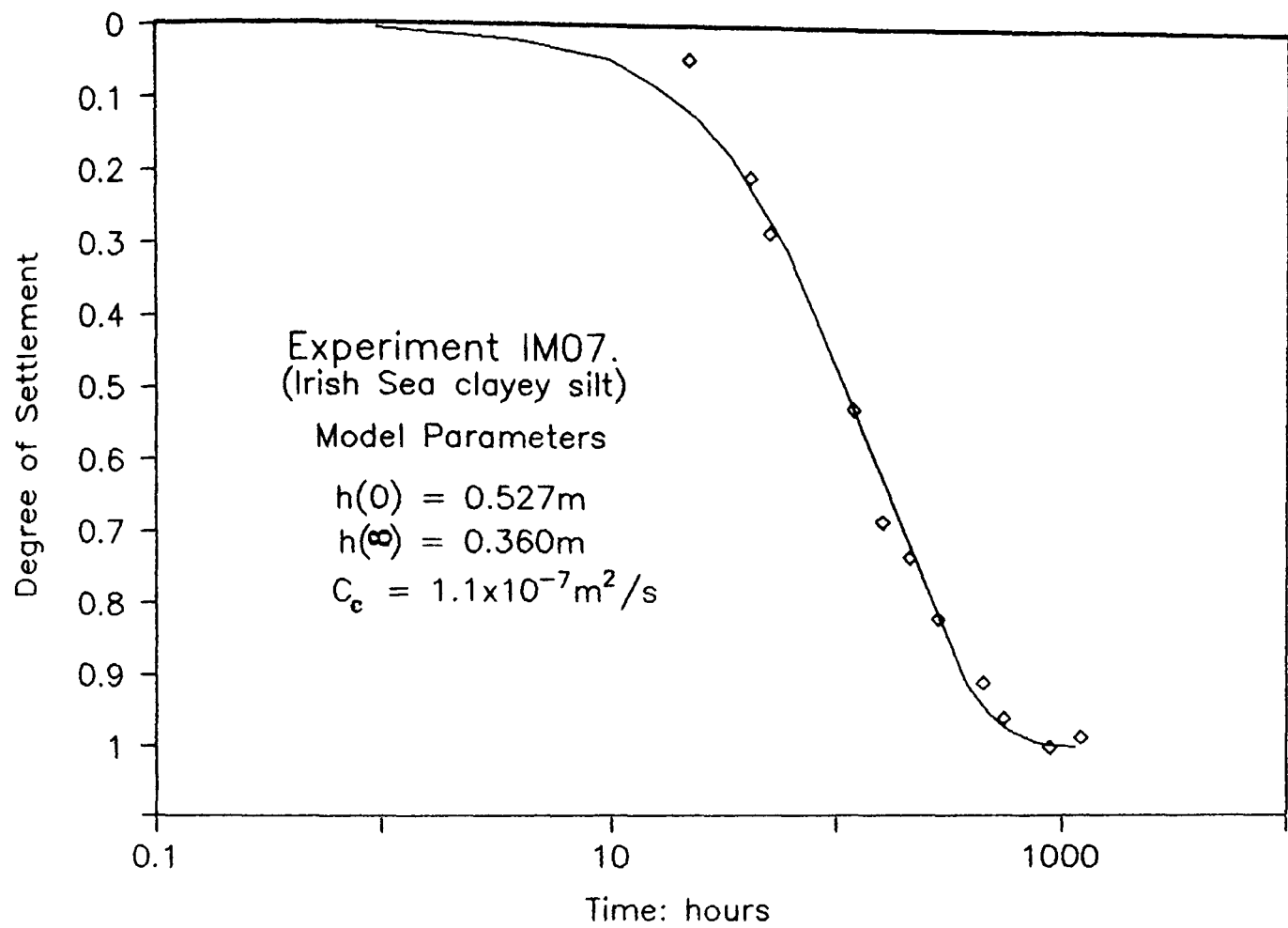
Figure 5.15 The Lee and Sills Model for Surface Settlement.

Experiment IM08.
(Irish Sea clayey silt)

Model Parameters

$h(0) = 0.592m$
$h(\infty) = 0.408m$
$C_c = 1.1 \times 10^{-7} m^2/s$
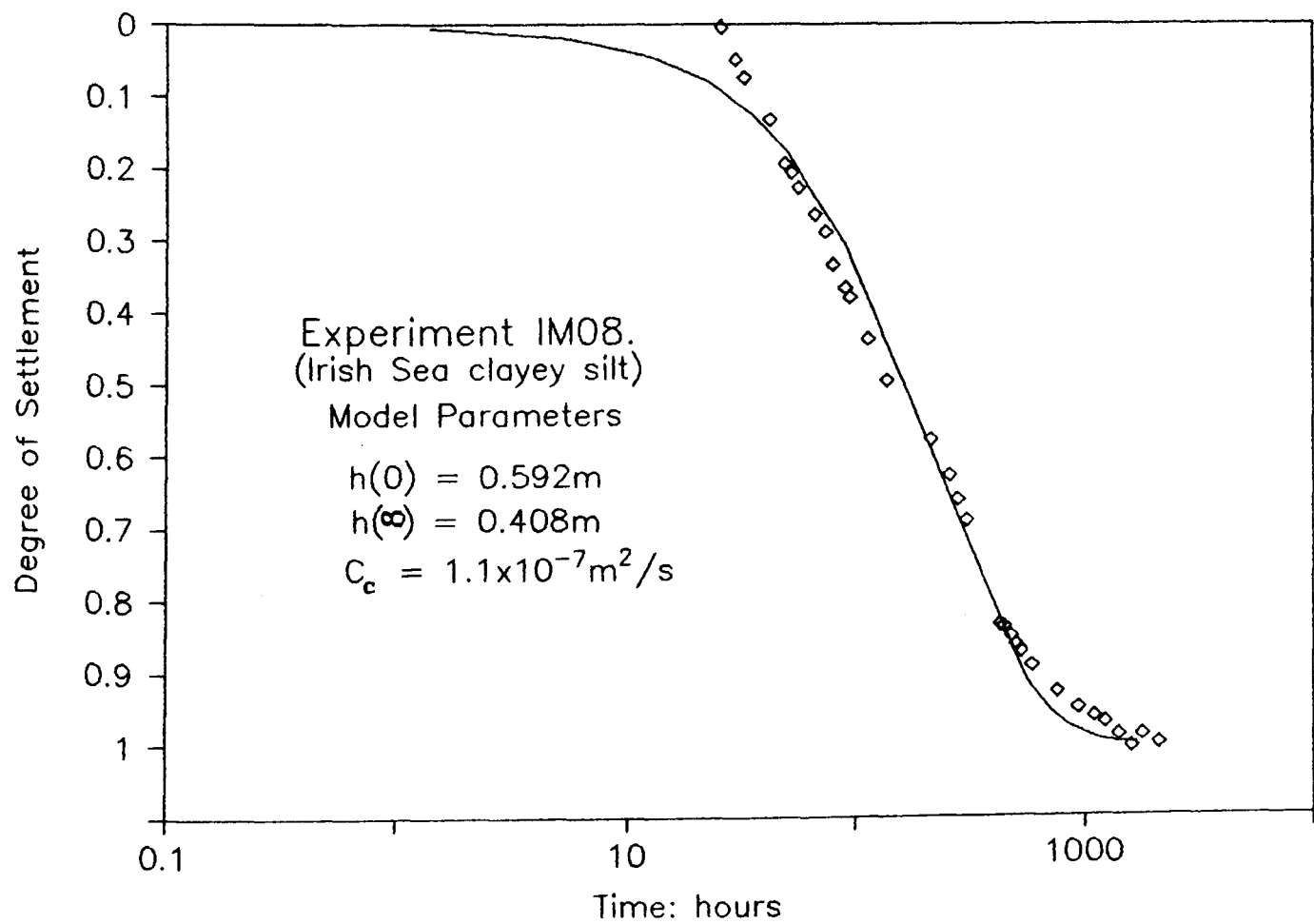
Figure 5.16 The Lee and Sills Model for Surface Settlement.

Experiment IM11.
(Irvine Bay mud)

Model Parameters

$h(0) = 0.488m$
$h(\infty) = 0.329m$
$C_c = 3.9 \times 10^{-7} m^2/s$

Time: hours
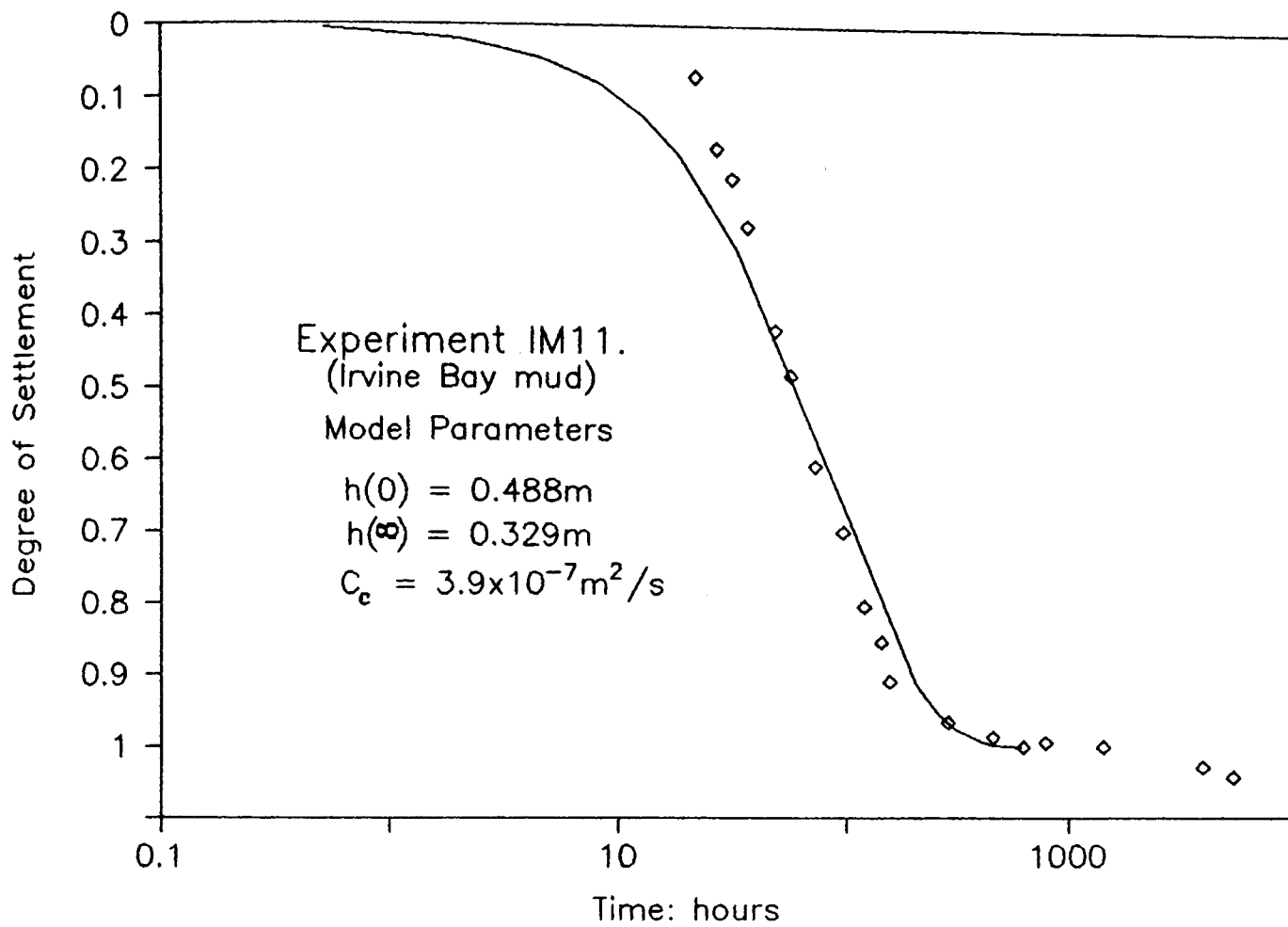
Figure 5.17 The Lee and Sills Model of Surface Settlement.

Experiment IM09.
(Irish Sea silty clay)

Model Parameters

$h(0) = 0.871m$
$h(\infty) = 0.605m$
$C_c = 6.5 \times 10^{-7} m^2/s$

Time: hours
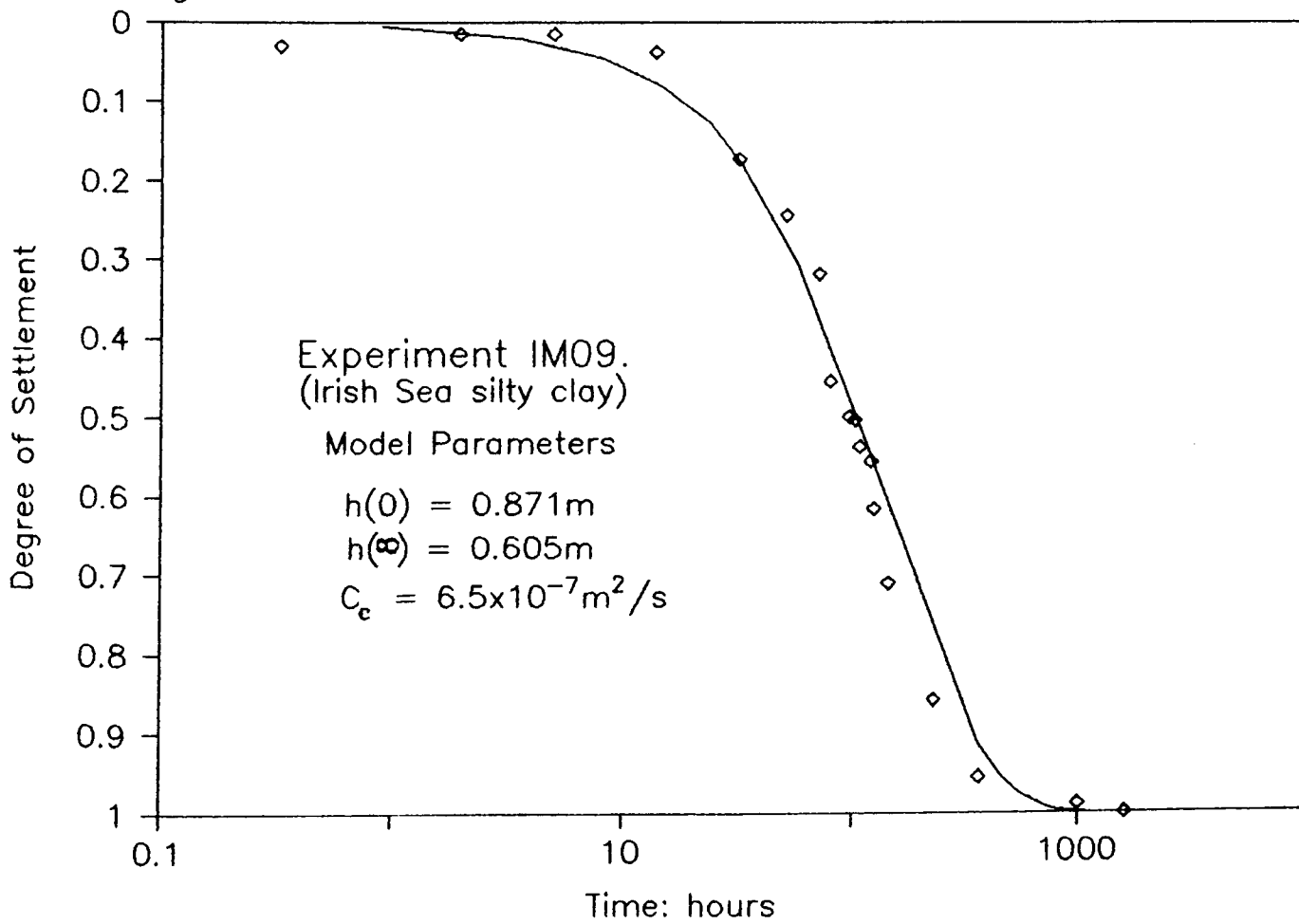
Figure 5.18   The Lee and Sills Model of Surface Settlement.
Elders data for experiment 10. (1985)

Experiment 10
(Combwich silty clay)

Model Parameters

$h(0) = 1.55m$

$h(\infty) = 0.946m$

$C_c = 4.7 \times 10^{-8} m^2/s$
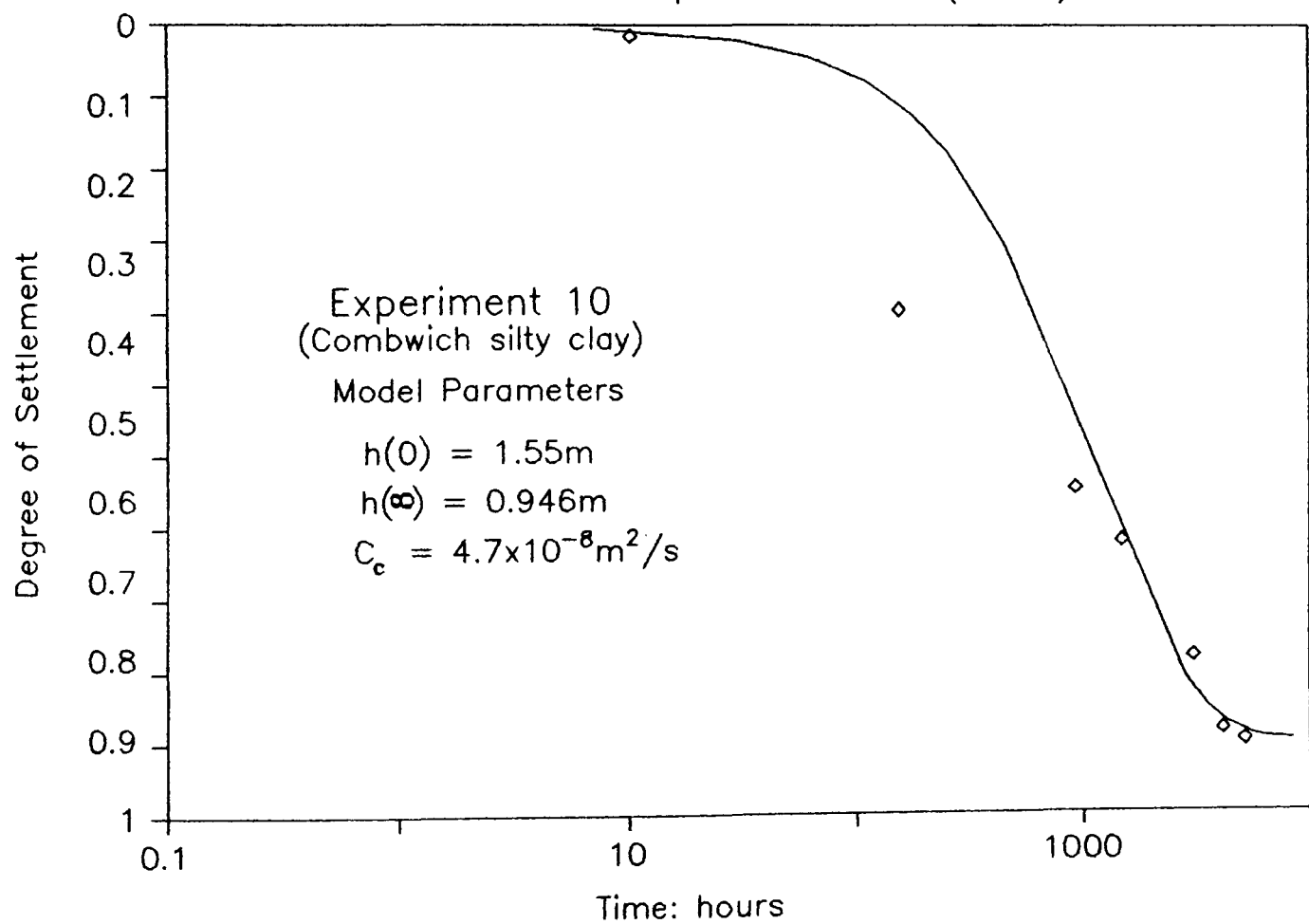
5.5.3 EXCESS PORE PRESSURE DISSIPATION MODELLING.

The Lee-Sills model has also been applied to the prediction of excess pore water pressure isochrones, shown in figures 5.19 to 5.21. The normalized excess pore pressure by U is given by

$$U = 2 \sum \frac{(-1)^N \sin (M\pi (1-y))}{M^2 \pi^2} \exp (-M^2 \pi^2 T_F) \qquad (2.6)$$

where
$$M = 0.5(2N + 1)$$
$$N = 0,1,2,\ldots\ldots$$
$$y = \text{normalized material co-ordinate} = z/z_0$$
$$T_F = \frac{C_c t}{z_0^2} = \text{Time Factor} \qquad (2.7)$$

The thickness of the consolidating layer (z_0) can be identified by the first non-zero excess pore pressure below the water/sediment interface. In most circumstances this coincides with the interface itself, but during the early stages of the experiment this is not always the case. The separation of the pore pressure ports does however limit the resolution with which this soil height can be identified.

The Lee-Sills model predictions have been compared to the observed pore pressure profiles of experiments IM07, IM08, and IM11 (figures 5.19 to 5.21). Initially the agreement appears to be poor due not only to the difficulty of identifying the zero excess pore pressure height, but due also to the models failure to predict the slow dissipation of pore pressures at the base of the column. With the passage of time, the Lee-Sills model begins to predict the behaviour of the soil with a higher degree of accuracy. The model input parameters and the value of consolidation coefficient thereby determined are shown in table 5.4.

The Lee-Sills model has been used to predict the pore pressure profile of experiment IM09, the soil exhibiting creep. As in the settlement predictions, the model fits the data well (see figure 5.22). Elder's (1985) results from experiment 10 are likewise predicted to a high degree, figure 5.23.

Table 5.4   The Lee-Sills excess pore pressure dissipation model
            input parameters

Expt. Ref.	Total Vertical Stress (kPa)	Time (hours)	Z_0 (m)	Time Factor T_F	Coef. of Consolidation ($\times 10^{-7}$ m^2/s)
IM07	1.034	42	0.470	0.1	1.46
		119	0.440	0.175	0.79
		283	0.398	0.35	0.54
		553	0.367	0.6	0.41
IM08	1.321	53	0.535	0.1	1.50
		260	0.503	0.24	0.65
		558	0.443	0.45	0.44
		937	0.425	0.9	0.48
IM09	1.908	1.1	0.842	0.001	1.79
		31	0.799	0.05	2.86
		51	0.780	0.125	4.14
		369	0.604	0.26	0.71
IM11	1.238	49	0.399	0.4	3.61
		49	0.399	0.18	1.62
		97	0.359	0.4	1.48
		120	0.344	0.45	1.23
		166	0.329	0.575	1.04
Elder	2.239	10	1.550	0.0005	0.007
		148	1.182	0.015	0.39
		912	1.086	0.1	0.36
		3000	0.701	0.25	0.11
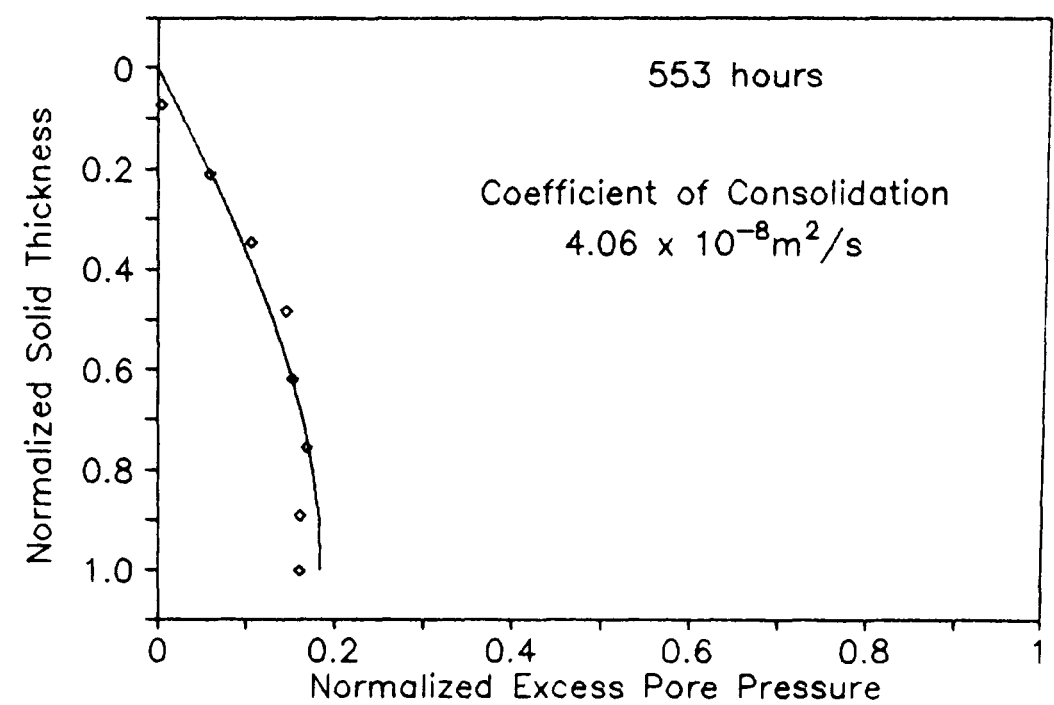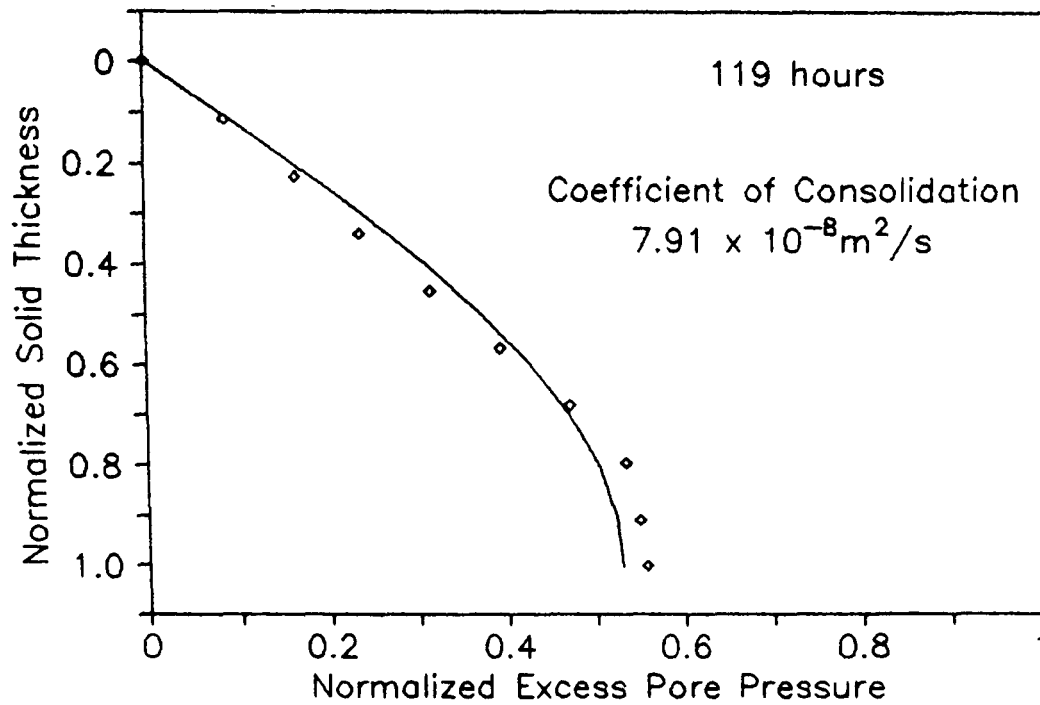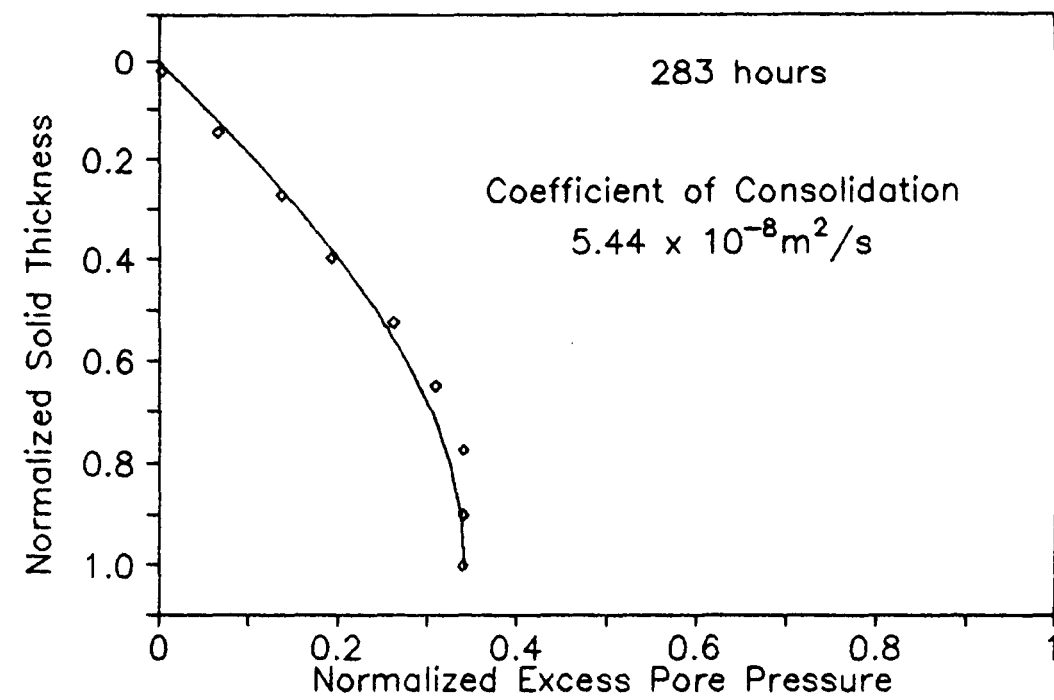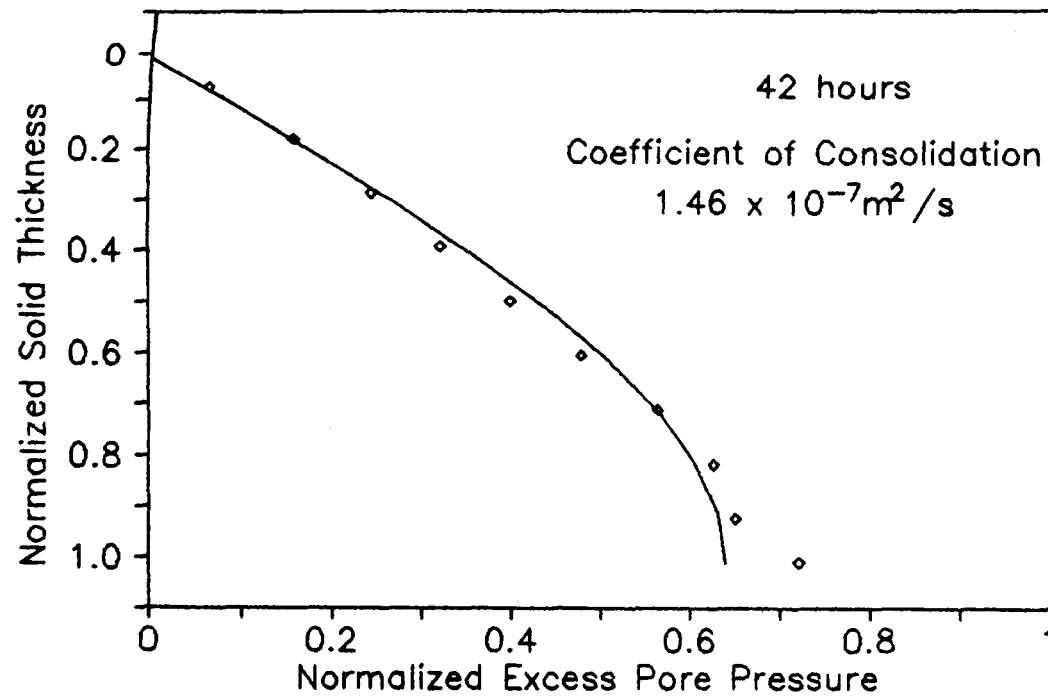
Figure 5.19 The Lee–Sills Model of Excess Pore Water Dissipation: Experiment IM07
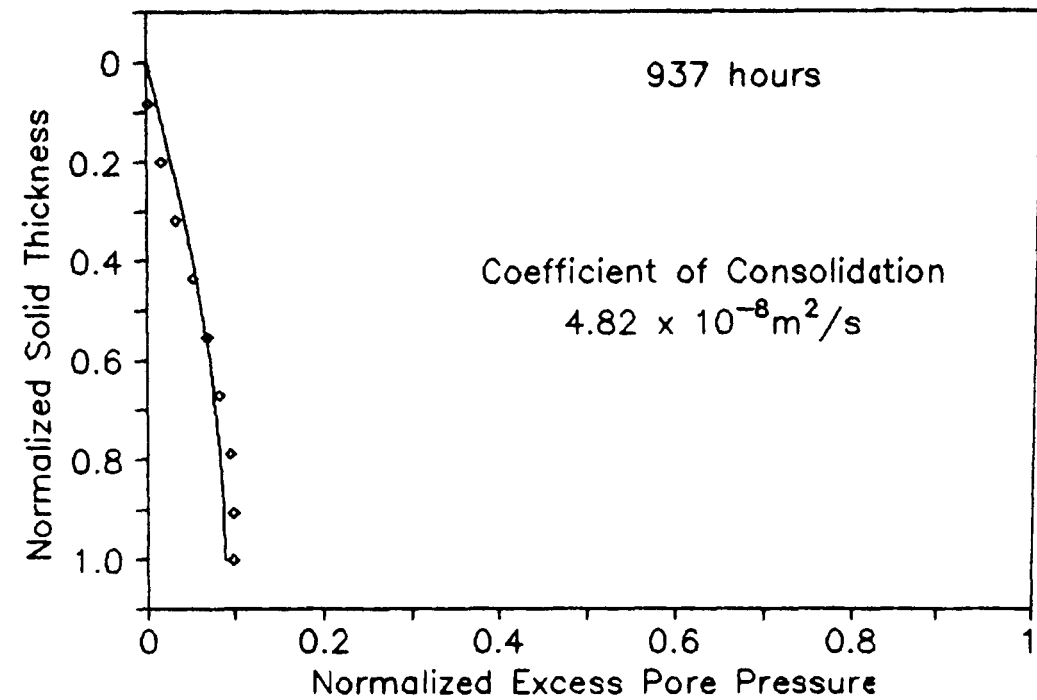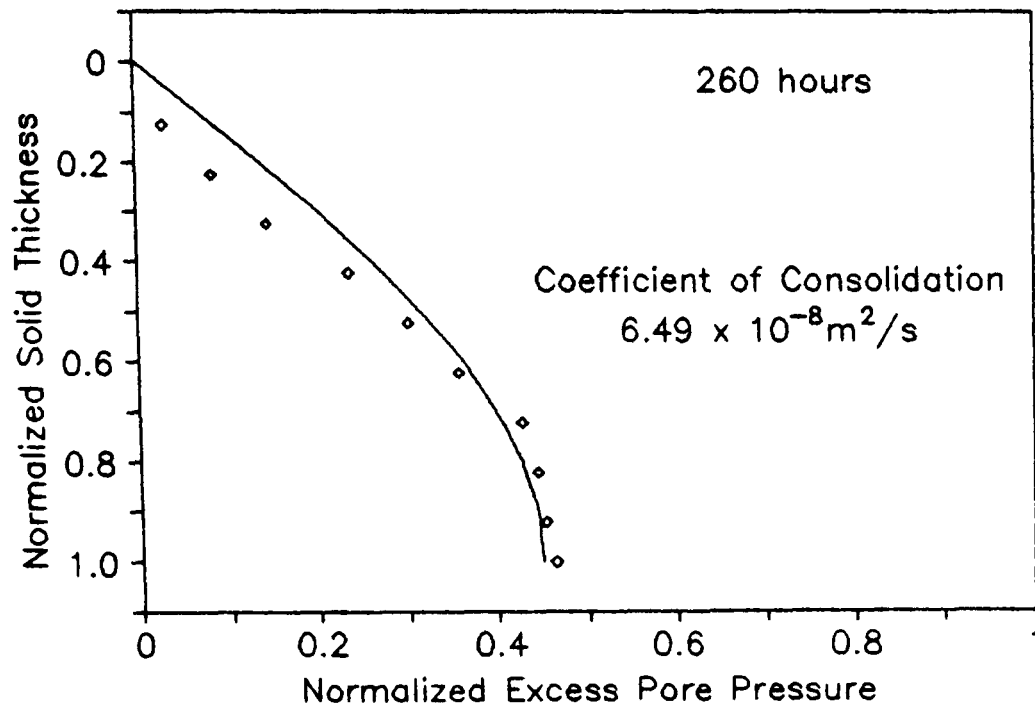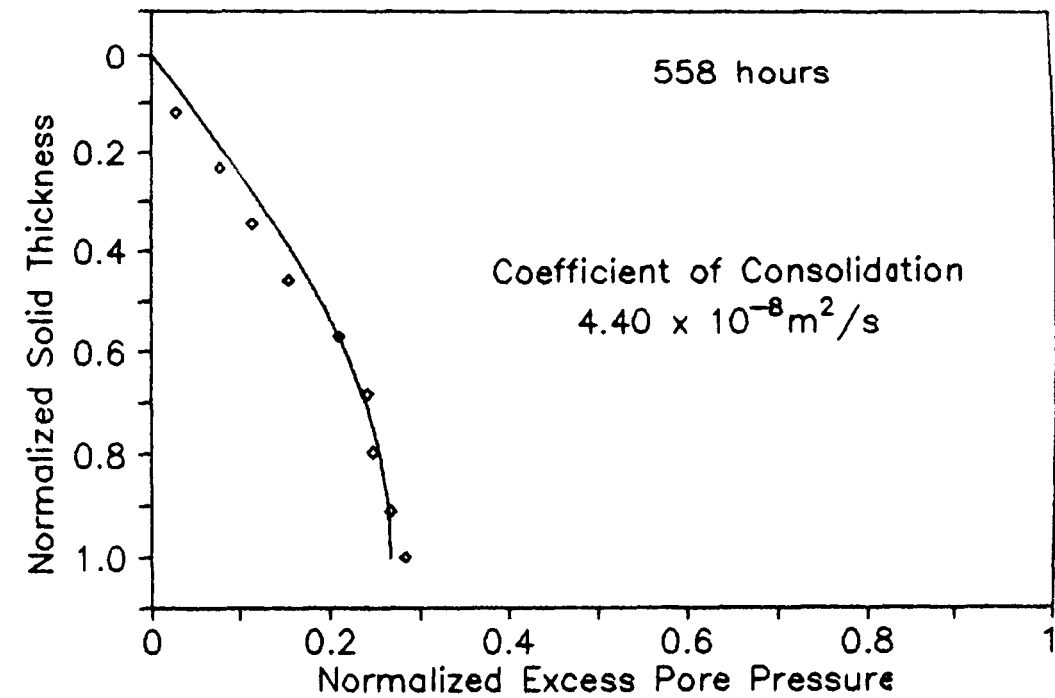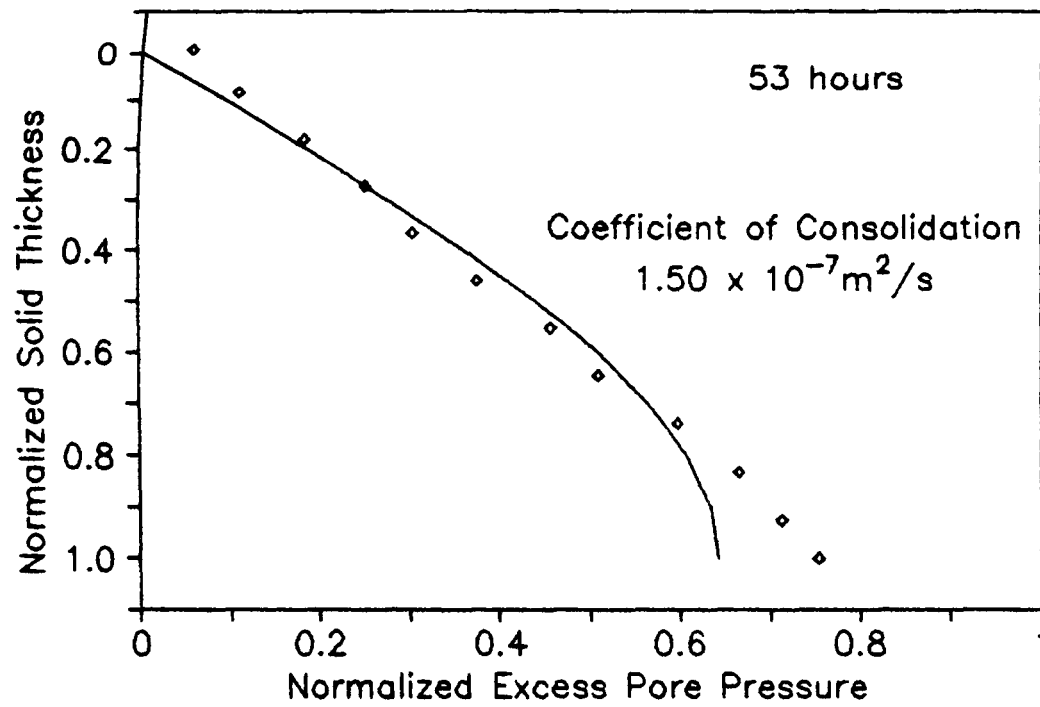
Figure 5.20 The Lee–Sills Model of Excess Pore Water Dissipation: Experiment IM08
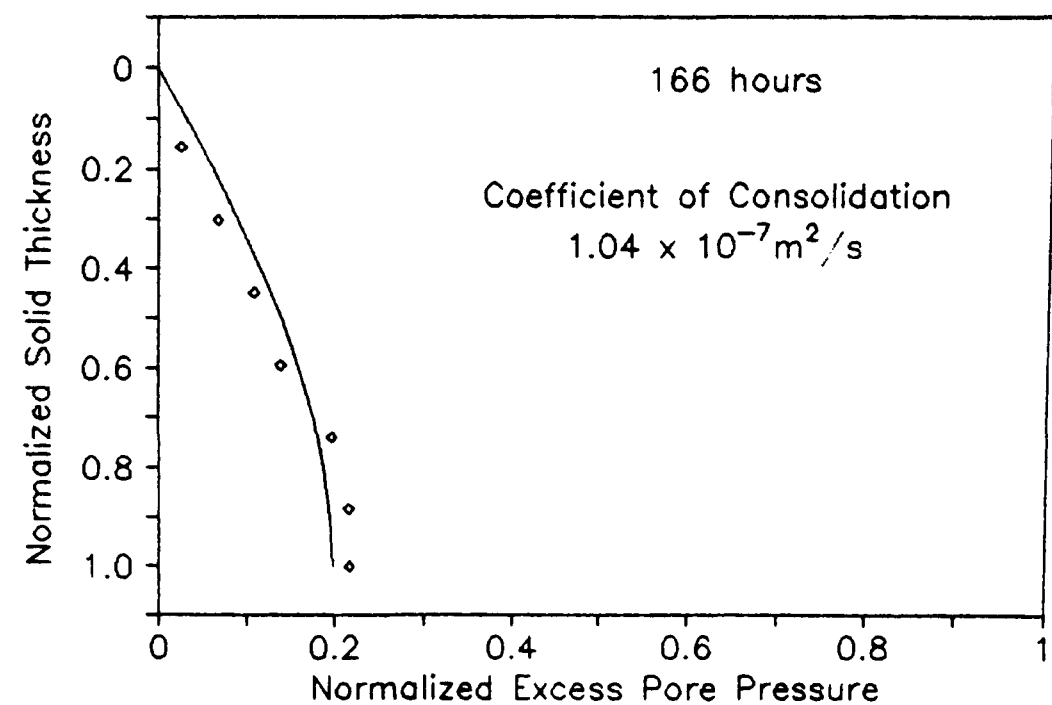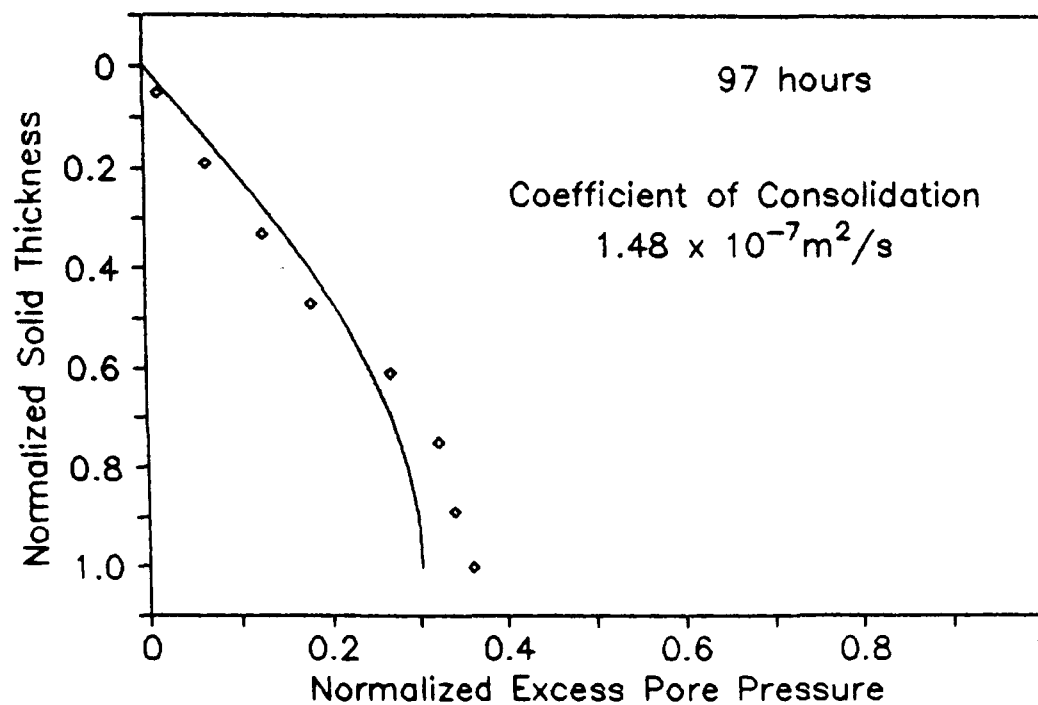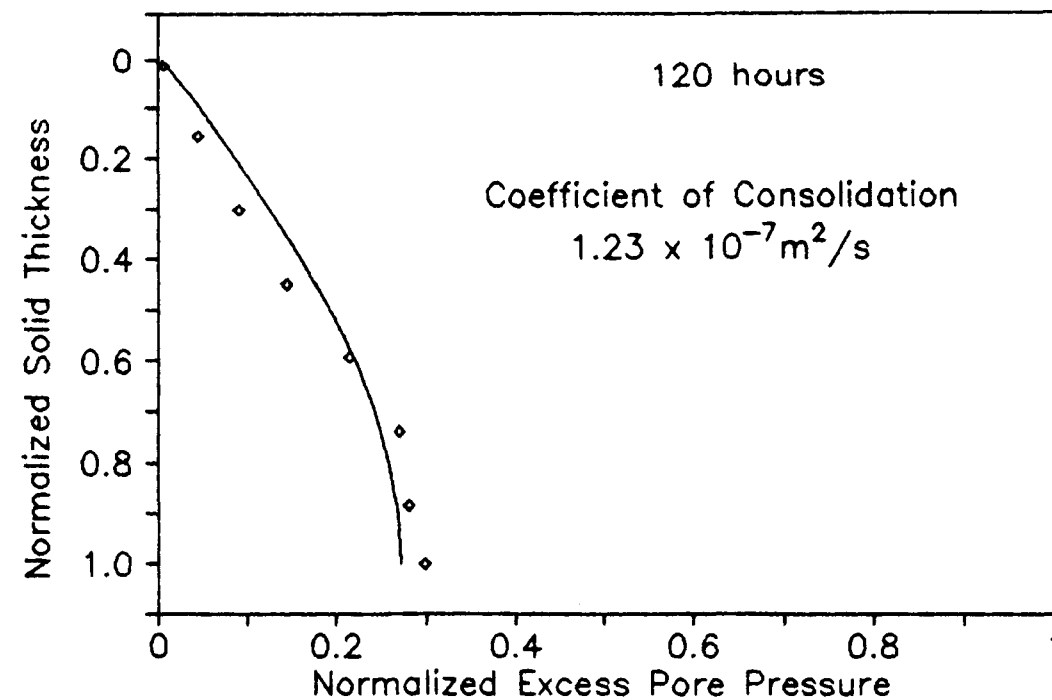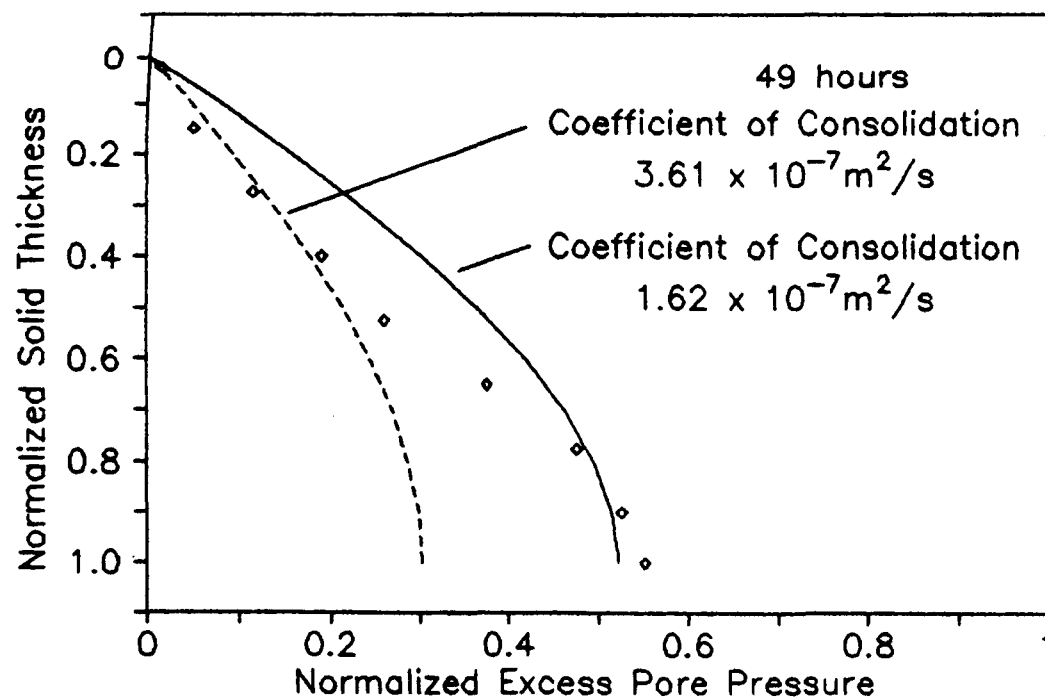
Figure 5.21 The Lee—Sills Model of Excess Pore Water Dissipation: Experiment IM11
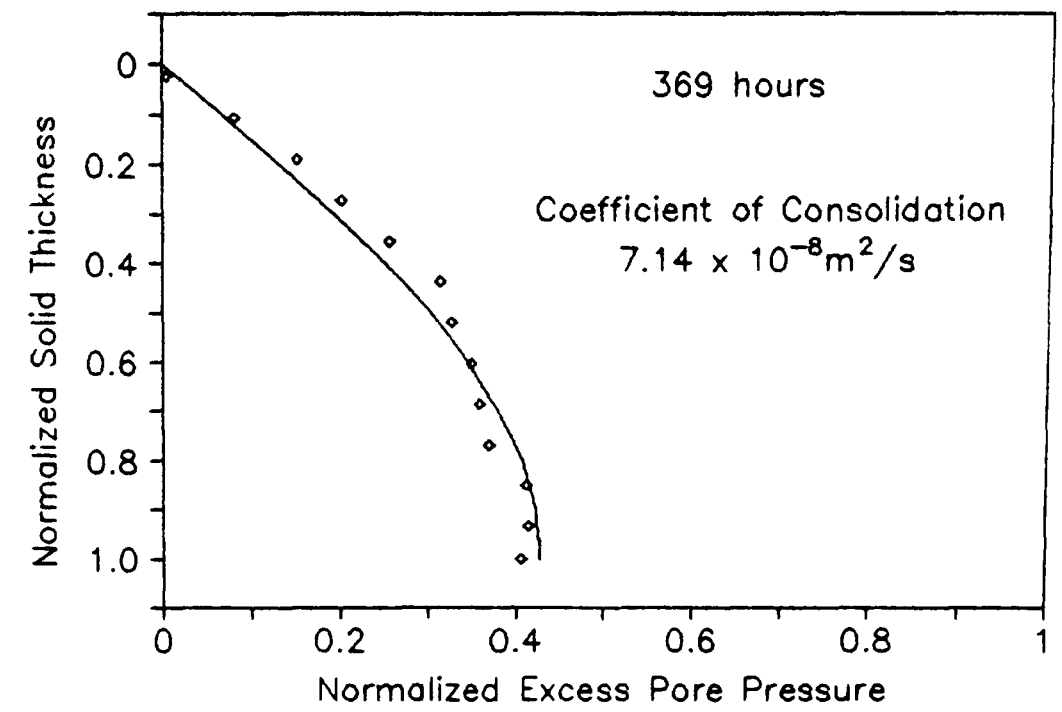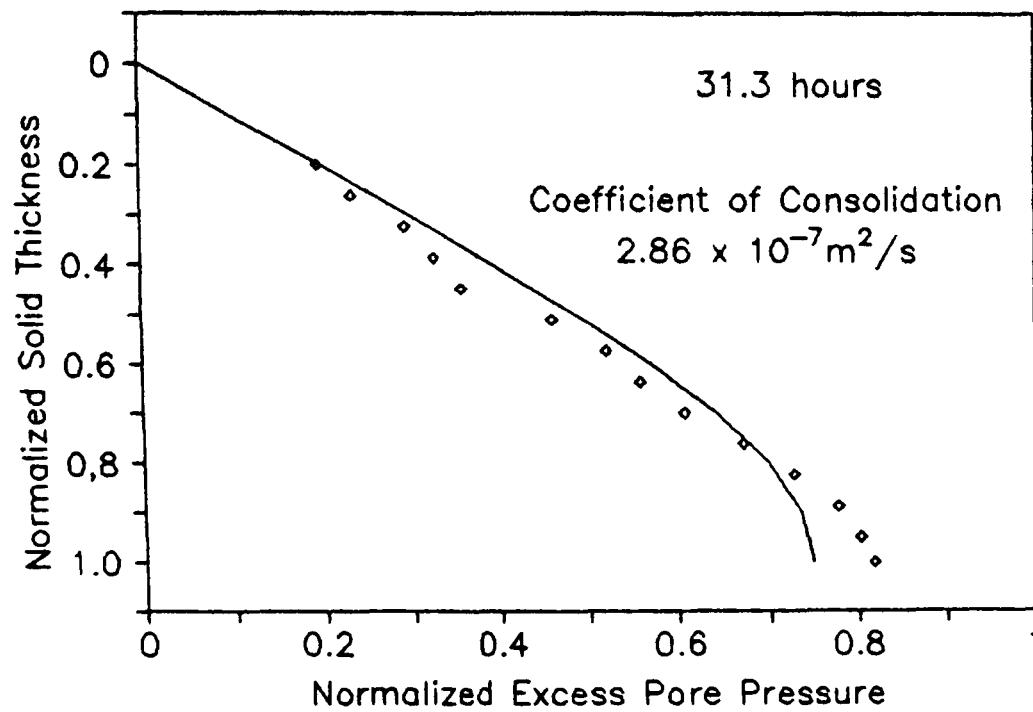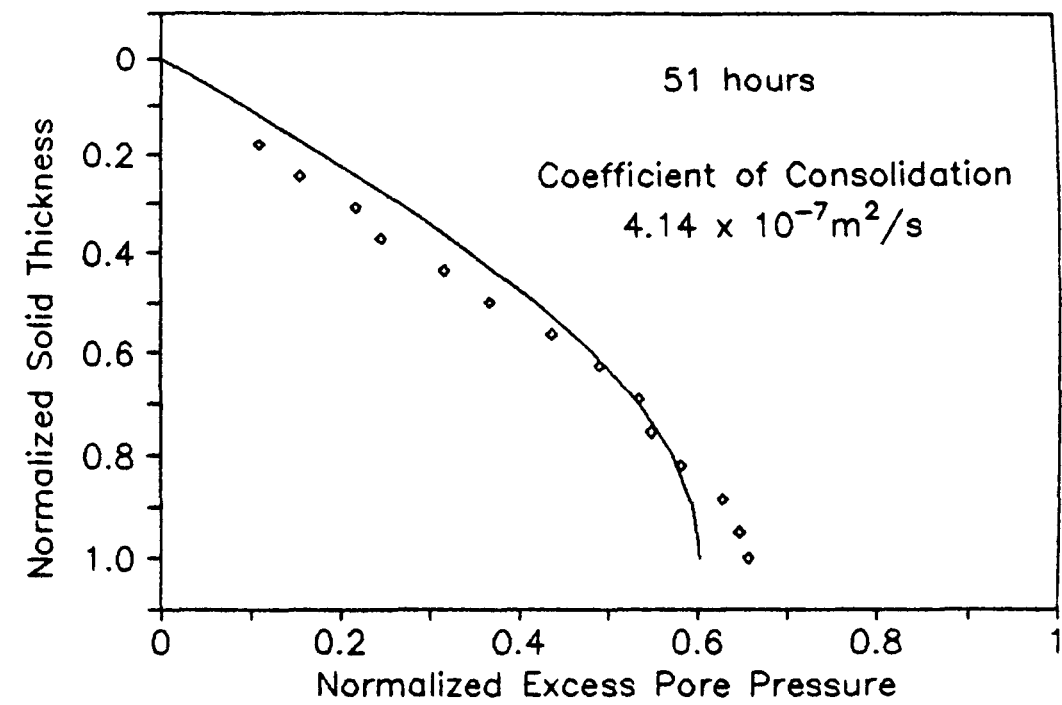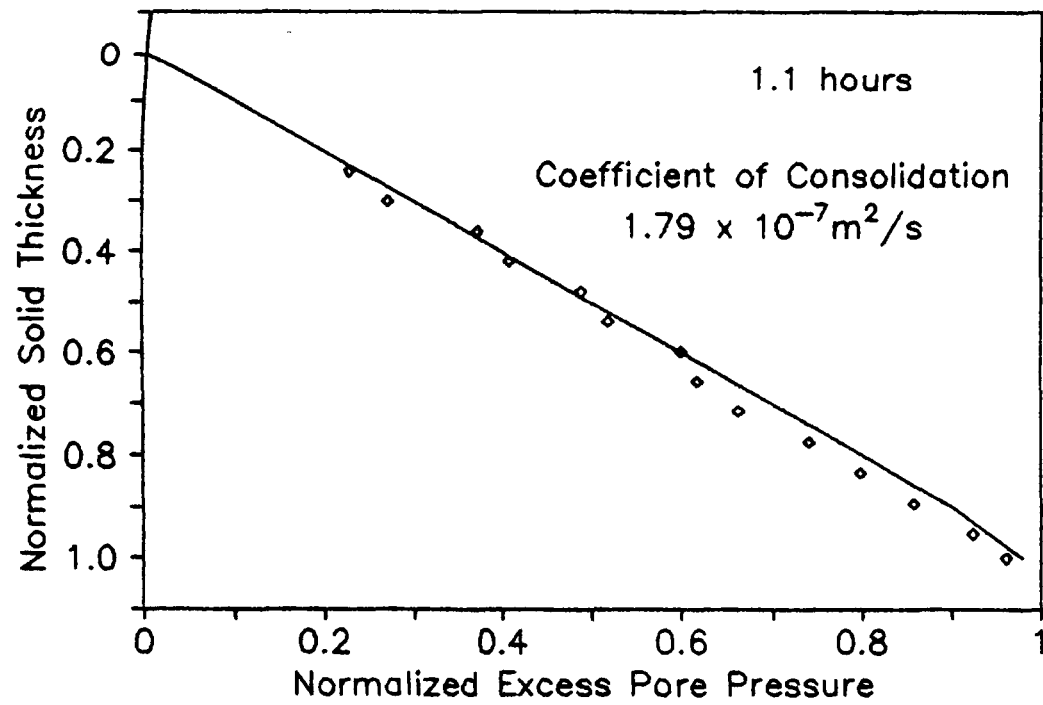
Figure 5.22 The Lee—Sills Model of Excess Pore Water Dissipation: Experiment IM09
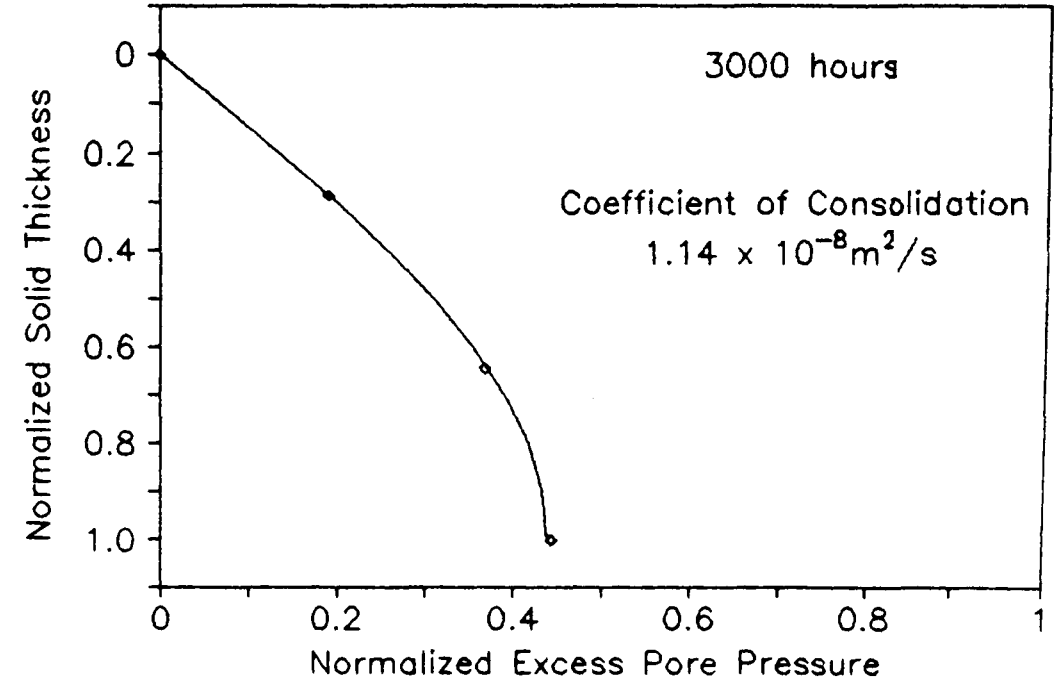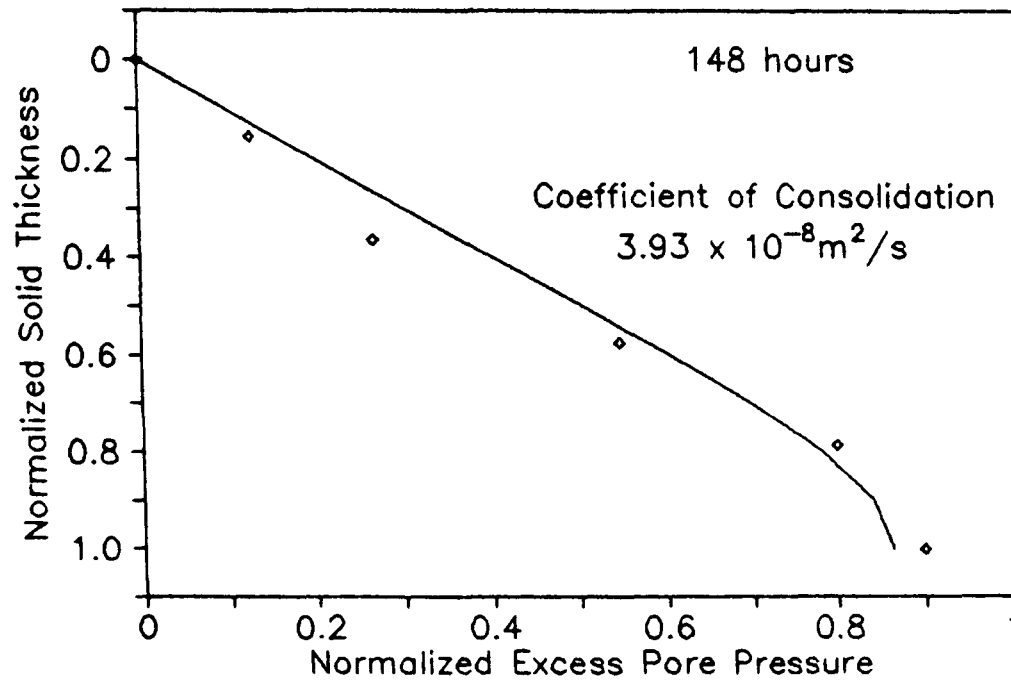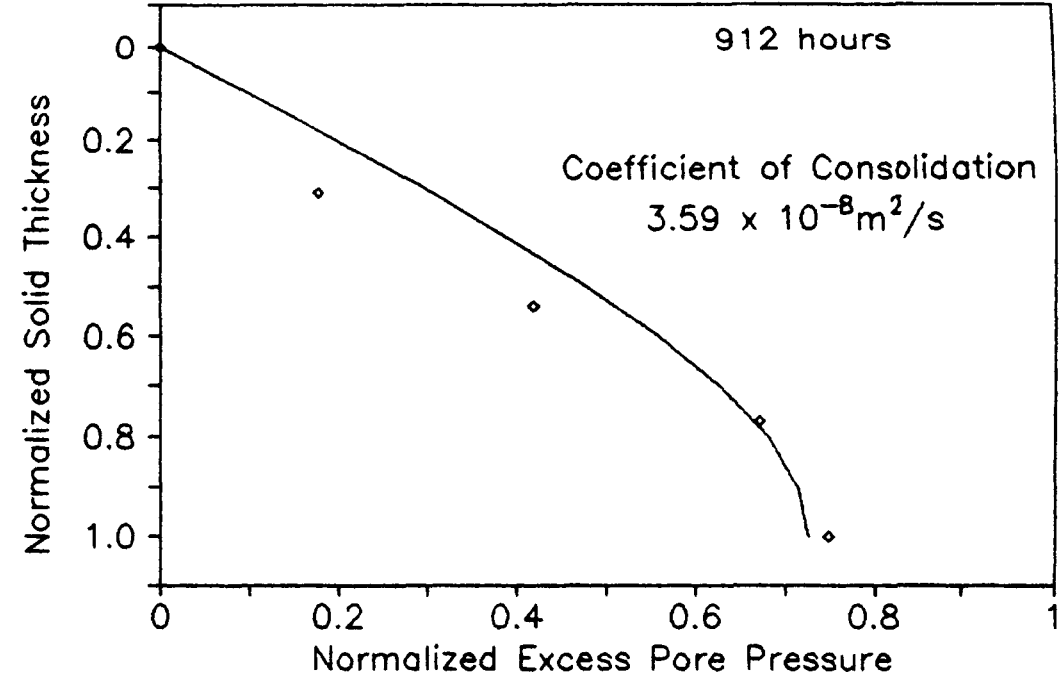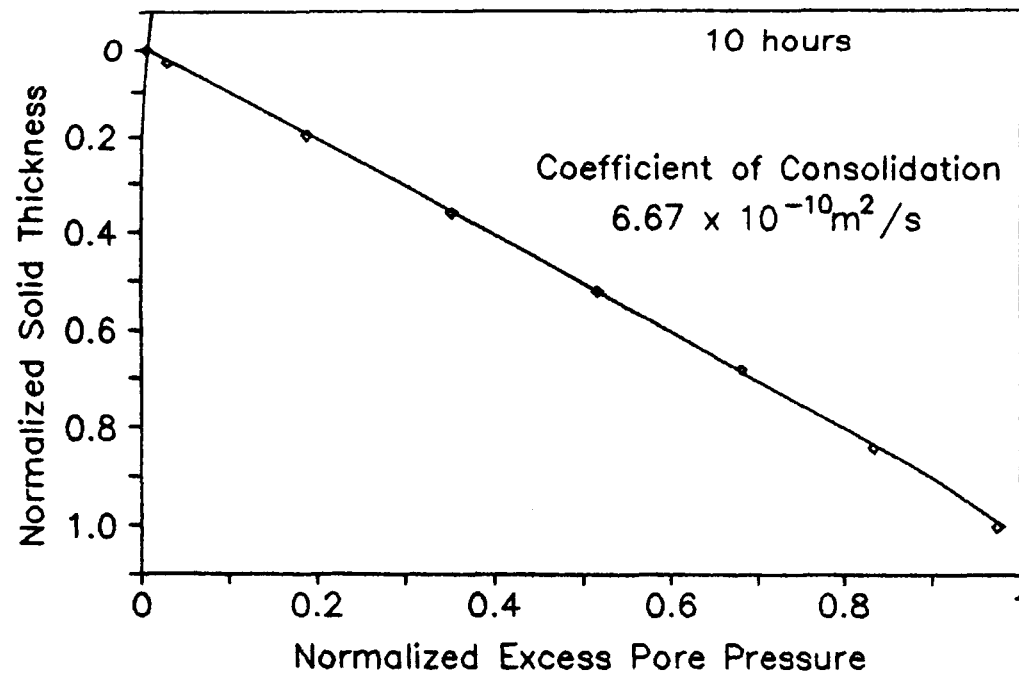
Figure 5.23 The Lee–Sills Model of Excess Pore Water Dissipation: Elders data (1985)

5.5.4 COEFFICIENT OF CONSOLIDATION BY CALCULATION.

The coefficient of consolidation, C_c, was defined by Gibson et al. (1967) as

$$C_c = \frac{-k}{\rho_w (1 + e)} \frac{d\sigma'}{de}$$

where C_c = coefficient of consolidation
       k = permeability
       e = voids ratio
       σ' = vertical effective stress
       z = the solid thickness??
       ρ_s = solid particle density
       ρ_w = fluid density

Using the empirical relationships of table 5.1 and 5.3 for the values of compressibility and permeability, C_c have been calculated for a range of voids ratio. The results are shown in table 5.5.

5.5.5 COEFFICIENT OF CONSOLIDATION DATA ANALYSIS SUMMARY.

A summary of the predicted coefficients of consolidation (C_c) are shown in table 5.5. If the results 5.5 are compared it will be seen that the settling curve models give a value of C_c that is in the upper limit of C_c obtained by modelling pore pressure dissipation. The value of C_c derived by calculation (method (c) above) is consistently lower than the other two methods, in addition it gives the most inaccurate results owing to the large error in permeability. For example if the error bands are taken into consideration, the range of C_c for experiment IM11 is $0.6 \times 10^{-8} \text{m}^2/\text{s}$ to $25.1 \times 10^{-8} \text{ m}^2/\text{s}$.

The variation in results may be explained by considering the parameters used to determine C_c in each case. The settlement curves rely on the measurement of deformation, pore pressure profiling rely on the measurement of pore pressure alone, whereas the method of calculation requires the measurement of

stress, deformation and pore pressure. There is no justification to say that one method is better than any other.

Table 5.5 Summary of Predicted Coefficient of Consolidation

Expt. Ref.	C_c from Pore Pressure modelling ($\times 10^{-8} m^2/s$)	C_c from Settlement curve modelling ($\times 10^{-8} m^2/s$)	C_c by Calculation ($\times 10^{-8} m^2/s$)
IM07	14.6 4.1	11	0.4 1.0 ($6.5 \geq e \leq 4$)
IM08	15.0 4.4	11	0.3 1.3 ($6.5 \geq e \leq 2$)
IM09	17.9 7.1	65	
IM11	36.1 10.4	39	1.3 13.0 ($5 \geq e \geq 2$)

5.6 Summary.

The consolidation behaviour of a rapidly deposited sediment slurry is greatly influenced by its initial input density. A slurry deposited in sea water above a critical voids ratio will exist initially as a fluid supported suspension before becoming a consolidating soil. Below this critical value the soil behaves immediately as a consolidating soil. The critical voids ratio for the soils studied in the column experiments settling in sea water was found to be less than 11.54.

The soils vertical effective stress distribution was determined using bulk density and pore pressure measurements. The tracking of individual soil elements allowed compression behaviour of the soil to be analysed in detail. Above the critical density the soil exhibited a largely unique voids ratio versus effective stress relationship. This relationship

could be differentiated to yield the frame compressibility at any point in the soil. The resulting frame compressibility was large, ranging from 10^{-3} to 10^{-5} Pa^{-1} for voids ratios between 6 and 2, illustrating the weak nature of the soil frame. Frame compressibility derived from the surface settlement curves represents, it is believed, some integrated compressibility over all soil all the elements. With regard to the one soil sample analysed which had a density greater than the critical value exhibited considerable time dependent compression, or creep.

The logarithm of permeability versus voids ratio relationship of the soils was found to be approximately linear over voids ratio ranges of 6 to 2. Permeabilities were found to range from 10^{-5} to 10^{-8} m/s in the soils studied in these experiments.

The coefficient of consolidation (C_c) of the soil was determined using three methods based on the large strain consolidation analysis of Gibson et al. (1967). The Lee-Sills formulation of this analysis was used to model the settlement behaviour and the excess pore pressure dissipation, whilst the third method calculated C_c from the permeability and compressibility relationships described above. Although the Lee-Sills model was successful in predicting consolidation behaviour, particularly in the later stages of consolidation, the resulting predictions of C_c spanned two orders of magnitude (10^{-9} to 10^{-7} m^2/s). The Lee-Sills analysis appeared to agree well with the observed consolidation behaviour of the soil sample exhibiting creep. The results of this data analysis will be used to appraise the success of using geophysical measurement, and in particular the Biot model, in predicting consolidating soil behaviour.

CHAPTER 6   ANALYSIS OF SEISMO-ACOUSTIC BEHAVIOUR.

6.1 Introduction.

In this chapter, the seismo-acoustic behaviour of soft soils will be analysed. Shear wave propagation will be studied in relation to soil porosity, effective stress, soil stiffness and to the soil frame compressibility (see section 6.3). Section 6.4 will consider how measurements of soil resistance may be utilized to estimate the soils mass coupling factor. Compressional wave propagation in soft soils will be considered in section 6.5. The geophysical measurements in this chapter will be used to make predictions of the geotechnical properties of the soil samples in chapter 7.

6.2 Apparatus Validation Experiment -Data Analysis.

In order to validate the instrumented sedimentation column as a practical geotechnical-geophysical apparatus, a set of geophysical measurements were made on a saturated sand sample. P-wave, S-wave and soil resistance measurements were made in the column and compared to similar measurements made in the Jackson Porosity Cell (Schultheiss 1983). The results of the experiment are shown in figures 6.1 to 6.3.

All measurements were corrected to a reference temperature and salinity of $20°C$ and $34°/°°$. Figure 6.1 shows the variation of compressional wave velocity with porosity as measured by the two sets of apparatus. A best line has been fitted to the column data (dashed line), similarly to the Jackson cell data (solid line) for comparison. The best line equations are given below.

$$V_P = 3003 - 4696\eta + 4286\eta^2 \qquad \text{(Sedimentation Column)}$$
$$V_P = 3035 - 5316\eta + 5631\eta^2 \qquad \text{(Jackson Cell)}$$

The agreement between both sets of apparatus is reasonably good. The estimated error in V_P is $\pm0.35\%$ thought to be
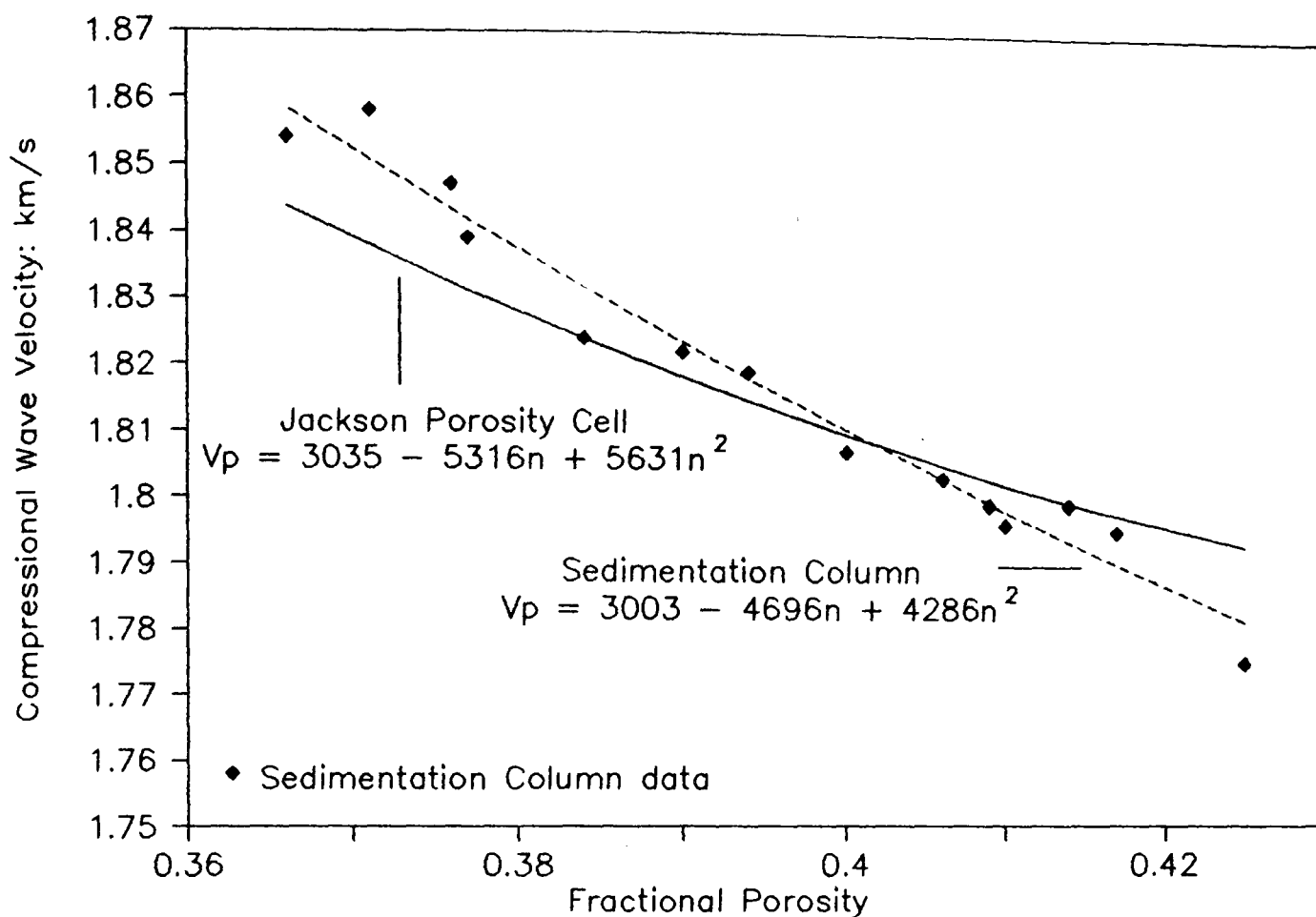
Figure 6.1 P—wave Velocity/Porosity Relationship: Experiment IMO6.
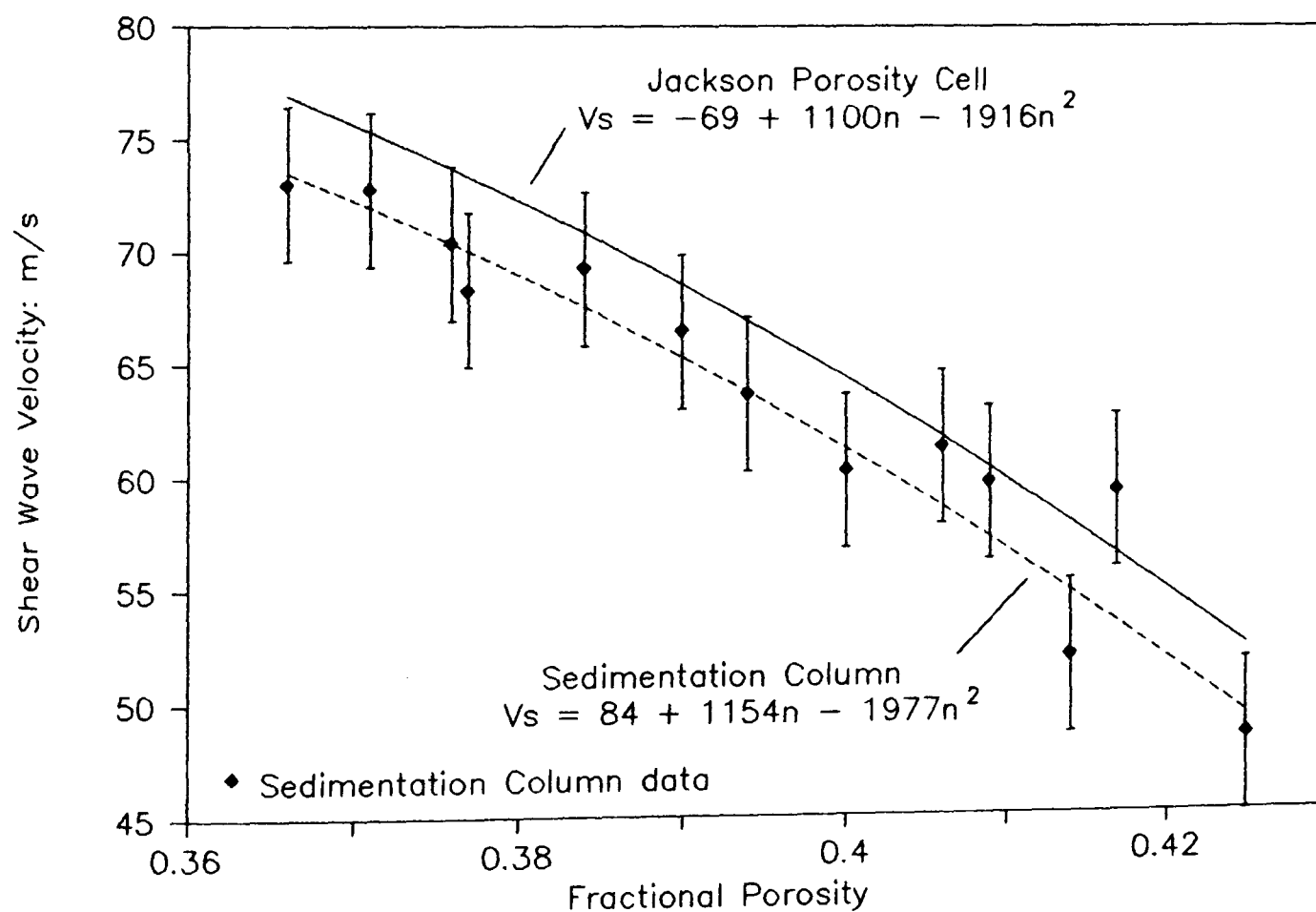
Figure 6.2 S—wave Velocity/Porosity Relationship: Experiment IMO6.
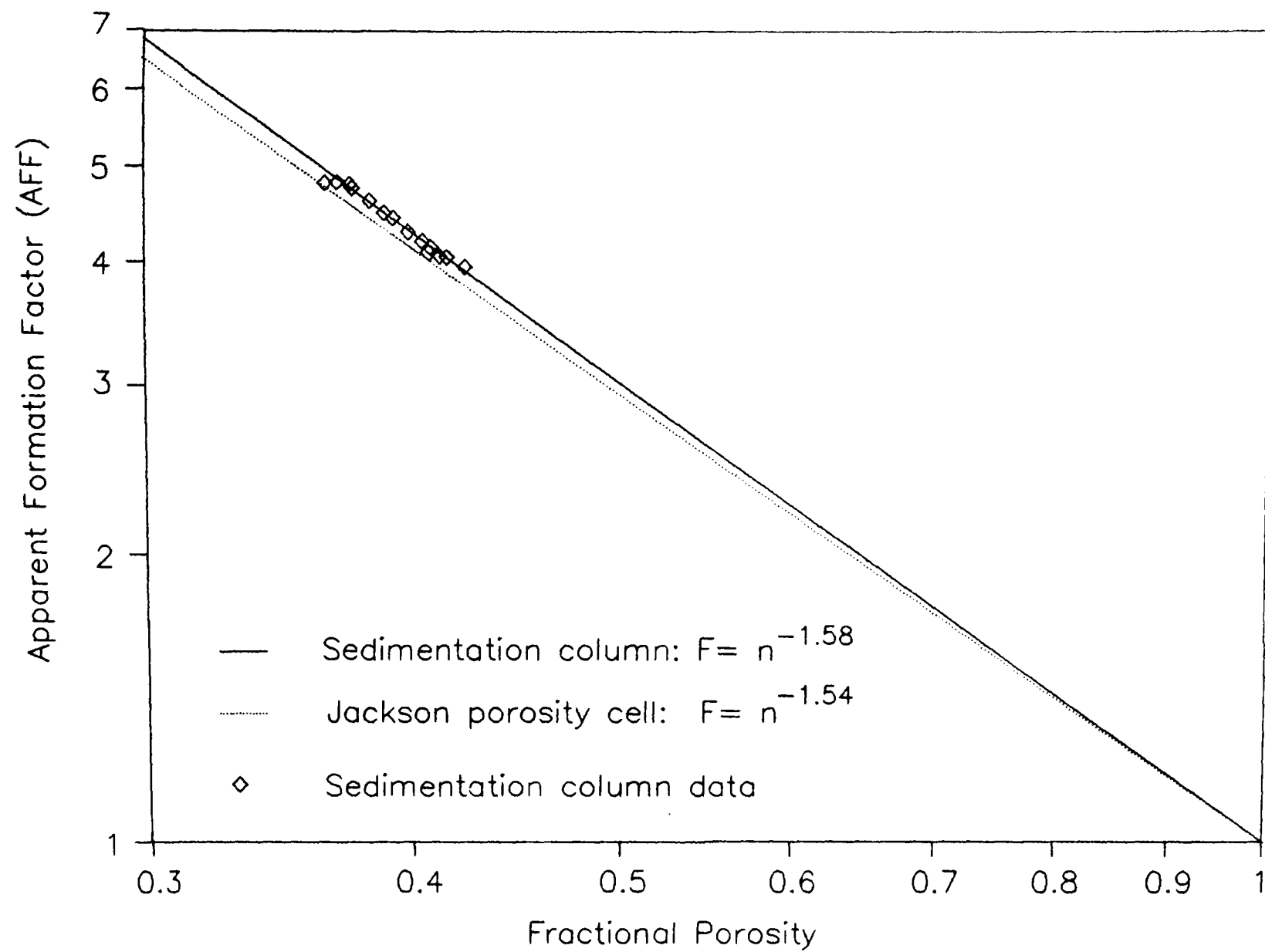
Figure 6.3   Apparent Formation Factor versus Fractional Porosity
Experiment IM06.

primarily due to the difficulty of measuring the samples temperature accurately. The estimated error of the fractional porosity measurement in the column was ±0.3%, and ±0.5% in the Jackson cell.

The shear wave velocity versus porosity data are displayed in a similar manner in figure 6.2. While the best fit line for the Jackson cell appears to be consistently higher than that for the column, the trend for both curves is the same. Applying a correction for applied frequency variation (Shirley and Bell 1978) to the experiment would result in a reduction of V_s in the Jackson cell by 1 or 2m/s thereby making best fit lines practically coincident. Shear wave velocity was measured to an accuracy of ±4.5m/s.

The plot of Formation factor versus porosity is shown in figure 6.3. The best fit equations to the data are given by

$$F = \eta^{-1.58} \qquad \text{(Sedimentation Column)}$$
$$F = \eta^{-1.54} \qquad \text{(Jackson Cell)}$$

The indices of these equations are related to the shape of the soil grains (index 2 ⇒ platey grains, index 1 ⇒ spherical grains) and is indicative of a non-cohesive marine sediment (refer to appendix 3 for typical values shown in figures A3.6 and A3.7). The agreement between the two sets of apparatus appears to be good, any variation in index can be accounted for by experimental error. It is concluded that the sedimentation column can justifiably be used in investigations into marine sands.

6.3 Shear Wave Data Analysis.

6.3.1 INTRODUCTION.

In this section measured shear wave velocity will be related to porosity, effective stress and soil compressibility. The rigidity modulus, which is a function of shear wave velocity and bulk density, will also be compared to effective stresses in the soil. The ultimate aim of the above study is to relate the measured geotechnical properties of the soil samples to shear wave propagation in order to explain the mechanism of propagation and to investigate possible practical applications of such shear wave measurements.

6.3.2 THE EFFECT OF CHANGING POROSITY ON SHEAR WAVE PROPAGATION.

The relationship between shear wave velocity and porosity is shown in figures 6.4 to 6.7. Figure 6.4 shows data from experiment IM07, where measurements were made on an Irish Sea clayey silt sample. Shear wave velocities range from 3m/s to over 8m/s ±8.5%. These velocities span a porosity range of 85% to 75% and the results compare well with those of Shirley and Hampton (1978) and Williams and Williams (1989a,b). It is tempting to fit a straight line through these data to produce a V_s-porosity relationship.

For experiment IM08 if the data for the near surface transducer data set (0.39m above the column base) are ignored, (on the grounds that the proximity to the sediment-water interface introduces additional complexities with respect to shear wave propagation) the data appears to be composed of a series of quadratic curves that asymptotically approach the curve

$$V_s = 241.4 - 564.1\eta + 317.4\eta^2 \qquad (6.1)$$

as illustrated in figure 6.5. Equation 6.1 represents shear
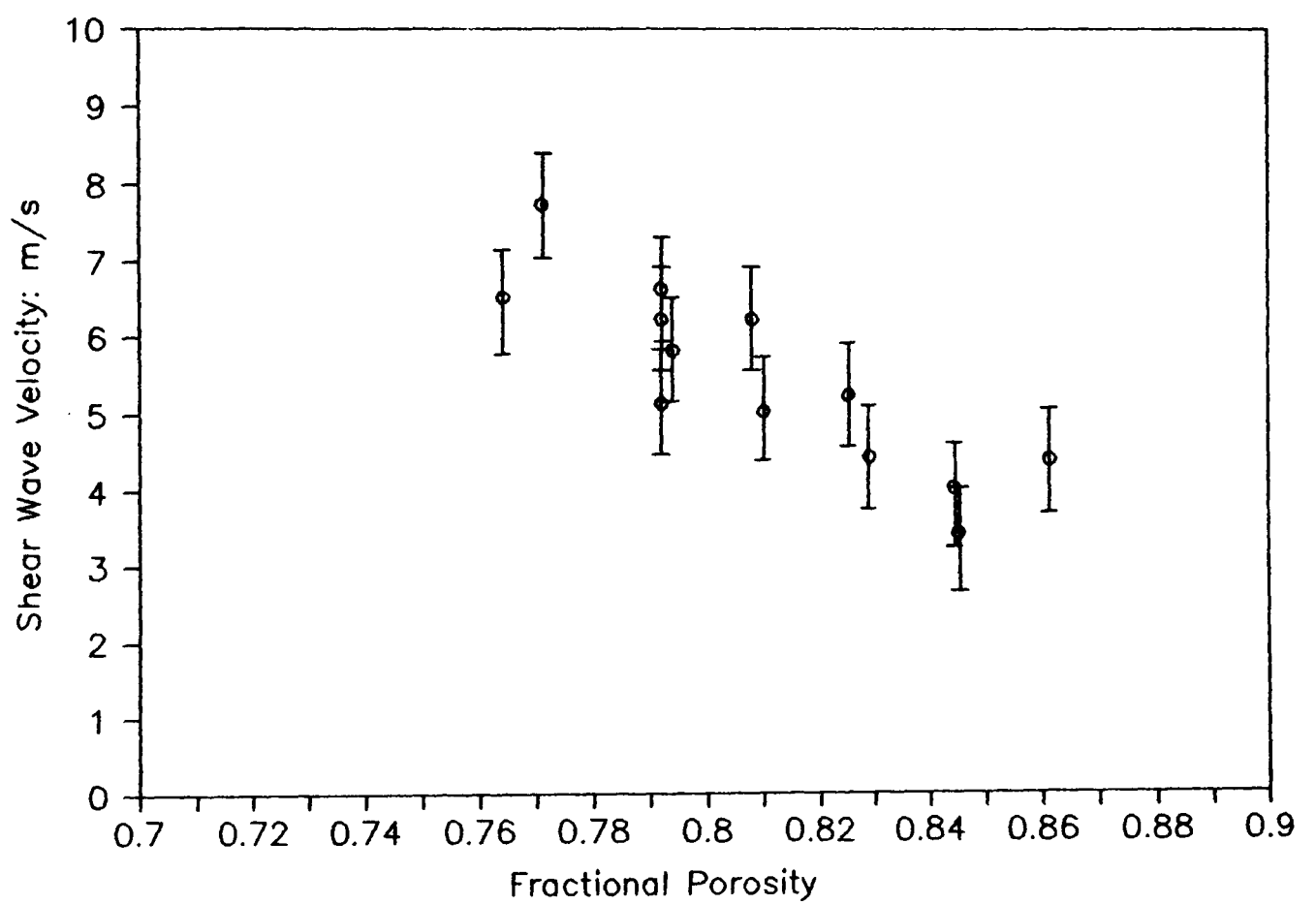
Figure 6.4   Shear wave velocity versus fractional porosity
Experiment IM07.
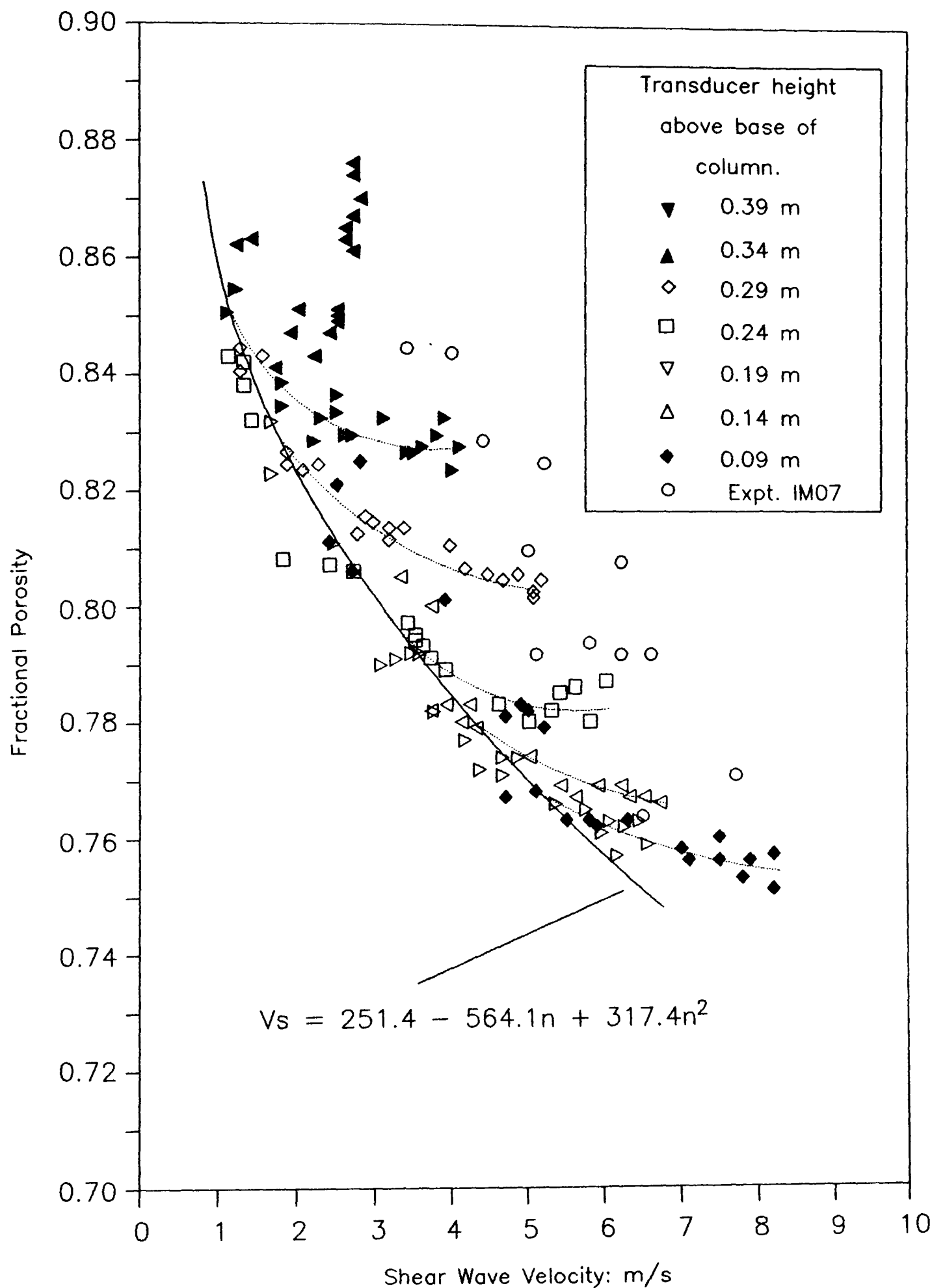
Figure 6.5   Shear wave velocity versus fractional porosity.
Experiments IM08 and IM07.

$$Vs = 251.4 - 564.1n + 317.4n^2$$

wave behaviour in the early stages of primary consolidation. Viewing experiment IM07 data in this context would imply that a straight line fit would be inappropriate.

Fitting polynomial equations to the V_s versus porosity data for each set of transducers gives the expressions shown in table 6.1. Figure 6.5 compares the curves represented by these equations with the postulated pattern and shows that the actual data are very closely mirrored by these equations.

Table 6.1   Shear wave velocity-porosity relationships for experiment IM08.

Transducer height(m)	Equation	Coef.of correlation
0.34	$V_s = 1912 - 4458\eta + 2600\eta^2$	66.1%
0.29	$V_s = 1869 - 4449\eta + 2650\eta^2$	96.4%
0.24	$V_s = 942 - 2246\eta + 1340\eta^2$	92.4%
0.19	$V_s = 1977 - 4954\eta + 3108\eta^2$	91.6%
0.14	$V_s = 499 - 1184\eta + 704\eta^2$	95.3%
0.09	$V_s = 689 - 1669\eta + 1015\eta^2$	74.7%

In section 4.6.2, figure 4.9, it was shown that shear wave propagation was greatly dependent upon overburden pressure. Propagation was first observed at the base, where the soil particles and flocs are pushed closest together. Such close proximity of soil particles enhances the electro-chemical bonding process of the clay minerals and initiates the creation of a soil matrix. This soil frame development migrates from the base upwards as indicated by the progressive ability of soil elements higher up the column to support shear wave propagation. The time delay between the soil matrix development in adjacent soil elements results in distinctly separate but nearly parallel Vs-porosity relationships. The later stages of primary consolidation are associated with relatively large changes in V_s for small changes in porosity. At any time in the consolidation process any value of porosity can be associated with a large range of shear wave velocities. The implications of such behaviour are that a time dependent shear wave velocity increase is occurring. This is believed to

be associated with the creep phenomena discussed in chapter 5.

Figures 6.6 and 6.7 show how Vs varies with porosity in experiments IM09 and IM11 respectively. The data for experiment IM09, a silty clay sample, was collected during the earliest stages of consolidation, that is 74 hours to 369 hours, primary consolidation being complete after approximately 1500 hours in this experiment. Velocities range from just below 1m/s to 5m/s and porosity ranges from 84% to 78%. From the interpretation of experiment IM08 and IM07, it was expected that the values of Vs would approximate to those defined by the asymptote (see equation 6.1). Having fitted a best fit line to the data, this does indeed seem to be the case (as shown in figure 6.6).

Figure 6.7 shows data from experiment IM11, for an Irvine Bay mud. This experiment was continued for the longest period of time after primary consolidation was complete. The clay fraction of the soil is believed to have preferentially settled at the top of the sedimentation column and the Vs-porosity relationship in this region (i.e. transducer heights 0.29m to 0.24m) displays the characteristic discrete and parallel relationship seen earlier. The data approaches equation 6.1 asymptotically as before. The coarser sediments, found at the base of the column (transducer heights 0.04m to 0.19m), display shear wave velocities of up to 11.5 m/s. The Vs-porosity relationship characterizing the clay component no longer holds, but instead the data show a tendency toward a single Vs-porosity curve. This change in behaviour is thought to be due to an increased proportion of sand and coarse silt in this region of the soil sample. This observation clearly illustrates the important role clay minerals play in the development of the soil frame and the soil frame's ability to sustain shear wave propagation. The soft soil frame cannot be observed directly with present day technology (Bowden 1989) however future studies into the relationship between shear wave velocity and rigidity modulus with clay mineralogy may reveal the chemistry/physics behind the development of soil fabric rigidity.
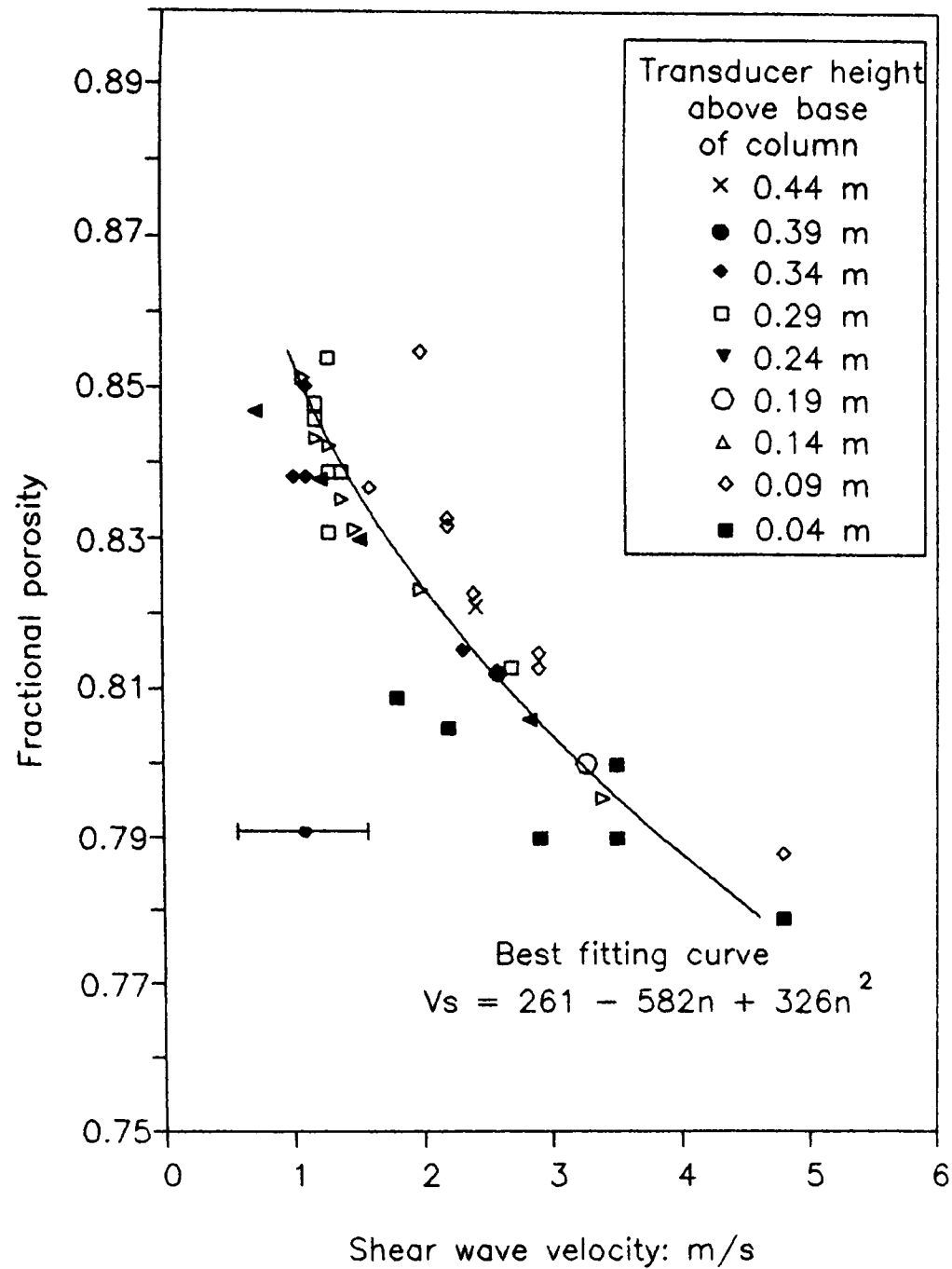
Figure 6.6   Shear wave velocity versus porosity.
Experiment IM09: Irish Sea silty clay
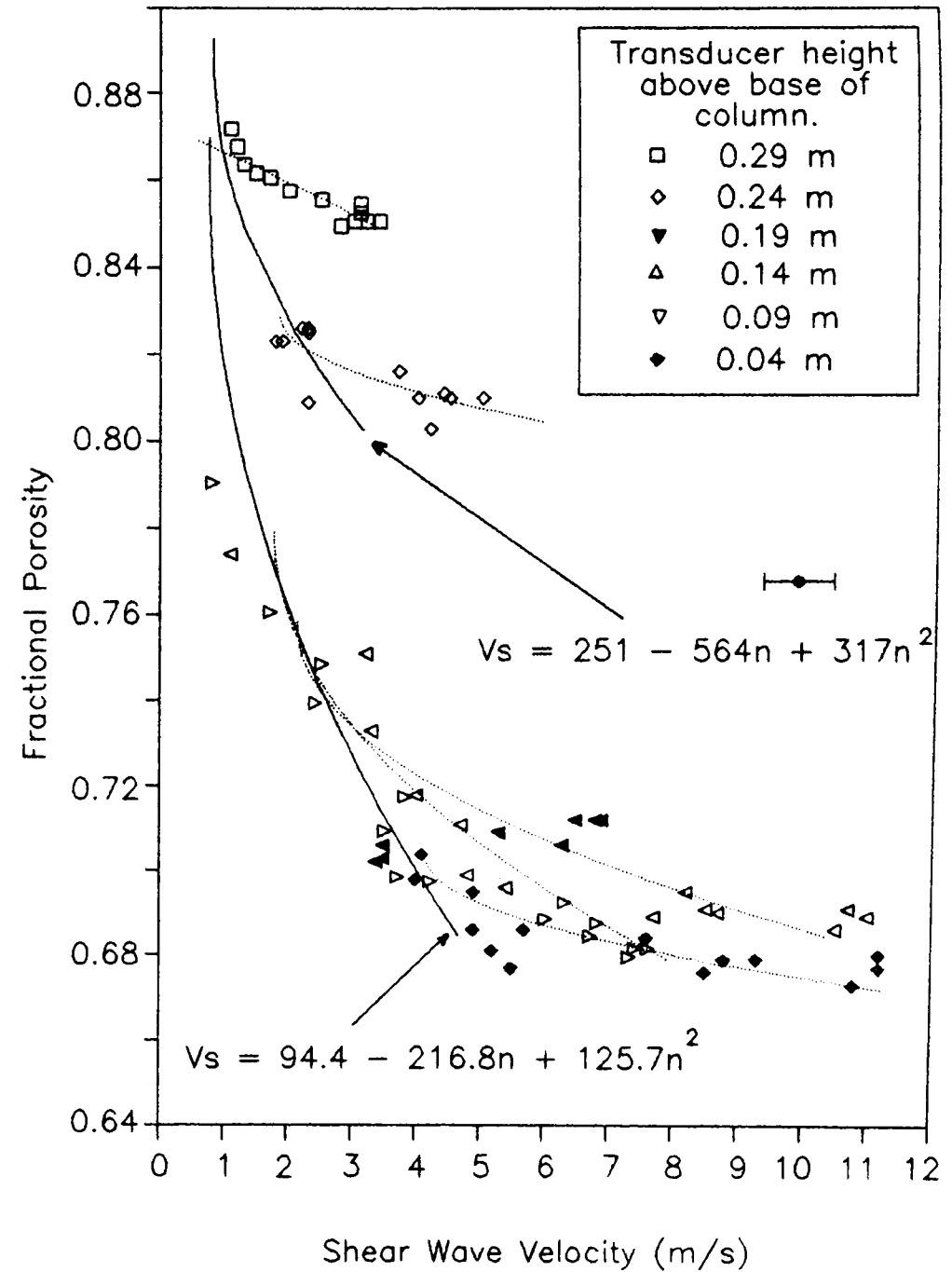
Figure 6.7   Shear wave velocity versus porosity.
Experiment IM11: Irvine Bay mud

The organic content of the sediment sample is known to influence the behaviour of the material significantly. Organic particles may be strongly adsorbed on clay mineral surfaces which may cause high plasticity, high shrinkage, high compressibility, low permeability and low strength (Grim 1962, Mitchell 1976). Data show that increasing the organic content by 1 or 2 percent may increase the liquid and plastic limits by 10 to 20 percent. Although the gross organic content of the samples examined in this thesis are lower than 2.6% (table A5.1) the process of sedimentation may result in preferential settling of the organics such that they form a much larger percentage of the soil at a particular height in the sediment column. This is likely to modify shear wave propagation in the sediment. Although the relationship between organic content and shear wave velocity or rigidity modulus cannot be defined within the present study it is an area that is of considerable interest to engineers and worthy of continued research.

6.3.3 THE INFLUENCE OF VERTICAL EFFECTIVE STRESS ON SHEAR WAVE VELOCITY AND SOIL STIFFNESS.

Figure 6.8 shows the relationship between shear wave velocity and vertical effective stress for experiment IM11. S-wave velocity has been interpolated for different soil elements using velocity gradient curves shown in table 6.2. at the end of this section. The data is typical of that seen in the other soils in this study. Each soil element demonstrates increasing V_s for increasing effective stress. Each element, on reaching maximum effective stress, shows a continued increase in velocity. This implies that shear wave velocity is sensitive to time dependent, or creep, influences.

The shear wave velocity data for experiments IM07 to IM11, are plotted in figure 6.9 against normalized effective stress σ'_n, or degree of consolidation,

where $$\sigma'_n = \frac{\sigma'}{\sigma_{max}} y$$

and σ' is the vertical effective stress, y is the percentage

mass above the soil element, and σ_{max} is the maximum vertical stress for a particular soil element. While the data are somewhat scattered, the linear trend of Vs-σ' can be seen. A line fitted to the data in the range $0 \leq \sigma' \geq 0.9$, thereby allowing creep effects to be discounted, is of the form

$$Vs = 4.44\sigma'_n + 1.077 \qquad \text{R-sq} = 0.395 \qquad N_N = 123$$

The fact that this equation gives a non-zero shear wave velocity at zero effective stress runs contrary to experimental observations. Since the soft soil under study possesses no residual stiffness, an equation of the form

$$Vs = 5.26(\sigma'_n)^{0.635} \qquad \text{R-sq} = 0.399 \qquad N_N = 123$$

fits the data equally well and gives a zero solution at zero effective stress. Figure 6.9 also shows that shear wave propagation does not generally occur until the degree of primary consolidation has reached 20% to 30%. Shear waves at this time have velocities ranging from 0.6m/s to 3.0m/s ±8.7%.

At the end of primary consolidation time dependent shear wave velocity increase continues. This effect illustrated in figure 6.10. The magnitude of velocity increase with time is found to be significant. In the limited period studied here, up to 2400 hours, velocity is seen to increase by roughly 0.001 ms^{-1}/hour. The phenomenon of shear wave velocity creep is believed to be due to continued soil frame development after primary consolidation. This continued soil development will manifest itself in terms of soil stiffness which is related to the rigidity modulus ($G=\rho Vs^2$). A plot of rigidity modulus versus normalized effective stress (figure 6.11) does show that the soil stiffness continues to increase after primary consolidation is complete. The soil is seen to have a wide range of rigidity modulus values for each state of effective stress. However, an upper boundary line does exist

$$G = 78\sigma'_n$$

for the soils primary consolidation stage. Rigidity modulus ranges from zero to 90kPa ± 8.7% during primary consolidation. The upper limit value is higher than rigidity modulus values

reported by other authors (see tables 2.1 and 2.2).

Anderson and Stokoe (1978) documented the time dependence of the rigidity modulus in kaolinite subject to large confining pressures. Thus the results from the sedimentation column have been analysed in a similar manner and figure 6.12 shows how rigidity modulus changes as a function of time. The curves seen in this figure are of a similar form to those observed by Anderson and Stokoe. Anderson and Stokoe identified two distinct phases which can be seen in the current figure; an initial phase was delimited by the zone where the modulus increases most rapidly with time. The second phase where the modulus increases linearly with the logarithm of time. The point of transition between the two phases, Anderson and Stokoe believed was coincident with the end of primary consolidation. However, this is not considered to be the case in the self weight consolidation studied here (100% primary consolidation being complete after approximately 1600 hours). Here the point of transition is seen to be a function of depth of burial i.e relating to transducer height, as well as time. Anderson and Stokoe defined a coefficient of rigidity modulus increase I_G

$$I_G = \frac{\Delta G}{\log_{10}(\Delta t)}$$

where ΔG is the change in rigidity modulus in the linear phase of the figure 6.12, and Δt is the associated time interval over which this change took place. In soft soil the values for I_G typically range from 0.65kPa for near surface soils to 60kPa at the base of the column (results are from experiment IM08).

As a conclusion to this analysis, the equation derived by Hardin and Black (1968) for clays with low surface activity

$$V_s = (18.4 - 6.20e)(\sigma')^{0.25}$$

was compared to the present experimental results. The equation is unsuccessful in predicting V_s in the soft soils studied here and is therefore considered inappropriate for use with

soft soils consolidating under self weight. The basic concept of the equation, that porosity and effective stress have a dual effect upon shear wave velocity, remains true.

Table 6.2 Shear wave velocity gradient curves for experiment IM11.

Time (hours)	Best fit curve	Coef. of Correlation
47.3	$V_s = 10.8 - 23.4z$	99.1%
55.7	$V_s = 7.44 - 12.0z$	96.4%
71.4	$V_s = 7.87 - 12.6z$	92.5%
97.2	$V_s = 9.05 - 14.2z$	95.7%
122	$V_s = 9.63 - 15.1z$	97.9%
146	$V_s = 9.85 - 15.3z$	98.7%
169	$V_s = 10.5 - 15.9z$	94.4%
289	$V_s = 14.3 - 21.3z$	88.8%
461	$V_s = 15.6 - 23.4z$	93.1%
627	$V_s = 16.0 - 23.6z$	93.2%
792	$V_s = 16.7 - 24.7z$	94.9%
1422	$V_s = 20.5 - 32.3z$	95.4%
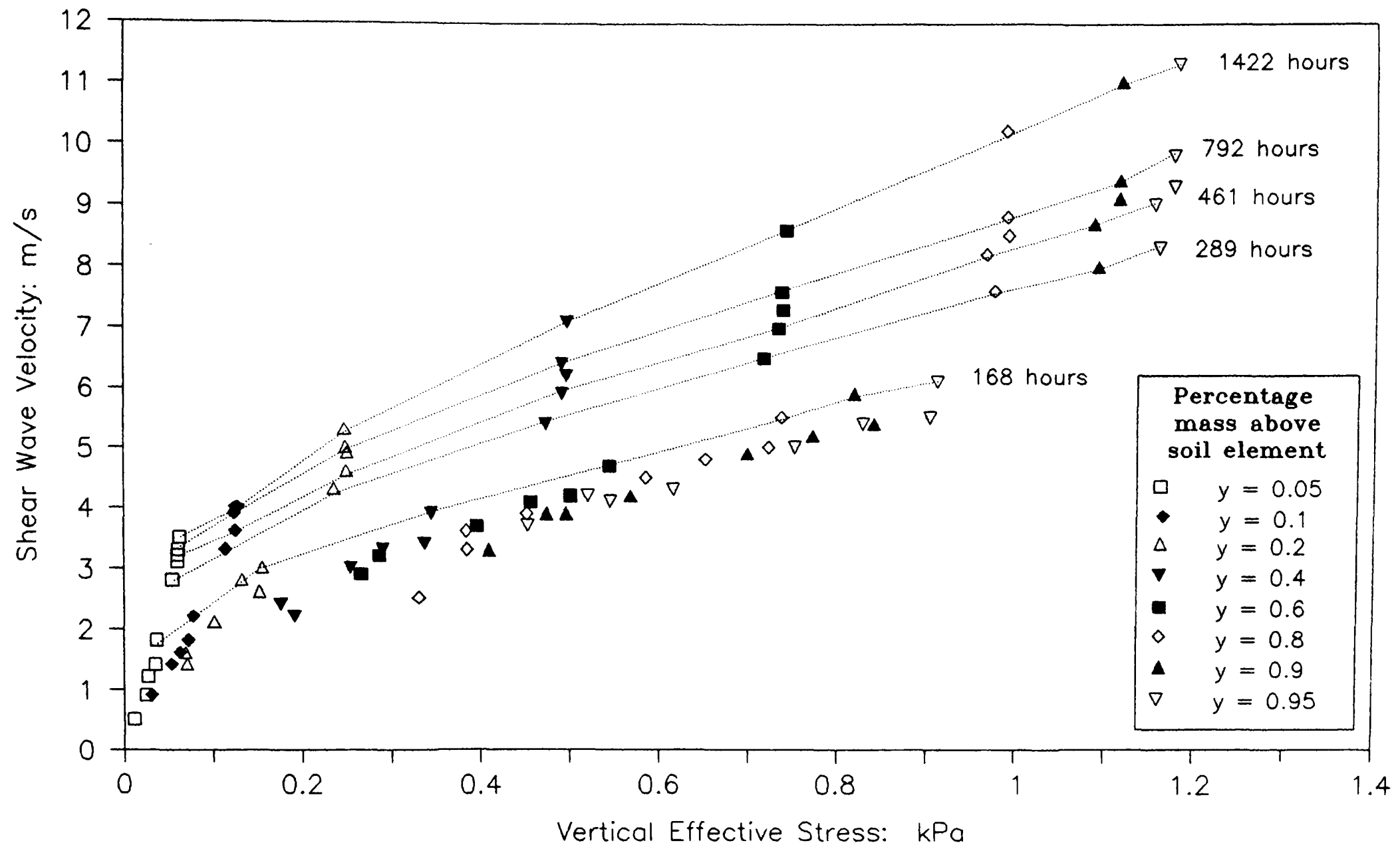
Figure 6.8 Shear wave velocity and vertical effective stress relationship.
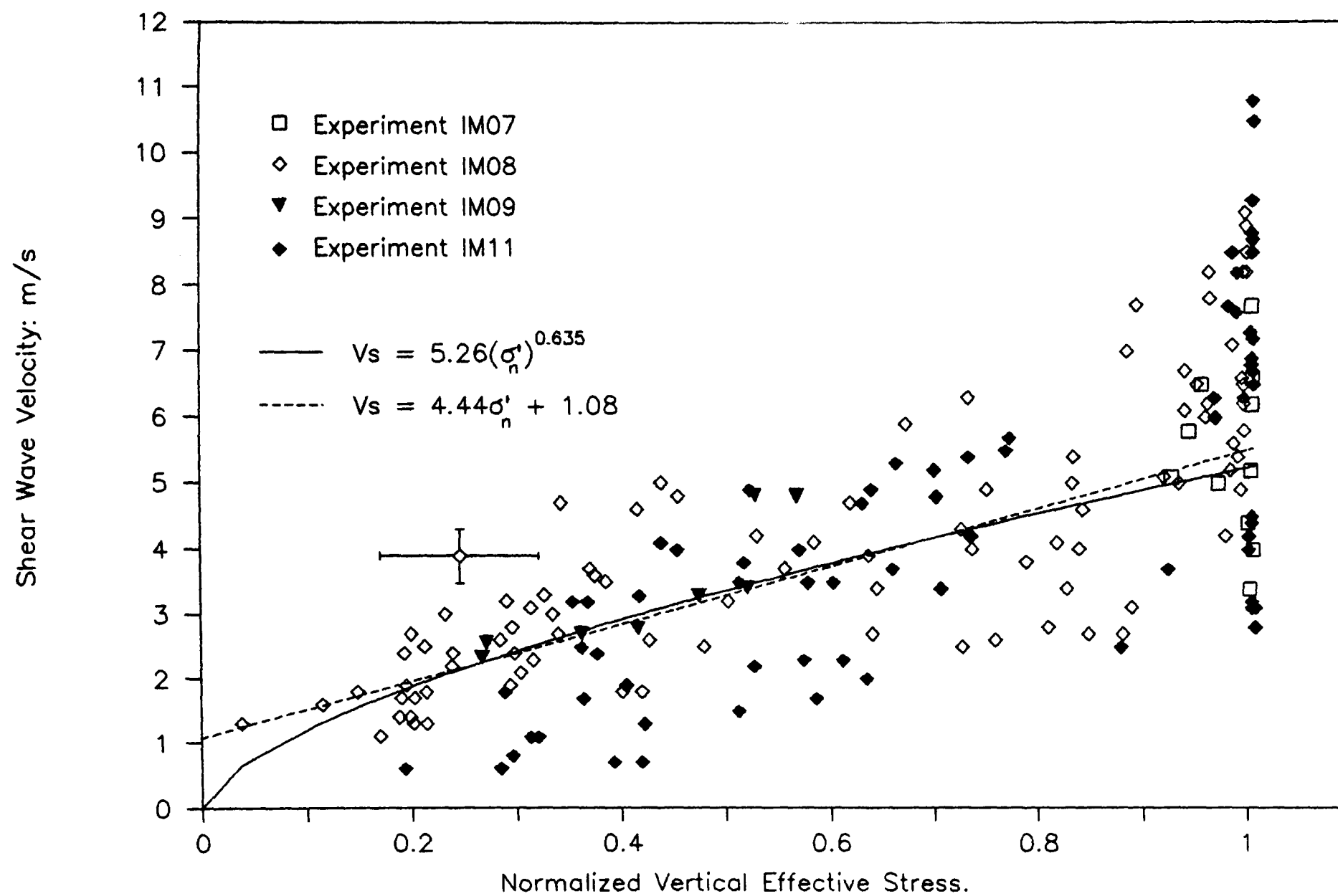
Figure 6.9   Shear wave velocity versus effective stress.
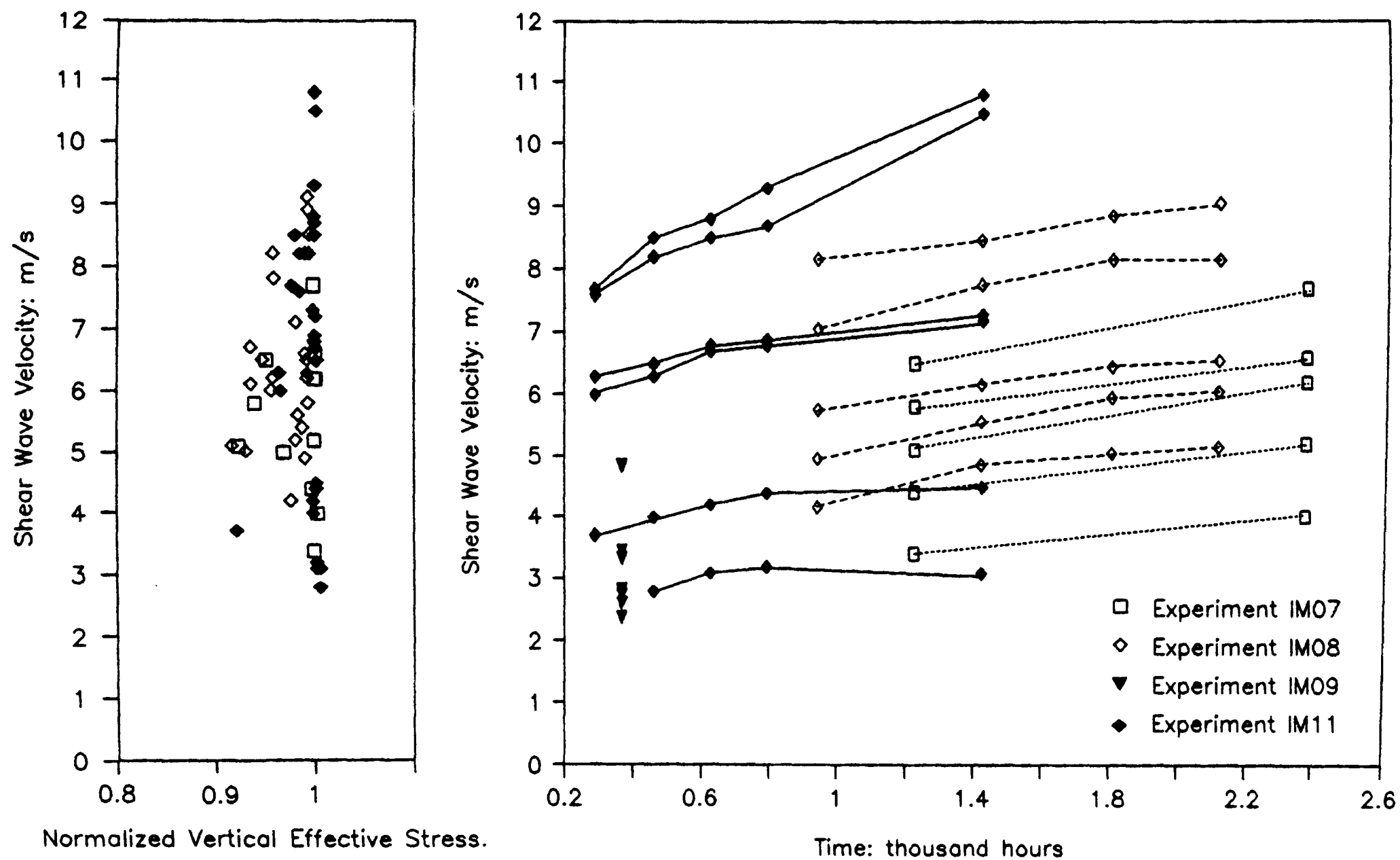
Figure 6.10 Time dependent shear wave velocity increase.
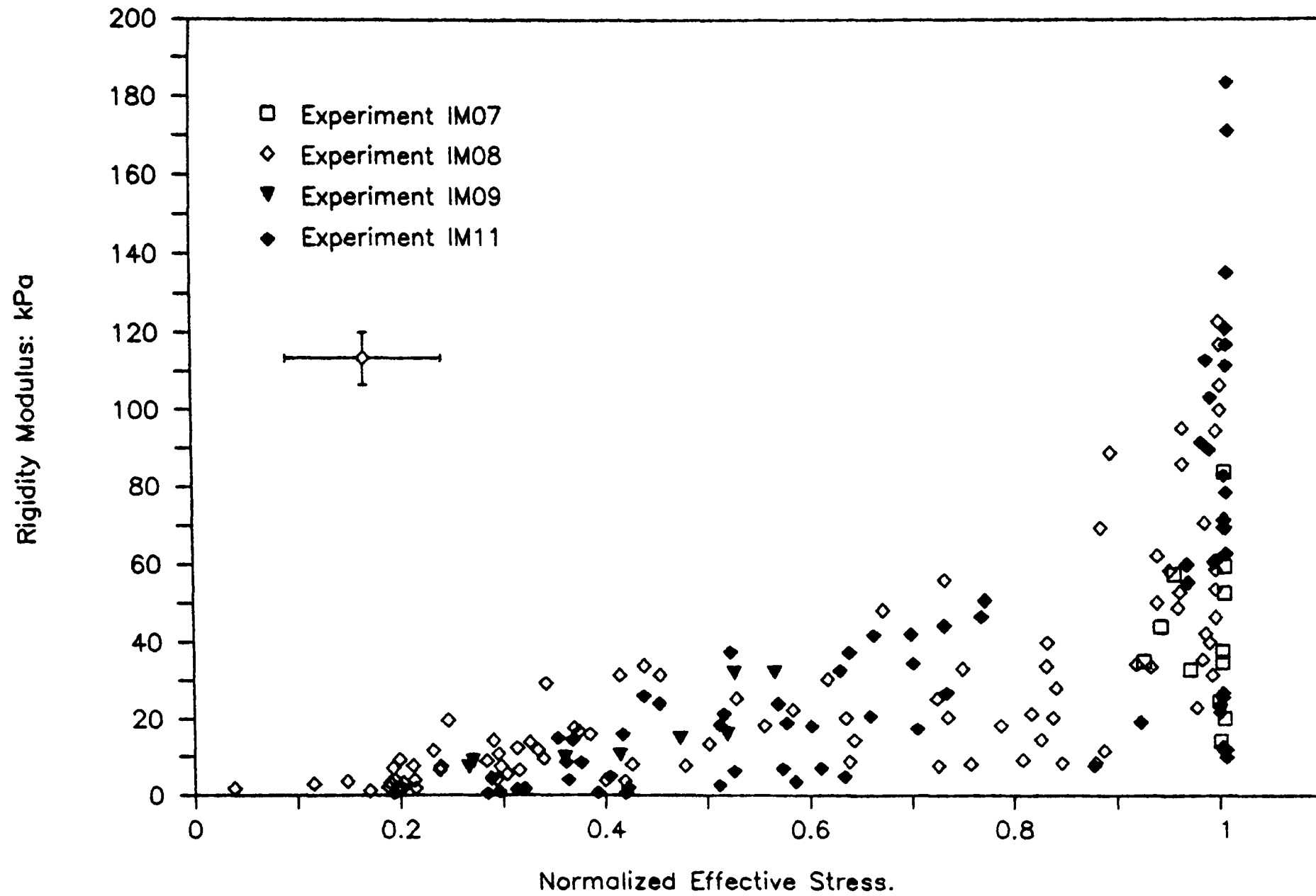
Figure 6.11   Soil Stiffness as a function of Effective Stress.
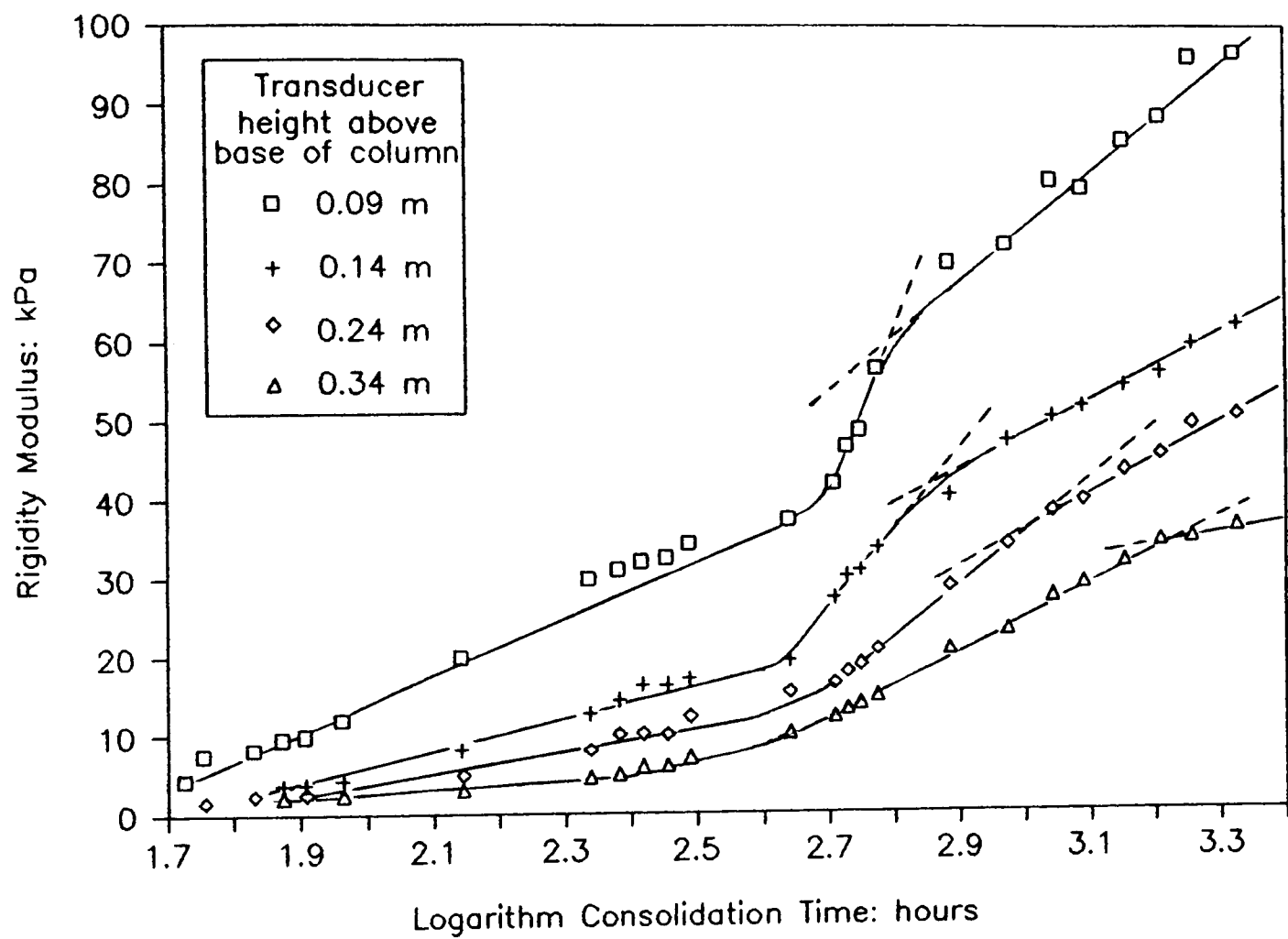
Figure 6.12. Rigidity modulus versus consolidation time.
Experiment IM08: Irish Sea clayey silt sample.

6.3.4 SHEAR WAVE PROPAGATION AS A FUNCTION OF FRAME COMPRESSIBILITY.

It was reported in section 2.2.3 that Taylor Smith (1986) had derived an empirical relationship relating shear wave velocity to soil frame compressibility, of the form

$$C_f = (0.001Vs^2)^{-1}$$

This equation has been compared to those derived empirically from the e versus σ' curves and the settlement curves of section 5.3.

The frame compressibility results shown in table 6.3 are found to agree to the first order of magnitude. The mean values of Taylor Smith's equation agree particularly well with the settlement curve result. It is concluded therefore that the Taylor Smith C_f versus V_s empirical relationship is valid for soft soils.

Table 6.3   Comparison of Frame Compressibility Results.

Expt. Ref	Vs (m/s)	$C_f=(0.001Vs^2)^{-1}$ ($\times10^{-4}Pa^{-1}$)	Void Ratio	C_f from e versus σ' curves ($\times10^{-4}Pa^{-1}$)	C_f from settlement curves ($\times10^{-4}Pa^{-1}$)
IM07	8 1	0.16 10.0	3 6	1.02 16.1	4.37
IM08	8 1	0.16 10.0	3 6	0.80 8.70	5.56
IM11	11 1	0.08 10.0	2 4 6	1.10 8.31 47.3	3.81

6.4   Soil Electrical Resistivity Data Analysis.

6.4.1   INTRODUCTION.

The soil electrical resistivity was continuously monitored during the course of the experiments. Converting the soil electrical resistivity to formation factor (F) eliminates the effects of pore fluid and therefore gives a meaningful measure of the properties of the soil fabric. The variation of formation factor with porosity will be reported in section 6.4.2, with section 6.4.3 describing how the mass coupling factor, as defined in Biot's theory, can be estimated using Brown's equation (described earlier in section 2.2.4). Finally the characteristic frequency of the soil will be estimated using the soil electrical resistivity and bulk density measurements (described in section 6.4.4).

6.4.2 THE EFFECT OF CHANGING POROSITY ON SOIL ELECTRICAL RESISTIVITY.

The soil electrical resistivity was corrected, to a reference temperature of $20^{\circ}C$ using the calibration curve given in appendix 3. The salinity of the pore fluid remained a constant $34^{\circ}/\circ\circ$ for all experiments. During the course of the experiments soil resistance was seen to increase, rapidly at first, then becoming a more gentle gradient with time. There was no apparent change in gradient which could be attributed to the onset of secondary consolidation.

The apparent formation factor (F) was calculated using equation 2.16. The bulk density measurements were used to determine an average porosity between the outer current electrodes. For each experiment the logarithm of apparent formation factor was plotted against logarithm porosity, (see figure 6.13). A linear trend was observed in the data and an empirical equation of the form suggested by Winsauer et al.
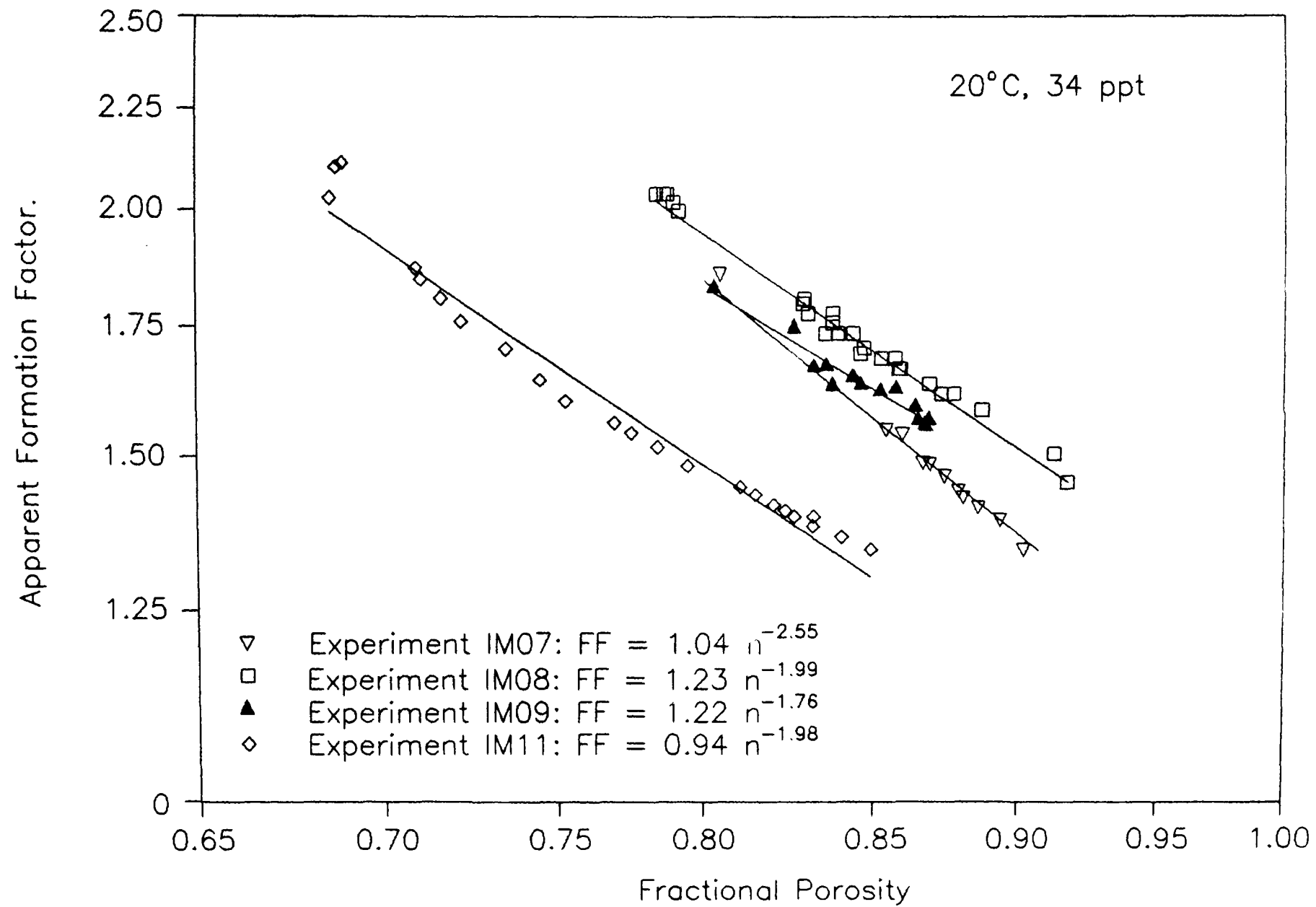
Figure 6.13 Apparent formation factor as a function of porosity.

(1952) could be fitted. The resulting equations relating apparent formation factor and porosity are presented in table 6.4.

Table 6.4 Empirical Relations between Apparent Formation
        Factor and Porosity.

Soil Classification	Equation
Experiment IM07 Irish Sea clayey silt	$F = 1.04 \; \eta^{-2.55}$
Experiment IM08 Irish Sea clayey silt	$F = 1.23 \; \eta^{-1.99}$
Experiment Im09 Irish Sea silty clay	$F = 1.22 \; \eta^{-1.76}$
Experiment IM11 Irvine Bay mud	$F = 0.94 \; \eta^{-1.98}$

All the results of the various experiments fall within the expected ranges described in the literature (see table 2.3 and figure A3.7). For experiment IM11 the data could have been interpreted as falling on two intersecting linear gradients. The apparent change in gradient was not associated with the onset of secondary consolidation (as was originally thought) but instead believed to be a consequence of either the encroachment of the sediment water interface into the sampling electric field, or perhaps related to a low density upper layer of predominantly clay particles, moving into the sampling field of the electrodes. Though one would expect such particles to lower the measured formation factor they would also greatly reduce the averaged porosity. The combined effect could be to produce the trend seen in figure 6.13. The lower portion of the curve has an empirical relation of

$$F = 1.05 \; \eta^{-1.49}$$

Such a relationship is probably acceptable since experiment IM11 comprised of a mud, having a larger sand fraction than previous experiments, and as a consequence the equation's index would be expected to be reduced (Jackson 1975). Similarly, fitting a line to the upper portion of the curve

produces the following relation which represents a very platey material representative of a clay.

$$F = 0.7 \, \eta^{-2.90}$$

6.4.3 THE ESTIMATION OF A SOFT SOILS MASS COUPLING FACTOR.

Using Brown's relationship the mass coupling factor can be estimated for a range of porosities using the empirical equation from table 6.4. The results of such a computation are presented in table 6.5.

The value of mass coupling factor "b" for these experiments are found to lie between Stoll's theoretical upper and lower limit of $1 \leq b \leq 3$. The trend of the calculated values of "b" in table 6.5 is thought to represent a soil matrix which in its highest porosity state is composed of large pore spaces with large "throats" between the soil particles. In such a soil the tortuosity would be small and may approximate very nearly to Stoll's theoretical lower limit (b=1) representing uniform and parallel pores. As the soil consolidates the pore spaces and "throats" would reduce in size, increasing tortuosity and giving rise to an increase in mass coupling factor.

Table 6.5   Estimation of Biot's Mass Coupling Factor using Brown's Relationship.($b = F.\eta$)

Soil Classification	Fractional Porosity	Mass Coupling Factor
Experiment IM07 Irish Sea clayey silt	0.90 0.80 0.70	1.22 1.47 1.81
Experiment IM08 Irish Sea clayey silt	0.90 0.80 0.70	1.36 1.53 1.75
Experiment IM09 Irish Sea silty clay	0.90 0.80 0.70	1.32 1.44 1.60
Experiment IM11 Irish Sea mud	0.90 0.80 0.70	1.04 1.17 1.33

6.5   Compressional Wave Data Analysis.

6.5.1 INTRODUCTION.

The correlation between compressional wave velocity and bulk density was illustrated in chapter 4. In this section a more detailed analysis of the P-wave data in terms of its relationship with porosity will be made. Compressional wave velocity (V_P) and porosity (η) data will be studied and empirical relationships derived. The relationships will then used to make back predictions to reconstruct the bulk density profiles using the velocity data. These profiles will be used in chapter 7 for comparison with density profiles predicted from the Biot model.

6.5.2 THE EFFECT OF CHANGING POROSITY ON COMPRESSIONAL WAVE PROPAGATION.

The compressional wave velocity has been normalized with respect to the velocity of sound in water and plotted against fractional porosity, determined from the bulk density profiles. The data are presented in figures 6.14 to 6.17. The scatter in the velocity data may be attributed to several factors: local temperature fluctuations, gas pockets caused by biological activity, and localised refraction events within the soil elements. The resulting V_P data are accurate to ±6m/s and the porosity to ±0.6%. However, at the sediment water interface the accuracy decreases as a result of surface inhomogeneities. Polynomial equations have been fitted to the porosity-V_P data, the resulting equations being given in table 6.6.

Figures 6.14, 6.15 and 6.17 exhibit a distinct minimum between 80% and 90% porosity. Compressional wave velocity is a function of bulk modulus, rigidity modulus and bulk density as shown in equation 2.10. The distinct V_P-porosity curve appears to result from a balance of influence between bulk density and rigidity modulus. At high porosity the bulk density term

dominates and V_p falls with decreasing porosity. The minimum is thought to represent the stage at which some critical development in the soil frame occurs resulting in an increase in frame rigidity which in turn causes the compressional wave velocity to rise with continued decreasing porosity. Comparing the data of table 6.6 to the figures of 6.4 to 6.7 may provide evidence to support this hypothesis. It is significant that the shear waves propagating in the sediments studied in this research programme first appear at porosities very nearly coincident (within 2% or 3%) with the porosity associated with the P-wave velocity minimum.

Ogushwitz (1985) considered that the definition of the porosity-V_p minimum was governed by the relative density of the solid and fluid constituents. The present investigation would support this view since the mud sample (experiment IM11), having a specific gravity of 2.643, displays a poorly defined minimum (figure 6.20), whilst the clayey silts of experiments IM07/IM08, having a larger specific gravity of 2.665, display a slightly more pronounced minimum.

The accuracy with which the empirical equations (table 6.7) could be used to reconstruct the bulk density profile was required for later comparison with Biot model predictions. The density profiles of experiment IM11 (shown in figure 4.10) were selected for reconstruction owing to the presence of an interesting density inversion. The P-wave velocity profiles for 2.4, 21.5, 49 and 1422 hours were used in the reconstruction. Velocities at the respective sampling heights were input into the appropriate equation of table 6.6 and the quadratic was solved for porosity. In cases were the measured V_p was less than that of the P-wave velocity minimum value, the velocity was assumed to be at the minimum porosity. The resulting density profiles are shown in figure 6.21 in which the density inversion is seen to be successfully reproduced. The correlation between predicted and real density profiles improved with time as the soil porosity decreased and V_p increased beyond the minimum value. Further comparisons will be made in chapter 7.
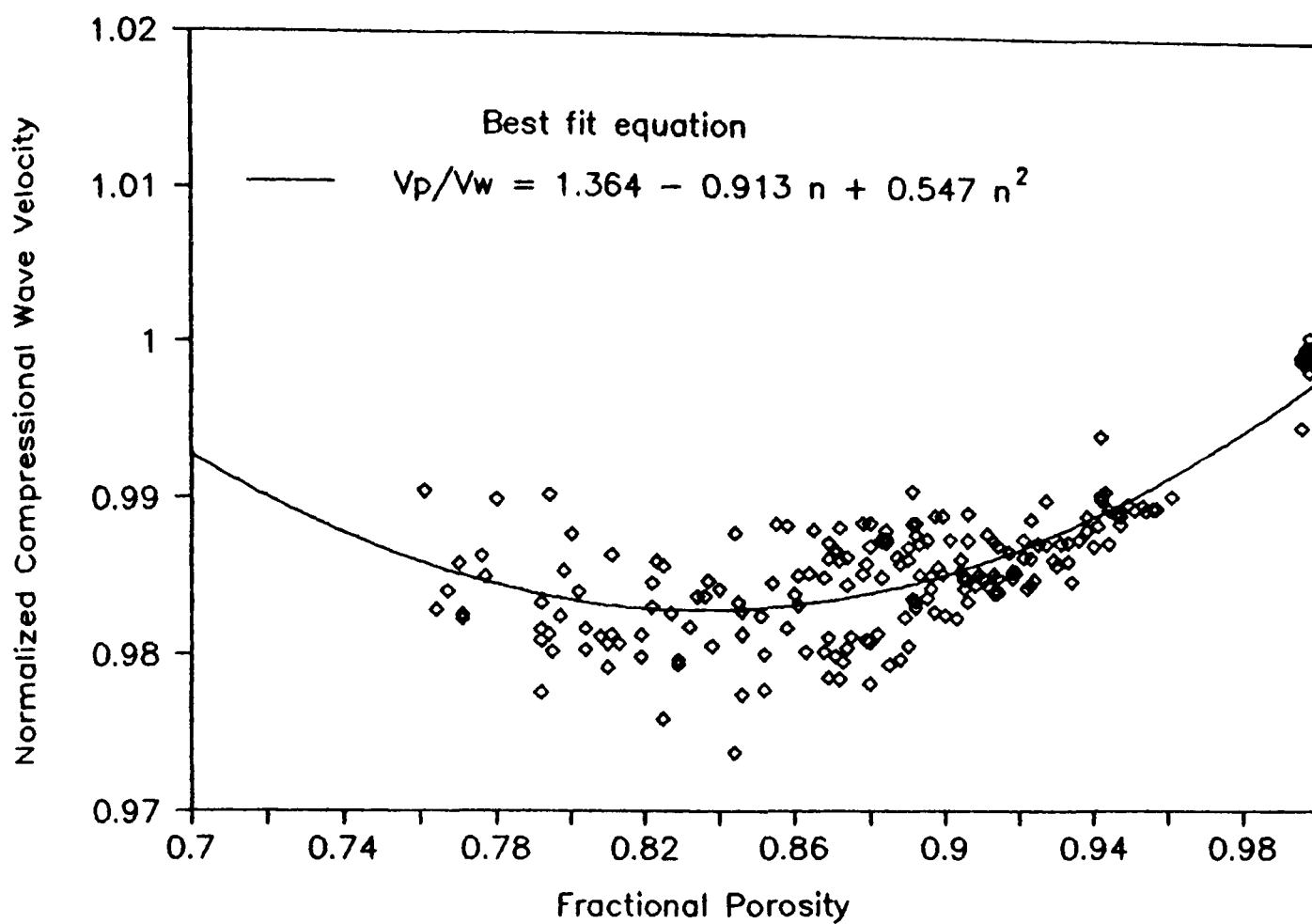
Figure 6.14 Normalized velocity versus porosity: Experiment IM07.
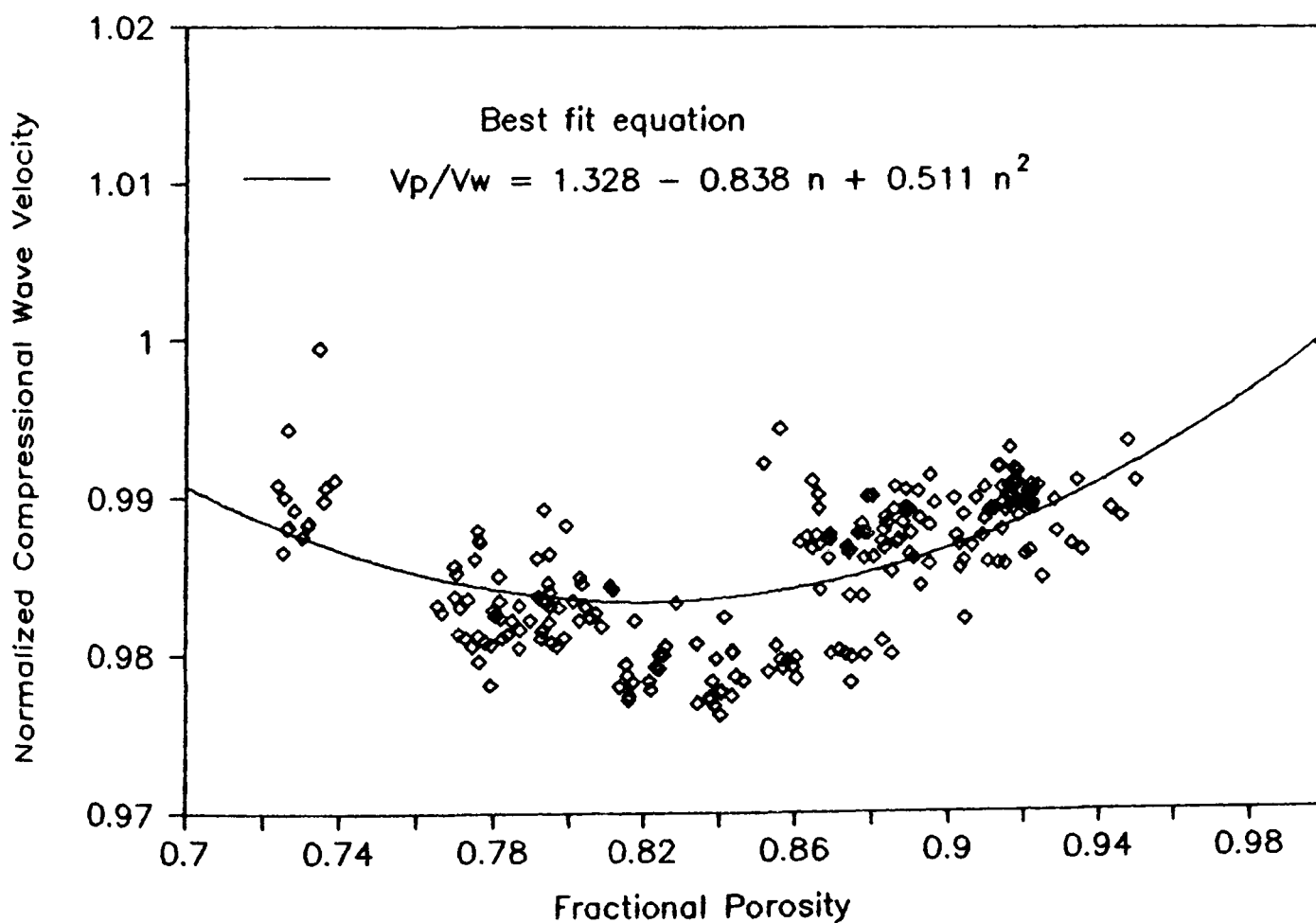
Figure 6.15 Normalized velocity versus porosity: Experiment IM08.
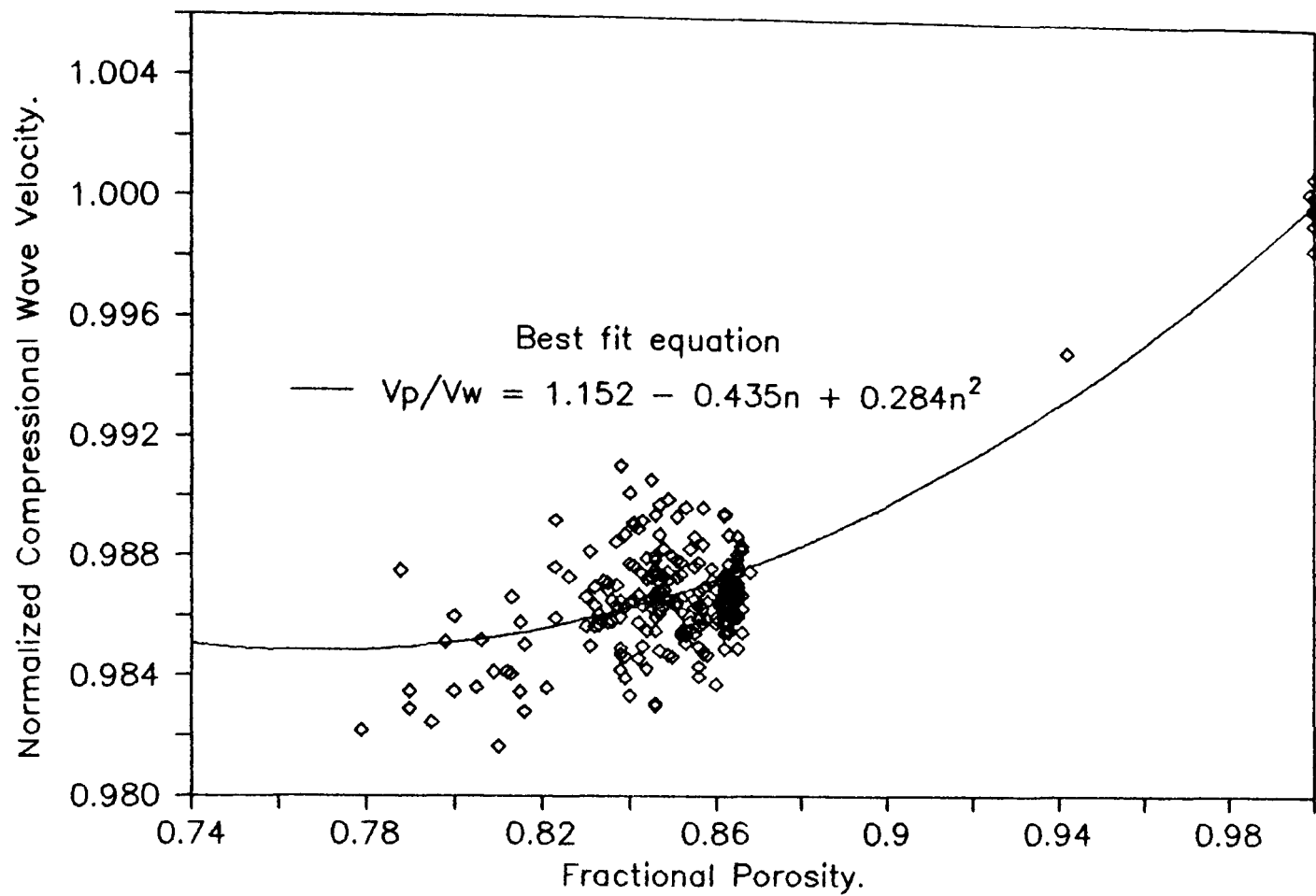
Figure 6.16   Normalized velocity versus porosity: Experiment IM09.
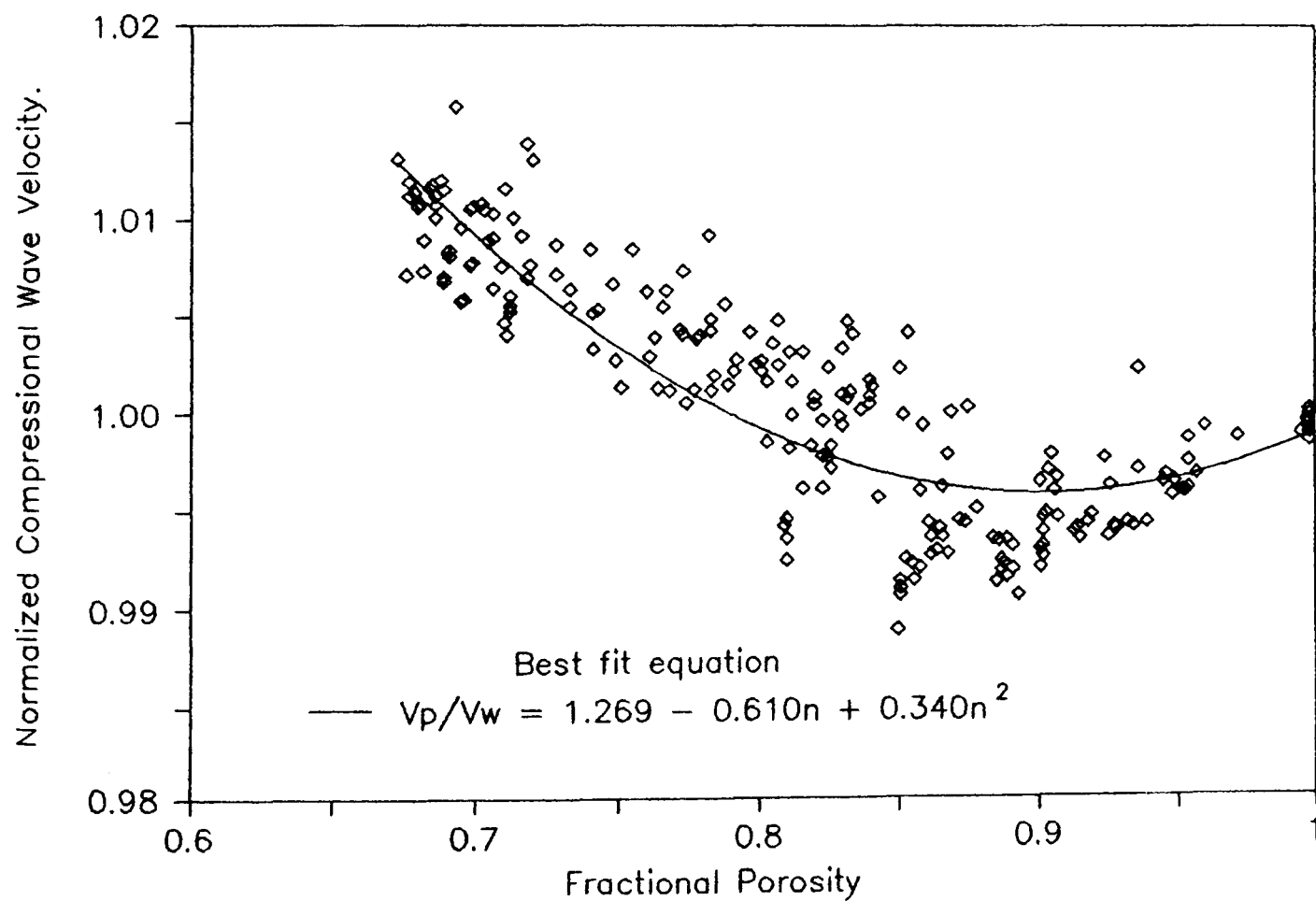
Figure 6.17   Normalized velocity versus porosity: Experiment IM11.

Table 6.6 Compressional wave velocity-porosity relationships.

Expt. Ref.	Soil type	G_s	Empirical Relationship	Porosity relating to V_P minimum
IM07	clayey silt	2.665	$\frac{V_P}{V_w} = 1.364 - 0.913\eta + 0.547\eta^2$ $N_N = 205 \quad R\text{-sq} = 0.775$	0.834
IM08	clayey silt	2.665	$\frac{V_P}{V_w} = 1.328 - 0.838\eta + 0.511\eta^2$ $N_N = 499 \quad R\text{-sq} = 0.851$	0.820
IM09	silty clay	2.684	$\frac{V_P}{V_w} = 1.152 - 0.435\eta + 0.284\eta^2$ $N_N = 226 \quad R\text{-sq} = 0.801$	0.766
IM11	mud	2.643	$\frac{V_P}{V_w} = 1.269 - 0.610\eta + 0.340\eta^2$ $N_N = 324 \quad R\text{-sq} = 0.753$	0.897

where N_N is the number of observations and R-sq is the coefficient of correlation.

Figure 6.18 Density Profiles produced from the Compressional Wave Velocity–Porosity Empirical Relationship.
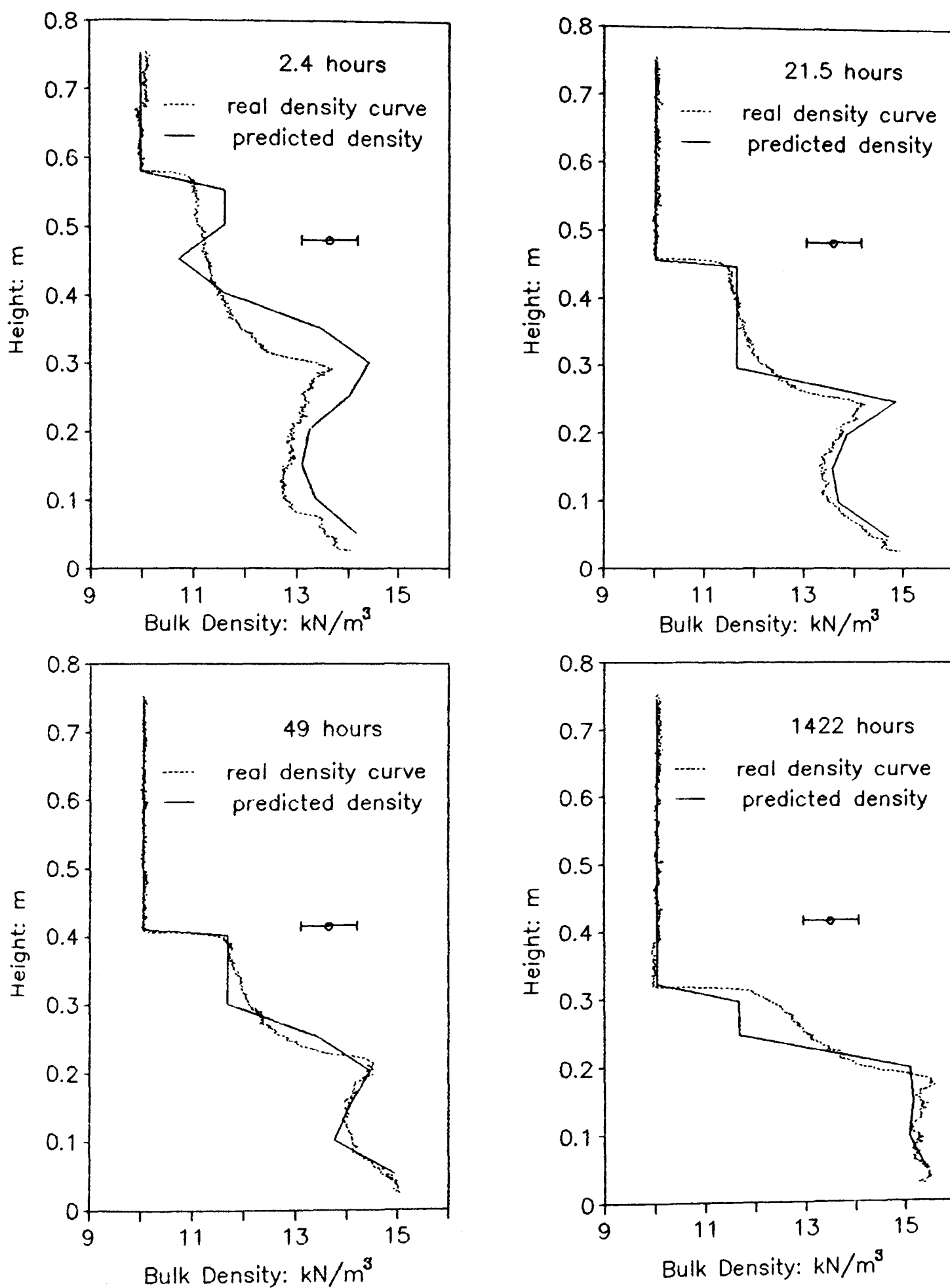
6.6   Summary.

The seismo-acoustic behaviour of a number of soft soils has been analysed. The changing behaviour of the sediment, as it consolidates, and as the soil structure develops, is shown to have considerable influence on the geophysical properties of the soil. The relationship between the consolidation phenomena and these changing geophysical properties will now be reviewed.

Soil electrical resistivity was measured during the course of the experiments to establish how the formation factor, a measurement indicative of the soil fabric, changed as a result of consolidation. A linear trend between the logarithm relationships of formation factor and porosity was observed. This is in agreement with current findings in the literature. Brown's equation was used to compute estimates for Biot's mass coupling factor. The result of this computation showed that in the soil samples studied in this thesis the soil fabric remained as a very open structure throughout the experiments. The soil pores could be considered to approximate to a set of uniform and parallel conduits although it must be stressed that the measurement of mass coupling factor indicated that the tortuosity of the soil pores increased during the course of the consolidation process.

Shear wave measurements within the consolidating soil revealed phenomena of considerable interest to geotechnical engineers. Shear waves generally behaved in much the way reported by previous authors. Small amplitude shear waves were recorded propagating at velocities ranging from below 1m/s up to 11m/s even after extensive periods of consolidation. Shear waves were observed to undergo time dependent increase, or creep. This increase was believed to be a result of continued clay particle floc interaction during secondary consolidation. Evidence for this is demonstrated as the effect reduces with increasing silt and sand content. The relationship between shear wave velocity (V_s) and porosity under the influence of creep took on a more complex form than had previously been

documented. However, some headway was made in the interpretation of these relationships.

The degree of consolidation (σ'_n) for these experiments could be estimated from shear wave velocity by using the empirical equation

$$V_s = 5.26 (\sigma'_n)^{0.635}$$

Taylor Smith's empirical equation for the estimation of soil frame compressibility (C_f) remains valid in soft soils for the

$$C_f = (0.001 V_s)^{-1}$$

Rigidity of the soil was again subject to creep effects, increasing after the termination of primary consolidation. The values of rigidity modulus (G) measured in these experiments were of the same magnitude as those recorded by other authors, using both geophysical and geotechnical techniques. Though no unique relationship between rigidity modulus and effective stress was observed in these soils, primary consolidation was bound by an upper limit defined by

$$G = 78 \, \sigma'_n$$

where σ'_n represents the degree of consolidation.

The results of this geophysical data analysis will be utilized in the following chapter to investigate the use of the Biot theory in predicting the geotechnical consolidation behaviour of the soil.

CHAPTER 7   THE MODELLING OF GEOTECHNICAL PROPERTIES OF SOFT SOILS USING GEOPHYSICAL MEASUREMENT.

7.1   Introduction.

It is the ability of the Biot theory to explain the dispersive behaviour of seismo-acoustic waves in a number of saturated porous media that justifies its use in the present study. The theory will be used to predict the consolidation properties of soft soils using the geophysical measurements so far described. Two modelling programs are utilized in this study which are based upon the theoretical treatment outlined in appendix 2. The first of these programs is based upon the Geertsma and Smit approximation of the Biot theory which make use of equations 2.19 to 2.23 in chapter 2. The second program is that of Stoll's based on the full Biot model (Stoll 1989) described in appendix 2.

The method of predicting the permeability and bulk density using the computer programs and geophysical measurements are described in section 7.2, the modelling programs will then be used in the following section (section 7.3) to predict the consolidation properties of the soil samples studied in the column experiments. The results of the modelling procedures will be discussed in the final section of this chapter.

7.2   The prediction of soil properties using geophysical measurements.

7.2.1 THE PREDICTION OF SOIL PERMEABILITY.

The coefficient of permeability (k) will be predicted for a number of Irish Sea soils using the Geertsma and Smit model and the Stoll full model. The modelling procedure is based upon the calculation of a compressional wave dispersion curve. The permeability, being an input parameter of the model, is adjusted until the predicted curve agrees with the observed

P-wave velocity measured at an applied frequency of 500kHz. The dispersion curve modelling routine is shown in the flow chart of figure 7.1.

In order to predict permeability using the Stoll full model it is necessary to have the following input parameters (listed below). Parameters that are common to the Geertsma and Smit's approximate solution are marked by an asterisk:

*(1)   Solid compressibility, C_s

*(2)   Liquid compressibility, C_w

*(3)   Frame compressibility, C_f
       or poissons ratio.

*(4)   Rigidity modulus, G.

*(5)   Bulk density, ρ

*(6)   Solid density, ρ_s

*(7)   Fluid density, ρ_w

*(8)   Mass coupling factor, b

*(9)   Applied frequency, f

*(10) Compressional wave velocity, V_P

(11)   Absolute viscosity of fluid

(12)   Logarithmic decrement for shear waves

(13)   Ratio edec/gdec

(14)   Pore size parameter, d

To use the Geertsma and Smit program (listed in appendix 4) to predict permeability the model input parameters 1-10 are required. Many of these parameters have already been established in previous chapters. The frame bulk modulus $(1/C_f)$ and rigidity modulus (G) have been found to be so small that they have negligible effect on the Biot model solution, and will be regarded here as zero representing a "weak frame" model. The solid and liquid compressibilities dominate the model under these circumstances. The liquid compressibility can be determined from the compressional wave velocity and water density. The value 2.78×10^{-11} Pa^{-1} for solid compressibility, is taken from previous authors work in Irish Sea soils (Hamdi and Taylor Smith (1982) and Hurley (1989)).

G & S MODEL

i/p parameters (1) to (10)

i/p guess for k

calculate dispersion curve

IS calc. Vp = obs. Vp at applied frequency

N

Y

IS $f \leqslant f_t$

Y

ACCEPT VALUE OF k

N

FULL MODEL

i/p parameters (1) to (14)

i/p guess for k

calculate "d"

calculate dispersion curve

IS calc. Vp = obs. Vp at applied frequency

N

Y

ACCEPT VALUE OF k
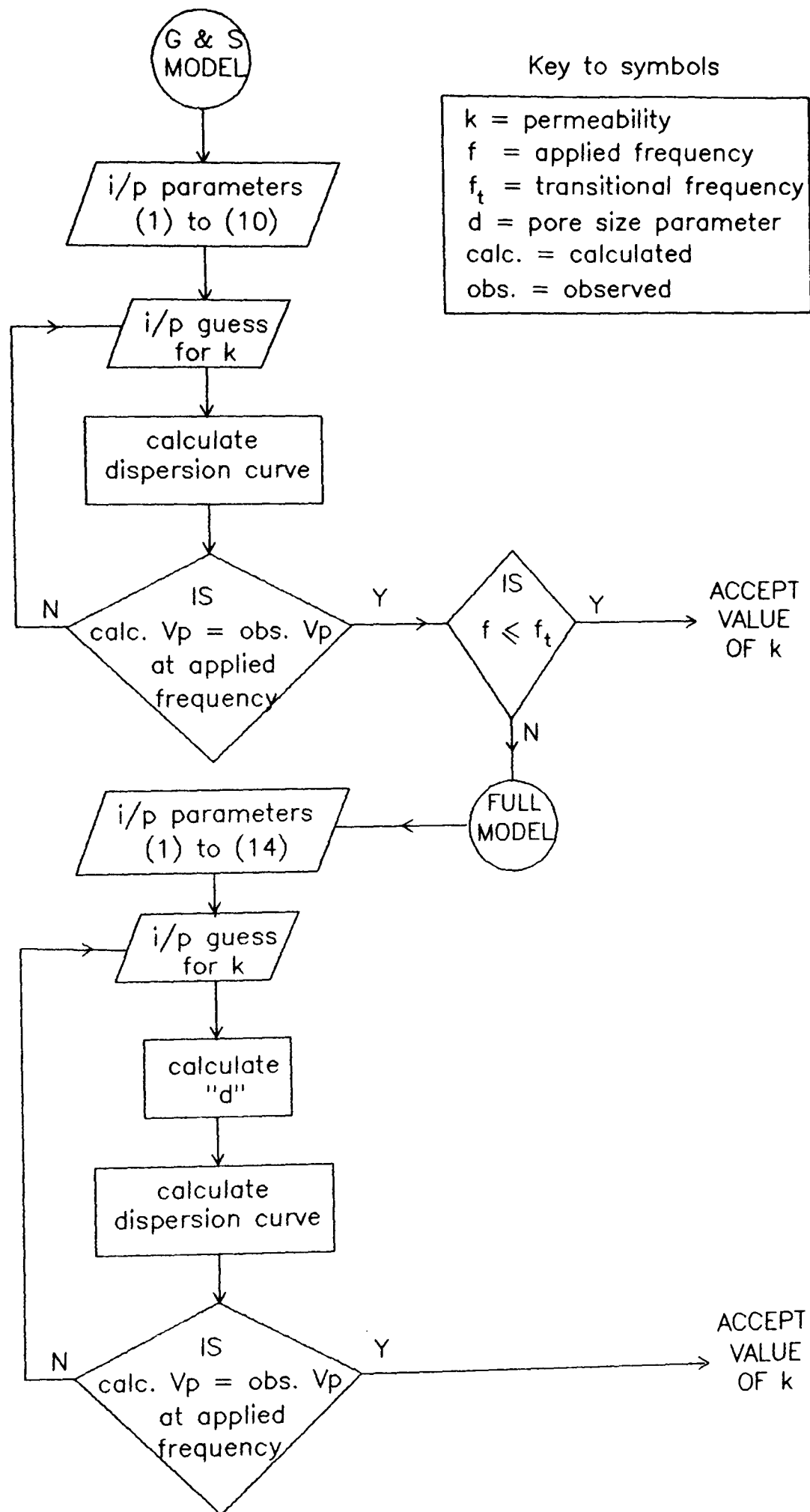
Figure 7.1   Flow chart of permeability prediction routine.

In order to use the full model program (listed in appendix 4) to predict permeability the input parameters 1 to 14 are required. The additional parameters include; the absolute viscosity of the fluid, logarithmic decrement for shear waves, and ratio of edec/gdec (where edec and gdec are the logarithmic decrements of longitudinal and torsional oscillations). Suitable values for these parameters were obtained from Stoll (1986). The pore size parameter (d) is also introduced (discussed in chapter 2) and will be estimated using the following formulae:

$$d' = \frac{a}{3} \cdot \left(\frac{\eta}{(1-\eta)} \right) \qquad \text{(Hovem and Ingram 1979)}$$

$$d'' = \left(\frac{8\ \phi}{\eta} \right) \qquad \text{(from Briggs 1991)}$$

where "a" is the mean grain diameter, "η" is fractional porosity and "ϕ" is permeability (units area). The permeability predictions will be made using the data from the Irish Sea clayey silt sample (experiments IM07 and IM08) and the Irvine Bay mud (experiment IM11) in section 7.3.

7.2.2 MODELLING COMPRESSIONAL WAVE BEHAVIOUR IN A SOFT SOIL WITH CHANGING POROSITY.

In section 6.5.2, the derivation of empirical equations to the V_P versus porosity data was considered. To have any confidence in such equations it is necessary to have a large data set. It may, however, be possible to use just a handful of data points to generate a representative curve for this relationship using the Geertsma and Smit model.

The "weak frame" soil parameters will be used in the Geertsma and Smit model to determine best fitting curves for the experimentally derived compressional wave velocity (V_P) versus porosity relationship. The characteristic frequency and mass coupling factor are regarded as the model variables and will be suitably modified, within sensible limits, until a best fit is obtained with the V_P-porosity data.

7.2.3 USING THE GEERTSMA AND SMIT MODEL TO REPRODUCE SOFT SOIL BULK DENSITY PROFILES FROM GEOPHYSICAL MEASUREMENT.

Having established a best fitting curve to the V_P-porosity relationship using the Geertsma and Smit model (section 7.2.2) the model is again used to reproduce bulk density profiles from the corresponding compressional wave velocity profiles. Bulk density profiles will be generated and compared to those directly observed at convenient stages during the consolidation process.

7.3 Predictions of consolidation phenomena using geophysical measurement.

7.3.1 INTRODUCTION.

In this section the Geertsma and Smit approximate solution to the Biot model will be used to model the compressional wave velocity-porosity relationship of the soils studied in the sedimentation columns. The approximate model is also used to reproduce bulk density profiles from P-wave velocities. The Geertsma and Smit and full model computer programs will be used to predict the coefficient of permeability of the soils studied in the instrumented settling column. This analysis considers each soil type in turn. The results are discussed in section 7.4.

7.3.2 EXPERIMENT IM03 AND IM04 IN AN IRISH SEA CLAY.

Experiments IM03 and IM04 were investigations into the settling behaviour of Irish Sea clays using the prototype column. The bulk density, and hence porosity, was measured using a PAAR density meter (see appendix 3 for details of the PAAR density meter) capable of measuring density to an accuracy of $\pm 1 kg/m^3$.

The Geertsma and Smit approximate solution was used to determine best fitting curves to the experimentally derived

compressional wave velocity (V_P) versus porosity relationship. The V_P versus porosity relationships for these experiments are shown in figures 7.2 and 7.3. The relationship was modelled using the input parameters shown in table 7.1. The prototype column had no means of measuring the soil's electrical resistivity therefore a value of 1 was assumed for the mass coupling factor in this instance. The effect of changing porosity and therefore permeability also, on the characteristic frequency (f_c) of the soil is clearly illustrated in figure 7.2. In this figure, experiment IM03 is shown to consist of two V_P profiles measured at time intervals of 1 hour and 23 hours after the slurry introduction to the sediment column. The V_P-porosity relationship is modelled in the first instance by using a value for f_c of 550kHz. After the passage of 23 hours the relationship can be modelled using the same "weak frame" parameters but with an increased f_c of 650kHz. It should be realized that the relationship depicted in figure 7.2 (and those of subsequent analyses) are based on instantaneous measurements of a soil system that is in a continual state of change. It must be emphasized that at such characteristic frequencies, as used in these models, the applied frequency of 500kHz would be expected to induce non-linear flow in the soils pore fluid. This makes any formal use of the approximate solution invalid. However, if the model is regarded as a purely curve fitting tool, as in this case, a number of characteristic frequencies may be selected to adequately represent the ever changing V_P-porosity relationship.

The Geertsma and Smit model is used to reproduce the bulk density profiles for experiment IM04. The profiles for 72, 311, 670 and 815 hours experiment duration were modelled using the corresponding compressional wave velocity profiles, the input parameters of table 7.1 and a characteristic frequency of 750kHz. The resulting profiles are shown in figure 7.4. The agreement between the observed and predicted profiles are reasonably good although it is realized that the data set is somewhat limiting.

Table 7.1   The Geertsma and Smit model input parameters for experiment IM03/IM04.

1. Fluid density = 1000 kg/m^3
2. Solid density = 2718 kg/m^3
3. Fluid compressibility = 4.55x10^{-10} Pa^{-1}
4. Solid compressibility = 2.78x10^{-11} Pa^{-1}
5. Characteristic frequency = 575kHz 1MHz
6. Applied frequency = 500 kHz
7. Frame compressibility = 0
8. Rigidity modulus = 0
9. Mass coupling factor = 1
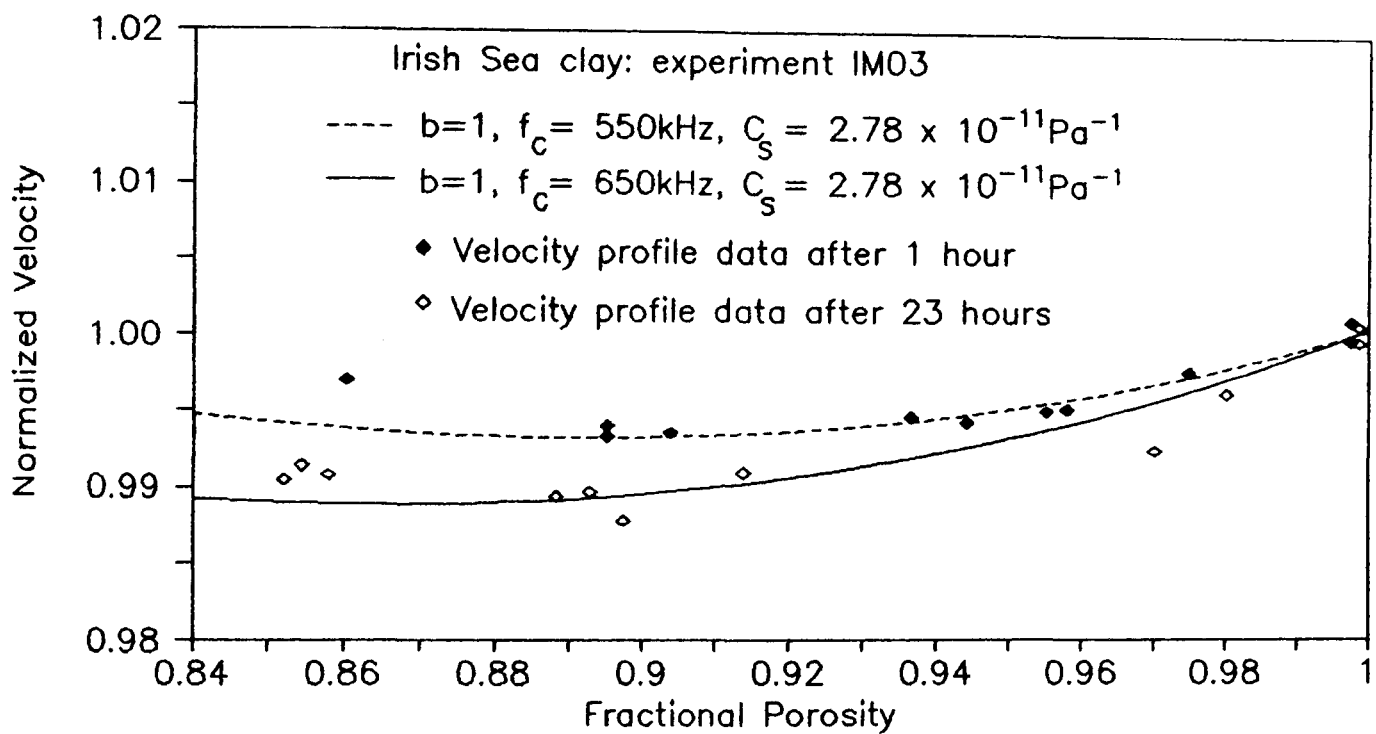
Figure 7.2 G & S model prediction of velocity–porosity relationship.
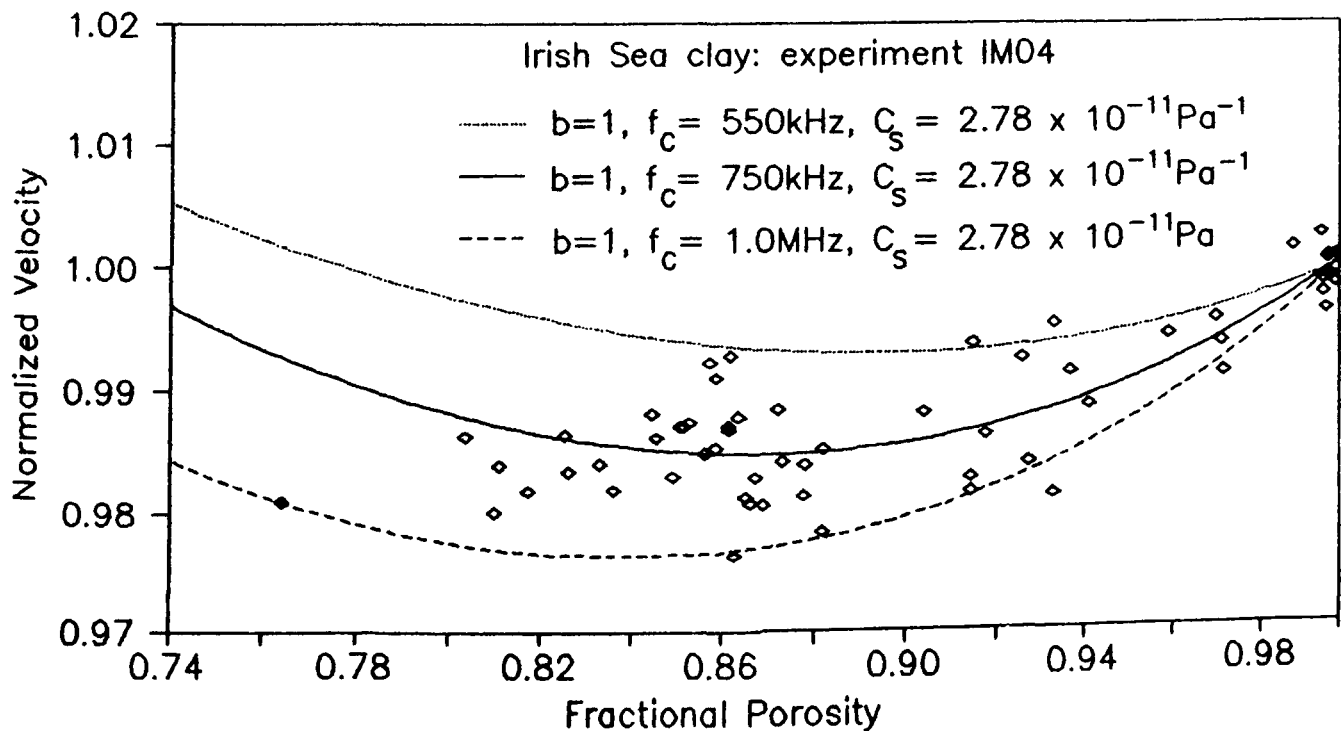
Figure 7.3 G & S model prediction of velocity–porosity relationship.

Figure 7.4   Density Profiles for an Irish Sea Clay using the Geertsma and Smit Model: Experiment IM04.
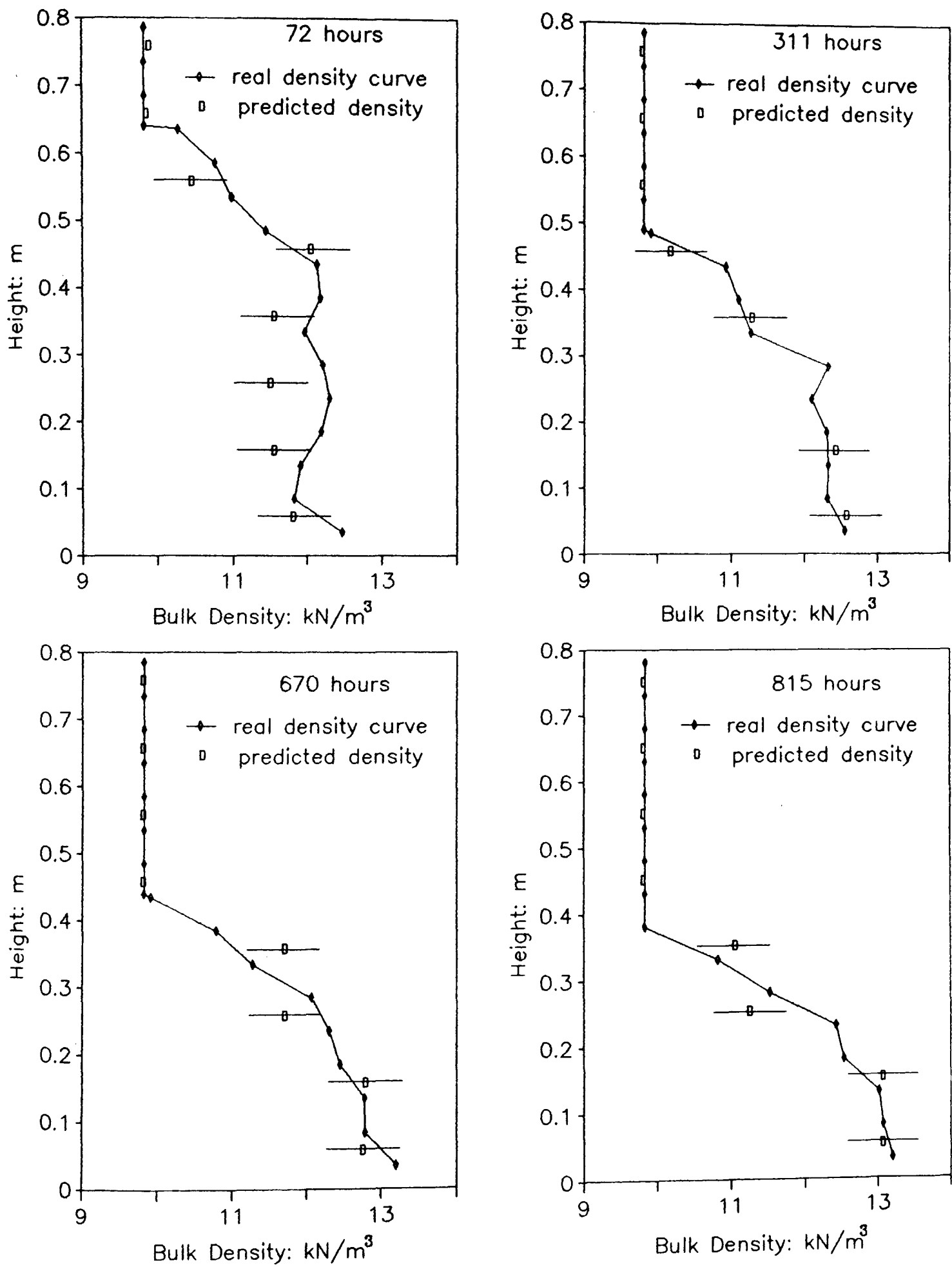
7.3.3 EXPERIMENT IM07 AND IM08 IN AN IRISH SEA CLAYEY SILT.

Experiments IM07 and IM08 were investigations into the settling behaviour of Irish Sea clayey silt using the instrumented settling column. The Geertsma and Smit approximate solution was used to determine best fitting curves to the compressional wave velocity versus porosity relationship. The relationship was modelled using the input parameters shown in table 7.2.

The model is compared with the observed data in figures 7.5 and 7.6. The data presented in these figures represent compressional wave velocities and porosity measured at different time and depths within the sediment column. The V_P-porosity relationship was first modelled using the mass coupling factor (b) derived from the electrical resistivity measurement and Brown's equation. This resulted in an under-estimation of V_P as shown in figure 7.5. A mass coupling factor equal to unity was found to improve the model. Characteristic frequencies ranging from 700kHz, in the initial stages of consolidation, to 1.2MHz in the final stages of the experiment were found to accurately model the V_P-porosity relationship. The same model parameters were used in the analysis of experiment IM08 (the same soil type but with different initial sedimentation conditions) resulting in good agreement with the measured data. The model predicts velocity minimum at porosities ranging between 0.864 and 0.814.

The compressional wave dispersion curves were calculated using the two modelling computer programs described earlier. The approximate and full model input parameters are shown in tables 7.2 and 7.3 respectively. The dispersion curves are calculated for soil porosities of 0.90 and 0.80 and are shown in figure 7.7 (In the diagram "Full model 1" refers to the pore parameter d being calculated using Hovem and Ingram's formula (1979) and "Full model 2" to the parameter being calculated using the formula from Briggs (1991)). In all cases the model predictions overestimate the observed permeability though agreement is improved when the soil is in the high porosity state. Prediction is poor in the 0.80 porosity case,

permeability being modelled an order of magnitude larger than that observed by direct measurement. The results are summarized in table 7.11 and displayed in figure 7.13. The results will be discussed in more detail in the following section (7.4.3).

The inability of the models to predict permeability in the low porosity soil state led to investigations into permeability anisotropy (experiment reference *IM07/IM08). In order to test for anisotropy a series of compressional wave velocity measurements were made down the length of the column using a pair of 500kHz piezoelectric transducers mounted at the top and bottom of the sediment column. A mean soil porosity was calculated from the corresponding bulk density profile. The full model was then used to calculate the dispersion curves for the soil sample. The values of permeability so derived were again found to be overestimates of those observed directly and are shown in table 7.9 and in figure 7.12. However what is encouraging about the modelled results is that they follow the same trend shown by the observed permeability values. These results would appear to imply that anisotropy does exist in this sample an observation that will be discussed further in section 7.4.

Table 7.2   The Geertsma and Smit model input parameters for the Irish Sea clayey silt sample (experiment IM07/IM08).

1. Fluid density = 1025 kg/m^3
2. Solid density = 2665 kg/m^3
3. Fluid compressibility = 4.22×10^{-10} Pa^{-1}
4. Solid compressibility = 2.78×10^{-11} Pa^{-1}
5. Characteristic frequency = 700 kHz 1.2 MHz
6. Applied frequency = 500 kHz
7. Frame compressibility = 0
8. Rigidity modulus = 0
9. Mass coupling factor = F.η 1

Table 7.3   The full model input parameters for the Irish Sea clayey silt sample (experiment IM07/IM08).

1. Solid compressibility	=	2.78×10^{-11} Pa^{-1}
2. Fluid compressibility	=	4.22×10^{-10} Pa^{-1}
3. Solid density	=	2665 kg/m^3
4. Fluid density	=	1025 kg/m^3
5. Rigidity modulus	=	10^5 Pa
6. Frame compressibility	=	10^{-5} Pa^{-1}
7. Mass coupling factor	=	1
8. Applied frequency	=	500 kHz
9. Poissons ratio	=	0.49
10. Logarithm decrement for shear	=	0.1
11. Ratio edec/gdec	=	1

full model parameters specific to individual experiments:

Porosity	V_P (m/s)	d' (m)	d'' (m)
0.90	1504	1.14×10^{-5}	3.6×10^{-6}
0.80	1498	5.07×10^{-6}	2.0×10^{-6}
0.80	15052	5.07×10^{-5}	2.2×10^{-6}

Experiment IM07: Irish Sea clayey silt

$b=1$, $f = 700kHz$, $C = 2.78 \times 10^{-11}Pa^{-1}$

$b=1$, $f_c = 900kHz$, $C_s = 2.78 \times 10^{-11}Pa^{-1}$

$b=1$, $f_c = 1.2MHz$, $C_s = 2.78 \times 10^{-11}Pa^{-1}$

$b=F.n$, $f_c = 1.2MHz$, $C_s = 2.78 \times 10^{-11}Pa^{-1}$

Figure 7.5 G & S model prediction of velocity—porosity relationship.

Experiment IM08: Irish Sea clayey silt

$b=1$, $f = 700kHz$, $C = 2.78 \times 10^{-11}Pa^{-1}$

$b=1$, $f_c = 900kHz$, $C_s = 2.78 \times 10^{-11}Pa^{-1}$

$b=1$, $f_c = 1.2MHz$, $C_s = 2.78 \times 10^{-11}Pa^{-1}$

$b=F.n$, $f_c = 1.2MHz$, $C_s = 2.78 \times 10^{-11}Pa^{-1}$
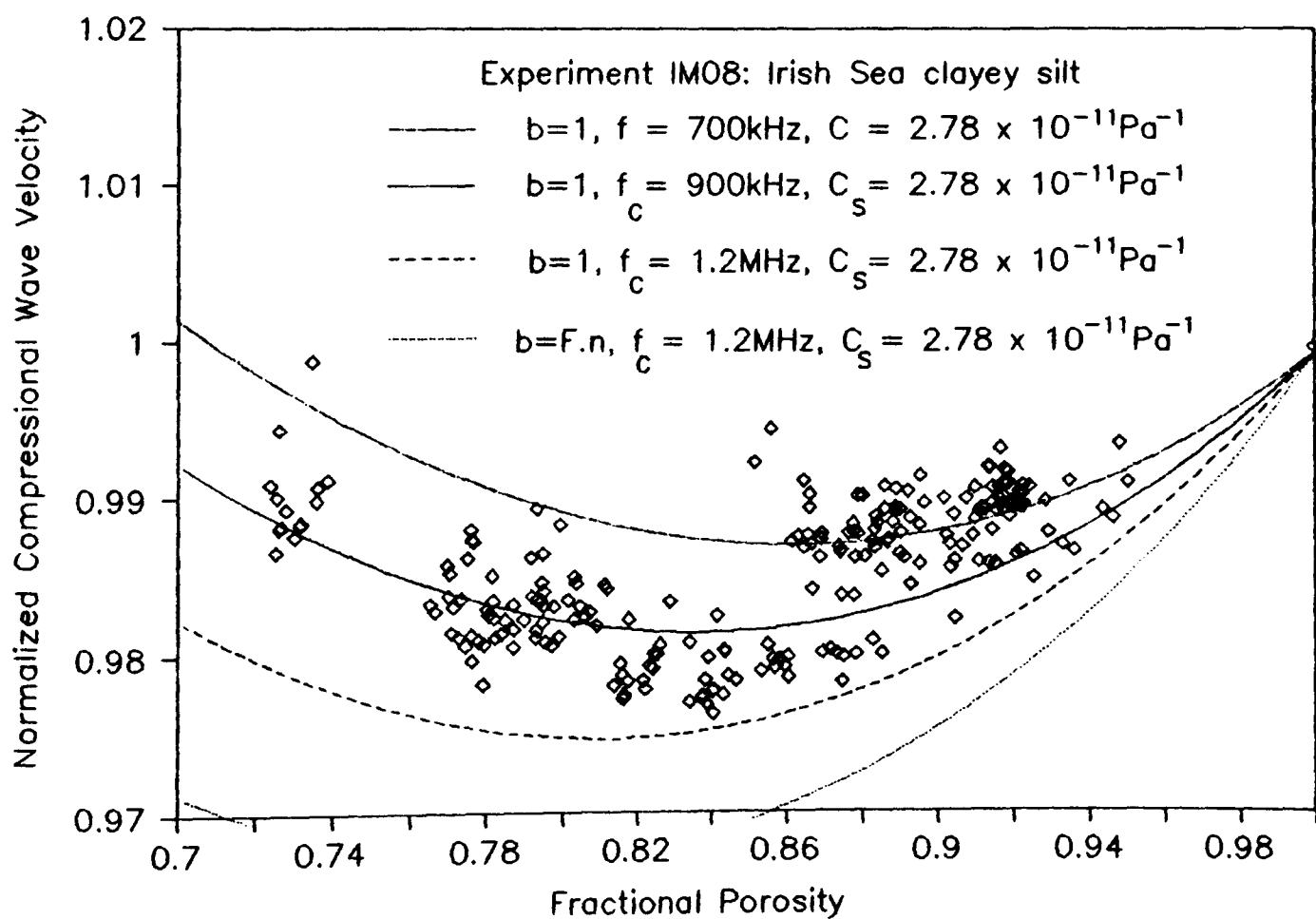
Figure 7.6 G & S model prediction of velocity—porosity relationship.
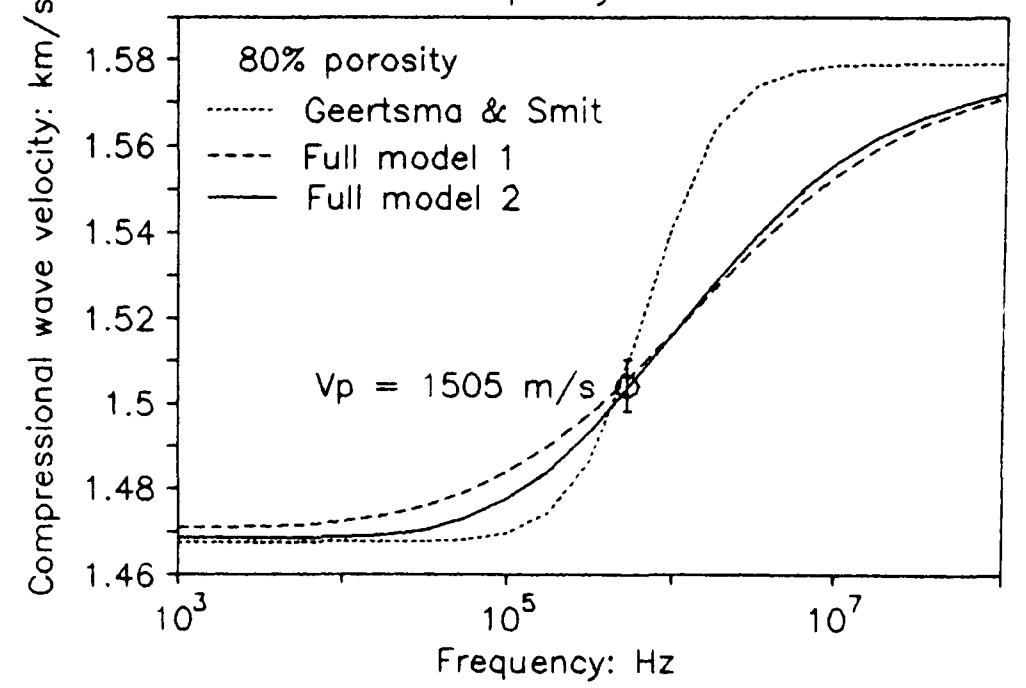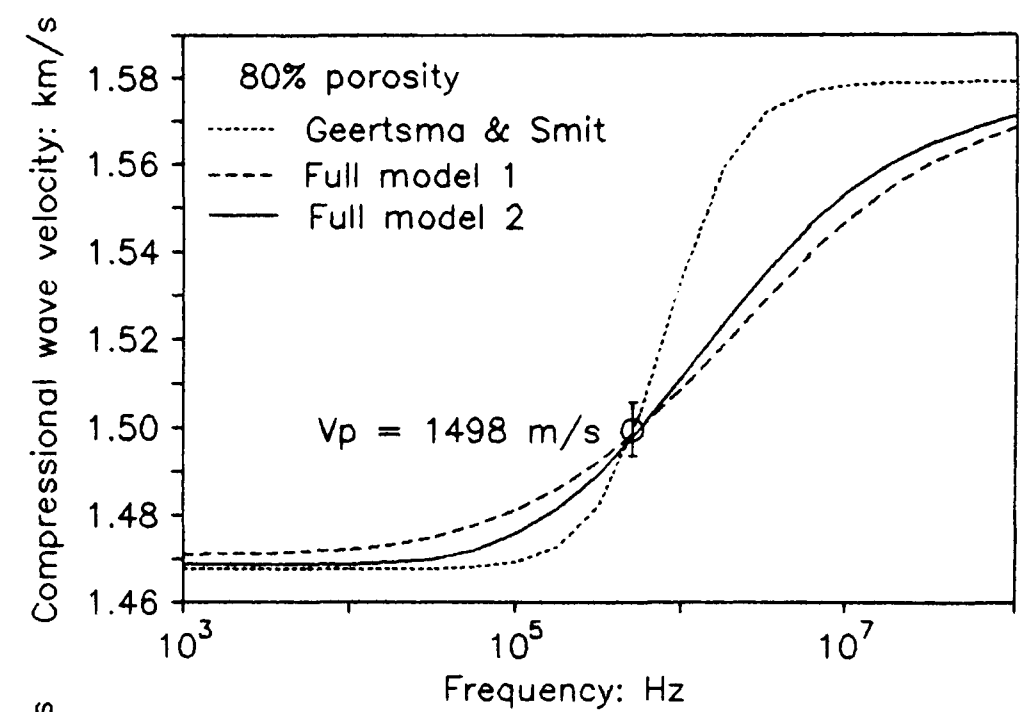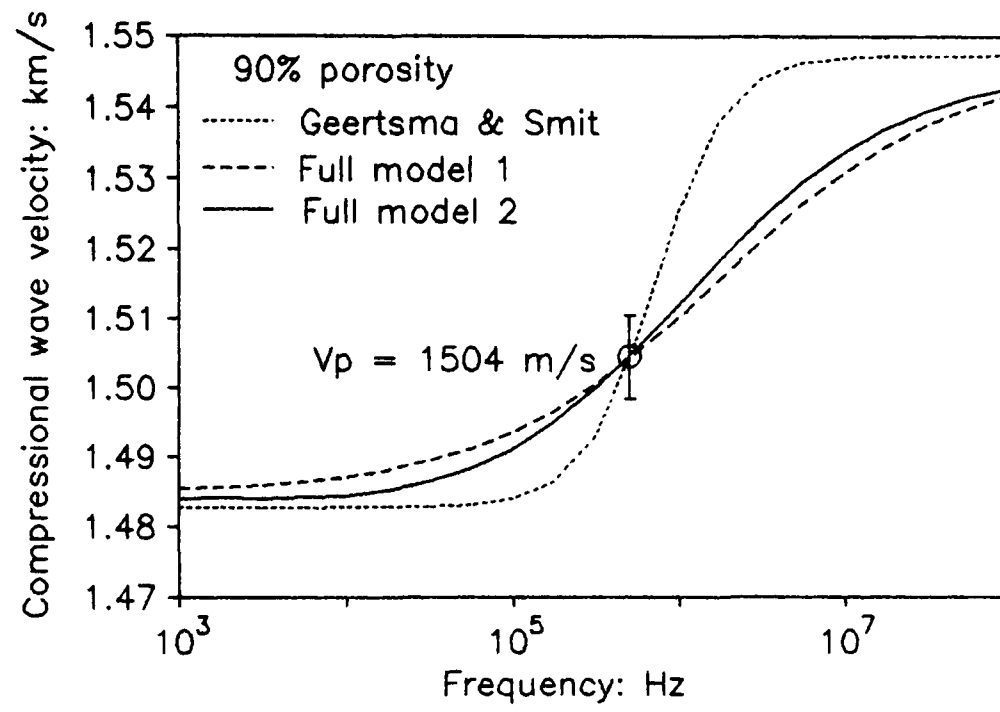
Figure 7.7 Predicted P−wave dispersion curves for an Irish Sea clayey silt.

7.3.4 EXPERIMENT IM11 IN AN IRVINE BAY MUD.

Experiment IM11 involved the study of an Irvine Bay mud. The V_P-porosity relationship was satisfactorily modelled using the approximate model with the input parameters shown in table 7.4. The best fitting models were obtained using soil characteristic frequencies ranging between 500kHz to 650kHz (shown in figure 7.8). The velocity minimum was found to range between a porosity of 0.922 and 0.876 for these curves.

Bulk density profiles were reproduced using the input parameters of table 7.4, using the corresponding V_P profiles for 2.4, 21.5, 49, and 1422 hours and using characteristic frequencies of 500kHz, 575kHz, 575kHz and 650kHz respectively. The resulting profiles shown in figure 7.9 validate the use of the Geertsma and Smit model in soft soil studies. The density inversion at 21.5 and 49 hours is accurately reproduced. Comparing figure 7.9 to the profile reconstructed using the empirical technique (figure 6.18) it can be seen that the Geertsma and Smit model is an improvement on the prediction using the empirical method.

The compressional wave dispersion curves were modelled using the approximate and full model computer programs described earlier. The model input parameters are shown in tables 7.4 and 7.5 respectively. The dispersion curves are calculated for soil porosities of 0.80 and 0.70 and are shown in figure 7.10. The results again show a tendency for the Biot theory to over estimate permeability and again prediction appears to be more successful in the high porosity soil. The prediction of permeability in the 0.70 porosity soil differs by almost two orders of magnitude from the observed value. The results of this analysis are summarized in table 7.9 and are shown in figure 7.12.

Table 7.4   Geertsma and Smit model input parameters for the Irvine Bay mud sample (experiment IM11).

1. Fluid density = 1025 kg/m^3
2. Solid density = 2643 kg/m^3
3. Fluid compressibility = 4.22×10^{-10} Pa^{-1}
4. Solid compressibility = 2.78×10^{-11} Pa^{-1}
5. Characteristic frequency = 500kHz 650kHz
6. Applied frequency = 500 kHz
7. Frame compressibility = 0
8. Rigidity modulus = 0
9. Mass coupling factor = 1

Table 7.5   Full model input parameters for the Irvine Bay mud sample (experiment IM11).

1. Solid compressibility	= 2.78×10^{-11} Pa^{-1}
2. Fluid compressibility	= 4.22×10^{-10} Pa^{-1}
3. Solid density	= 2643 kg/m^3
4. Fluid density	= 1025 kg/m^3
5. Rigidity modulus	= 10^5 Pa
6. Frame compressibility	= 10^{-5} Pa^{-1}
7. Mass coupling factor	= 1
8. Applied frequency	= 500 kHz
9. Poissons ratio	= 0.49
10. Logarithm decrement for shear	= 0.1
11. Ratio edec/gdec	= 1

full model parameters specific to individual experiments:

Porosity	Vp (m/s)	d' (m)	d'' (m)
0.80	1507	1.7×10^{-5}	3.1×10^{-6}
0.80	1518	1.7×10^{-5}	4.3×10^{-6}
0.70	1532	7.0×10^{-6}	2.3×10^{-6}
0.80	1542	7.0×10^{-6}	2.7×10^{-6}

Normalized Compressional Wave Velocity.

Fractional Porosity

1.02

1.01

1.00

0.99

0.98

0.6   0.7   0.8   0.9   1

Experiment IM11: Irvine Bay mud

$- - -$ b=1, f_c= 500kHz, C_s = 2.78 x $10^{-11}Pa^{-1}$

$- - -$ b=1, f_c= 575kHz, C_s = 2.78 x $10^{-11}Pa^{-1}$

$---$ b=1, f_c= 650kHz, C_s = 2.78 x $10^{-11}Pa^{-1}$

Figure 7.8 The Geertsma and Smit model prediction of the compressional wave velocity—porosity relationship.

Figure 7.9 Density Profiles for an Irvine Bay Mud using the
Geertsma and Smit Model: Experiment IM11.
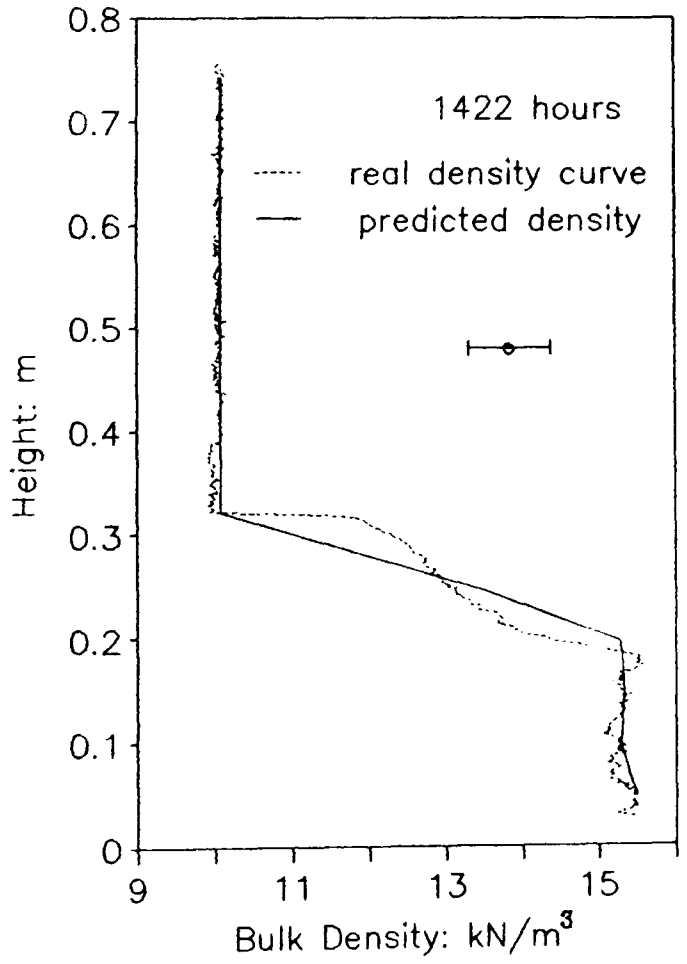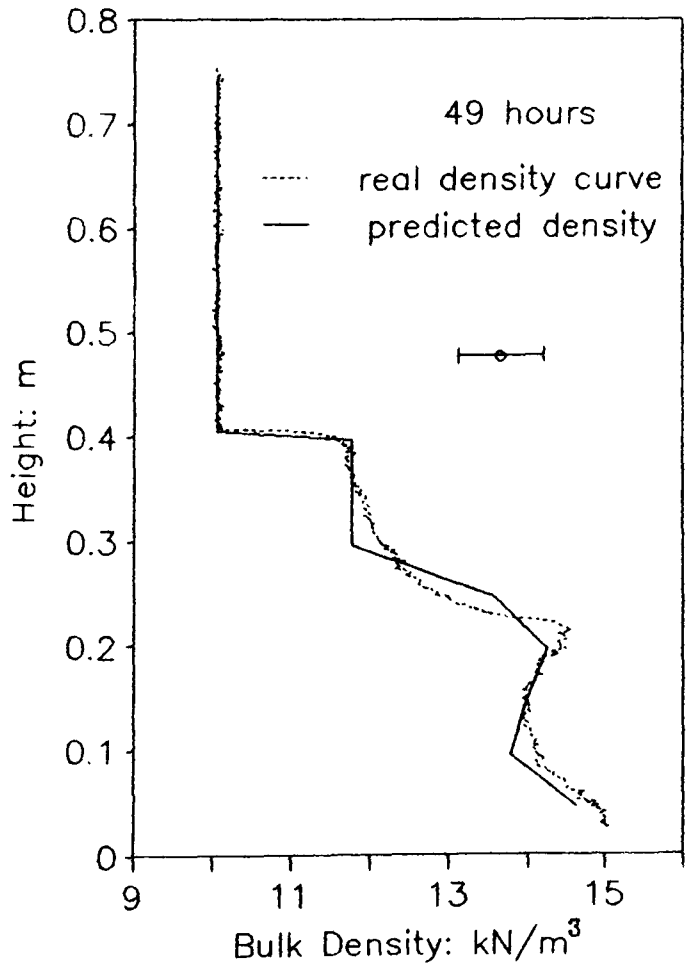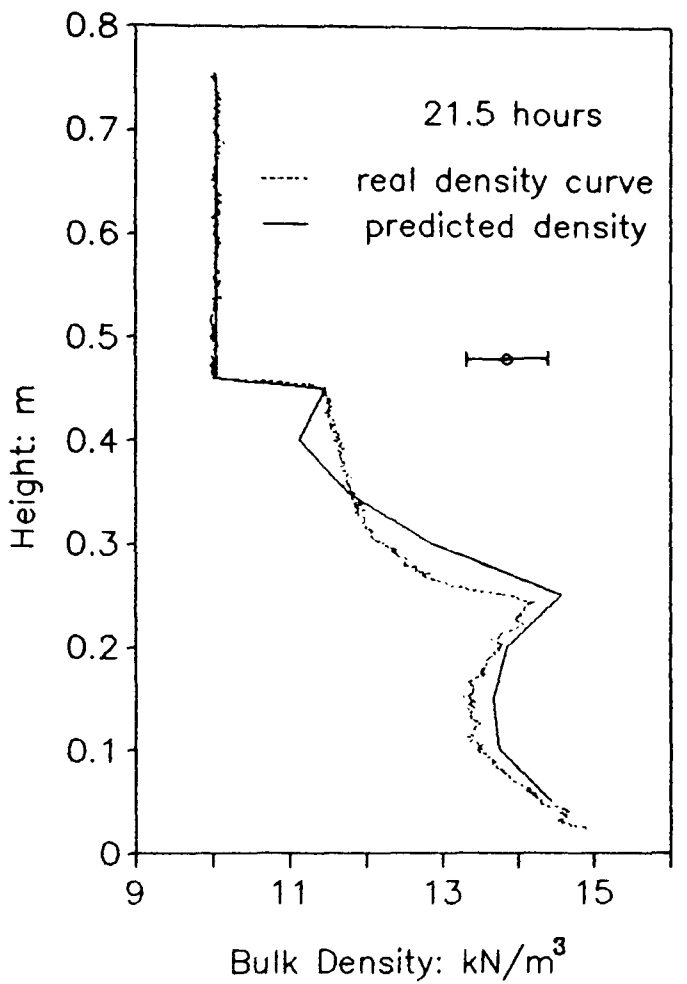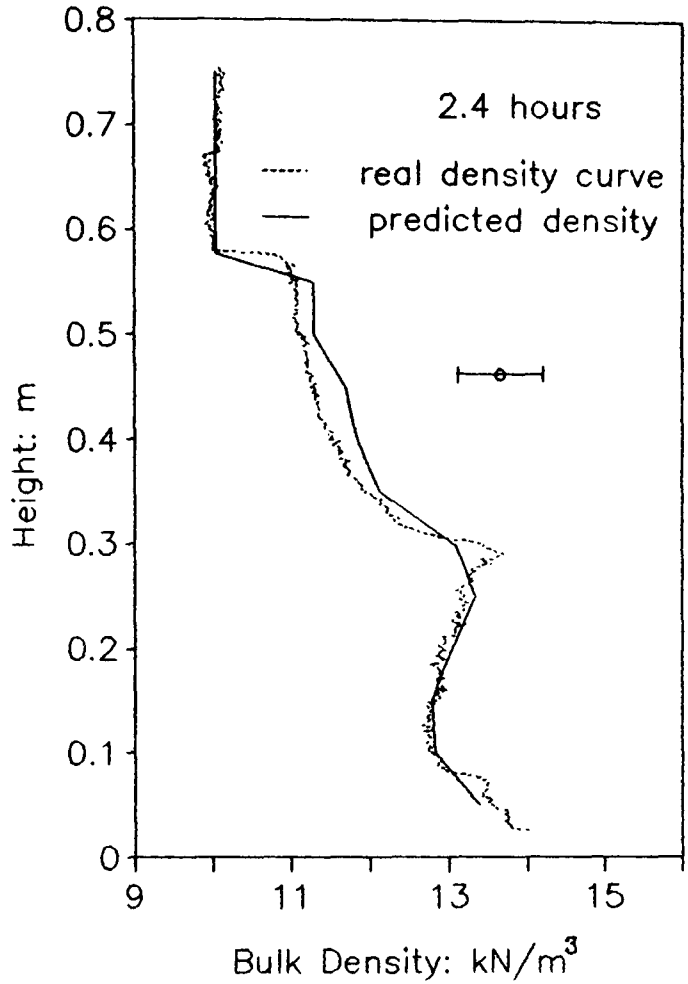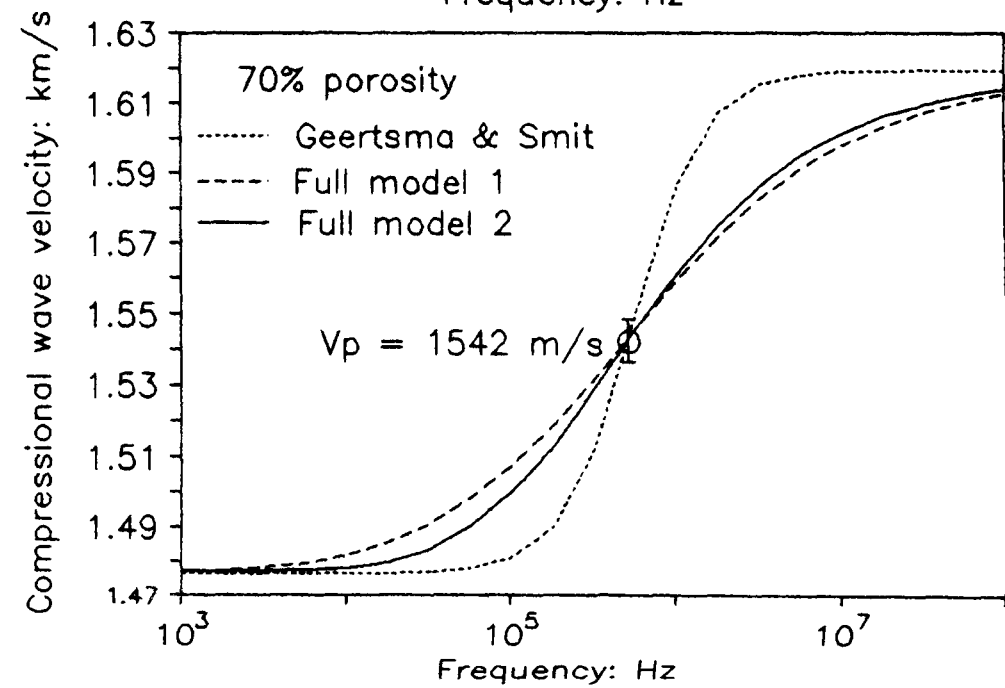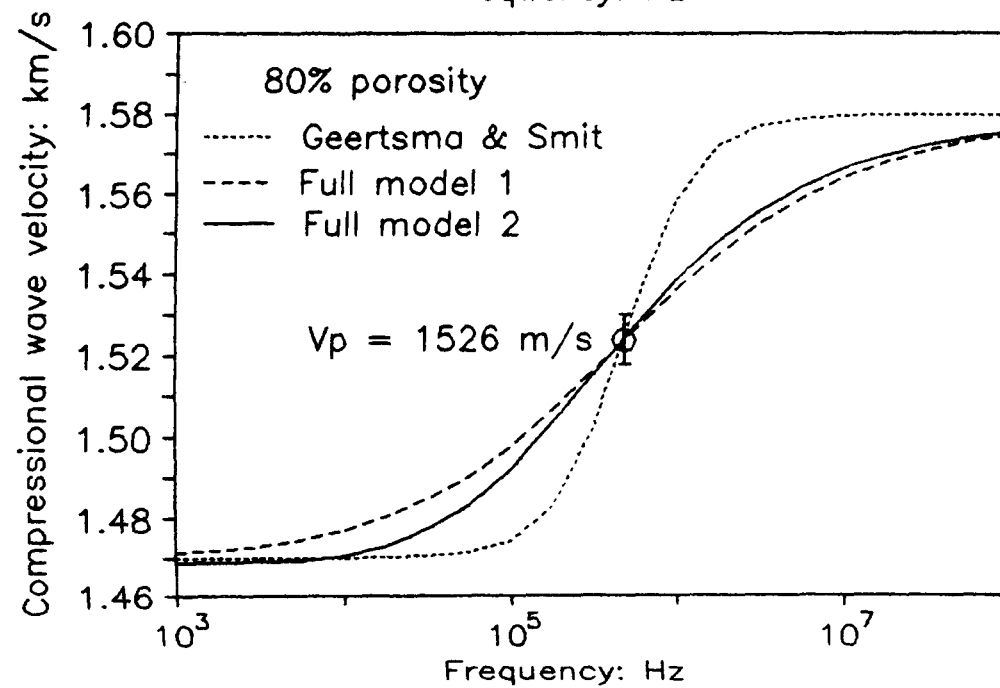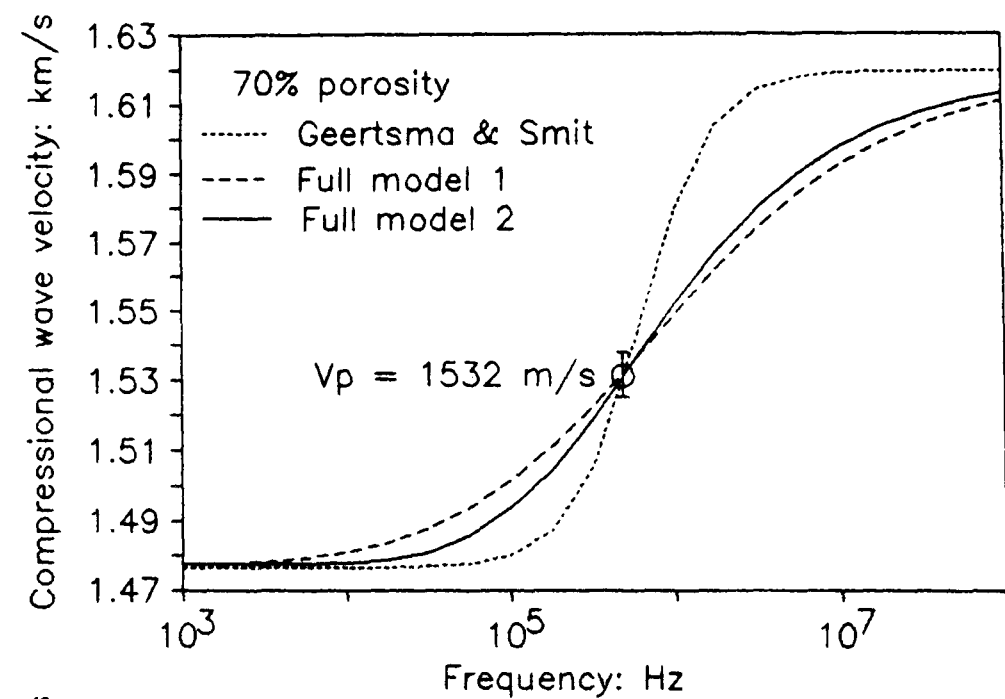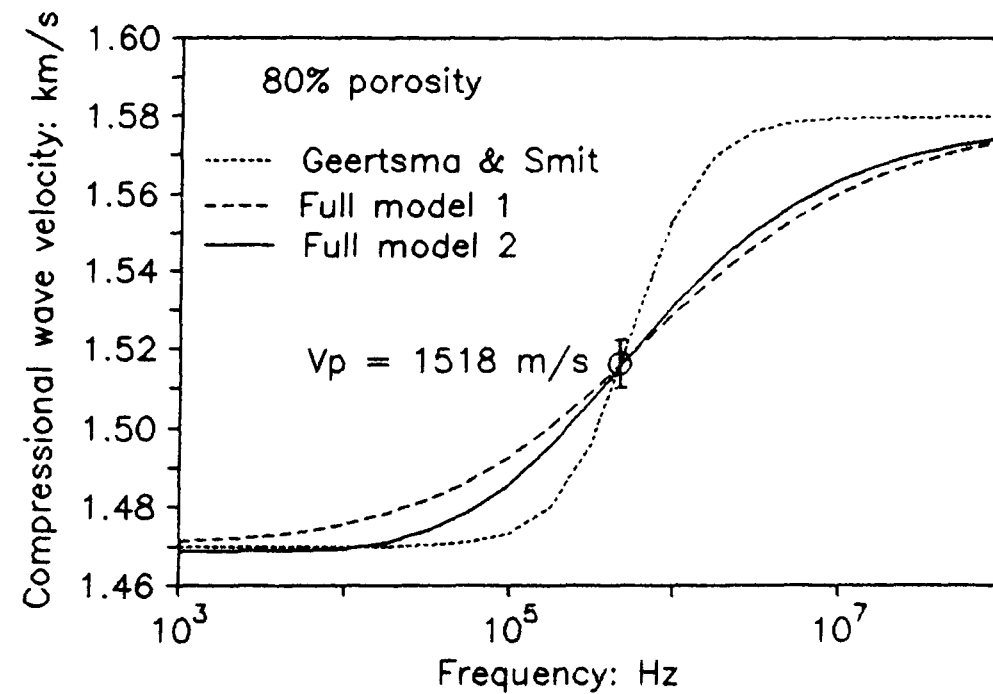
Figure 7.10 Predicted P-wave dispersion curves for an Irvine Bay mud

7.4 Discussion.

7.4.1 THE MODELLING OF COMPRESSIONAL WAVE VELOCITY-POROSITY RELATIONSHIP.

The compressional wave velocity-porosity relationship was modelled using the Geertsma and Smit approximate solution. The model assumes a weak frame soil (i.e. a soil in which frame bulk modulus and rigidity modulus are zero). The soil is assumed to consist of large pores and large pore "throats" such that the mass coupling factor assumes a value of 1. In order to satisfactorily model the relationship the soil characteristic frequency was increased as a function of the degree of consolidation. The resulting models were found to reproduce the soils V_P-porosity relationship with a high degree of accuracy. The relationship cannot therefore be satisfactorily modelled by a single empirical relationship (as in section 6.5.2) since the soil properties are in a continual state of change. No single porosity can be associated with a P-wave velocity minimum, rather that velocity minima are observed for a range of porosities, the magnitude of this minimum changing as a function of degree of consolidation.

Since the Geertsma and Smit model proved successful in the column experiments the model was used to reproduce compressional wave velocity-porosity relationships observed by other authors (Urick (1947), Hampton (1967), Dewes and McCann (1972)). These authors describe P-wave velocity measurement in a variety of sediments at a range of applied frequencies.

The model has been used to predict the V_P-porosity relationship observed by Urick (1947) in a sample of kaolinite (the model parameters are shown in table 7.6). The model successfully predicts the compressional wave velocity to within 0.5% and accurately predicts the velocity minimum shown in figure 7.11. Hampton's data was compared to the model in a similar manner using the parameters shown in table 7.7. In this case the model fails to predict the observed compressional wave velocity-porosity relationship (figure

Table 7.6   The Geertsma and Smit model input parameters for
             Urick's data (1947).

1. Fluid density = 1025 kg/m^3
2. Solid density = 2665 kg/m^3
3. Fluid compressibility = 4.22x10^{-10} Pa^{-1}
4. Solid compressibility = 0.98x10^{-11} Pa^{-1}(from Urick 1948)
5. Characteristic frequency = 4MHz
6. Applied frequency = 1MHz
7. Frame compressibility = 0
8. Rigidity modulus = 0
9. Mass coupling factor = 1

Table 7.7   The Geertsma and Smit model input parameters for
             Hampton's data (1967).

1. Fluid density = 1025 kg/m^3
2. Solid density = 2665 kg/m^3
3. Fluid compressibility = 4.22x10^{-10} Pa^{-1}
4. Solid compressibility = 0.98x10^{-11} Pa^{-1}
5. Characteristic frequency = 1.2mHz
6. Applied frequency = 50kHz and 200kHz
7. Frame compressibility = 0
8. Rigidity modulus = 0
9. Mass coupling factor = 1

Table 7.8   The Geertsma and Smit model input parameters for
             Dewes and McCann data (1972).

1. Fluid density = 1025 kg/m^3
2. Solid density = 2665 kg/m^3
3. Fluid compressibility = 4.22x10^{-10} Pa^{-1}
4. Solid compressibility = 2.78x10^{-11} Pa^{-1}
5. Characteristic frequency = 1.0 MHz
6. Applied frequency = 250 kHz
7. Frame compressibility = 0
8. Rigidity modulus = 0
9. Mass coupling factor = 1
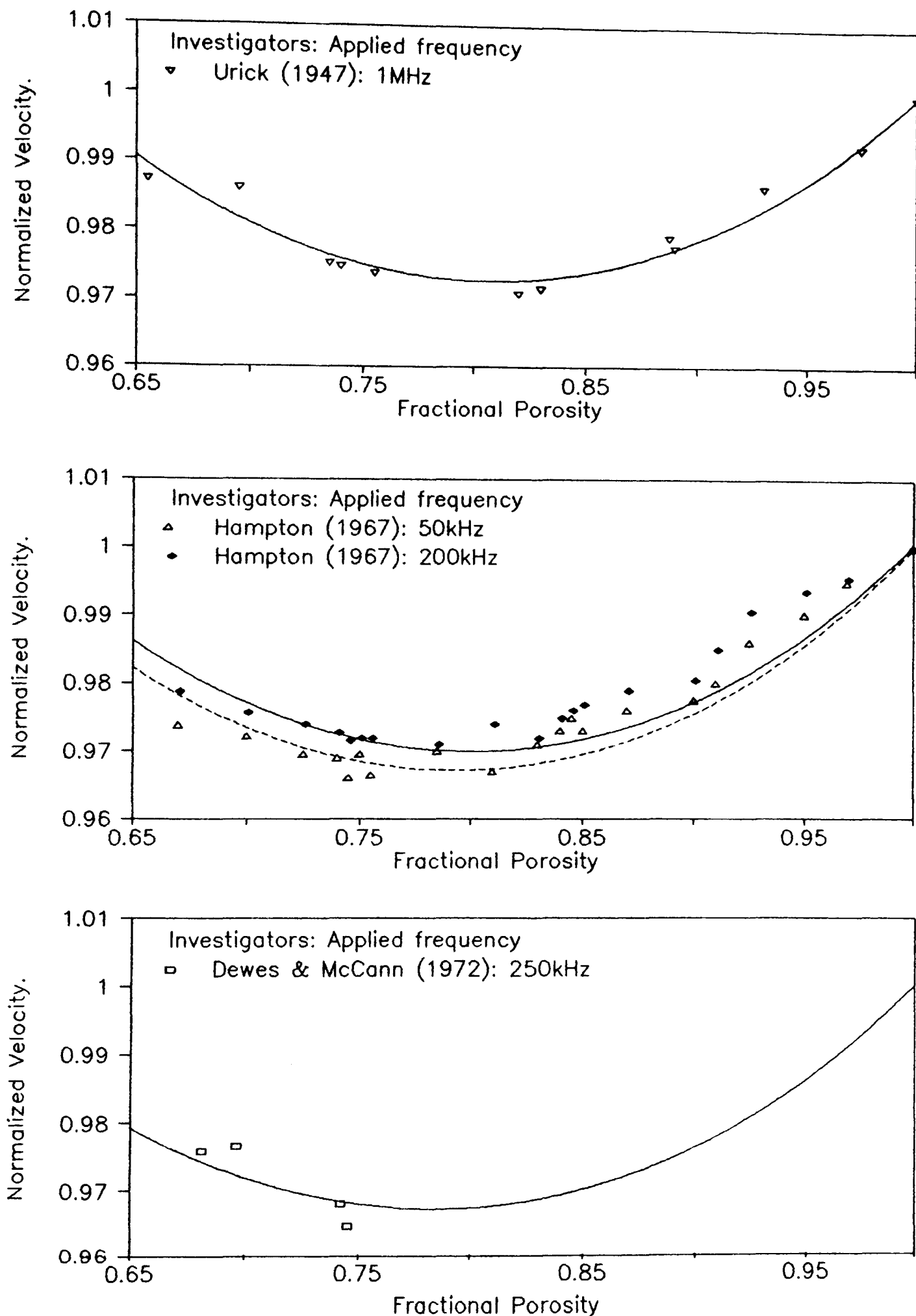
Figure 7.11 Geertsma and Smit prediction of P—wave velocity
versus porosity relationship for other authors data.

7.11). There are thought to be two reasons that may account for this; the model parameters may be incorrect or else the soil sample has been allowed to consolidate during the experiment and hence the relationship would need to be modelled using more than one characteristic frequency. Dewes and McCann's (1972) limited data set is of particular interest because it represents a natural sediment from the North Atlantic. The model parameters are shown in table 7.8 and the model predictions are compared to the data in figure 7.11. Though data is limited the model still appears to make reasonable predictions of the relationship.

7.4.2 DISCUSSION OF BULK DENSITY PROFILE RECONSTRUCTION.

Two examples have been given (figure 7.4 and 7.9) to illustrate the validity of using the Geertsma and Smit model to fit curves to the P-wave velocity-porosity relationship and thence to reproduce the bulk density profile. This exercise served to illustrate that it was possible to reconstruct a detailed and accurate P-wave velocity-porosity relationship from just a few data points. This relationship could then be used to generate an accurate bulk density profile from the P-wave velocity measurements. It was hoped that the bulk density of the soft soil could ultimately be measured remotely using P-waves. The application of this technique falls far short of its aim however. The compressional wave velocity-porosity relationship represents a change in velocity of the order of 2% for a 30% change in porosity. In the laboratory it was possible to measure P-wave velocity to approximately 0.4%, *in-situ* the velocity is at best measured to within 1% to 5% making velocity measurement too insensitive for the purpose of recreating the bulk density profile.

It is suggested that bulk density may be more accurately determined using electrical resistivity measurement. Referring to figure 6.13 which shows the relationship between Apparent Formation Factor (AFF) and porosity it is possible to see that 15% change in porosity is accompanied by approximately 60% change in AFF. The electrical resistivity method being far

more sensitive to changes in porosity than P-wave velocity would serve as a better geophysical tool in measuring bulk density of the soil. The draw-back of using an electrical resistivity probe is that it would invariably be an intrusive device which would result in the destruction of the soil fabric as in the case of the gamma ray density probe described by Kirby and Parker (1977).

7.4.3   DISCUSSION OF PERMEABILITY PREDICTIONS.

The applied frequency of the compressional wave measurements (500kHz) appear to be too high for the Geertsma and Smit approximation to be valid. The applied frequency, though lower than the characteristic frequency, is in excess of the transitional frequency indicating that the applied wave causes non-linear flow of the pore fluid. For the approximation to be successfully used the applied frequency would need to be in the range of 100kHz to 140kHz for the Irish Sea clayey silt of experiments IM07 and IM08, and 50kHz to 100kHz for the Irvine Bay mud of experiment IM11. In the applicable frequency range for the application of the Geertsma and Smit model the observed compressional wave velocity must be very close to V_0, so much so that it would be necessary to measure V_p to many decimal places as well as predicting V_0 to the same order of magnitude in order to make meaningful permeability predictions. In this study V_p was measured to an accuracy of ±6m/s, with considerable efforts taken to reduce this error. A further lowering of the compressional wave applied frequency would be likely to increase the picking errors. Thus considerable doubt is cast upon the method as a viable experimental technique to predict permeability.

Prior to discussing the permeability predictions of the full model it is useful to consider the mode of permeability measurement in the experiments considered so far. The direct method, described in chapter 5, is based on a passive monitoring of the relative motion of the solid and fluid phases of the soil in a vertical direction. The seismo-acoustic measurements uses forced vibration to induce

fluid motion in the pore spaces. With the exception of experiment *IM07/IM08 the seismo-acoustic waves are generated across the sediment column and in a horizontal propagation direction. With these facts established the permeability predictions will now be considered.

The coefficient of permeability predictions made using the approximate and full models are summarized in table 7.9 and are presented in figure 7.12. Considering the predictions made using the P-wave velocity logged across the column it will be seen from figure 7.12 that the full model is reasonably successful in predicting permeability of the soils in the high porosity state but with decreasing porosity the model fails badly in its predictions. This is in agreement with findings of Hurley (1989).

The modelled P-wave velocities measured vertically down the column (experiment *IM07/IM08) appear to be successful in recording the trend of permeability but fails in its ability to predict its actual value. This ability of the model to monitor the trend in the vertical direction is not apparent in the horizontal permeability predictions. This result would suggest that the soil exhibits anisotropy with respect to permeability. Such anisotropic behaviour could explain why the models using the P-wave velocity profiling data are more successful in predicting permeability in the high porosity soil state. It is suggested that the high porosity state represents a relatively homogeneous soil condition and that the soil becomes increasingly anisotropic with the continued consolidation. If the above comments are correct then it is possible to make a number of observations using figure 7.12. The permeability in the horizontal plane (i.e. across the column) reduces by over 66% during the consolidation process. In contrast the permeability of the same soil in the vertical direction is observed to change by approximately 95% during the same consolidation period. The ratio of the horizontal to vertical permeability of both the Irish Sea clayey silt and the Irvine Bay mud is roughly 4:3. This compares to laboratory measurements of London clay with voids ratio's ranging from 0.89 to 0.81 having a ratio of 2:1 for horizontal to vertical

Expt. Ref.	Observed values			Geertsma and Smit model				Full model predictions			
	k $\times 10^{-6}$ m/s	n	V_p m/s	k $\times 10^{-6}$ m/s	f_c kHz	V_o m/s	V_∞ m/s	d' $\times 10^{-6}$ m	k' $\times 10^{-6}$ m/s	d'' $\times 10^{-6}$ m	k'' $\times 10^{-6}$ m/s
				Compressional wave velocity logged horizontally.							
IM07/ IM08	2.2 − 2.3	0.90	1503−1504	8.2	765	1483	1547	11.7	35.0	3.6	15.0
IM07/ IM08	0.11−0.15	0.80	1498−1505	3.5−4.1	896−769	1468	1579	5.2	7.0−9.0	2.0−2.2	4.0−5.0
IM11	2.79	0.80	1518−1526	5.1−5.9	622−538	1470	1580	12.0	27.5−35.0	3.2−3.9	10.0−15.0
IM11	0.1	0.70	1532−1542	3.0−3.4	703−610	1476	1619	7.0	10.0−13.0	2.3−2.7	4.5−6.5
				Compressional wave velocity measured vertically down the column.							
*IM07 /IM08	0.06	0.703	1517							1.8	3.0
	0.1	0.798	1512							2.3	5.0
	0.5	0.859	1504							2.9	9.0

k' predicted using d' derived using Hovem and Ingram's formula (1979)
k'' predicted using d'' derived using formulae from Briggs (1991)

Table 7.9 Comparison of observed permeability to the model predictions.

Figure 7.12 Comparison of Coefficient of Permeability.
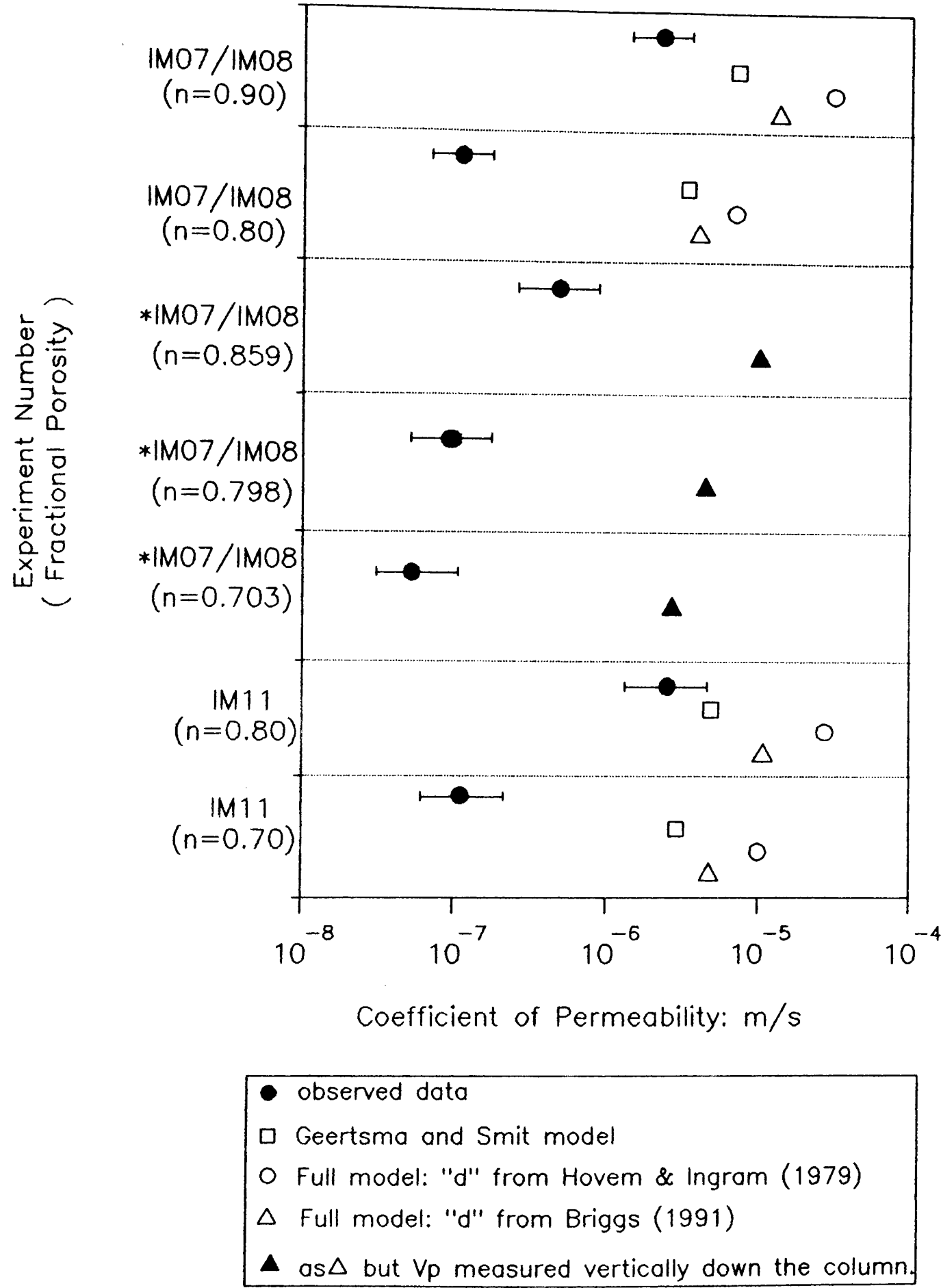
permeability (Chandler et al. 1990). In the light of this experimental evidence it seems reasonable to assume that the anisotropic ratio be closer to unity for more porous sediments. It is worthwhile at this point to reflect on the experience of other researchers.

The possible existence of permeability anisotropy in soft soils is supported by the work of Partheniades (1965) and Bowden (1989). Partheniades gives a possible explanation for the anisotropy and describes it in terms of a mechanism whereby pore water is piped sideways, rather than flowing immediately upwards, to zones of higher permeability, thus allowing the escape of the pore fluid to the sediment surface. If such a mechanism is operating within the soils studied here then permeability is likely to be greater in the horizontal direction as compared to the vertical. Bowden (1989) attempted to study the degree of horizontal particle alignment and its effect on soft soil permeability. Although unsuccessful, his research clearly demonstrated that he suspected anisotropy of this kind.

Though the model using the P-wave velocity measured down the column (experiment *IM07/IM08) may make observation of permeability trend possible the actual prediction of the coefficient of permeability was disappointing. This was thought to be due to a problem inherent in the model. The most likely source of difficulty is the correct selection of the pore size parameter "d". The Hovem and Ingram formula (1979) used here is strictly for use with uniform spherical grains, clearly not the case for these experiments. Using the formula from Briggs (1991) to estimate "d" does appear to improve permeability predictions slightly although the results remain very similar to the other computer models. However to describe the highly complex nature of the soil matrix and in particular the distribution of effective pore radius or "throats" in terms of a simple formula of this kind must surely be a gross approximation and a main source of error.

There is the possibility that the Biot theory fails to predict values of permeability close to those observed directly

because it depends upon the use of forced vibration to cause fluid motion in the interstitial pores. Such forced vibrations are likely to induce high rates of pore water flow at the microscopic level and it should be no surprise therefore that the Biot model predicts consistently high permeability values. An argument against this hypothesis is the relatively low values of permeability resulting from the oedometer method of analysis which subjects the soil sample to much larger forces than the seismo-acoustic method (Hurley 1989). The permeability as predicted by the Biot theory may well have its application as a measure of maximum flow rates in soils but to consider using the Biot theory to monitor macroscopic permeability is likely to prove unsuccessful.

8.1 Concluding Remarks.

The research described in this thesis was envisaged as a pilot study into the relationship between seismo-acoustic properties of soft soils and consolidation phenomena. For the most part the study has concerned itself with the fundamental philosophy of this subject, however section 8.2 will briefly address the possible applications of the research. The application of geophysics to soft soil research has produced more questions than it can provide answers. However, it is hoped that this thesis has gone some way to extend the work of the Oxford University soft soil group. It is useful at this point to summarize the main successes of the research and to make some concluding remarks.

An instrumented sedimentation column has been developed and used in a laboratory investigation into the relationship between seismo-acoustic properties of cohesive marine soils and self weight consolidation phenomena. The instrumented column was successful in allowing measurement of compressional wave velocity, shear wave velocity, electrical resistivity and pore pressures in a number of natural marine sediments initially introduced as a homogeneous slurry. The instrumented column was designed such that it could be used in conjunction with the X-ray apparatus located at the Department of Engineering, Oxford in order to provide information on bulk density.

Measurements have shown that the consolidation behaviour of a rapidly deposited sediment slurry is greatly influenced by its initial input density. A slurry deposited in sea water above a critical voids ratio will exist initially as a fluid supported suspension before becoming a consolidating soil. Below this critical value the soil behaves immediately as a consolidating soil.

The soils vertical effective stress distribution was determined using bulk density and pore pressure measurements.

The tracking of individual soil elements allowed the compression behaviour of the soil to be analysed in detail. Above the critical voids ratio the soil exhibited a largely unique voids ratio versus effective stress relationship. Differentiating this curve enabled the frame compressibility to be determined at any point in the soil and was found to range between 10^{-3} to 10^{-5} Pa^{-1} for voids ratios of 6 to 2. For the soil sample characterized by an initial voids ratio less than the critical value considerable time dependent compression, or creep, was observed.

The changing permeability of the soils during the consolidation process was measured by tracking soil element displacements over a known duration and by using an average hydraulic gradient determined from pore pressure and density profiles. The logarithm of permeability versus voids ratio relationship of the soils was found to be approximately linear over voids ratio ranges of 6 to 2. For the soils studied in the column permeabilities were found to range from 10^{-5} to 10^{-8} m/s. The coefficient of consolidation was determined using analytical techniques based on Gibson et al. (1967) large strain consolidation theory. The coefficient was also found by direct calculation and by using the Lee-Sills formulation of this analysis to model the settlement behaviour and the excess pore pressure dissipation in the soils. The resulting predictions of the coefficient of consolidation spanned two orders of magnitude (10^{-9} to 10^{-7} m^2/s).

Shear wave measurements within the consolidating soft soil revealed phenomena of considerable interest. Shear waves were generally not observed until the soil reached 20% degree of consolidation. The shear waves were found to be small amplitude waves propagating at velocities ranging from below 1m/s to a maximum of 11m/s for a consolidation time of up to 5427 hours. Shear wave velocity was also observed to undergo time dependent increase or creep, the increase probably being a result of continued clay particle floc interaction during secondary consolidation. The creep effect was less prevalent in the mud sample, comprising a greater percentage of sand and silt, which would support the hypothesis above. Under the

influence of creep the V_s-porosity relationship takes on a more complex form than had previously been documented. Shear wave velocity increases with decreasing porosity and with increasing overburden, as would be expected, however no unique V_s-porosity relationship exists such that any porosity may be associated with a wide range of velocities. The degree of consolidation (σ'_n) for these experiments could be estimated from shear wave velocity by using the empirical equation.

$$V_s = 5.26 (\sigma'_n)^{0.635}$$

Taylor Smith's empirical equation for the estimation of soil frame compressibility (C_f) remains valid in soft soils .

$$C_f = (0.001 \ V_s^2)^{-1}$$

The rigidity of the soil was also subject to creep. The values of rigidity modulus (G) measured in these experiments were of the same magnitude as those observed by other authors using both geophysical and geotechnical techniques. Though no unique relationship between rigidity modulus and effective stress was observed in these soils, primary consolidation was bound by an upper limit defined by

$$G = 78 \ \sigma'_n$$

where σ'_n represents the degree of consolidation.

The Geertsma and Smit approximate solution to the Biot theory was used to model the compressional wave velocity (V_P) and porosity (η) relationship of the soil. This was achieved by assuming a "weak frame" condition in which the soil frame bulk modulus and rigidity approximated to zero. In addition, a soil frame consisting of large pore spaces and large "throats" was assumed so that the soil properties could be modelled on the premise that the mass coupling factor was equal unity. The Geertsma and Smit model successfully reproduced the V_P-porosity curves for a wide variety of sediments and indicated that the characteristic frequency of the soil significantly increased as consolidation progressed. The model was also able to reproduce bulk density profiles from measured

compressional wave velocities with considerable accuracy however, the method was believed to be too insensitive to have any practical application.

The Stoll full model was used to construct compressional wave dispersion curves in order to determine the coefficient of permeability. The curves were modelled using "weak frame" soil parameters, whilst the value of permeability was adjusted until the curve matched the measured velocity at an applied frequency of 500kHz. The full model necessitates the estimation of a pore size parameter which was achieved using the Hovem and Ingram formula (1979) and also a formula from Briggs (1991). The analysis of the permeability data appeared to show that the soils studied in the column were at first homogeneous becoming increasingly anisotropic with respect to permeability as consolidation progressed. The ratio of horizontal to vertical permeability was found to be approximately 4:3.

8.2 Implications of results and conclusions.

Two areas of potential application for the results of this work, namely the dredging and waste disposal industries, were discussed in the introduction to this thesis and at this point it is appropriate to discuss what contribution the results of this research have upon these areas of application?

In chapter 1, Parker and Kirby's (1977) method of defining navigable depth in terms of a bulk density of 1200 kg/m^3 was described. Bowden's (1989) objection to the use of such a definition was that density was not the criterion which determines the safe passage of a vessel and that a limiting value of soil stiffness or resistance to shear was the correct property to be measured in order to sensibly define navigable depth. In this thesis soil stiffness has been quantified through the rigidity modulus which was determined in the laboratory by measuring shear wave velocity and bulk density through X-ray attenuation measurements. It is therefore possible to envisage a gamma ray density measuring probe

fitted with shear wave velocity measuring apparatus to perform the same task *in situ*. Considerable testing would of course need to be done in order to relate soil rigidity modulus to navigable depth. The inherent problem of the probe destroying the soil fabric remains a difficulty. However it may be economically astute of the dredging industry to invest in the development of an *in situ* probe which is capable of monitoring navigable depth in terms of the soils rigidity modulus.

It was hoped that the shear wave velocity or rigidity modulus measurements would demonstrate some unique relationship with that of effective stress. The samples examined in the sediment column showed that during primary consolidation the degree of consolidation (σ'_n) was related to shear wave velocity (Vs) by the empirical relationship

$$Vs = 5.26 \ (\sigma'_n)^{0.635}$$

Such a relationship may have particular relevance to the waste disposal industry as will be described below.

The U.K. has a policy of disposing of certain industrial waste materials at sea. The waste material, depending on its chemical composition, will often become chemically bound to soil particles either in suspension or on the sea bed. Contaminated soil particles associated with the sea bed may undergo consolidation during which the pollutant may be released into the pore fluid as a result of changing chemical conditions within the soil. The consolidation process may result ultimately in the pollutant being re-introduced into the water column above the bed. When considering localities suitable for the dumping of industrial waste it is important to consider various factors amongst which is the state of consolidation of the sea bed. Here then is the possible application of the Vs-σ'_n relationship described above. If the relationship is valid for all sediments then the consolidation state of the sea bed could be monitored using shear wave velocity measurement. This may enable further dumping of industrial waste to be deferred until the soil has reached a state of consolidation equilibrium. A similar application may

131

be envisaged for disposal of mine tailings.

8.3 Apparatus development.

There are a few aspects of the apparatus that require further development. It was realized at an early stage that the electrode arrangement used in the resistivity apparatus induced a large toroid electric field. Initially this was considered to be desirable in order to sample all of the sediment. However the electrical resistivity data collected in the Irvine Bay mud sample showed some anomalous results that could not be satisfactorily explained. It was also considered desirable to measure electrical resistivity in the same orientation as the seismo-acoustic beam. For these reasons a more focused electrode array is thought to be required such as the arrangement used in the Jackson porosity cell (Jackson 1975). It may be that the electrical resistivity is no longer a requirement of the apparatus if the mass coupling factor of all soft soils assume the value of unity. Perhaps the electrical resistivity in both the horizontal and vertical directions will be of interest to future researchers thus necessitating a combination of both types of electrode arrays.

The accuracy of the compressional wave and shear wave velocity measurements could be improved by adopting a more detailed monitoring of temperature at different points within the soil. The possibility of localised biological activity may substantially alter the temperature of the soil which, in the present column, would lead to a significant reduction in the accuracy of both V_p and V_s. In addition the shear wave measurements might be improved if there was a more accurate means of determining the bender element separation. This might take the form of a vernier or micrometer screw arrangement.

In order to improve the application of the Lee-Sills model, more pore pressure ports need to be incorporated into the column walls. These ports need to be of a smaller diameter than in the present column, since air entrapment proved a problem and called for frequent de-airing.

On a more general note, the considerable insight into the geotechnical properties using the lagrangian system of measurement makes a P-wave and S-wave tracking device very desirable. While there are considerable technical difficulties associated with S-wave tracking, P-wave tracking devices are now commercially available and would be useful in such studies.

8.4 Recommendations for future research.

A major aim of future research should be to obtain more data on the lines described in this thesis. This would give more credence to the trends already established between seismo-acoustic measurement and consolidation properties of the soil. Of particular interest would be the continued research into soft soil anisotropy with respect to permeability perhaps utilizing techniques already described in this thesis.

Continued research would be desirable into the relationship between shear wave velocity and rigidity modulus with effective stress making use of the apparatus improvements described section 8.3. The changes in column design would greatly improve the accuracy of the shear wave system reducing the scatter on the V_s-effective stress curves. Long term experiments into the effects of creep on the sediment samples are also of importance. Several questions need to be answered in this field of work. Does the creep continue at the rate observed in these column experiments, or does it stop at some point in time? Is creep affected by temperature, pressure, or by biological activity? Ideally, laboratory experiments concerned with these questions need to be continued until the laboratory sample has similar geophysical properties to those measured *in situ* prior to sampling. As a note of caution to future researchers in soft soil sedimentation, the behaviour of the consolidating soils above and below the critical input voids ratio should be observed and studied in isolation from each other. This would simplify all aspects of the research

ranging from the design of apparatus to the interpretation of results.

The relationship between shear wave propagation and organic content and clay mineralogy are of growing interest to engineers. A column design based on the proto-type column fitted with shear wave transducers should be sufficient to make such studies. The effects of biologically produced gas upon the seismo-acoustic properties of a sediment is again of interest to engineers and geophysicists alike. A research programme involving the study of gas concentration and its effect upon compressional wave reflectivity and penetration could be envisaged in a modified column experiment.

Continued laboratory research into the use of the Geertsma and Smit model using "weak frame" soil parameters to model P-wave velocity-porosity relationship is envisaged. Such research may answer questions such as when can a soil no longer be described by the "weak frame" parameters? Does the model break down with increasing sand/organic content? If so at what percentage of sand/organic content does this occur?

The method of modelling compressional wave dispersion curves to a single measurement of compressional wave velocity in order to predict permeability is questionable. On the one hand the approximate solution to the Biot theory, the Geertsma and Smit model, has severe practical limitations as described in section 7.4. On the other hand the full model requires information about the sediment sample which is difficult or even impossible to obtain. The main problem with the model appears to be in defining the size of the soil pore space. Present methods of determining pore size rely on either empirical relationships or else use simplistic models based on circular pores and slits, and upon the geometry of pores created by stacking spherical particles. The problem of defining a pore size parameter may be insurmountable for soft cohesive soils owing to their highly complex structure. It is doubtful as to whether pore size is the correct parameter needed and that researchers should be looking for ways of

defining pore throats as these clearly have an over-riding influence upon the sediments permeability.

The answer may lie in proving that the boundaries of the pores are fractal. The difficulty here is that it is virtually impossible to obtain a visible record of the soil fabric (Bowden 1989) and so the mathematicians have nothing with which to compare their fractal models. Given these difficulties it is worthwhile considering technological development of a system capable of measuring compressional wave velocity over several decades of frequency. If this could be done then the full model could be used with a great deal more confidence than at present.

Future research into the relationship between seismo-acoustic propagation and consolidation phenomena is likely to based upon the Biot theory. The theory, based on a two phase soil model, may need to be modified in order to include a gas phase or even an organic phase to the soil model. To date the Biot theory remains the most successful model in predicting soil properties; however it does not represent a truly unifying theory which is capable of relating geophysical measurement to geotechnical properties of the soil. This unifying theory remains the aim of all engineering geophysicists and for the present such a theory remains a distant goal.

A1.1 Soil Bulk Density Measurement Using X-Ray Attenuation.

The soil bulk density was determined non-destructively by measuring the degree of X-ray attenuation in the soil sample. The measurement technique has been initially described by Been (1982) and developed further by Elder (1985). The method by which the soil bulk density is determined from X-ray attenuation measurements is outlined below.

If a hypothetical narrow, monoenergetic beam of X-ray radiation of initial intensity I_0 is incident upon a sample of homogeneous material then the X-rays would be attenuated in accordance with the following equation (Kohl et al 1961):

$$I = I_0 \exp (-\mu_m \rho x) \qquad\qquad (A1.1)$$

where I_0 = incident radiation intensity

I = transmitted radiation intensity

μ_m = total mass absorption coefficient

ρ = bulk density of absorbing material

x = radiation path length in the absorber

This equation may be re-written in terms of a quantity that is more easily measured, namely the X-ray count rate

$$N_s = N_0 \exp (-\mu_m \rho x) \qquad\qquad (A1.2)$$

where N_0 = detected count rate with no sample present

N_s = detected count rate with sample present

In reality it is virtually impossible to use equations A1.1 and A1.2 to determine the soils bulk density directly due to X-ray source energy spectrum broadening, beam intensity fluctuations, and inhomogeneities in the soil sample and soil container (see Elder 1985 and Bowden 1989). However the problem of relating X-ray attenuation to density can be best

treated empirically as described by Elder (1985).

The problems encountered in applying equation A1.1 and A1.2 can be overcome by creating an all encompassing average attenuation constant that includes the effects of material inhomogeneities and sample geometry. Calibration of the X-ray apparatus is achieved by back calculation of the average attenuation equation constants from each attenuation profile, assuming a known mass of solids in each column. Applying equation A.1.2 to a sample of water, density (ρ_w) and then to a sample of a homogeneous soil/water mixture of density (ρ) the incident count rate N_s is eliminated to give

$$\rho - \rho_w = \frac{1}{\chi} \, \mathrm{Ln} \left(\frac{N}{N_w} \right) \qquad (A1.3)$$

where N = observed count rate through soil/water mixture
       N_w = observed count rate through water sample
       χ = average attenuation constant = μ_m x

If χ is known then ρ can be determined. In order to determine χ the total vertical stress above hydrostatic at the bottom of the soil sample must be defined as

$$\sigma = \int_0^{z_0} (\rho - \rho_w) \, g \, dz \qquad (A1.4)$$

where z = thickness of soil sample
       z_0= total thickness of sample
       g = acceleration due to gravity

Combining equations A.1.3 and A.1.4 and replacing the integral by the summation of discrete linear segments gives

$$\sigma = \frac{-g}{2\chi} \left[\sum \left(\mathrm{Ln} \left(N_i \cdot N_{i+1} \right) \Delta z_i \right) - 2z_0 \cdot \mathrm{Ln} \, N_w \right] \qquad (A1.5)$$

where N_i and N_{i+1} are count rates at consecutive elevation
       Δz_i being the difference in elevation

The quantity σ was determined in each experiment by inputting the measured initial slurry density and height into equation

A.1.4. Equation A.1.5 was then solved to yield χ. Each count rate value was then converted to a bulk density using equation A.1.3.

The vertical total stress acting upon any element within the soil mass can be determined in a similar manner by changing the integration/summation limits of equations A1.4 and A1.5.

A1.2. Determination of Total Vertical Stress.

Making use of the analysis technique described by Been (1980) and Elder (1985), in which individual elements within the soil can be tracked it is necessary to set up a Lagrangian co-ordinate system and define normalized material co-ordinate, y, using the soil surface as a datum.

$$y = \frac{\text{mass of solids above element}}{\text{total mass of solids present}} \qquad (A1.6)$$

The total vertical stress above hydrostatic pressure acting on a particular soil element can be determined using

$$\sigma = \int_0^z (\rho - \rho_w) \, g \, dz \qquad (A1.7)$$

where σ = vertical total stress
z = total thickness of soil sample
ρ = bulk density of the soil
ρ_w = density of the pore fluid
g = acceleration due to gravity

Integrating the equation over the interval 0 to z_0 gives the total vertical stress acting at the base of the column of the soil, and should remain a constant throughout the experiment so long as no material is added or taken away.

138

A1.3 Determination of Vertical Effective Stress.

Using the principal of effective stress, the vertical effective stress is given by

$$\sigma' = \sigma - u \qquad (A1.8)$$

where σ' = vertical effective stress

σ = vertical total stress

u = pore pressure

Effective stress can be determined for a particular soil element by using (figure A1.1)

(1) the bulk density to determine the total stress acing on that element.

(2) the pore pressure profiles to determine the excess pore pressure acting on that same element.

The soils frame compressibility (C_f) can be determined from differentiation of e versus σ' curves.

$$C_f = \frac{\frac{d\sigma'}{de}}{(1 + e_0)} \qquad (A1.9)$$

where e_0 = initial voids ratio

Voids ratio derived directly from density profiles using the expression

$$e = \frac{(G_s\rho_w - \rho)}{(\rho - \rho_w)} \qquad (A1.10)$$

where G_s = specific gravity of soil grains

ρ_w = density of fluid

ρ = bulk density

A1.4 Determination of Permeability.

The permeability, k, of the consolidating soft soil can be estimated from the experimental results, assuming Darcy's law

$$c = k \, i \tag{A1.11}$$

where c = relative velocity of the fluid to the solid phase
       k = the permeability (units m/s)
       i = hydraulic gradient

The equation of continuity gives the following

$$c_s (1 - \eta) + c_f \eta = 0 \tag{A1.12}$$

where c_s = velocity of the solid phase
       c_f = velocity of the fluid phase
       η = porosity

The relative velocity is given by

$$c = (c_s - c_f) = \frac{c_s}{\eta} \tag{A1.13}$$

combing equations A1.11 and A1.13, the permeability is given as

$$k = - \frac{c_s}{i\eta} \tag{A1.14}$$

The mean velocity of the solid phase c_s can be deduced by recording the displacement of a soil element between two density profiles. The change in height of the element divided by the time between profiles gives c_s.

$$c_s = \frac{(z_1 - z_2)}{(t_1 - t_2)} \tag{A1.15}$$

A mean hydraulic gradient and porosity can be determined directly from the pore pressure and density profiles

respectively, and hence an average permeability for the soil
element is found.

$$i = \frac{i_1 + i_2}{2}$$

$$= \quad 0.5 \left(\frac{u_{11} - u_{12}}{z_1 + z_2} + \frac{u_{22} - u_{21}}{z_1 - z_2} \right) \qquad (A1.16)$$

$$k = \frac{c_s}{i} = \frac{(z_1 - z_2)}{2(t_1 - t_2)(u_{11} - u_{12} + u_{22} - u_{21})} \qquad (A.1.17)$$

DENSITY PROFILE

PORE PRESSURE PROFILE

Height

Total vertical stress
acting on soil elament

$$\sigma = \int_o^z (\rho - \rho_w)g \, dz$$

Z

soil element

$y = Z/Z_0$

Z_0

$\rho_w g$

Bulk Density $(\rho \, g)$

Height

pore pressure u

Pore Pressure

Vertical Effective Stress

$$\sigma' = \sigma - u$$
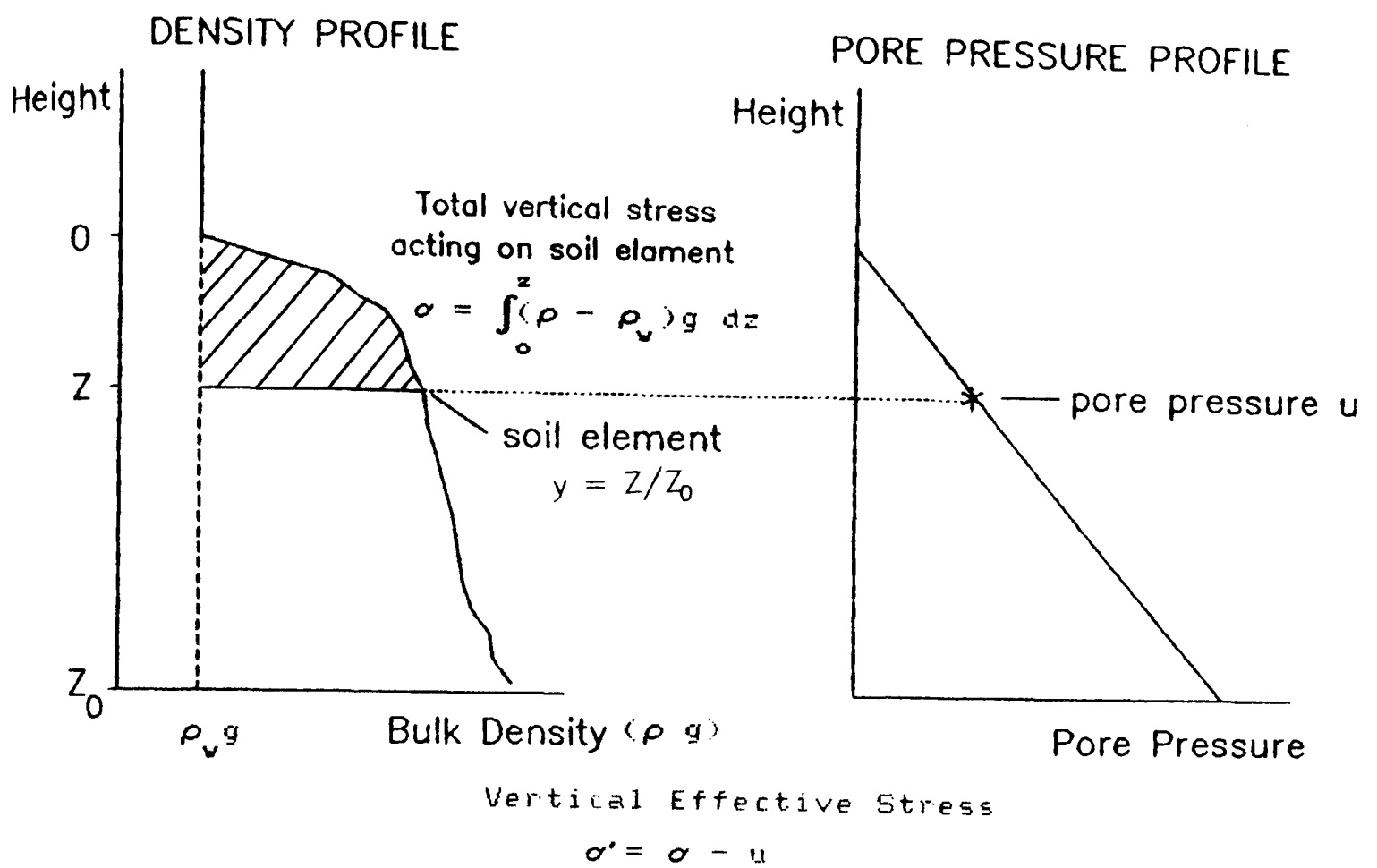
Figure A1.1   Method to determine vertical effective stress

DENSITY PROFILE 1

$y = 0.2$

Z_1

PORE PRESSURE
PROFILE 1

U_{11}

U_{12}

DENSITY PROFILE 2

$y = 0.2$

Z_2

PORE PRESSURE
PROFILE 2

U_{21}

U_{22}

Profiles at time t1

Profiles at time t2

(t1 < t2)
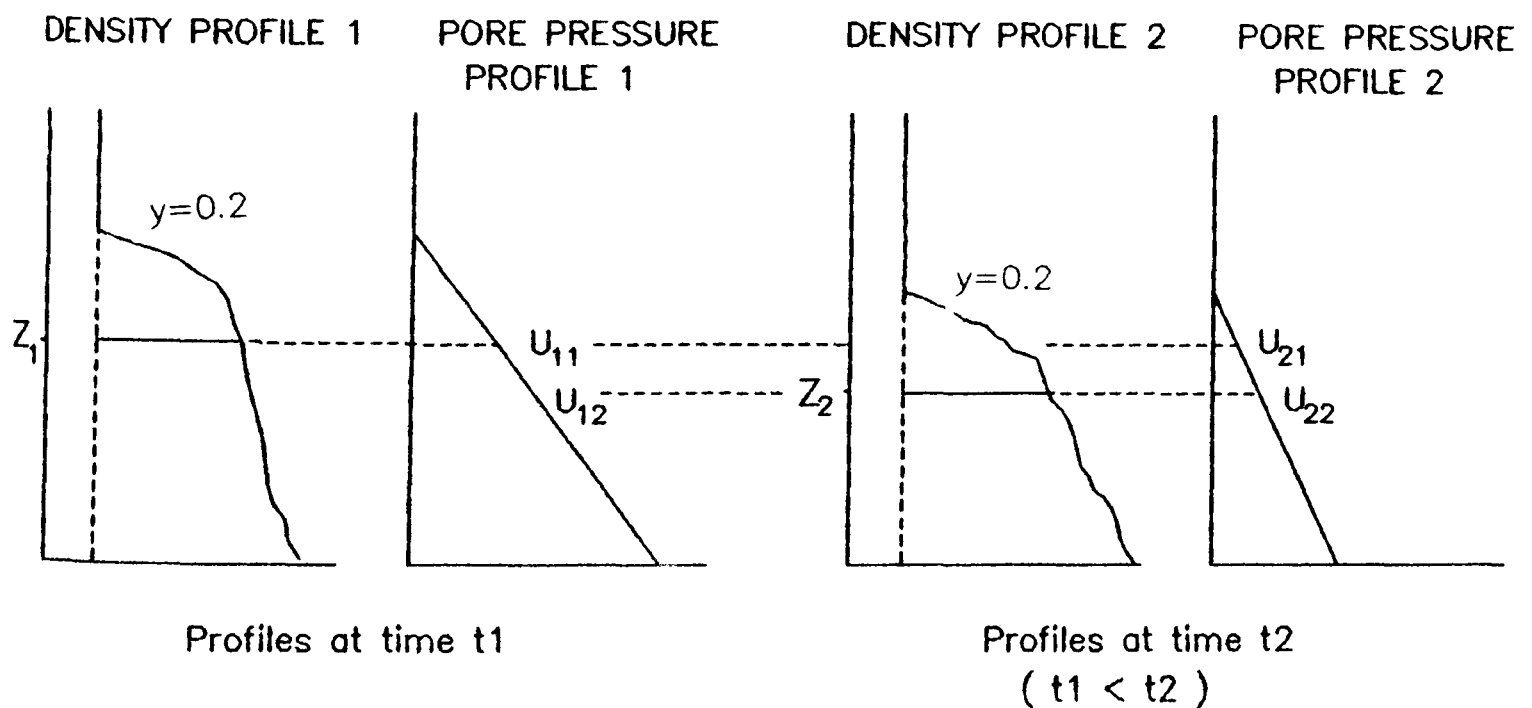
Figure (A1.2)   Method to determine permeability.

APPENDIX 2 THE BIOT THEORY.

A2.1 INTRODUCTION.

A general theory of three dimensional propagation of elastic waves in a fluid saturated porous solid was presented by Biot (1956a,b). The theory is reviewed briefly below in its application to ocean sediments saturated by sea water.

A seismo-acoustic wave incident upon a porous solid will cause deformation to the solid structure and in general will change the pore volume also. If this pore volume contains fluid, this fluid can change its volume owing to its own compressibility. As the fluid compressibility in most cases will differ from that of the pore volume, the fluid will try to flow through the porous medium under the influence of the induced pressure gradient. If an elemental volume associated with the porous solid is considered in terms of continuity equations then the balance between the fluid displacement and change in fluid volume can be determined. The stress-strain equations of the two phases, the equations of motion of the solid and fluid, together with equations of continuity, are sufficient to determine the behaviour of the fluid saturated porous solid, provided the effect of temperature changes due to dissipation of energy as heat can be neglected.

A2.2 THE BIOT MODEL ASSUMPTIONS.

(1) The wavelength of the wave passing through the medium is larger than the largest dimension of soil particle which comprises the pore structure.
(2) The pore fluid saturating the porous medium is viscous and compressible.
(3) The solid phase is isotropic and porous (The anisotropic condition was later treated in Biot 1962).

A2.3 THE STRESS-STRAIN EQUATIONS.

$$\sigma_x = X\Delta - 2G \left(\varepsilon_y + \varepsilon_z \right) - Y\zeta \qquad (A2.1)$$

$$\sigma_y = X\Delta - 2G \left(\varepsilon_z + \varepsilon_x \right) - Y\zeta \qquad (A2.2)$$

$$\sigma_z = X\Delta - 2G \left(\varepsilon_x + \varepsilon_y \right) - Y\zeta \qquad (A2.3)$$

$$\tau_{xy} = G \, \gamma_{xy} \qquad (A2.4)$$

$$\tau_{yz} = G \, \gamma_{yz} \qquad (A2.5)$$

$$\tau_{xz} = G \, \gamma_{xz} \qquad (A2.6)$$

$$u = Z\zeta - Y\varepsilon \qquad (A2.7)$$

where σ = normal stresses on an element of the soil frame
τ = shear stresses on an element of the soil frame
ε_{xyz} = strain components due to normal stresses
γ_{xyz} = strain components due to shear stresses
G = shear modulus of the soil bulk material.
u = pore pressure
X, Y, Z = Generalized elastic coefficients

the volumetric strain of the elemental soil frame is given by

$$\varepsilon = \varepsilon_x + \varepsilon_y + \varepsilon_z = \text{div } \underset{\sim}{\upsilon} \qquad (A2.8)$$

the volume of fluid that has flowed in and out of the element is given by

$$\zeta = \eta \, \text{div} \left(\underset{\sim}{\upsilon} - \underset{\sim}{\xi} \right) \qquad (A2.9)$$

where η = porosity
$\underset{\sim}{\upsilon}$ = frame displacement
$\underset{\sim}{\xi}$ = fluid displacement

The parameters X,Y and Z can be related to the compressibilities of the constituents of the two phase media. (Refer to Stoll 1974, 1986 for more detail of these

parameters).

$$X = \frac{(1 - R)}{(1 - \eta - R)C_s + \eta C_w} + \frac{1}{C_f} + \frac{4G}{3} \qquad \text{(A2.10)}$$

$$Y = \frac{(1 - R)}{(1 - \eta - R)C_s + \eta C_w} \qquad \text{(A2.11)}$$

$$Z = \frac{1}{(1 - \eta - R)C_s + \eta C_w} \qquad \text{(A2.12)}$$

where C_s = compressibility of the soil grains
C_w = compressibility of the pore fluid
C_f = compressibility of the skeletal frame
$R = C_s/C_f$

A2.4 EQUATIONS OF MOTION IN A SATURATED POROUS MEDIUM.

If equations A2.10, A2.11, A2.12 are combined with the stress strain equations (A2.1 to A2.7) and assuming that Darcy's equation for flow through a porous medium holds, then two coupled equations of motion result. These differential equations predict the existence of two plane compressional waves referred to by Biot as waves of the "first kind" and "second kind". (refer to Biot 1956a and Geertsma 1961).

$$\nabla^2 (X\varepsilon - Y\zeta) = \frac{\partial^2}{\partial t^2} (\rho\varepsilon - \rho_w \zeta) \qquad \text{(A2.13)}$$

$$\nabla^2 (Y\varepsilon - Z\zeta) = \frac{\partial^2}{\partial t^2} (\rho_w \varepsilon - m\zeta) - \frac{\mu}{\phi} \frac{\partial \zeta}{\partial t} \qquad \text{(A2.14)}$$

where ρ_s = soil grains density
ρ_w = pore fluid density
ρ = bulk density of the two phase system
$= (1 - \eta)\rho_s + n\rho_w$
μ = viscosity of the pore fluid

ϕ = coefficient of permeability (units of area)

m = apparent mass density

A2.5 APPARENT MASS DENSITY AND MASS COUPLING FACTOR.

As a result of a small strain seismo-acoustic wave passing through a saturated porous medium, a macroscopic pressure gradient will propagate through the soil. Owing to the tortuous and multi directional nature of the interconnecting pore spaces, not all the pore fluid will move in the direction of this pressure gradient. As a consequence of the restricted movement, an opposing pressure gradient will be induced in the fluid. Biot (1962) introduced this concept to his theory in the form of a mass coefficient "m". Such a coefficient is a function of the mass of the fluid plus an additional "apparent mass" which arise within the fluid as a consequence of the opposing gradient. Biot defined this quantity as

$$m = \frac{b \, \rho_w}{\eta} \qquad\qquad (A2.15)$$

The term "b" is referred to as the mass coupling factor and is a measure of the tortuosity of the interconnected pore spaces within the soil. Stoll (1974) states that theoretically

$$1 \geq b \leq 3$$

The lower limit, b = 1, represents uniform pores with axes parallel to the seismo-acoustic pressure gradient, while the upper limit, b = 3, represents a random system of uniform pores with all possible orientations. In a real soil, however, the distribution of the pores is far more complex and it is impossible to calculate theoretically. Therefore the mass coupling factor must be determined experimentally. One method, suggested by Brown (1980), for determining an estimate of mass coupling factor is to use the analogy between hydraulic and electrical tortuosity in the porous medium

$$b = F\eta \qquad\qquad (A2.16)$$

where F = apparent formation factor

$$= \frac{\text{electrical resistivity of the sediment}}{\text{electrical resistivity of the pore fluid}}$$

A2.6 SOLUTIONS TO THE EQUATIONS OF MOTION.

The simultaneous differential equations (A2.13) and (A2.14) are satisfied by the solutions of the form

$$\varepsilon = A_1 \exp (i(\omega t - lx)) \qquad \text{(A2.17)}$$

$$\zeta = A_2 \exp (i(\omega t - lx)) \qquad \text{(A2.18)}$$

where ω = angular frequency
            l = wave number

the velocity of these waves is given by

$$V = \omega/l \qquad \text{(A2.19)}$$

Biot considers solutions to these equations within a low frequency range where Poiseuille flow is valid (Biot 1956(a)), and extends the solution to higher frequency ranges were such flow breaks down (1956(b)). The complexity and impracticability of the Biot model has led a number of authors, in particular Geertsma and Smit (1961) and Geertsma (1961), to derive approximate solutions to the Biot theory.

A2.7 GEERTSMA AND SMIT'S APPROXIMATE SOLUTION.

The exact solution for the wave of the "first kind", the compressional wave normally observed in sediments, can be easily arrived at but is impractical for engineering purposes. Geertsma and Smit (1961) introduced additional constraints to the Biot theory:
(a) Darcy's law of fluid flow should be obeyed.
(b) Temperature variation due to energy losses are negligible. Geertsma and Smit derived a suitable approximation which makes

use of two velocities: the "zero frequency velocity" V_o for applied frequencies very much lower than the characteristic frequency of the material; and the "infinite frequency velocity" V_∞ where the applied frequency is very much higher than the characteristic frequency. The compressional wave of the "first kind" V_P is given by

$$V_P^2 = \frac{V_\infty^4 + V_o^4 (\omega_c/\omega)^2}{V_\infty^2 + V_o^2 (\omega_c/\omega)^2} \qquad (A2.20)$$

where

$$V_o^2 = X/\rho \qquad (A2.21)$$

$$V_\infty^2 = \frac{Z + Xm - Y\rho_w}{m\rho - \rho_w^2} \qquad (A2.22)$$

and the characteristic angular frequency of the sediment ω_c

$$\omega_c = \frac{\mu\rho}{(m\rho - \rho_w^2)} \cdot \frac{1}{\phi} \qquad (A2.23)$$

where ϕ is the coefficient of permeability defined in units of area. To convert into units of velocity

$$k = (\phi \, g \, \rho_w)/\mu \qquad (A2.24)$$

where k = permeability (units m/s)

g = acceleration due to gravity

Equation A2.20 is valid so long as the relative motion of the pore fluid is Darcyian (assumption 4). Biot defines a frequency below which Poiseuille flow exists, above which turbulent flow occurs and Poiseuille flow breaks down. Biot

147

calls this the transitional frequency f_t (Biot 1956a) and
defines it as

$$f_t = \frac{\pi \ \mu}{(4 \ \rho_w d^2)} \approx 0.15 \ f_c \qquad (A2.25)$$

where   d = pore size parameter

It is necessary to point out that the relationship between
Poiseuille flow and Darcy's flow is not well documented. Many
authors use the terms indiscriminately where as theoreticians
such as Biot and Geertsma and Smit have been very precise in
their use of the two terms.

A2.8 THE BIOT FULL MODEL.

The Geertsma and Smit approximate solution to the low
frequency Biot theory breaks down at applied elastic wave
frequencies above the transitional frequency. Above this
frequency the impinging pressure wave induces non-linear flow
in the interstitial fluid. Biot (1956,b) analysed the subject
of seismo-acoustic wave propagation in a fluid saturated
porous medium at high frequency by introducing a complex
viscosity correction factor $(F(\Phi))$ through the dimensionless
ratio $\Phi = f/f_c$ where f_c is the characteristic frequency of the
soil. Separating the real and imaginary parts of $F(\Phi)$ as
follows

$$F(\Phi) = F_r(\Phi) + F_i(\Phi)$$

The viscosity correction factor represents the deviation from
Poiseuille flow as frequency increases. Setting $F(\Phi)=1$ means
that Φ 0 which corresponds to Poiseuille flow, and the return
to the low frequency Biot model and the Geertsma and Smit
approximation. The full assessment of non-linear flow involves
the use of a complex Kelvin function which requires the
determination of a pore size parameter (d) which may be
determined experimentally for coarser sediments but as yet not
for clays and silts. Many authors choose to use approximations
of "d" but these are based on ideal structures such as spheres
and circular ducts (Hovem and Ingram 1979, Stoll 1986,

Yamamoto and Turgut 1988). Computer programs modelling the Biot full model and the Geertsma and Smit approximate solution are given in appendix 4.

APPENDIX 3   AUXILIARY DIAGRAMS
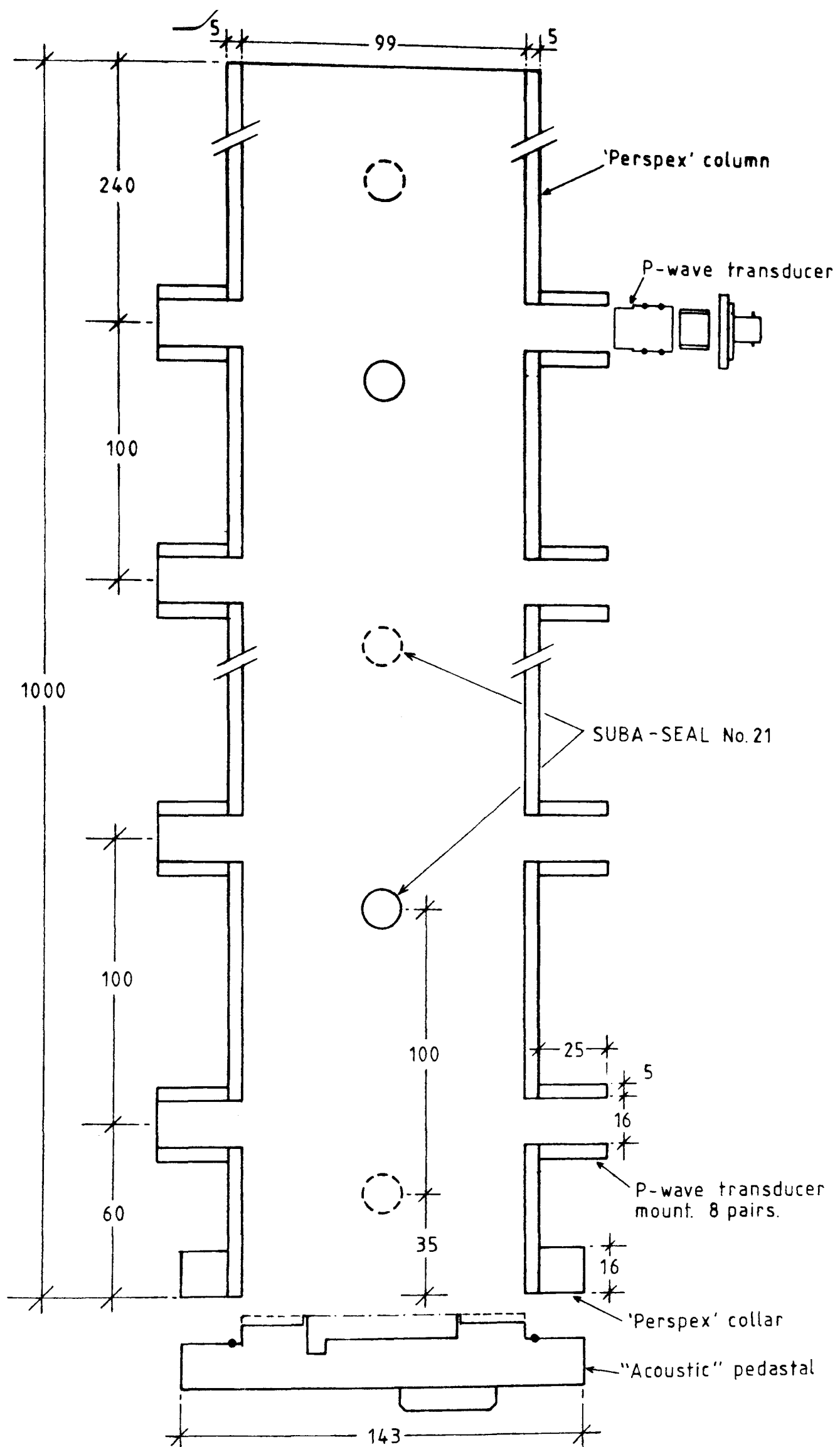
All dimensions in millimetres.

Figure A3.1 Prototype sedimentation column.

SECTION BB

2 mm. drainage channel

99

66

52

Porous disc

22

6·25

3

'O' ring

24·5

Seismic transducer port

16

Pressure transducer port

142

PLAN AA

2 mm. drainage channel and holes.

'O' ring channel

30°

Transducer recess

Pedastal to base screw holes.
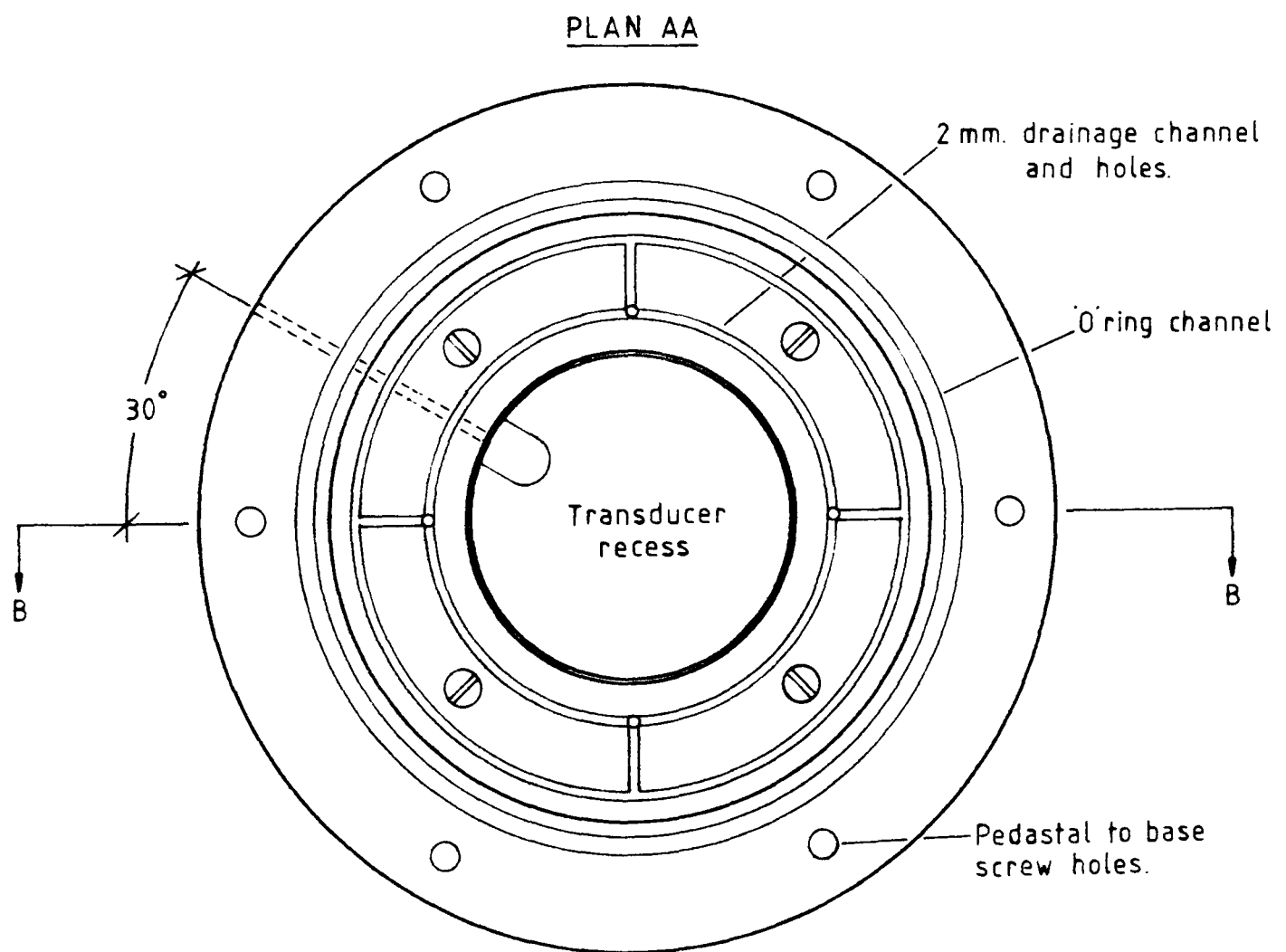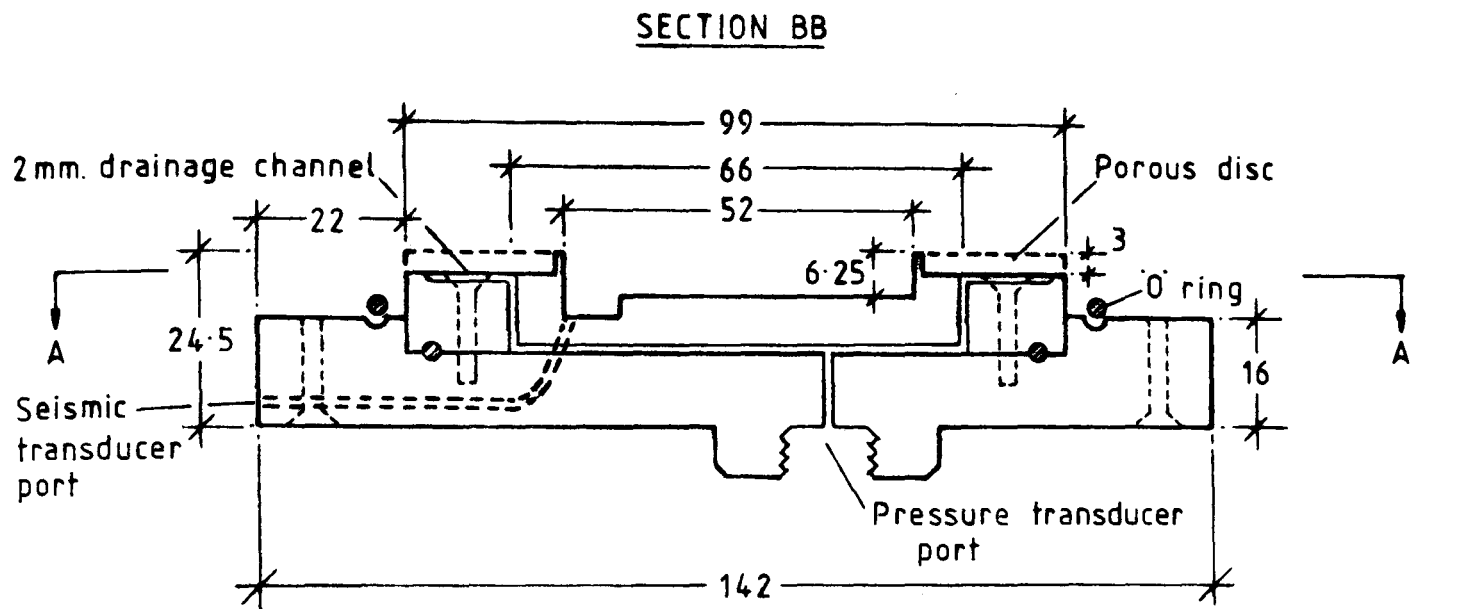
All dimensions in millimetres.

Figure A3.2   Acoustic pedestal of the prototype column.

Plan A-A

Plan B-B

'PERSPEX'
TRANSDUCER
RECEPTICLE

Ashton precision
O-ring seal
Ref: 0100TA0147 OMN

'PERSPEX' SPACER

BNC
CONNECTOR
Sq/skt 50 Ω
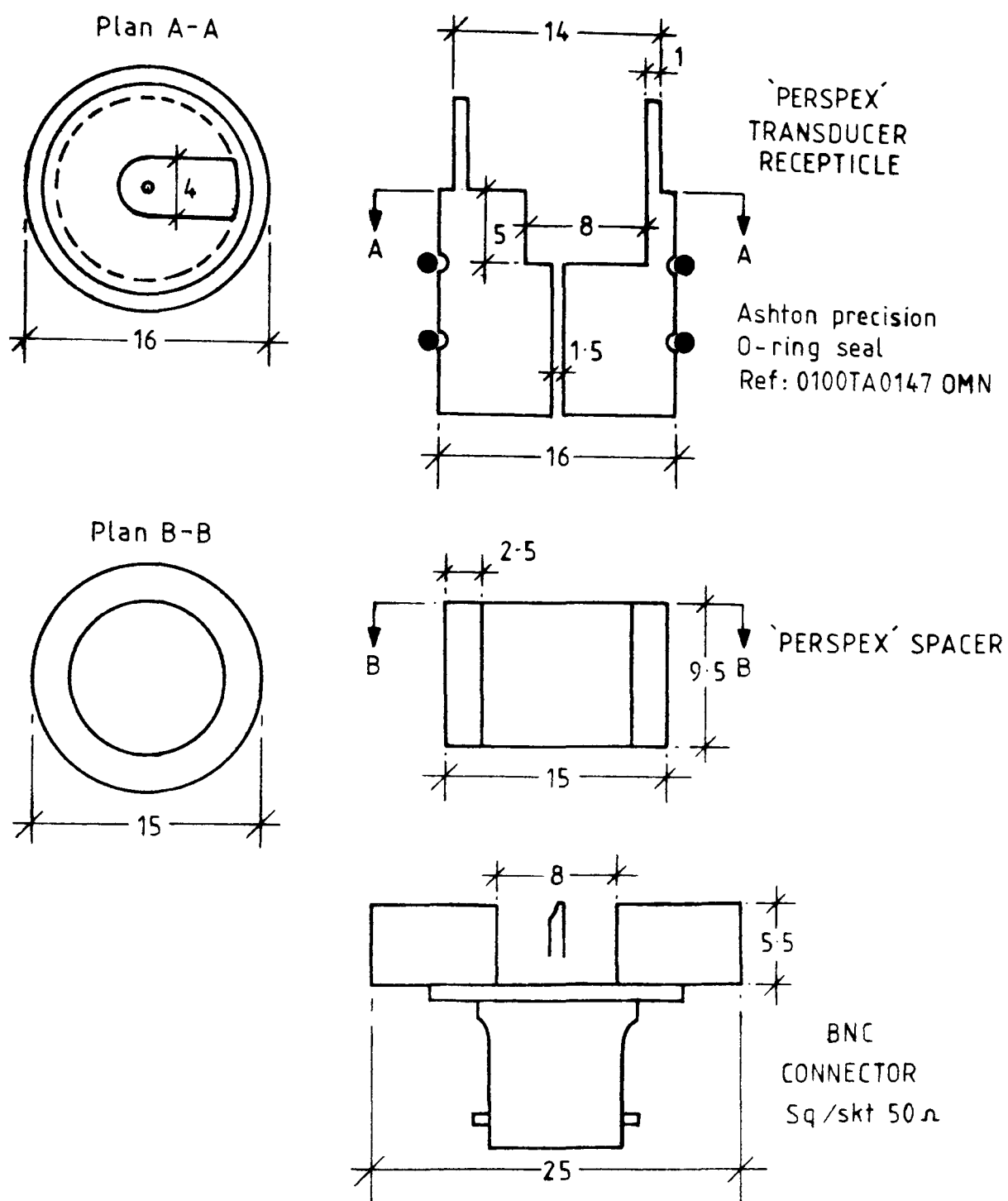
All dimensions in millimetres.

Figure A3.3 Compressional wave transducer assembly.

Figure A3.4 Settling column temperature–resistance calibration curve.

$$R = 2.35 - 0.0584T + 0.00069T^2$$
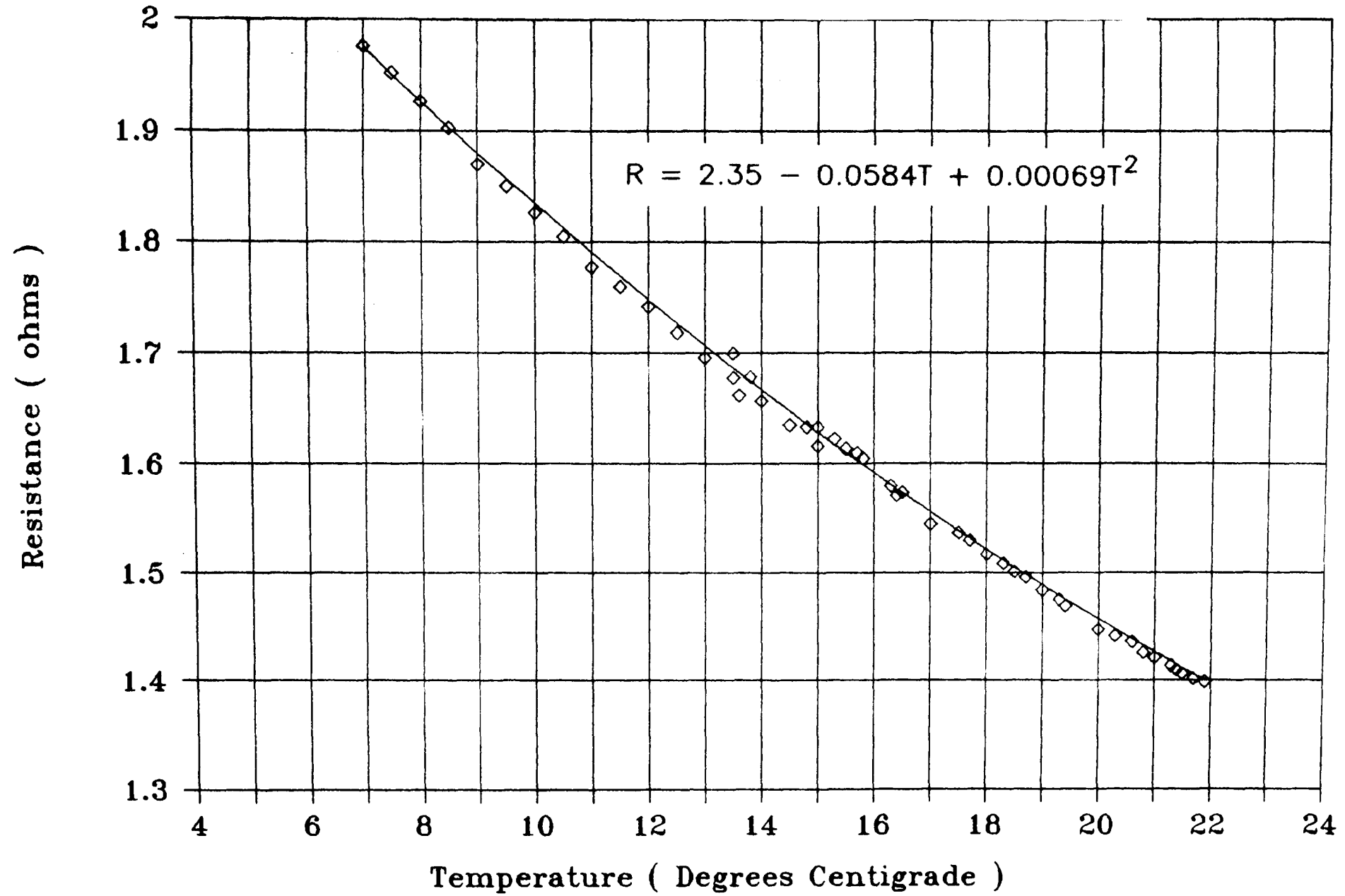
Figure A3.5 Experiment IM06 X—ray calibration curve.
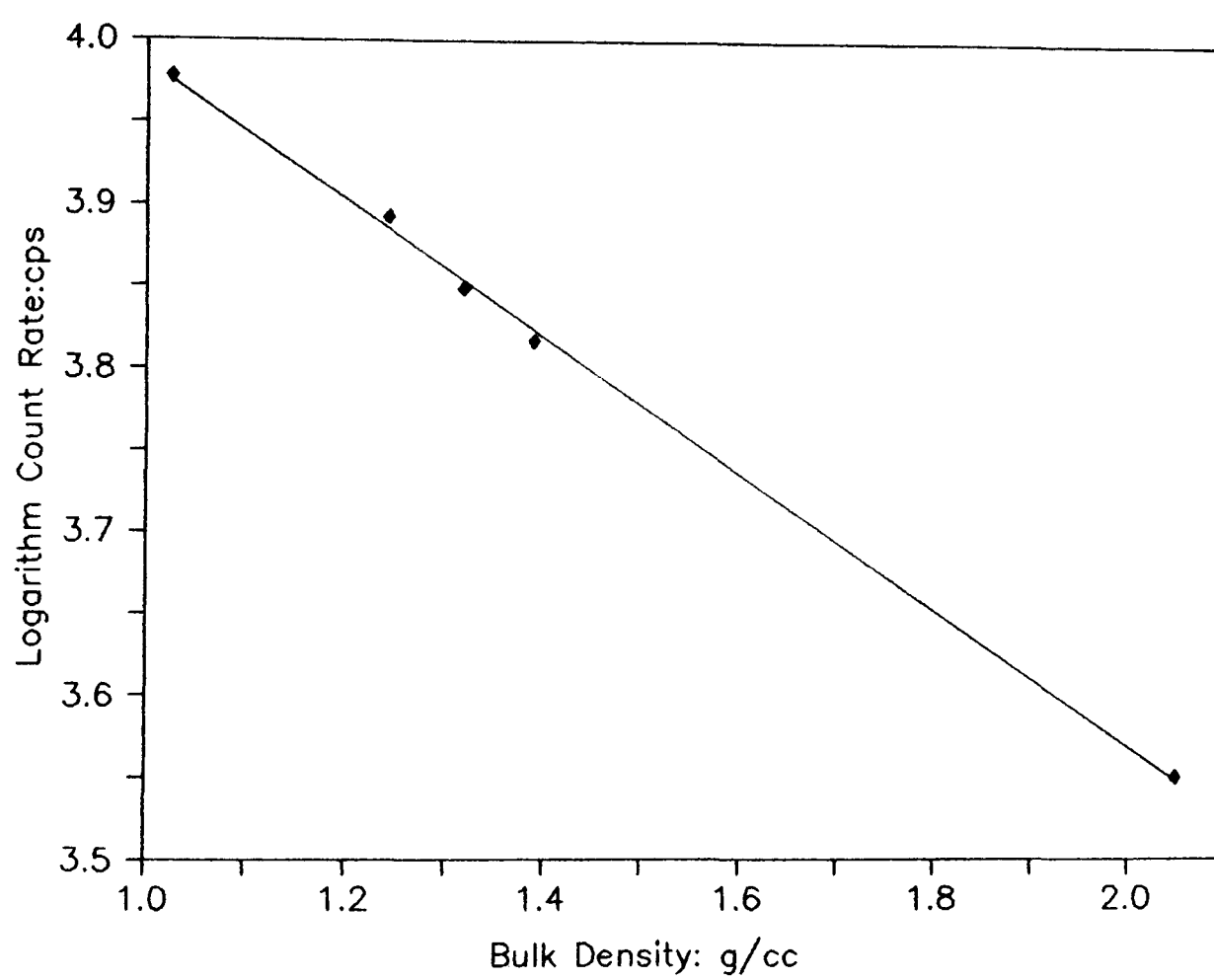
Figure A3.6 Formation Factor versus porosity relationship for marine sediments of different particle sizes and shapes (from Jackson et al 1978)

Figure A3.7 Typical ranges of Formation Factor in cohesive
and non-cohesive marine sediments.

(from Jackson et al 1978)
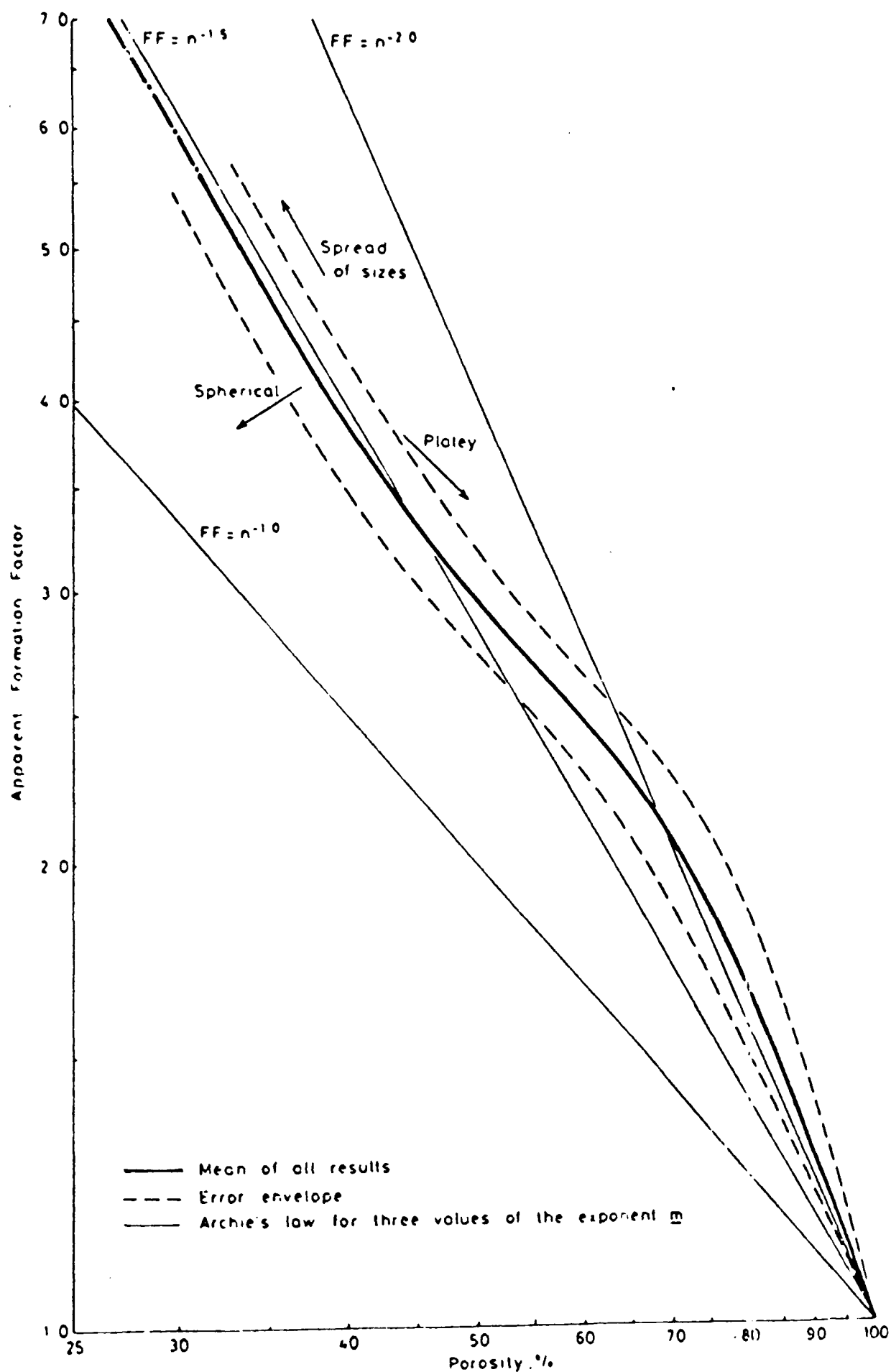
DMA 35 DIGITAL DENSITY METER

The new DMA 35 portable density meter incorporates a density measuring device based upon the mechanical oscillator technique and a digital thermometer, which uses a thermistor as the sensor. The thermometer measures sample temperature and also provides for compensation of temperature influences.
Calibration constants for the oscillator cell are stored in a non-volatile digital memory.
Weighing only 550g and being powered by a standard 9v battery means that the DMA 35 can truly be described as a portable hand-held unit for use wherever a rapid and convenient method of density measurement is required without the need to send samples back to laboratories for test.

The instrument is available as

• density meter

• relative-density meter

• concentration meter (e. g. °Brix)

• accurate
• fast
• easy to operate
• no external power
• no external thermostat
• digital density display
• digital temperature display
• special versions: intrinsically safe (Ex) i; soft rubber housing (also intrinsically safe (Ex) i)

Specifications
Density measuring range: 0.5 to 1.999 gcm⁻³

Density measuring range: 0.5 to 1.999 gcm^{-3}
Accuracy: ± 0.001 gcm^{-3}
Temperature range: Filling: Ambient temperature up to 80° C
Measuring: Ambient temperature ±5 K within 0 to 40° C
Resolution: 0.1 K
Sample volume: 2 cm³
Power requirements: 3.5mA (from standard 9v battery)
Weight: 550 g
Size: 80 x 280 x 35 (85) mm
Storage temperature range: − 10 to 60° C
The sample is in contact with borosilicate glass, PTFE and the stainless steel filling nozzles (mat. no. 1.4436). The suction device is made of glass and silicone rubber. Special filling nozzles made of Ni, Ti, PTFE. Other material upon request.
With automatic LCD segment test when switched on, low battery indicator, and LCD protection when battery exhausted.

Principle of measurement

The sample to be measured is introduced into a hollow U-shaped oscillator [4] made of borosilicate glass DURAN 50. This sample tube is electromagnetically excited to perform undamped oscillations.
Since the volume of sample participating in the vibration is kept constant by the construction of the oscillator, the period depends only on the sample's density and the temperature of the sample tube.
In order to eliminate the temperature coefficient of the oscillator the temperature of the oscillator is determined.
From the period a built-in digital processor calculates according to the equation

$$\rho = A \ (T^2 - T_0^2)$$

the true density of the sample, where:

T is the actual period, T_0 the period of the empty oscillator forming one calibration constant and A the second, for the individual oscillator. A and T_0 are determined at manufacture and are stored in the processor's non-volatile memory. When measuring relative density or concentration A and T_0 are modified accordingly.

APPENDIX 4   **COMPUTER PROGRAMS**

```
10 '************************************************************************
20 '*                                                                      *
30 '*          ################ XLOG2 ##########################           *
40 '*      X-ray to IBM interface program via DAS-8PGA board               *
45 '*      Screen display and Lotus file in metres and volts               *
50 '*  I.McDermott/G.Sills                                                  *
60 '*                                                                5-12-89  *
70 '************************************************************************
80 SCREEN 0,0,0 : KEY OFF : WIDTH 80
90 'Make initial screen announcement
100 CLS
110 'Program performs ADC in bursts of two channels
120 '        channel 0 = Rig height
130 '        channel 1 = Count rate
140 '        pin connections as follows
150 '              (1) CLK.2 OUT (PIN 6) to CLK.0 IN (PIN 2)
160 '              (2) CLK.0 OUT (PIN 3) to INTE (PIN24)
170 '              (3) IP1 (PIN 25) external trigger high/no adc, low/start adc
180 '              (4) Jump one of the interrupt lines 2-7 on DAS-8 board"
190 'Clock 2 acts as both the Interrupt and the SAMPLE/HOLD source.
200 PRINT:PRINT:PRINT:COLOR 0,7
210 PRINT"************************************************************************
220 PRINT"*
230 PRINT"*                      X-RAY LOGGING PROGRAM XLOG2
235 PRINT"*                      Lotus file in metres and volts
240 PRINT"*
250 PRINT"************************************************************************
260 B=0
300 '
310 '--- Step 1:  Initialize DAS-8 with mode 0 -----------------------------
320 DEF SEG = &H5000       'Load base address
330 BLOAD "DAS8.BIN",0     'Load driver routine
340 OPEN "DAS8.ADR" FOR INPUT AS#1
350 INPUT #1,BASADR%
360 CLOSE#1
370 DAS8 = 0               'Load offset = 0
380 MD% = 0                'initialize mode
390 FLAG% = 0              'declare error variable
400 CALL DAS8 (MD%,BASADR% , FLAG%)
410 IF FLAG% <> 0 THEN PRINT "Error in initialization":END
420 '
430 '--- Step 2: Set timer rate -------------------------------------------
440 MD% = 10               'Mode 10 for setting counter configuration
450 D%(0) = 2              'Operate on counter #2
460 D%(1) = 3              'Configuration #2 = rate generator
470 CALL DAS8 (MD%, D%(0), FLAG%)
480 IF FLAG% <> 0 THEN PRINT "Error in setting counter 2 configuration":END
490 '
500 'Enter desired sample rate
510 F = 1      'desired output frequency in Hz  (suggested range 0.1-10 Hz)
520 'Set clock 2 to output 1kHz square wave to be fed into clock 0
530 D = 1000    ' Let clock 2 divisor =1000
540 K = 1000000!/D  'desired o/p frequency from clock 0
550           '     Output frequency = (1000.0/N KHz if DAS8-PGA)
560 N = 1000000!/K
570 IF N < 2 OR N >65535! THEN PRINT"Warning! A sample rate of ";F;" samples/se
is outside the range of Counter 2 ":STOP
580 MD% = 11                'Mode 11 to load counter
590 D%(0) = 2               'Operate on counter #2
600 IF N < 32767 THEN D%(1) = N ELSE D%(1) = N - 65536!  'correct for integer
610 CALL DAS8 (MD%, D%(0), FLAG%)
620 'clock 2 will now be sending a 1KHz square wave
630 IF FLAG% <> 0 THEN PRINT "Error in loading counter 2":END
640 MD% = 10                'Mode 10 for setting counter configuration
```

```
650 D%(0) = 0                  'Operate on counter #0
660 D%(1) = 3                  'Configuration #3 = rate generator
670 CALL DAS8 (MD%, D%(0), FLAG%)
680 IF FLAG% <> 0 THEN PRINT "Error in setting counter 0 configuration":END
690 '
700          'Calculate the desired sample rate
710 N = K/F   'ex. N = 1 kHz/ 2 Hz
720 IF N < 2 OR N >65535! THEN PRINT"Warning! A sample rate of ";F;" samples/se
 is outside the range of Counter 2 change statement 580":STOP
730 MD% = 11                   'Mode 11 to load counter
740 D%(0) = 0                  'Operate on counter #0
750 IF N < 32767 THEN D%(1) = N ELSE D%(1) = N - 65536!   'correct for integer
760 CALL DAS8 (MD%, D%(0), FLAG%)    'desired frequency now emitted from clock
 o/p (pin 3)
770 IF FLAG% <> 0 THEN PRINT "Error in loading counter 2":END
780 '
790 '***************** USER DEFINED PARAMETERS  ****************************
800 '--- Step 3: Select the channel(s) to scan  ---------------------------
810 MD% = 1       'Set scan limits
820 LS%=0         'Set lower limit to channel 0
830 US%=1         'Set upper limit to channel 1
840 D%(0)=LS% : D%(1)=US%:CHAN%=(1+(US%-LS%))
850 CALL DAS8 (MD%, D%(0), FLAG%)
860 IF FLAG% <> 0 THEN PRINT "Error in setting channel scan limits":END
870 '
880 'Now fetch duration of scan in seconds by converting rig height into travel
890 ' time
892 GOTO 895
893 CLS:PRINT:INPUT "SET RED SWITCH TO OFF.   ENTER ANY VALUE EXCEPT N WHEN DONE
 ",SWTH$
894 GOTO 897
895 PRINT:PRINT:INPUT "IS THE RED SWITCH OFF? (Y/N)   ",SWTH$
897 IF SWTH$ = "" GOTO 895
898 IF SWTH$ = "N" OR SWTH$ = "n" THEN 893
900 CLS:PRINT:PRINT:INPUT "Enter height of column base (in metres) =   " ,BH
905 IF BH = 0 GOTO 900
910 PRINT:INPUT "Enter height of top of the column (in metres) =   ",TH
915 IF TH =   0 GOTO 910
920 PRINT:INPUT "Enter whether UP or DOWN SCAN  (U/D) ",SCAN$
924 PRINT:PRINT:PRINT:PRINT:PRINT:PRINT" - Do you wish to continue (y/n)? - ";:C
OLOR 7,0
925 A$ = INKEY$
926 IF A$ = "y" OR A$ = "Y" THEN GOTO 930 ELSE IF A$ <>"" THEN CLS:END
927 GOTO 925
930 IF SCAN$="U" OR SCAN$="u" THEN 950
940 IF SCAN$="D" OR SCAN$="d" THEN 960 ELSE 920
950 DS=INT((TH-BH)*604.99):GOTO 990     'Calc duration of the UP scan
960 DS=INT((TH-BH)*603.8)               'Calc duration of the DOWN scan
964 PRINT:PRINT:PRINT:PRINT:PRINT:PRINT" - Do you wish to continue (y/n)? - ";:C
OLOR 7,0
970 'Translate duration in a number of conversions for mode 5
980 'Number of conversions = duration x sample rate
990 NC = (DS * F * CHAN%)
1000 '-- Step 4: Dimension data array for A/D data and check sufficient memory -
1010 'Check there is enough memory to hold this array
1020 IF (FRE(0) - 2000 - NC*2) < 0 THEN PRINT "Warning! There is inadequate memo
ry within BASIC to hold this data":PRINT"Re-run program":END
1030 DIM A%(NC)    'o.k. dimension an array
1040 '*********************************************************************
1050 '--- Step 5: Set DAS-8PGA gain amplifier -----------------------------
-
1060 MD%=19
1070 D%(0)=11     'Set range to 0 to 1 Volt
1080 CALL DAS8(MD%,D%(0),FLAG%)
```

```
1090 '
1100 '--- Step 6: Set mode 21 going and acquire data ------------------------
1110 '
1120 '    Mode 21, do conversions direct to array with trig. channel
1130 '    Note: Counter 2 output (pin 6) should be jumpered to
1140 '    interrupt input (pin 24)
1150 CLS:COLOR 0,7
1160 PRINT:PRINT" Put red switch on to start A/D conversions ...";:COLOR 7,0
1170 MD% = 21: D%(0) = 0          ' FIRST CALL......LOAD/SET interrupt
1180 D%(1) = VARPTR(A%(0))        ' Segment of storage array
1190 D%(2) = NC                   ' Size in words
1200 'Remember this isn't required when using DAS8DI.SYS simply leave as 0 ...
1210 D%(3) = 3                    ' Interrupt level 2-7 (not required on PS/2)
1220 CALL DAS8 (MD%, D%(0), FLAG%)
1230 MD% = 21: D%(0) = 1          ' SECOND CALL.... START interrupt
1240 D%(1) = 0                    ' software trigger or 0 no trig.
1250 CALL DAS8 (MD%, D%(0), FLAG%)
1260 MD% = 21: D%(0) = 2          ' THIRD CALL......CHECK interrupt
1270 D%(1) = 0                    ' 0 - Don't terminate interrupt
1280 D%(2) = 0                    ' Number of formats on this pass
1290 CALL DAS8 (MD%, D%(0), FLAG%)
1300 IF D%(3)<>NC GOTO 1260       'wait until done ....
1310 IF FLAG% <> 0 THEN PRINT:PRINT "Error in setting mode 21 Error code : ";Fl
G%:END
1320 '--- STEP 7:CHOOSE TYPE OF FILE REQUIRED ------------------------------
1330 '
1340 CLS:PRINT:PRINT "Choose from the following:-"
1350 PRINT:PRINT"   <1> - Generate a Lotus 1-2-3 compatible import file"
1360 PRINT:PRINT"   <2> - Generate a data file and plot using the DAS-8 graphics
package"
1370 PRINT"          (option not yet available).
1380 PRINT:PRINT"   <3> - Display data on screen"
1390 PRINT:PRINT"   <4> - Complete this run"
1400 PRINT:PRINT"Enter selection number (1-4): ";
1410 A$=INKEY$:IF A$="" GOTO 1410
1420 PRINT A$
1430 IF VAL(A$)=1 THEN GOTO 1510
1440 IF VAL(A$)=2 THEN GOTO 1490
1450 IF VAL(A$)=3 THEN GOTO 1630
1460 IF VAL(A$) = 4 AND B = 0 THEN PRINT:PRINT:PRINT " YOU HAVE NOT SAVED THE D
TA.  DO YOU WISH TO DO SO?  Y/N  " ELSE IF VAL(A$) = 4 AND B = 1 THEN CLS:END
1464 IF VAL(A$) = 4 AND B = 0 THEN A$ = INKEY$:IF A$ = "N" OR A$ = "n" THEN CLS
END ELSE IF A$ <>"" THEN GOTO 1330
1465 GOTO 1464
1470 PRINT"[";A$;"] IS NOT A VALID ENTRY. PLEASE RE-ENTER":GOTO 1400
1480 '
1490 '--- Generate DAS-8 graphics package data file and plot ----------------
1500 ' option not yet available
1510 '--- Generate a Lotus 1-2-3 .PRN import file -------------------------
1520 CLS
1530 LOCATE 1,1:INPUT "LOTUS .PRN FILE NAME [DRIVE]:NAME (automatic .PRN ext.)
";F$
1535 IF F$="" GOTO 1530
1540 F$=F$+".PRN"
1550 OPEN F$ FOR OUTPUT AS #1
1560 'store every 4th data set
1570 FOR I=0 TO NC-1 STEP CHAN%
1580 PRINT #1,(I/F)/CHAN%,((2.0373788#*(A%(I)/4095))-.002645),(A%(I+1)*1/4095)
1590 NEXT I
1600 CLOSE#1
1605 B=1
1610 GOTO 1740
1620 '
```

```
1630 '--- Display data on screen and return to menu ----------------------
1640 CLS
1650 LOCATE 25,1:PRINT "Press any key to STOP/START display, <ESC> key to retu:
 to data storage menu";:LOCATE 1,1
1660 PRINT"Time          Rig Height          Count rate"
1665 PRINT"(sec)            (m)               (Volts) "
1670 FOR I=0 TO (NC-1) STEP CHAN%
1680 PRINT USING "###.##"; (I/F)/CHAN%,:PRINT USING "######.###";((2.0373788#*(
%(I)/4095))-.002645),:PRINT USING "###########.###";(A%(I+1)*1/4095)
1690 A$=INKEY$
1700 IF A$=CHR$(27) THEN I=NC+3
1710 IF A$<>"" THEN GOTO 1770
1720 NEXT I
1730 IF I=NC+3 GOTO 1330
1740 COLOR 0,7:PRINT "Press any key to return to data storage menu";:COLOR 7,0
1750 IF INKEY$="" GOTO 1750
1760 GOTO 1330
1770 FOR K=1 TO 50 :NEXT K            'delay
1780 IF INKEY$="" GOTO 1780
1790 GOTO 1720
1800 END
```

```
10 REM        M E N U
20 REM
30 MODE 1
40 COLOUR 1
45 PRINT'"****************************************"
50 PRINT'"******* C O L U M N   S O F T ********"
60 PRINT'"****************************************"
70 PROCfnkey
80 COLOUR 2
90 PRINT''"          MAIN MENU "
100 PRINT'"(0) VELOCITY LOG...............fnkey<0>"
110 PRINT'"(1) REFLECTION PROFILE.........fnkey<1>"
112 PRINT'"(2) REFLECTION PROFILE PLOT....fnkey<2>"
114 PRINT'"(3) P-WAVE VELOCITY LOG PLOT...fnkey<3>"
115 PRINT'"(4) S-WAVE VELOCITY LOG PLOT...fnkey<4>"
116 PRINT'"(5) CONVERT LOGGING DATA TO"
117 PRINT "    VAX FORMAT.................fnkey<5>"
118 PRINT'"(6) CONVERT PROFILE DATA TO"
119 PRINT "    VAX FORMAT.................fnkey<6>"
120 PRINT'"(9) END......................fnkey<9>"
130 PRINT''" Enter option"
135 X=GET
140 COLOUR3
150 END
200 DEF PROCfnkey
210 *KEY0! CHAIN "LOGGER"|M
220 *KEY1! CHAIN "STACKER"|M
222 *KEY2! CHAIN "PRFLPLT"|M
224 *KEY3! CHAIN "PLOGPLT"|M
225 *KEY4! CHAIN "SLOGPLT"|M
226 *KEY5! CHAIN "CONVERT"|M
227 *KEY6! CHAIN "PROVERT"|M
230 *KEY9! END|M
240 ENDPROC
```

```
  10 REM       P L O G
  20 REM
  30 REM *** COLUMN VELOCITY LOGGING PROGRAMME ***
  40 REM Column P-wave velocity logging programmme
  50 REM For use with the HP54200A-BBC Master-Aries B488 Interface
  60 REM  I.McDermott 22.4.90
  70
  80 CLEAR:MODE 7
  90
 100 REM     E n a b l e   S c o p e
 110 PROCIEINIT(0,TRUE)
 120 scope%=7
 130 PROCIELA(scope%)
 140 PROCIETA(scope%)
 150
 160 PROCmemlcn
 170 PROCreaddata
 180 PROCfnkeys
 190 PROCscreen
 200
 210 END
 220
 230 REM ------------------------------------------------
 240 REM             S C R E E N
 250 DEF PROCscreen
 260 *DRIVE O
 270 CLS:PRINT'''"USE THE FUNCTION KEYS FOR ONE OF THE FOLLOWING"
 280 PRINT''"(1) PLOT DATA............fn key<1>"
 290 PRINT' "(2) STORE DATA ON DISC...fn key<2>"
 300 PRINT' "(3) ACQUIRE MORE DATA....fn key<3>"
 310 PRINT' "(9) RETURN TO MAIN MENU..fn key<9>"
 320 X=GET
 330 ENDPROC
 340 REM------------------------------------------
 350 REM       M E M O R Y   L O C A T I O N S
 360 REM
 370 DEF PROCmemlcn
 380 REM Set up a main memory Z%, and a scratch memory scatch%
 390 DIM Z%16000
 400 REM Set up variable locations initial values
 410 D%=Z%:E%=Z%+1000
 420 ENDPROC
 430 REM------------------------------------
 440 REM       R E A D   D A T A
 450 REM
 460 DEF PROCreaddata
 470 REM loops collecting data from each port
 480 port%=1
 490 REPEAT
 500 CLS:PRINT'''''''"GET PORT ";port%;" READY FOR DATA COLLECTION"
 510 PRINT'"PRESS ANY KEY WHEN READY":X=GET
 520 PROCIEWRIT(scope%,0)
 530 PROCIEPUTS("CHAN1,STORE NORM")
 540 PROCrange
 550 PROCoffset
```

```
555 IF P=1 THEN 540:REM safety net to return to previous menu
560 PROCwaveform
570 REM
580 REM Transfer data from scope to BBC
590 REM
600 PROCdata
610 REM
620 REM update memory locations for next port
630 D%=E%+1:E%=D%+1000
640 port%=port%+1
650 REM ************** USER DEFINED **************
660 UNTIL port%=16
670 REM ***********************************************
680 ENDPROC
690 REM----------------------------------
700 REM      W A V E F O R M
710 REM
720 DEF PROCwaveform
730 PROCIEWRIT(scope%,0)
740 PROCIEPUTS("CHAN1,STORE AVE,64")
750 PROCIEPUTS("WAVEFORM,SOURCE CHAN 1, FORMAT BYTE,DATA?")
760 PROCIEREAD (scope%,0)
770 ENDPROC
780 REM----------------------------------
790 REM          D A T A
800 REM
810 DEF PROCdata
820 ct%=0:REM Set up counter
840 CLS:PRINT ''"ACQUIRING DATA - PORT";port%
850 FOR I%=D% TO E%
870 REM counts the no. of data points transfered from scope
880 ct%=ct%+1
900 REM get new value from scope
910 byte%=FNIEGETB
930 IF ct%<=4 THEN 880
935 IF ct%=50 THEN 936 ELSE 940
936 REM alarm to sound end of data
937 SOUND 1,-11,100,2:SOUND 1,-11,53,2
938 PRINT''"  CHANGE PORTS"
940 ?I%=byte% :REM  put byte% into mem
950 NEXT I%
964 REM ready tone
965 SOUND 1,-11,130,4
966
970 ENDPROC
980 REM----------------------------------
990 REM      F U N C T I O N   K E Y S
1000 REM
1010 DEF PROCfnkeys
1020 *KEY1¦ CHAIN "PLOGPLT"¦M
1030 *KEY2¦ PROCstoredata¦M
1040 *KEY3¦ GOTO 70¦M
1050 *KEY9¦ CHAIN "MENU"¦M
1060 ENDPROC
1070 REM----------------------------------
1080 REM  S T O R E   D A T A   O N   D I S C
1090 REM
1100 DEF PROCstoredata
1110 E%=Z%+15015
```

```
1120 CLS:PRINT'''"What is the name of the File"
1130 PRINT' "  (Seven characters only)";:INPUT Name$
1140 CLS:PRINT'''"STORING FILE ";Name$
1150 *DRIVE 1 80
1160 CLOSE£0
1170 C=OPENOUT Name$
1180 ct%=1
1190 FOR I%=Z% TO E%
1200 BPUT£C,?I%
1210 ct%=ct%+1
1220 NEXT I%
1230 CLOSE£C
1240 PROCscreen
1250 ENDPROC
1260
1270 REM--------------------------------------
1280 REM        R A N G E
1290 DEF PROCrange
1295 P=0
1300 REM introducing keys to be used
1310 CLS:PRINT '''"    CHANGE VOLTAGE RANGE - PORT ";port%
1320 PRINT''" UP = increase range"
1330 PRINT' "DOWN= decrease range"
1340 PRINT' " RTN = accept range"
1350 PRINT''"ENTER CHOICE........."
1360
1370 REM loop to change voltage range
1380 REM disable cursor edit keys
1390 *FX4,1
1400 STP=0: REM initial step value
1410 range=.2: REM initial range value
1420 REPEAT
1430 PROCIEWRIT(scope%,0)
1440 PROCIEPUTS("CHANNEL 1,RANGE"+STR$(range))
1450 X=GET
1460 IF INKEY(-58) THEN STP=100E-3:REM increase range by 100mV
1470 IF INKEY(-42) THEN STP=-100E-3:REM decrease range by 100mV
1480 range=range+STP:REM calculate range value
1490 IF range<0 THEN range=40E-3
1500 REM test to see if RTN is pressed
1510 UNTIL INKEY(-74)
1520 *FX4,0
1530 ENDPROC
1540 REM --------------------------------------
1550 REM
1560 REM      O F F S E T
1570 REM
1580 DEF PROCoffset
1590 REM introducing keys to be used
1600  CLS:PRINT '''"*********************************"
1610 PRINT '''"    CHANGE OFFSET VOLTAGE - PORT ";port%
1620     PRINT '''"*********************************"
1630 PRINT''" UP = increase offset"
1640 PRINT' "DOWN= decrease offset"
1650 PRINT' "RTN = accept offset"
1655  PRINT' " P = return to previous menu"
1660 PRINT''"ENTER CHOICE........."
1670 REM loop to change offset voltage
1680 REM disable cursor edit keys
```

```
1690 *FX4,1
1700 REPEAT
1710 STP=0: REM initial step value
1720 X=GET
1730 IF INKEY(-58) THEN STP=0.01:REM increase offset by 0.01V
1740 IF INKEY(-42) THEN STP=-0.01:REM decrease range by 0.01V
1745 IF INKEY(-56) THEN P=1:GOTO 1790
1750 offset=offset+STP:REM calculate offset value
1760 PROCIEWRIT(scope%,0)
1770 PROCIEPUTS("CHANNEL 1,OFFSET"+STR$(offset))
1780 REM test to see if RTN is pressed
1790 UNTIL INKEY(-74) OR INKEY(-56)
1800 *FX4,0
1810 ENDPROC
1820 REM ------------------------------------------------
1830REM BBILIB library version 1.04 (C) 1985 ARIES COMPUTERS
1840END
1850DEFPROCIEINIT(A%,S%):DIMIEBUF%256:IECAF%=FALSE:IEEOIF%=FALSE:B%=&FC20:IEISR
0%=B%:IEISR1%=B%+1:IEASR%=B%+2:IEBSR%=B%+3:IECPTR%=B%+6:IEDIR%=B%+7:IEIMR0%=B%:I
EIMR1%=B%+1:IESCR%=B%+2:IEACR%=B%+3:IEAR%=B%+4:IESPR%=B%+5:IEPPR%=B%+6:IEDOR%=B%
+7:PROCIEACM1(0):PROCIEACM1(19)
1860?IEIMR0%=0:?IEIMR1%=0:IELADD%=A%:?IEAR%=IELADD%:IESCF%=S%:IFIESCF%THEN?IESC
R%=1ELSE?IESCR%=0
1870PROCIEACM1(3):IERFDH%=0:IEEOIOF%=TRUE:DIMIEASM%176:FORI%=0TO2STEP2:P%=IEASM
%:[OPT I%:.IEGETA:LDA&74:BEQ IEG4:INC&75:.IEG4:JSR IEGBO:LD/£0:STA(&70),Y:TAY:DE
C&74:BNE IEG3:DEC&75:BEQ IEGEND:.IEG3:TXA:AND£&08:BNE IEG5:LDA&79:BNE IEG2:CPY&7
8:BEQ IEG5:.IEG2:INC&70:BNE IEG4
1880INC&71:BNE IEG4:.IEG5:DEC&75:.IEGEND:RTS:.IEGBO:LDA&7A:STA IEACR%:LDA£2:STA
&7A:.IEGB1:LDA&FF:ROL A:BCC IEGB2:RTS:.IEGB2:LDA IEISR0%:STA&7B:TAX:AND£&20:BEQ
IEGB1:LDA IEDIR%:RTS:.IEPUTA:LDA&74:BEQ IEP1:INC&75:.IEP1:DEC&74:BNE IEP4:DEC&75
:BEQ IEP2:.IEP4
1890JSR IEPB2:INC&70:BNE IEP1:INC&71:BNE IEP1:.IEP2:LDA&78:BEQ IEPB2:.IEPB1:LDA
£8:STA IEACR%:.IEPB2:LDY£0:LDA(&70),Y:.IEPB0:PHA:.IEPB3:LDA&FF:ROL A:BCC IEPB4:P
LA:RTS:.IEPB4:LDA IEISR0%:AND£&10:BEQ IEPB3:PLA:STA IEDOR%:RTS:.IESPA:LDA£12:STA
IEACR%:LDA£24
1900JSR IEPB0:LDA&70:ORA£&4:JSR IEPB0:LDA£128+9:STA IEACR%:LDA£11:STA IEACR%:JS
R IEGBO:STA&71:LDA£12:STA IEACR%:LDA£25:JMP IEPB0:]:NEXTI%:PROCIEACMO(0):IFNOTIE
SCF%THENENDPROC
1910PROCIEACM1(15):PROCIEACM1(16):PROCIEACMO(15):PROCIEGTS:PROCIETC:ENDPROC
1920DEFPROCIESPOL(N%,D%,R%):D%=D%-1:R%=R%-1:FORI%=1TON%:?&70=D%?I%:CALLIESPA:R%
?I%=?&71:NEXTI%:PROCIECLR:ENDPROC
1930DEFPROCIEPPC(L%,S%):PROCIEPUTB(5):IFL%=0THENL%=17
1940PROCIEPUTB(95+L%+(S%*8)):PROCIECLR:ENDPROC
1950DEFFNIEPPOL:PROCIECLR:PROCIEACM1(14):IETEMP%=?IECPTR%:PROCIEACMO(14):=IETEM
P%
1960DEFPROCIEPPU:PROCIECLR:PROCIEPUTB(21):ENDPROC
1970DEFPROCIEWRIT(D%,S%):PROCIETC:PROCIETALK(31,-1):PROCIELIST(D%,S%):PROCIEGTS
:ENDPROC
1980DEFPROCIEREAD(D%,S%):PROCIETC:PROCIETALK(D%,S%):PROCIELIST(31,-1):PROCIEGTS
:ENDPROC
1990DEFPROCIECLR:PROCIETC:PROCIEUNT:PROCIEUNL:ENDPROC
2000DEFPROCIETALK(D%,S%):PROCIEUNT:IFD%=31THENPROCIEACM1(10)ELSEPROCIETA(D%)
2010IFS%<>-1THENPROCIESA(S%)
2020ENDPROC
2030DEFPROCIELIST(D%,S%):PROCIEUNL:IFD%=31THENPROCIEACM1(9)ELSEPROCIELA(D%)
2040IFS%<>-1THENPROCIESA(S%)
2050ENDPROC
```

```
10 REM        S L O G
20 REM
30 REM *** COLUMN VELOCITY LOGGING PROGRAMME ***
40 REM Column S-wave velocity logging programmme
50 REM For use with the HP54200A-BBC Master-Aries E488 Interface
60 REM  I.McDermott 22.4.90
70
80 CLEAR:MODE 7
90
100 REM      E n a b l e   S c o p e
110 PROCIEINIT(0,TRUE)
120 scope%=7
130 PROCIELA(scope%)
140 PROCIETA(scope%)
150 PROCmemlcn
160
170 REM ******* USER DEFINED VARIABLES ********
180 REM -------   S-WAVE PORT DATA    ---------
190 REM quantity of ports being used
200        p%=8
210 REM reference numbers of ports being used
220      DATA 4,5,6,7,12,13,14,15
230 REM ***********************************
232
234 REM read port data
236 FOR I%=1 TO p%:READ uport%(I%):NEXT I%
240
250
270 PROCreaddata
280 PROCfnkeys
290 PROCscreen
300
310 END
320
330 REM ------------------------------------------
340 REM             S C R E E N
350 DEF PROCscreen
360 *DRIVE 0
370 CLS:PRINT'''"USE THE FUNCTION KEYS FOR ONE OF THE FOLLOWING"
380 PRINT''"(1) PLOT DATA.............fn key<1>"
390 PRINT' "(2) STORE DATA ON DISC...fn key<2>"
400 PRINT' "(3) ACQUIRE MORE DATA....fn key<3>"
410 PRINT' "(9) RETURN TO MAIN MENU..fn key<9>"
420 X=GET
430 ENDPROC
440 REM------------------------------
450 REM    M E M O R Y   L O C A T I O N S
460 REM
470 DEF PROCmemlcn
480 REM Set up a main memory Z%
490 DIM Z%15015,uport%(15)
500 REM Set up variable locations initial values
510 D%=Z%:E%=Z%+1000
520 ENDPROC
```

```
530 REM-------------------------------
540 REM        R E A D    D A T A
550 REM
560 DEF PROCreaddata
570 REM loops collecting data from each port
580 port%=1
581
590 REPEAT
591
600 REM routine checks if port is being used
610 I%=1
620 IF port%=uport%(I%) THEN 630
622 IF I%=p% THEN 625
623 I%=I%+1:GOTO 620
625 PROCstuffing:GOTO 740
626
630 CLS:PRINT'''''''"GET PORT ";port%;" READY FOR DATA COLLECTION"
640 PRINT'"PRESS ANY KEY WHEN READY":X=GET
650
655 PROCIEWRIT(scope%,0)
656 PROCIEPUTS("CHAN1,STORE NORM")
657 IF port%=4 OR port%=12 THEN 658 ELSE 660:REM***** extra line *****
658 PROCIEPUTS("TIMEBASE,RANGE 50E-3,DELAY 0"):REM ****** extra line ****
660 PROCrange
665 REM position of PROCoffset
666
670 PROCwaveform
672
690 REM Transfer data from scope to BBC
710 PROCdata
720
730 REM update memory locations for next port
740 D%=E%+1:E%=D%+1000
750 port%=port%+1
755
760 REM ************** USER DEFINED **************
770 UNTIL port%=16
780 REM *******************************************
781 ENDPROC
782 REM-------------------------------
785 REM      S T U F F I N G
786
787 DEF PROCstuffing
788 FOR I%=D% TO E%
789 ?I%=0
800 NEXT I%
801 ENDPROC
809 REM-------------------------------
810 REM       W A V E F O R M
820 REM
830 DEF PROCwaveform
840 PROCIEWRIT(scope%,0)
845 PROCIEPUTS("CHAN1,STORE AVE,64")
850 PROCIEPUTS("WAVEFORM,SOURCE CHAN 1, FORMAT BYTE,DATA?")
860 PROCIEREAD (scope%,0)
870 ENDPROC
880 REM-------------------------------
890 REM            D A T A
900 REM
910 DEF PROCdata
920
```

```
1000 ct%=0 :REM initialise count
1010
1020 CLS:PRINT ''"ACQUIRING DATA - PORT";port%
1030 FOR I%=D% TO E%
1040
1050 REM counts the no. of data points transfered from scope
1060 ct%=ct%+1
1080 REM get new value from scope
1090 byte%=FNIEGETB
1110 IF ct%<=4 THEN 1060
1112 IF ct%=50 THEN 1116 ELSE 1120
1115 REM alarm to sound end of data collection
1116 SOUND 1,-11,100,2:SOUND 1,-11,53,2
1117 PRINT'''"CHANGE PORTS"
1120 ?I%=byte%
1160
1170 NEXT I%
1180 REM ready tone
1185 SOUND 1,-11,130,4
1190 PROCIEWRIT(scope%,0):REM**** extra line
1200 PROCIEPUTS("TIMEBASE,RANGE 20E-3,DELAY 5E-3"):REM **** extra line
1260 ENDPROC
1270 REM-------------------------------
1420 REM     F U N C T I O N   K E Y S
1430 REM
1440 DEF PROCfnkeys
1450 *KEY1| CHAIN "SLOGPLT"|M
1460 *KEY2| PROCstoredata|M
1470 *KEY3| GOTO 70|M
1480 *KEY9| CHAIN "MENU"|M
1490 ENDPROC
1500 REM-----------------------------
1510 REM   S T O R E   D A T A   O N   D I S C
1520 REM
1530 DEF PROCstoredata
1540 E%=Z%+15015
1550 CLS:PRINT''"What is the name of the File"
1560 PRINT' "  (Seven characters only)";:INPUT Name$
1570 CLS:PRINT'''"STORING FILE ";Name$
1580 *DRIVE 1 80
1590 CLOSE£0
1600 C=OPENOUT Name$
1610 ct%=1
1620 FOR I%=Z% TO E%
1630 BPUT£C,?I%
1640 ct%=ct%+1
1650 NEXT I%
1660 CLOSE£C
1670 PROCscreen
1680 ENDPROC
1690 REM-------------------------------------------
1700 REM     R A N G E
1710 DEF PROCrange
1720 CLS:PRINT'''"CHANGE VOLTAGE RANGE-PORT";port%
1721 PRINT''"UP = increase range"
1722 PRINT''"DOWN = decrease range"
1723 PRINT''"RETURN = accept range"
1725 PRINT''"ENTER CHOICE........."
1730 *FX4,1
```

```
1740 STP=0:range=.1
1750 REPEAT
1760 PROCIEWRIT(scope%,0)
1770 PROCIEPUTS("CHANNEL 1,RANGE"+STR$(range))
1780 X=GET
1790 IF INKEY(-58) THEN STP=100E-3
1800 IF INKEY(-42) THEN STP=-100E-3
1810 range=range+STP
1820 IF range<0 THEN range=40E-3
1830 UNTIL INKEY(-74)
1840 *FX4,0
1850 ENDPROC
1860 REM-------------------------------------------------
2040REM BBILIB library version 1.04 (C) 1985 ARIES COMPUTERS
2050END
2060DEFPROCIEINIT(A%,S%):DIMIEBUF%256:IECAF%=FALSE:IEEOIF%=FALSE:B%=&FC20:IEISR
0%=B%:IEISR1%=B%+1:IEASR%=B%+2:IEBSR%=B%+3:IECPTR%=B%+6:IEDIR%=B%+7:IEIMR0%=B%:I
EIMR1%=B%+1:IESCR%=B%+2:IEACR%=B%+3:IEAR%=B%+4:IESPR%=B%+5:IEPPR%=B%+6:IEDOR%=B%
+7:PROCIEACM1(0):PROCIEACM1(19)
2070?IEIMR0%=0:?IEIMR1%=0:IELADD%=A%:?IEAR%=IELADD%:IESCF%=S%:IFIESCF%THEN?IESC
R%=1ELSE?IESCR%=0
2080PROCIEACM1(3):IERFDH%=0:IEEOIOF%=TRUE:DIMIEASM%176:FORI%=0TO2STEP2:P%=IEASM
%:[OPT I%:.IEGETA:LDA&74:BEQ IEG4:INC&75:.IEG4:JSR IEGBO:LDY£0:STA(&70),Y:TAY:DE
C&74:BNE IEG3:DEC&75:BEQ IEGEND:.IEG3:TXA:AND£&08:BNE IEG5:LDA&79:BNE IEG2:CPY&7
8:BEQ IEG5:.IEG2:INC&70:BNE IEG4
2090INC&71:BNE IEG4:.IEG5:DEC&75:.IEGEND:RTS:.IEGBO:LDA&7A:STA IEACR%:LDA£2:STA
&7A:.IEGB1:LDA&FF:ROL A:BCC IEGB2:RTS:.IEGB2:LDA IEISR0%:STA&7B:TAX:AND£&20:BEQ
IEGB1:LDA IEDIR%:RTS:.IEPUTA:LDA&74:BEQ IEP1:INC&75:.IEP1:DEC&74:BNE IEP4:DEC&75
:BEQ IEP2:.IEP4
2100JSR IEPB2:INC&70:BNE IEP1:INC&71:BNE IEP1:.IEP2:LDA&78:BEQ IEPB2:.IEPB1:LDA
£8:STA IEACR%:.IEPB2:LDY£0:LDA(&70),Y:.IEPBO:PHA:.IEPB3:LDA&FF:ROL A:BCC IEPB4:P
LA:RTS:.IEPB4:LDA IEISR0%:AND£&10:BEQ IEPB3:PLA:STA IEDOR%:RTS:.IESPA:LDA£12:STA
 IEACR%:LDA£24
2110JSR IEPBO:LDA&70:ORA£64:JSR IEPBO:LDA£128+9:STA IEACR%:LDA£11:STA IEACR%:JS
R IEGBO:STA&71:LDA£12:STA IEACR%:LDA£25:JMP IEPBO:]:NEXTI%:PROCIEACMO(0):IFNOTIE
SCF%THENENDPROC
2120PROCIEACM1(15):PROCIEACM1(16):PROCIEACMO(15):PROCIEGTS:PROCIETC:ENDPROC
2130DEFPROCIESPOL(N%,D%,R%):D%=D%-1:R%=R%-1:FORI%=1TON%:?&70=D%?I%:CALLIESPA:R%
?I%=?&71:NEXTI%:PROCIECLR:ENDPROC
2140DEFPROCIEPPC(L%,S%):PROCIEPUTB(5):IFL%=0THENL%=17
2150PROCIEPUTB(95+L%+(S%*8)):PROCIECLR:ENDPROC
2160DEFFNIEPPOL:PROCIECLR:PROCIEACM1(14):IETEMP%=?IECPTR%:PROCIEACMO(14):=IETEM
P%
2170DEFPROCIEPPU:PROCIECLR:PROCIEPUTB(21):ENDPROC
2180DEFPROCIEWRIT(D%,S%):PROCIETC:PROCIETALK(31,-1):PROCIELIST(D%,S%):PROCIEGTS
:ENDPROC
2190DEFPROCIEREAD(D%,S%):PROCIETC:PROCIETALK(D%,S%):PROCIELIST(31,-1):PROCIEGTS
:ENDPROC
2200DEFPROCIECLR:PROCIETC:PROCIEUNT:PROCIEUNL:ENDPROC
2210DEFPROCIETALK(D%,S%):PROCIEUNT:IFD%=31THENPROCIEACM1(10)ELSEPROCIETA(D%)
2220IFS%<>-1THENPROCIESA(S%)
2230ENDPROC
2240DEFPROCIELIST(D%,S%):PROCIEUNL:IFD%=31THENPROCIEACM1(9)ELSEPROCIELA(D%)
2250IFS%<>-1THENPROCIESA(S%)
2260ENDPROC
2270DEFPROCIEUNT:PROCIEPUTB(95):PROCIEACMO(10):ENDPROC
2280DEFPROCIEUNL:PROCIEPUTB(63):PROCIEACMO(9):ENDPROC
2290DEFPROCIETA(D%):PROCIEPUTB(D%+64):ENDPROC
```

```
2300DEFPROCIELA(D%):PROCIEPUTB(D%+32):ENDPROC
2310DEFPROCIESA(S%):PROCIEPUTB(S%+96):ENDPROC
2320DEFPROCIEPUTS(S$):$IEBUF%=S$:PROCIEPUTA(IEBUF%,LEN(S$)):ENDPROC
2330DEFFNIEGETS(T%,L%):PROCIEGETA(IEBUF%,T%,L%):IEBUF%?IELEN%=13:=$IEBUF%
2340DEFPROCIEPUTA(A%,L%):!&70=A%:!&74=L%:?&78=IEEOIOF%:CALLIEPUTA:ENDPROC
2350DEFPROCIEGETA(A%,T%,L%):!&70=A%:!&74=L%:!&78=T%:?&7A=IERFDH%:CALLIEGETA:IEL
EN%=L%-!&74:IERFDH%=?&7A:IEEOIF%=?&7BANDS:ENDPROC
2360DEFPROCIEPUTB(B%):IEEOIOF%=FALSE:?&79=B%:PROCIEPUTA(&79,1):IEEOIOF%=TRUE:EN
DPROC
2370DEFPROCIEENDB(B%):?&79=B%:PROCIEPUTA(&79,1):ENDPROC
2380DEFFNIEGETB:PROCIEGETA(&7C,-1,1):=?&7C
2390DEFPROCIETC:IFIECAF%THENENDPROC
2400IFFNIETADSTHENREPEAT:UNTIL?IEISRO%AND16
2410PROCIEACMO(12):IECAF%=TRUE:ENDPROC
2420DEFPROCIEGTS:PROCIEACMO(11):IECAF%=FALSE:ENDPROC
2430DEFFNIESRQS=?IEBSR%AND4
2440DEFFNIETADS=?IEASR%AND2
2450DEFFNIELADS=?IEASR%AND4
2460DEFPROCIEACMO(C%):?IEACR%=C%:ENDPROC
2470DEFPROCIEACM1(C%):?IEACR%=C%+128:ENDPROC
```

```
 10 REM              P L O G P L T
 20 REM  Plotting routine for use with the BBC model B.
 30 REM Requires PRINTMASTER ROM  for hardcopy
 40 MODE 0
 50 DIM D%1001
 60 *FX6,0
 70 PROCfilename
 80 PROCopenfile
 90*FX4,1
100 PROCselectport
110 PROCreadfile
120 PROCAxis
130 PROCplotdata
140 PROCCursor
150*FX4,0
160 PROCbranch
170 CLS:END
180 REM---------------------------------------
190 REM         A X I S
200 DEF PROCAxis
210 REM set up text/graphics windows
220 VDU 24,0;1279;0;800;
230 VDU 28,0,1,60,0
240 @%=&20103
250 REM ************** USER DEFINED VARIABLES ********
260 YMIN=-10:XMIN=65:div=1:REM div=1 10us
270 REM ********************************************************
280 REM draw axis
290 CLS:MOVE 100,100:DRAW 100,740:MOVE 100,100:DRAW 1100,100
300 REM draw x-axis interval
310 FOR I= 0 TO 10
320 X=100+100*I:MOVE X,100:DRAW X,90
330 VDU5
340 MOVE X-20,70:PRINT;XMIN+(I/div)
350 NEXTI
360 REM draw y-axis interval
370 FOR I=0 TO 10
380 Y=100+64*I::MOVE 100,Y:DRAW 90,Y
390 MOVE 20,Y+10:PRINT;(YMIN+(I*2))/10
400 NEXT I
410 PROCTitle
420 VDU4
430 ENDPROC
440 REM-------------------------------------
450 REM         T I T L E
460 DEF PROCTitle
470 MOVE 400,30:PRINT;" Travel Time (us) "
480 MOVE 0,830:PRINT;"Normalized":MOVE 0,780:PRINT;"Amplitude"
490 ENDPROC
500 REM------------------------------------------
510 REM         C U R S O R
520 DEF PROCCursor
530 @%=&20307
540 Y1=110:Y2=730:CPOS=100
550 REPEAT
560 STP=0
570 X=GET
580 REM cursor left move one left
```

```
590 IF INKEY(-26) THEN STP=-1
600 REM cursor right move one right
610 IF INKEY(-122) THEN STP=1
620 REM if press SHIFT=CURSOR then fast move
630 IF INKEY(-1) THEN STP=STP*8
640 PROCdrawcursor(CPOS)
650 REM calculate cursor position
660 CPOS=CPOS+STP
670 REM if cursor at extreme right loop back to left
680 IF CPOS>1100 THEN CPOS=100
690  IF CPOS<100 THEN CPOS=1100
700 PROCdrawcursor(CPOS)
710 UNTIL INKEY(-99)
720 ENDPROC
730 REM------------------------------------
740 REM          D R A W    C U R S O R
750 DEF PROCdrawcursor(X)
760 GCOL 3,1
770 IF X=100 THEN 800
780 MOVE X,Y1
790 DRAW X,Y2
800 PRINT "Time = ";((X-100)/(div*100))+XMIN;" us"
810 GCOL 0,3
820 ENDPROC
830 REM------------------------------------
840 REM       F I L E     N A M E
850 DEF PROCfilename
860 CLS:PRINT'''"Enter File Name or Return to Cancel";:INPUT Name$
870 REM Return True If file open, False if cancelled
880 IF Name$="" THEN 860
890 ENDPROC
900 REM------------------------------------
910 REM         O P E N    F I L E
920 DEF PROCopenfile
930 CLOSE£0:REM First close any open files
940 *DRIVE 1 80
950 C=OPENUP(Name$)
960  REM decide if file exists if not print error message
970 IF C=0 THEN PRINT CHR$(7);"FILE DOES NOT EXIST":PROCfilename
980 ENDPROC
990 REM------------------------------------
1000 REM        R E A D    F I L E
1010 DEF PROCreadfile
1020 PRINT "LOADING FILE ";Name$
1030 PTR£C=point%:REM pointer from select port
1040 E%=D%+1000
1050 FOR I%=D% TO E%
1060 ?I%=BGET£C
1070 NEXT I%
1080 CLOSE£C:CLS
1090 *DRIVE 0 80
1100 ENDPROC
1110 REM------------------------------------
1120 REM       P L O T    D A T A
1130 DEF PROCplotdata
1140 @%=10:VDU5:MOVE 400,800:PRINT;"FILE ";Name$;"....PORT NO.";port%:VDU4
1150 ct%=100
```

```
1160 FOR I%=D% TO E%-1
1170 byte%=?I%
1180 byte%=((byte%-64)*5)+420
1190 IF ct%=100 MOVE ct%,byte%
1200 DRAW ct%,byte%
1210 ct%=ct%+1
1220 NEXT I%
1230 ENDPROC
1240 REM-----------------------------------------
1250 REM        S E L E C T   D A T A
1260 DEF PROCselectport
1270 @%=10
1280 REM Select which port is required for plotting
1290 point%=1:REM Data start pointer
1300 CLS:PRINT''"S E L E C T    P O R T    N U M B E R"
1310 PRINT''"Input ort number (1-15)":INPUT port%
1320 IF port%>15 OR port%<1 THEN 1300
1330 point%=(1001*(port%-1))+1:REM calculate data pointer
1340 CLS
1350 ENDPROC
1360 REM-----------------------------------------
1370 REM          B R A N C H
1380 DEF PROCbranch
1390 VDU26:REM reset text/graphics windows
1400 PROCfnkeys:REM define function keys
1410 CLS:PRINT''"USE THE FUNCTION KEYS TO SELECT ONE OF THE FOLLOWING"
1420
1430 PRINT''"(1) HARDCOPY.........................fnkey<1>"
1440 PRINT' "(3) SELECT PORT......................fnkey<3>"
1450 PRINT' "(5) NEWFILE..........................fnkey<5>"
1460 PRINT' "(7) RETURN TO MAIN MENU..............fnkey<7>"
1470 PRINT' "(9) END..............................fnkey<9>"
1480 PRINT'''"ENTER OPTION....."
1490 X=GET
1500 ENDPROC
1510 REM-----------------------------------------
1520 REM      F U N C T I O N    K E Y S
1530 DEF PROCfnkeys
1540 *KEY1; PROChardcopy ;M
1550 *KEY3; GOTO 80 ;M
1560 *KEY5; GOTO 140 ;M
1570 *KEY7; CHAIN "MENU";M
1580 *KEY9; END;M
1590 ENDPROC
1600 REM-----------------------------------------
1610 REM        H A R D    C O P Y
1620 DEF PROChardcopy
1630 REM using Printmaster ROM
1640 CLS:CLG
1650 PROCAxis
1660 PROCplotdata
1670 VDU2: REM enable printer
1680 *GDUMP 0 0 1 2 10
1690 VDU3: REM disable printer
1700 PROCbranch
```

```
  10 REM           S L O G P L T
  20 REM  Plotting routine for use with the BBC model B.
  30 REM Requires PRINTMASTER ROM  for hardcopy
  40 MODE 0
  50 DIM D%1001
  60 *FX6,0
  70 PROCfilename
  80 PROCopenfile
  90*FX4,1
 100 PROCselectport
 110 PROCreadfile
 120 PROCAxis
 130 PROCplotdata
 140 PROCCursor
 150*FX4,0
 160 PROCbranch
 170 CLS:END
 180 REM--------------------------------
 190 REM         A X I S
 200 DEF PROCAxis
 210 REM set up text/graphics windows
 220 VDU 24,0;1279;0;800;
 230 VDU 28,0,1,60,0
 240 @%=&20103
 250 REM ************* USER DEFINED VARIABLES ********
 260 YMIN=-10:XMIN=0:div=0.2:REM div=1 10ms record, div=2 5ms record
 270 REM *****************************************************
 280 REM draw axis
 290 CLS:MOVE 100,100:DRAW 100,740:MOVE 100,100:DRAW 1100,100
 300 REM draw x-axis interval
 310 FOR I= 0 TO 10
 320 X=100+100*I:MOVE X,100:DRAW X,90
 330 VDU5
 340 MOVE X-20,70:PRINT;XMIN+(I/div)
 350 NEXTI
 360 REM draw y-axis interval
 370 FOR I=0 TO 10
 380 Y=100+64*I::MOVE 100,Y:DRAW 90,Y
 390 MOVE 20,Y+10:PRINT;(YMIN+(I*2))/10
 400 NEXT I
 410 PROCTitle
 420 VDU4
 430 ENDPROC
 440 REM-------------------------------
 450 REM       T I T L E
 460 DEF PROCTitle
 470 MOVE 400,30:PRINT;" Travel Time (ms) "
 480 MOVE 0,830:PRINT;"Normalized":MOVE 0,780:PRINT;"Amplitude"
 490 ENDPROC
 500 REM--------------------------------
 510 REM        C U R S O R
 520 DEF PROCCursor
 530 @%=&20307
 540 Y1=110:Y2=730:CPOS=100
 550 REPEAT
 560 STP=0
 570 X=GET
 580 REM cursor left move one left
```

```
590 IF INKEY(-26) THEN STP=-1
600 REM cursor right move one right
610 IF INKEY(-122) THEN STP=1
620 REM if press SHIFT=CURSOR then fast move
630 IF INKEY(-1) THEN STP=STP*3
640 PROCdrawcursor(CPOS)
650 REM calculate cursor position
660 CPOS=CPOS+STP
670 REM if cursor at extreme right loop back to left
680 IF CPOS>1100 THEN CPOS=100
690  IF CPOS<100 THEN CPOS=1100
700 PROCdrawcursor(CPOS)
710 UNTIL INKEY(-99)
720 ENDPROC
730 REM------------------------------------------
740 REM         D R A W     C U R S O R
750 DEF PROCdrawcursor(X)
760 GCOL 3,1
770 IF X=100 THEN 800
780 MOVE X,Y1
790 DRAW X,Y2
800 PRINT "Time = ";((X-100)/(div*100))+XMIN;" ms"
810 GCOL 0,3
820 ENDPROC
830 REM----------------------------------------
840 REM       F I L E     N A M E
850 DEF PROCfilename
860 CLS:PRINT'''"Enter File Name or Return to Cancel";:INPUT Name$
870 REM Return True If file open, False if cancelled
880 IF Name$="" THEN 860
890 ENDPROC
900 REM-------------------------------------------
910 REM          O P E N     F I L E
920 DEF PROCopenfile
930 CLOSE£0:REM First close any open files
940 *DRIVE 1 80
950 C=OPENUP(Name$)
960  REM decide if file exists if not print error message
970 IF C=0 THEN PRINT CHR$(7);"FILE DOES NOT EXIST":PROCfilename
980 ENDPROC
990 REM---------------------------------------------
1000 REM          R E A D     F I L E
1010 DEF PROCreadfile
1020 PRINT "LOADING FILE ";Name$
1030 PTR£C=point%:REM pointer from select port
1040 E%=D%+1000
1050 FOR I%=D% TO E%
1060  ?I%=BGET£C
1070 NEXT I%
1080 CLOSE£C:CLS
1090 *DRIVE 0 80
1100 ENDPROC
1110 REM-----------------------------------------
1120 REM        P L O T     D A T A
1130 DEF PROCplotdata
1140 @%=10:VDU5:MOVE 400,800:PRINT;"FILE ";Name$;"....PORT NO.";port%:VDU4
1150 ct%=100
```

```
1160 FOR I%=D% TO E%-1
1170 byte%=?I%
1180 byte%=((byte%-64)*5)+420
1190 IF ct%=100 MOVE ct%,byte%
1200 DRAW ct%,byte%
1210 ct%=ct%+1
1220 NEXT I%
1230 ENDPROC
1240 REM----------------------------------------
1250 REM       S E L E C T   D A T A
1260 DEF PROCselectport
1270 @%=10
1280 REM Select which port is required for plotting
1290 point%=1:REM Data start pointer
1300 CLS:PRINT''"S E L E C T   P O R T   N U M B E R"
1310 PRINT''"Input ort number (1-15)":INPUT port%
1320 IF port%>15 OR port%<1 THEN 1300
1330 point%=(1001*(port%-1))+1:REM calculate data pointer
1340 CLS
1350 ENDPROC
1360 REM----------------------------------------
1370 REM            B R A N C H
1380 DEF PROCbranch
1390 VDU26:REM reset text/graphics windows
1400 PROCfnkeys:REM define function keys
1410 CLS:PRINT''"USE THE FUNCTION KEYS TO SELECT ONE OF THE FOLLOWING"
1420
1430 PRINT''"(1) HARDCOPY.........................fnkey<1>"
1440 PRINT' "(3) SELECT PORT.....................fnkey<3>"
1450 PRINT' "(5) NEWFILE.........................fnkey<5>"
1460 PRINT' "(7) RETURN TO MAIN MENU.............fnkey<7>"
1470 PRINT' "(9) END.............................fnkey<9>"
1480 PRINT'''"ENTER OPTION....."
1490 X=GET
1500 ENDPROC
1510 REM----------------------------------------
1520 REM       F U N C T I O N   K E Y S
1530 DEF PROCfnkeys
1540 *KEY1! PROChardcopy !M
1550 *KEY3! GOTO 80 !M
1560 *KEY5! GOTO 140 !M
1570 *KEY7! CHAIN "MENU"!M
1580 *KEY9! END !M
1590 ENDPROC
1600 REM----------------------------------------
1610 REM          H A R D   C O P Y
1620 DEF PROChardcopy
1630 REM using Printmaster ROM
1640 CLS:CLG
1650 PROCAxis
1660 PROCplotdata
1670 VDU2: REM enable printer
1680 *GDUMP 0 0 1 2 10
1690 VDU3: REM disable printer
1700 PROCbranch
```

```
10 REM ************ STOLL FULL MODEL **********
20 REM
30 REM from Stoll,R.D. (1989). Sediment Acoustics, Springer-Verlag, New York
40 REM Input parameters are in c.g.s units
50 REM
60 CLS
70 WIDTH "lpt1:",132
80 DEFINT I,J,N
90 DIM F(100),IP(4),DEC(100)
100 FF$="##.###`  ":FFF$="#####.## ":FFFF$="##.#### ":FZ$="##.##```"
110 PI=4*ATN(1):R=SQR(2)
120 INPUT "heading";H$
130 INPUT "porosity";PHI
140 INPUT "permeability (cm**2)";PERM
150 INPUT"raadius of aver. pore (cm)";RAD
160 INPUT"shear modulus of frame (dynes/cm**2)";GR
170 INPUT "poisson's ratio of frame";FRMNU
180 INPUT "constant or variable complex modulus (C orV)";G$:REM select C
190 IF G$="C" OR G$="c" THEN INPUT "shear log decrement";GDEC
200 INPUT"edec/gdec";EGRAT
205 REM   ##########  input parameters ##################
210 READ RMOD,FMOD,RDEN,FRHO,VISCF,FAC:REM see lines 200-330
220 DATA 3.6e11,2.37e10,2.665,1.025,.01,1
225 REM   #############################################
230 RHO=RDEN*(1-PHI)+PHI*FRHO
240 LPRINT CHR$(15):LPRINT DATE$,TIME$:LPRINT
250 LPRINT" ":LPRINT" ":LPRINT TAB(10)"**********************************
PRINT TAB(10) H$:LPRINT TAB(10) "*********************************":LPRI
" "
260 LPRINT TAB(10) "specific gravity of grains ---------------";RDEN
270 LPRINT TAB(10) "specific gravity of fluid ----------------";FRHO
280 LPRINT TAB(10) "ab viscosity of fluid (dyne-sec/cm**2) ---";VISCF
290 LPRINT TAB(10) "bulk mod of grains (dynes/cm**2) ---------";RMOD
300 LPRINT TAB(10) "bulk mod of fluid (dynes/cm**2)-----------";FMOD
310 LPRINT TAB(10) "density coupling factor ------------------";FAC
320 LPRINT TAB(10) "porosity----------------------------------";PHI
330 LPRINT TAB(10) "permeability (cm**2) ---------------------";PERM
340 LPRINT TAB(10) "radius of aver. pore (cm) ----------------";RAD
350 LPRINT TAB(10) "shear mod of frame (dynes/cm**2) ---------";GR
360 LPRINT TAB(10) "poisson's ratio --------------------------";FRMNU
370 LPRINT TAB(10) "ratio edec/gdec --------------------------";EGRAT
380 LPRINT TAB(10) "total specific gravity -------------------";RHO
390 IF G$="V" OR G$="v" THEN GOSUB 1540
400 IF G$="C" OR G$="c" THEN LPRINT TAB(10) "log decrement for shear --------
---";GDEC
410 INPUT "no. frequency decades";NFRQ
420 N=0
430 FOR F=0 TO NFRQ STEP .25
440 N=N+1
450 F(N)=10^F:GOSUB 1640
460 NEXT F
470 LPRINT TAB(10) "frequency    V1  "
480 LPRINT TAB(10) "   (Hz)     m/sec "
490 FOR I=1 TO N
500 GDEC = DEC(I):GI=GDEC*GR/PI
510 EMODR=(FRMNU+1)*GR*2
520 EMODI=EGRAT*GI/GR*EMODR
530 BR=GR*EMODR/(3*GR-EMODR)/3
540 BI=(3*GR*GR*EMODI-EMODR*EMODR*GI)/(3*GR-EMODR)/(3*GR-EMODR)/3
550 BDEC=BI/BR*PI
560 M=FAC*FRHO/PHI
570 D=RMOD*(PHI*(RMOD/FMOD-1)+1)
580 DNOM=(D-BR)*(D-BR)+BI*BI
590 HR=(((RMOD-BR)*(RMOD-BR)-BI*BI)*(D-BR)+2*BI*BI*(RMOD-BR))/DNOM+BR+4*GR/3
```

```
600 HI=(((RMOD-BR)*(RMOD-BR)-BI*BI)*BI-2*BI*(RMOD-BR)*(D-BR))/DNOM+BI+4*GI/3
610 KR=((RMOD*RMOD-BR*RMOD)*(D-BR)+BI*RMOD*BI)/DNOM
620 KI=((RMOD*RMOD-BR*RMOD)*BI-BI*RMOD*(D-BR))/DNOM
630 DR=RMOD*RMOD*(D-BR)/DNOM
640 DI=RMOD*RMOD*BI/DNOM
650 Z=SQR(F(I)*2*PI*FRHO/VISCF)*RAD
660 Z=SQR(F(I)*2*PI*FRHO/VISCF)*RAD
670 IF Z>8 GOTO 920
680 BER=1:DBER=0:SIGN=-1
690 FOR J=4 TO 32 STEP 4
700 DEN=1
710 FOR JJ=2 TO J STEP 2
720 DEN=JJ*JJ*DEN
730 NEXT JJ
740 BER=SIGN*Z^J/DEN+BER
750 DBER=SIGN*Z^(J-1)/DEN*J+DBER
760 SIGN=-SIGN
770 NEXT J
780 BBEI=0:DDBEI=0
790 SIGN=1
800 FOR J=2 TO 30 STEP 4
810 DEN=1
820 FOR JJ=2 TO J STEP 2
830 DEN=JJ*JJ*DEN
840 NEXT JJ
850 BBEI=SIGN*Z^J/DEN+BBEI
860 DDBEI=SIGN*Z^(J-1)/DEN*J+DDBEI
870 SIGN=-SIGN
880 NEXT J
890 TR=(BBEI*DDBEI+BER*DBER)/(BER*BER+BBEI*BBEI)
900 TI=(BER*DDBEI-BBEI*DBER)/(BER*BER+BBEI*BBEI)
910 GOTO 1010
920 T1=1/R-3/(8*Z)-15/(64*R*Z^2)-45/(512*Z^3)+315/(8192*R*Z^4)
930 T2=1/R+1/(8*Z)+9/(64*R*Z^2)+39/(512*Z^3)+75/(8192*R*Z^4)
940 D4=1+1/(4*R*Z)+1/(64*Z^2)-33/(256*R*Z^3)-1797/(8192*Z^4)
950 TR=T1/D4
960 TI=T2/D4
970 REM
980 REM Viscous correction factors: for Geertsma and Smit model
990 REM  set FFR=1   REAL
1000 REM set FI=0    IMAGINARY
1010 FFR=(.25*Z*(TR*(1-2*TI/Z)+TI*TR*2/Z))/((1-2*TI/Z)^2+(2*TR/Z)^2)
1020 FI=(.25*Z*(TI*(1-2*TI/Z)+TR*TR*2/Z))/((1-2*TI/Z)^2+(2*TR/Z)^2)
1030 REM
1040 VMOD=BR+4*GR/3
1050 OMEG=F(I)*PI*2
1060 AR=(KR*KR-KI*KI-HR*DR+HI*DI)/(VMOD*VMOD)
1070 AI=(2*KR*KI-HI*DR-HR*DI)/(VMOD*VMOD)
1080 ER=(HR*M/RHO+DR-2*KR*FRHO/RHO+(FFR*HI+FI*HR)*VISCF/(RHO*PERM*OMEG))/VMOD
1090 EI=(HI*M/RHO+DI-2*KI*FRHO/RHO+(FI*HI-FFR*HR)*VISCF/(RHO*PERM*OMEG))/VMOD
1100 CR=FRHO*FRHO/(RHO*RHO)-M/RHO-FI*VISCF/(RHO*PERM*OMEG)
1110 CI=FFR*VISCF/(RHO*PERM*OMEG)
1120 D2=2*(AR*AR+AI*AI)
1130 RR=ER*ER-EI*EI-4*(AR*CR-AI*CI)
1140 RI=2*EI*ER-4*(AI*CR+AR*CI)
1150 RTMOD=(RR*RR+RI*RI)^.25
1160 IF ABS(RI/RR)>1 THEN ANGL=PI/2-ABS(ATN(RR/RI)) ELSE ANGL=ABS(ATN(RI/RR))
1170 IF RR<0 THEN BATA=(PI-ANGL)/2 ELSE BATA=ANGL/2
1180 IF RI<0 THEN BATA = -BATA
1190 R1=RTMOD*COS(BATA)
1200 R2=RTMOD*SIN(BATA)
1210 D1=(ER+R1)*(ER+R1)+(EI+R2)*(EI+R2)
1220 X1=-2*(CR*(ER+R1)+CI*(EI+R2))/D1
1230 X2=(AR*(-ER-R1)-AI*(EI+R2))/D2
```

```
1240 Y1=2*(CI*(-ER-R1)+CR*(EI+R2))/D1
1250 Y2=(AI*(ER+R1)-AR*(EI+R2))/D2
1260 CC=OMEG*SQR(RHO/VMOD)
1270 IF ABS(Y1/X1)>1 THEN AA=PI/2-ABS(ATN(X1/Y1)) ELSE AA=ABS(ATN(Y1/X1))
1280  IF X1<0 THEN AA=(PI-AA)/2 ELSE AA=AA/2
1290 IF Y1<0 THEN AA=-AA
1300 IF ABS(Y2/X2)>1 THEN AB=PI/2-ABS(ATN(X2/Y2)) ELSE AB=ABS(ATN(Y2/X2))
1310 IF X2<0 THEN AB=(PI-AB)/2 ELSE AB=AB/2
1320 IF Y2<0 THEN AB=-AB
1330 P1=(X1*X1+Y1*Y1)^.25
1340 P2=(X2*X2+Y2*Y2)^.25
1350 V1=OMEG/(P1*COS(AA)*CC*100)
1360 A1=P1*SIN(AA)*CC*100
1370 V2=OMEG/(P2*COS(AB)*CC*100)
1380 A2=P2*SIN(AB)*CC*100
1390 Q1=V1*A1/F(I):Q2=V2*A2/F(I)
1400 E1=GR*M*OMEG*OMEG+GR*VISCF*OMEG*FI/PERM+GI*FFR*VISCF*OMEG/PERM
1410 E2=GI*M*OMEG*OMEG+GI*VISCF*OMEG*FI/PERM-GR*FFR*VISCF*OMEG/PERM
1420 XR=(RHO*M-FRHO*FRHO)*OMEG^4+VISCF*OMEG*FI/PERM*RHO*OMEG*OMEG
1430 XI=(-RHO*VISCF*FFR*OMEG^3)/PERM
1440 E1=E1/1E+15:E2=E2/1E+15:XR=XR/1E+15:XI=XI/1E+15
1450 X=(XR*E1+XI*E2)/(E1*E1+E2*E2)
1460 Y=(XI*E1-XR*E2)/(E1*E1+E2*E2)
1470 P=(X*X+Y*Y)^.25:THETA=ATN(Y/X)/2:GOTO 1480
1480 V3=OMEG/(P*COS(THETA)*100)
1490 A3=P*SIN(THETA)*100:Q3=V3*A3/F(I)
1500 LPRINT TAB(10) F(I) TAB(20):LPRINT V1
1510 NEXT I
1520 END
1530 'sub'
1540 INPUT "low frequency decrement"; LOWDEC
1550 INPUT "amplitude factor";AMFAC
1560 INPUT "alpha";ALPHA
1570 INPUT "frequency at peak decrement";PEAKFREQ
1580 LPRINT:LPRINT TAB(10) "parameters for viscoelastic frame"
1590 LPRINT
1600 LPRINT TAB(10) "low freq log decrement ---- ";LOWDEC
1610 LPRINT TAB(10) "amplitude factor -----------";AMFAC
1620 LPRINT TAB(10) "alpha ---------------------";ALPHA
1630 LPRINT TAB(10) "freq at peak decrement ---- ";PEAKFREQ
1640 IF G$ = "c" OR G$ = "C" THEN DEC(I) = GDEC:GOTO 1770
1650 TAU = 1/(2*PI*PEAKFREQ)
1660 MR1=GR
1670 MI1=LOWDEC*MR1/PI
1680 MR2 = MR1*AMFAC
1690 AIA=1 - ALPHA
1700 OMEGA = F(I)*2*PI
1710 DENOM = 1 +2*(OMEGA*TAU)^A1A*SIN(ALPHA*PI/2)+(OMEGA*TAU)^(2*A1A)
1720 MR3=MR2-(MR2*(1+(OMEGA*TAU)^A1A*SIN(ALPHA*PI/2)))/DENOM
1730 MI3=MR2*(OMEGA*TAU)^A1A*COS(ALPHA*PI/2)/DENOM
1740 MR=MR1+MR3
1750 MI=MI1+MI3
1760 DEC(I)=MI/MR*PI
1770 RETURN
```

```
5 PI=3.141592654#
10 REM GEERTSMA AND SMIT APPROXIMATION
12 REM
13 REM author Jim Bennell (1991)
14 REM
20 INPUT "INPUT COMPRESSIBILITIES OF SOLID AND FLUID CONSTITUENTS"; CS,CW
30 INPUT "INPUT DENSITIES OF SOLID AND FLUID COMPONENTS"; RS,RW
40 INPUT "POROSITY, MASS COUPLING FACTOR, FRAME COMPRESSIBILITY AND SHEAR MOD
S"; N,FF,CF,G
45 B=FF
50 R1=N*RW+(1-N)*RS
60 M=B*RW/N
70 R=CS/CF
80 Z=1/((1-N-R)*CS+N*CW)
90 Y=Z*(1-R)
100 X=Z*((1-R)^2)+1/CF+4*G/3
110 VZERO=SQR(X/R1)
120 VINF=SQR((Z*R1+X*M-2*Y*RW)/(M*R1-RW^2))
130 LPRINT "Vzero = "; VZERO; "  Vinf = ";VINF; " MASS COUPLING FACTOR = ";B
140 INPUT "VELOCITIES OR PERMEABILITY 1 OR 2"; N1
150 IF N1=1 THEN 160 ELSE 500
160 INPUT "INPUT PERMEABILITY M/S"; P
170 WC=(9.810001*N*R1)/(P*(B*R1-N*RW))
175 LPRINT "CHARACTERISTIC ANGULAR FREQUENCY =  ";WC
180 FOR F= 0 TO 10 STEP .25
190 F1=10^F
200 VP= (VINF^4+VZERO^4*(WC/(2*PI*F1))^2)/(VINF^2+VZERO^2*(WC/(2*PI*F1))^2)
205 VP=SQR(VP)
210 LPRINT "FREQ. = ";F1; "  Velocity = ";VP
220 NEXT F
230 GOTO 40
500 INPUT "INPUT VELOCITY  AND FREQUENCY ";VP,F
510 AA=(VZERO/VINF)^2
520 BB=(VP/VZERO)^2
530 CC=(VP/VINF)^2
540 A=AA*SQR((BB-1)/(1-CC))
550 P=A*N*9.810001*R1/(2*PI*F*(B*R1-N*RW))
560 LPRINT "PERMEABILITY = ";P
570 GOTO 40
```

APPENDIX 5   SEDIMENT SAMPLE DESCRIPTION
                 AND PROPERTIES

Expt. Ref.	Soil Type	Sample Location	Sediment Properties					Source of data
			Liquid Limit	Plastic Limit	Specific Gravity	Calcium Carbonate	Organic Content	
IM03	Clay	Traeth Lligwy Anglesey long 4° 16.30' lat 53° 22.00' (see fig. A5.1)	44%	16%	2.706	0.3%	<1%	Clarke (1982)
IM04	Clay		40%	14%	2.718	0.3%	<1%	
IM05	Clayey silt	Irish Sea C6 lat 54° 10.00' long 5° 09.83' (see fig. A5.2)	80%	23%	2.665	15.8%	1.8%	F. Yuan (personal communication)
IM07	Clayey silt							
IM08	Clayey silt							
IM09	Silty clay	Irish Sea C1 lat 53° 52.59' long 5° 40.99' (see fig. A5.2)	65%	34%	2.684		2.5%	F. Yuan (personal communication)
IM11	Mud	Irvine Bay Northing 633771 Easting 226363 (see fig. A5.3)	72%	30%	2.643	12.2%	2.6%	Cronan (1970)

Table A5.1   Sediment Sampling Locations and Sediment Properties.

Sediment Sample Clay Mineralogy

Table A5.2   Probable clay mineralogy of sample used in Experiment IM03 and IM04.

Sample location: Clay sample from Traeth Lligwy, Anglesey, U.K. (see figure A5.1)

Source of data: Younis (1983)

Clay mineral	Particle size					
	$2.0-0.63\mu$m		$0.63-0.2\mu$m		$<0.2\mu$m	
	$\bar{x}$	std	$\bar{x}$	std	$\bar{x}$	std
Hydrous mica	23.7	14.3	30.7	14.4	25.5	11.3
Chlorite	28.2	7.2	22.0	6.0	25.2	16.0
Kaolinite	<5	-	<5	-	<5	-
Vermiculite	11.0	7.1	12.2	15.9	17.2	11.6
Verm/Hyd. mica	15.5	1.2	13.2	8.3	17.5	5.4
Quartz	16.7	5.6	21.7	3.3	14.7	9.2

Comparative table of mean percentiles ($\bar{x}$) of minerals and standard deviation (std) based X-ray diffraction analysis per area, in the clay size fractions of drift derived soils. (5 samples were analysed)

Table A5.3   Probable clay mineralogy of sample used in
                  Experiment IM05,IM07,IM08 and IM09.

Sample location: Irish Sea (see figure A5.2)

Source of data: Younis (1983)

Clay mineral	Particle size					
	2.0-0.63μm		0.63-0.2μm		<0.2μm	
	$\bar{x}$	std	$\bar{x}$	std	$\bar{x}$	std
Hydrous mica	19.5	6.1	30.7	9.0	27.2	5.3
Chlorite	18.5	7.2	23.2	11.2	22.5	12.2
Kaolinite	23.2	5.7	<5	-	<5	-
Vermiculite	10.3	5.0	8.8	6.7	11.8	5.7
Verm/Hyd. mica	11.4	4.9	19.0	6.6	17.8	5.5
Quartz	18.5	6.0	18.4	3.7	20.4	9.5

Comparative table of mean percentiles ($\bar{x}$) of minerals and
standard deviation (std) based X-ray diffraction analysis per
area, in the clay size fractions of drift derived soils.
(7 samples were analysed)

Table A5.4   Probable clay mineralogy of sample used in
                   Experiment IM11.

Sample location: Mud sample from Irvine Bay, Firth of Clyde, U.K.
                      (see figure A5.3)

Source of data: Cronan (1970)

Clay mineral	Percentile
Vermiculite/Hydrous mica	75
Kaolinite	<5
Calcite & quartz	<15
Chlorite	<5

5km

IMO3/IMO4

Bangor

Anglesey sampling site

Holy
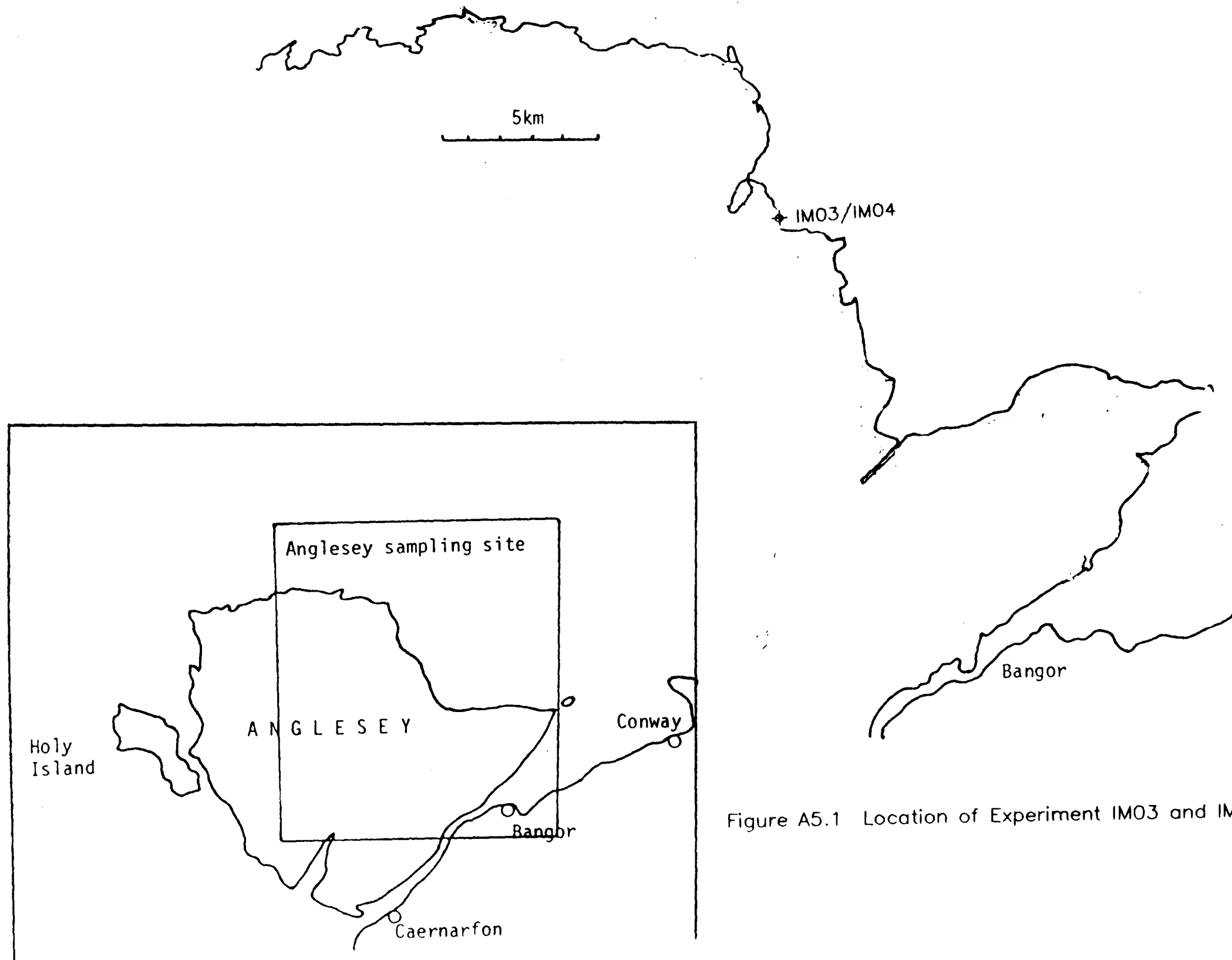Island

A N G L E S E Y

Conway

Bangor

Caernarfon

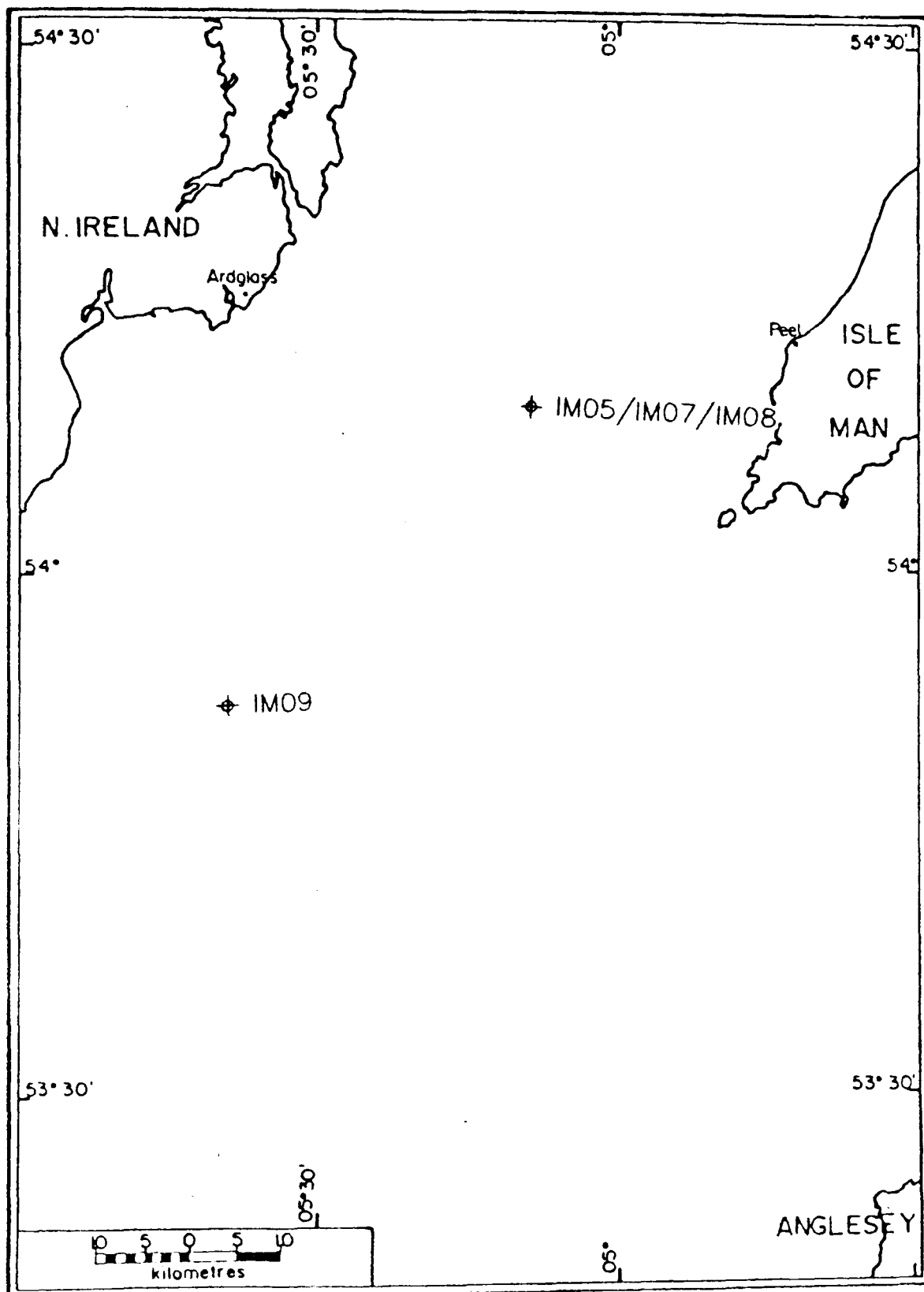Figure A5.1   Location of Experiment IMO3 and IMO4 Clay Sample Site.

Figure A5.2   Location of Experiment IM05,IM07,IM08 and IM09
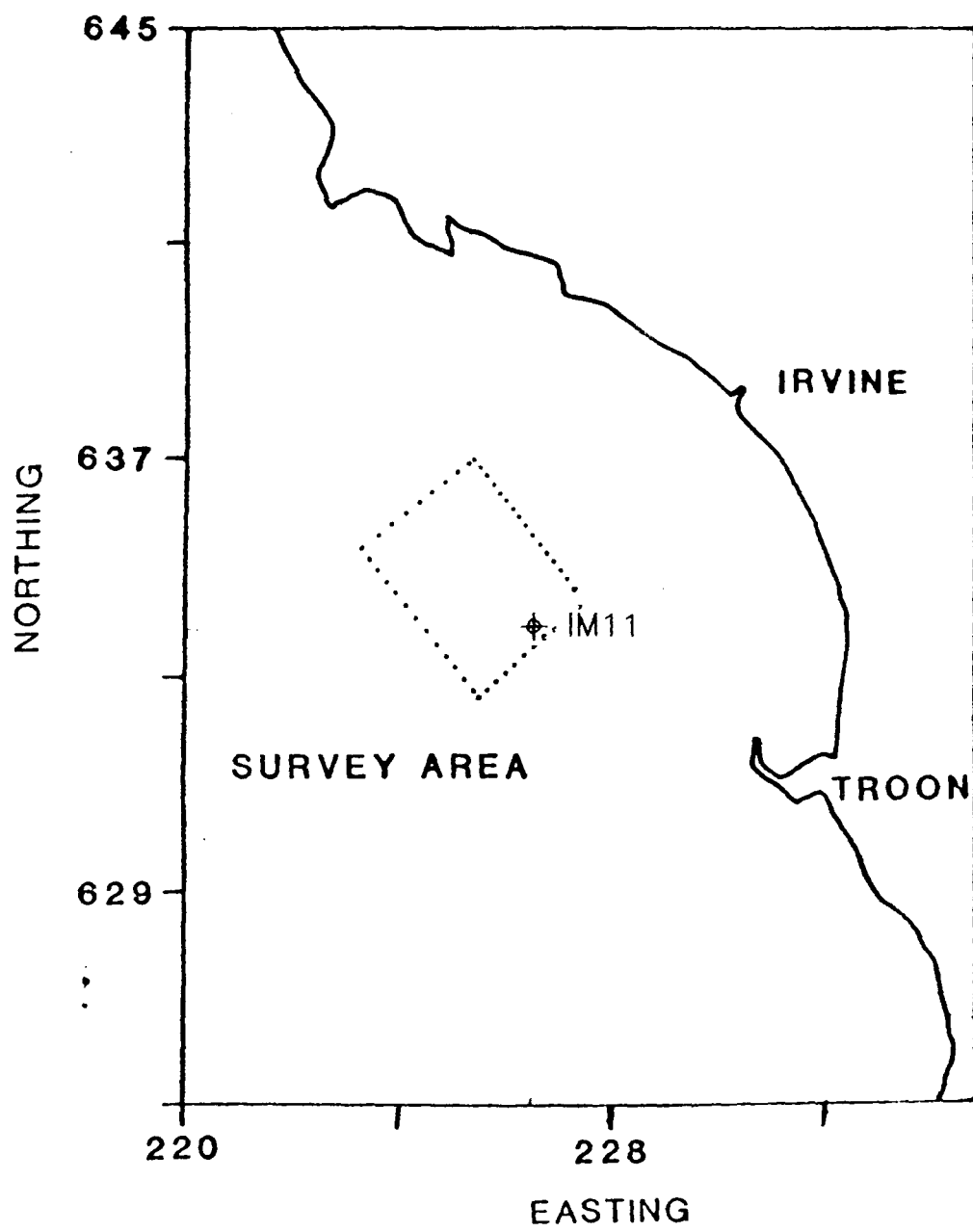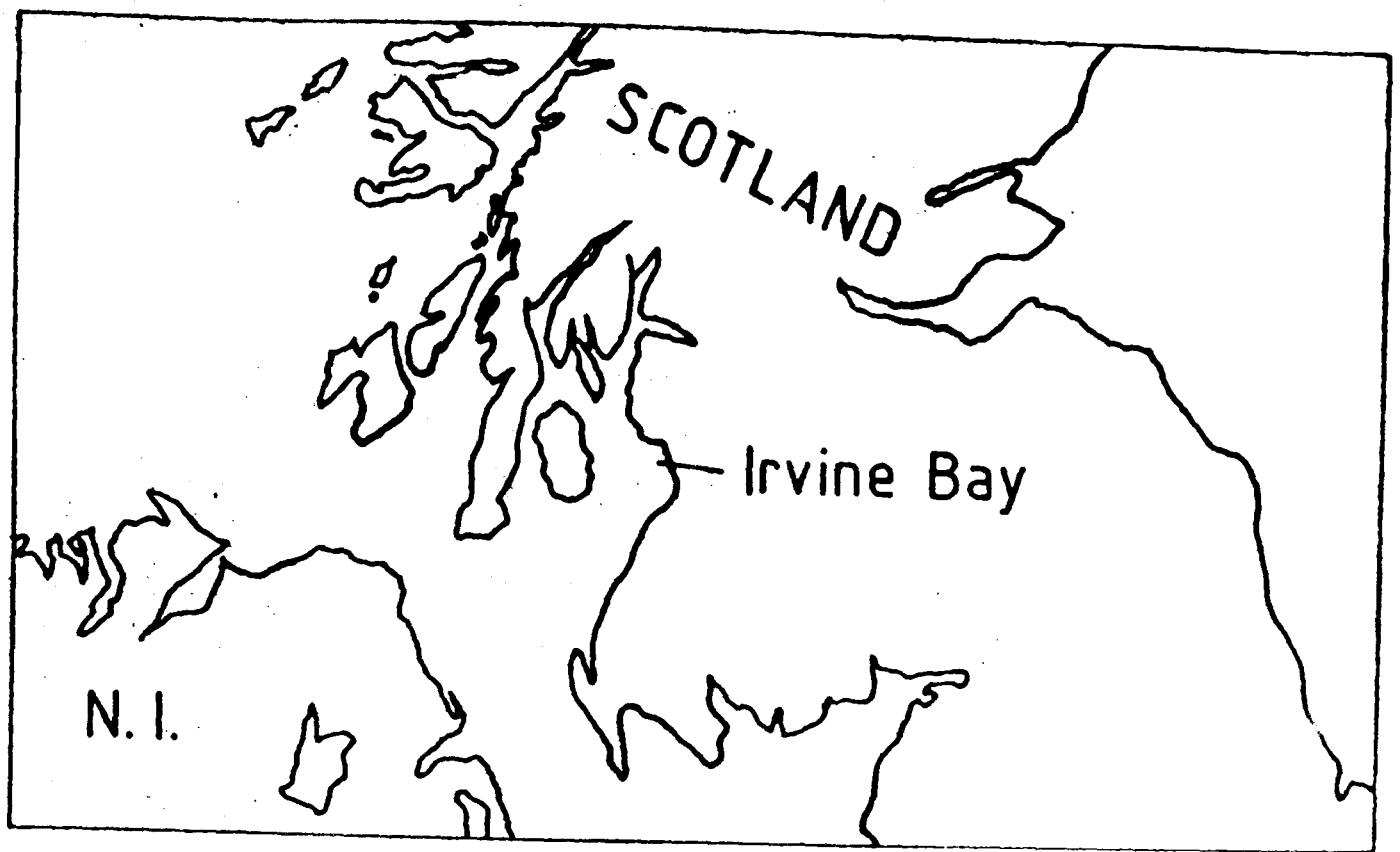Irish Sea Sediment Sample Sites.

Figure A5.3   Location of Experiment IM11 Irvine Bay Mud Sample Site.

REFERENCES

Akal, T. (1972)   The relationship between the physical properties of underwater sediments that affect bottom reflection. Marine Geology,13, p. 251-266.

Anderson, D.G. and Stokoe, K.H. (1978)   Shear modulus: A time-dependent soil property. Dynamical Geotechnical Testing, ASTM STP 654, 1978, pp. 66-90.

Anstey, N.A. (1991)   Velocity in thin section. First Break 9(10) p.449-457.

Archie, G.E. (1942)   Electrical resistivity as an aid in core analysis interpretation. Trans. AIME, 146, p. 54-63.

Been, K. (1980)   Stress strain behaviour of a cohesive soil deposited under water. D. Phil. Thesis Oxford University.

Been K. and Sills G.C. (1981)   Self weight consolidation of soft soils: an experimental and theoretical study. Geotechnique 31,No. 4, p. 519-535.

Bell, D.W. and Shirley, D.J. (1980)   Temperature variation of the acoustical properties of laboratory sediments. J. Acoust. Soc. Am. 68(1) p. 227-231.

Bennell, J.D., Taylor Smith, D. and Davis, A.M. (1984). Resonant column testing of marine sediments. Oceanology Int. 84.

Bennell, J.D. and Taylor Smith D. (1991).   A review of laboratory shear wave techniques and attenuation measurements with particular reference to the resonant column. In Shear Waves in Marine Sediments, Hovem, Richardson, and Stoll (eds.)Kluwer Academic Press, 83-93.

Biot, M. A. (1941). General theory of three-dimensional consolidation. J. Applied Phys. Am., 28, p. 168-178.

Biot, M. A. (1956a). The theory of elastic waves in a fluid saturated solid.I. Low-frequency range, J. Acoust. Soc. Am., 28, p. 168-178.

Biot, M. A. (1956b). The theory of elastic waves in a fluid saturated solid.II. High-frequency range, J. Acoust. Soc. Am., 28, 179-191.

Biot, M. A. (1961). The generalized theory of acoustic propagation in porous dissipative media, J. Acoust. Soc. Am., 34, p. 1254-1264.

Biot, M. A. (1962). Mechanics of deformation and acoustic propagation in porous media, J. Appl. Phys., 33, p. 1482-1498.

Bjerrum, L. (1967). Engineering geology of Norwegian normally consolidated marine clays as related to settlement of buildings. Geotechnique, 17, p 81-118

Bobber, R.J. (1970). Underwater electro-acoustic measurements. Naval Research Laboratory, Washington D.C. Library of Congress catalog card no. 72-608304 p.92-95

Bourbie, T., Coussy O., and Zinszer B. (1987) Acoustics of Porous Media. Editions Techniq (Paris), p 9-97.

Bowden R.K. (1989) Compression behaviour and shear strength characteristics of a natural silty clay sedimented in the laboratory. D. Phil. thesis University of Oxford

Boyce, R. E. (1968)   Electrical resistivity of modern marine sediments from the Bering Sea, J. of Geophysical Research, 73, p. 4759-4766.

Boyce, R.E. (1980)   Determination of the relationships of electrical resistivity, sound velocity, and density/porosity of sediments and rock by laboratory techniques and well logs from DSDP sites 415 and 416 off the coast of Morocco. Initial Reports of the Deep Sea Drilling Project, 50, p. 305-318.

Briggs, K.B. (1991)   Comparison of measured compressional and shear wave velocity values with predictions from Biot theory. In Shear Waves in Marine Sediments, Hovem, Richardson and Stoll (eds.) Kluwer Academic Press, p. 121-130.

British Standards Institution BS1377 (1975). Methods for testing for soils for civil engineering purposes.

Brown, R.J.S. (1980)   Connection between formation factor for electrical resistivity and fluid-solid coupling factor in Biot's equation for acoustic waves in fluid filled porous media, Geophysics, 45, p. 1269

Bryant, W.R., Deflache, A.P. and Trabant, P.K.(1974) Consolidation of marine clays and carbonates. in Deep Sea Sediments Physical and Mechanical Properties ed. Inderbitzen, Plenum Press, p 204-244.

Bueche, F.J. (1980)   Introduction to Physics for Scientists and Engineers, McGraw-Hill p. 253-263.

Chandler, R.J.S., Lorelliel, S. and Trenter, N.A. (1990) Measurements of the permeability of London clay using a self boring permeameter. Geotechnique 40(1) p. 113-124

Clarke, H. (1982)   Geotechnical and slope stability aspects of North Wales tills. MSc Thesis (University of Wales)

Clay, C.S. and Medwin, H. (1977)   Acoustical Oceanography. John Wiley and Sons, p 3.

Cronan, D.S. (1970)   Geochemistry of recent sediments from the central and north eastern Irish Sea. Rep. No. 70/17, Inst. Geol. Sci. p.20.

Davis,A.M. & Bennell, J.D. (1986)   Dynamic properties of sediments. In Ocean Seismo-acoustics vol.4., p 501-510 ed. Akal, T. and Berkson, J.M. Plenum press.

Dewes, F.C.D. & McCann, D.M. (1972)   Acoustic reflectors in the surface layers of deep sea sediments. Marine Geophysical Researches. D.Reidel publishing company, p 373.

Dullien, F.A. (1979)   Porous media fluid transport and pore structure. Academic press (London), p 35-40.

Dyer, K.R. (1986)   Coastal and Estuarine Sediment Dynamics. John Wiley and Sons, p 202-230.

Dyvik, R. & Madshus, C. (1985)   Laboratory measurement of Gmax using bender elements, Advances in of the art of soil testing under cyclic loads. Am. Soc. Civ. Engrs., New York.

Einstein, H.A. and Krone, R.B. (1962)   Experiments to determine modes of cohesive sediment transport in salt water. J. Geophysical Research. 67, No. 4, p. 1451-1461.

Einsele, G., Overbeck, R., Schwarz, H.U. & Unsold, G. (1974) Mass physical properties, sliding and erodibility of experimentally deposited and differently consolidated clayey muds. Sedimentology 21, p. 339-372.

Elder, D.McG and Sills G.C. (1984) Time and stress dependent compression in soft sediments. University of Oxford Soil Mechanics Report No. SM048/84.

Elder, D.McG. (1985) Stress strain and strength behaviour of very soft soil sediment. D. Phil. Thesis Oxford University.

Gartenhaus, S. (1977) Physics basic principles. Holt, Reinhart & Winston (pub) p. 42.

Gaudin, A.M. and Fuerstenau, M.C. (1958) The transviewer-X-rays to measure suspended solids concentration. Eng. & Mining J. V159,9, p. 110-112.

Geertsma J. (1961) Velocity log interpretation: the effect of rock bulk compressibility. J. Soc. Pet. Eng., 1, p. 235-246.

Geertsma J. and Smit D.C. (1961) Some aspects of elastic wave propagation in fluid saturated media, Geophysics, 26, p. 169-181.

Gibson, R.E., England, G.L. & Hussey, M.J.L. (1967) The theory of one dimensional consolidation of saturated clays. Geotechnique, 17, p. 261-273.

Grim, R.E. (1962) Applied Clay Mineralogy. McGraw-Hill. New York, p.4-47, p.204-275.

Hamdi, F.A.I. (1981) Variations of seismic velocity with depth in near surface marine sediments. Ph.D. Thesis. (University of Wales).

Hamdi, F.A.I. and Taylor Smith D.(1981)   Soil consolidation behaviour assessed by seismic velocity measurements, Geophysical Prospecting, 29, p. 715-729.

Hamdi, F.A.I. and Taylor Smith D.(1982)   The influence of permeability on compressional wave velocity in marine sediments, Geophysical Prospecting, 30, p. 622-640.

Hamilton, E.L. (1971)   Elastic properties of marine sediments. Journal of Geophysics Research, 76, 2,p.579-604.

Hamilton, E.L. & Backman, R.T. (1982)   Sound velocity and related properties of marine sediments. J. Acoust. Soc. 72(6), p. 1891-1903.

Hampton, L.D. (1967)   Acoustic properties of sediments. J. Acoust. Soc. Am. 42(4), p. 882-890.

Hardin, B.O. & Black, W.L. (1968)   Vibration modulus of normally consolidated clay. J. Soil Mech. and Found. Div., ASCE, 94,p. 353-369.

Hovem, J,M & Ingram, G,D (1979)   Viscous attenuation of sound in saturated sand. J. Acoust. Soc. Am. 66(6) p. 1807-1812.

Hovem, J.M. (1980)   Viscous attenuation of sound in suspensions and high porosity marine sediments. J. Acoust. Soc. Am. 67(5), p. 1559-1563.

Hurley, M.T. (1989)   The application of Biot's theory to sea bed sedimentation. Ph.D. Thesis (University of Wales).

Huws, D.G., Davis, A.M. & Bennel, J.D. (1991)   Mapping of the sea bed via an *in situ* shear wave (SH) velocities in Shear Waves in Marine Sediments, Hovem, J.M., Richardson, M.D. & Stoll,R.D. (eds.) Kluwer Academic Press p. 337-343.

Huws, D.G. (1992)   An integrated approach to the stability evaluation of prospective offshore sites. Ph.D. Thesis (University of Wales) in prep.

Ishihara, K. (1968)   Propagation of compressional waves in saturated soil, in Wave Propagation and Dynamics Properties of Earth Materials. Triandafilidis (ed.). University of Mexico Press.

Jackson, P.D. (1975)   Electrical properties of Irish Sea sediments. PhD Thesis (University of Wales).

Jackson, P.D., Taylor Smith, D. and Stanford, P.N. (1978) Resistivity-porosity-particle shape relationships for marine sands. Geophysics 43: 1250-68.

James, A.E., Williams D.J.A. & Williams, P.R. et al. (1989) Small strain, low shear rate rheometry of cohesive sediments. In Physical Processes in Estuaries eds. Dronkers,J. and van Leussen,W. Springer-Verlag publishers. p.488-500

Johnson, D.L. and Plona, T.J. (1982)   Acoustic slow waves and the consolidation transition, J. Acoust. Soc. Am., 72, p. 556-565.

Kinsler, L.E. and Frey, A.R. (1962)   Fundamentals of Acoustics (2nd edition). John Wiley and Sons, 194-197.

Kirby, R. and Parker, W.R. (1977)   Fine sediment studies relevant to dredging practice and control. 2nd Int. Symp. on Dredging Technology, Paper B2 p. 15-26.

Kranck (1973)   Flocculation of suspended sediment in the sea. Nature, 246, pp.348-350.

Krone R.B. (1962)   Flume studies of the transport of sedimentation in estuarial shoaling processes. University Kalif, Hyd. Eng. Lab. and Sanit. Eng. Res. Lab, 179-191.

Krumbein, W.C. & Pettijohn, F.J. (1938)   Manual of Sedimentary Petrography. Appleton-Century-Croft, p. 54.

Kynch G.J. (1952)   A theory of sedimentation. Trans. of the Faraday Soc. 48, p. 166-176.

Lambe, T.W. and Whitman R.V. (1979). Soil Mechanics. John Wiley and Sons, p 71-75.

Laughton, A.S. (1957)   Sound propagation in compacted ocean sediments. Geophysics 22, p. 233-260.

Lee K. and Sills G.C. (1981)   The consolidation of a soft soil stratum, including self weight effects and large strains. International J. for Numerical and Analytical Methods in Geomechanics 5,405-428.

Lovell, M.A. (1984)   Thermal conductivity and permeability assessment by electrical resistivity measurements in marine sediments, Marine Geotechnology, 6, p. 205 - 240.

McCann, D.M. (1968)   Acoustic properties of North Atlantic cores. PhD. thesis University of Wales.

Michaels, A.S. & Bolger, J.C. (1962)   Settling rates and sediment volumes of flocculated kaolin suspensions, Industrial & Engineering Chemistry Fundamentals, 1, p. 24-33.

Mikasa, M. (1964)   The consolidation of soft clay, Japan Soc. of Civil Eng., p. 21-26

Mitchel, J.K. (1976)   Fundamentals of Soil Behaviour. John Wiley and Sons Inc, p 186-195.

Mizra, N.A. (1991)   Geophysical modelling of sediment permeability. Phd Thesis (University of Wales).

Nafe, J.E & Drake, C.L. (1963)   Physical properties of marine sediments. In The Sea, vol. 3, p. 794-815. Interscience Publishers, New York.

Ogushwitz, P.R. (1985)   Applicability of the Biot theory .I. Low-porosity materials, J. Acoust. Soc. Am., 77, p. 429-440.

Ogushwitz, P.R. (1985)   Applicability of the Biot theory .II. Suspensions, J. Acoust. Soc. Am., 77, p. 441-451.

Pantin, H.M. (1978)   Quanternary sediments from the N.E. Irish Sea: Isle of Man to Cumbria, Bull. Geol. Surv. Great Britain (Institute of Geological Sci.) 64, p.39.

Partheniades, (1965)   Erosion and deposition of cohesive soils. J. Hydraul. Div. ASCE, 91, HY1, p.105-139.

Paul, M.A. & Jobson, L.M. (1987)   On the acoustic and geotechnical properties of soft sediments from the Witch Ground Basin, Central North Sea. Internal Report Dept. Civil Eng. Heriot Watt University, Edinburgh.

Richards, A.F. and Parker H.W. (1968)   Surface coring for shear strength measurements. in Civil Engineering in the Oceans, Am. Soc. of Civil Eng. New York Press p. 445-489.

Richards, A.F. (1984)   Modelling and consolidation of marine soils. in <u>Seabed Mechanics</u> ed. Dennes B. Graham & Trotman Press, p 3-8.

Schultheiss, P.J. (1981)   Development of seismic shear wave devices. University of Wales. No. F60/A1/30.

Schultheiss, P.J. (1983)   The influence of packing structures on seismic wave velocities in sediments. Marine Geological Report No. 83/1, University of Wales.

Shirley, D.J. & Bell, D.W.(1978)   Acoustics of in situ laboratory sediments. Applied Research Lab., Austin, Texas. Report ARL-TR-78-36.

Shirley, D.J. & Hampton, L.D. (1978)   Shear-wave measurements in laboratory sediments. J. Acoust. Am. 63(2),p. 607-613.

Shirley, D.J. (1980)   Sediment Acoustics. Applied Research Lab., Austin, Texas.ARL-TR-80-17.

Sills, G.C. and Thomas, R.C (1984)   Settlement and consolidation in the laboratory of steadily deposited sediments. In Sea Bed Mechanics ed. Dennes B. pub. Graham & Trotman, p. 41-49.

Smith, G.N. (1978)   Elements of soil mechanics for civil and mining engineers. Granada, p.281-282.

Stoll, R.D. and Bryan G.M. (1969)   Wave attenuation in saturated sediments, J. Acoust. Soc. Am., 47, p. 1440-1447.

Stoll,R.D. (1974)   Acoustic waves in saturated sediments. In <u>Physics of Sound in Marine Sediments</u>. Hampton L. (ed). Plenum (New York), p. 19-39.

Stoll, R.D. (1977)   Acoustic waves in ocean sediments, Geophysics, 44, p. 715-725.

Stoll, R.D. (1980)   Theoretical aspects of sound transmission in sediments, J. Acoust. Soc. Am., 68, p. 1341-1349.

Stoll, R.D. (1985)   Marine sediment acoustics, J. Acoust. Soc. Am., 77, p. 1789-1799.

Stoll, R.D. (1986)   Acoustic waves in marine sediments. In Ocean Seismo Acoustics. Akal, T. and Berkson J.M. (eds). Plenum (New York) p. 417-433.

Stoll, R.D. (1989)   Sediment Acoustics, Springer-Verlag, New York.

Swartzendruber, D. (1969)   The flow of water in unsaturated soils.   In Flow Through Porous Media.   ed.   De Weist,R.J.M. Academic Press. New York, p. 318-323.

Tan, S.A, Tan, T.S. Ting, L.C., Yong, K.Y., Kauruanaratne, G.P. and Lee, S.L. (1988)   Determination of consolidation properties for very soft clay. Geotechnical Testing Journal, 11, No. 4, p. 233-240.

Taylor Smith, D. (1971)   Acoustic and electric techniques for sea floor sediment identification. In Proceedings of International Symposium on Engineering Properties of Sea Floor Soils and their Geophysical Identification. Seattle, p 235-267.

Taylor Smith, D. (1974)   Acoustic and mechanical loading of marine sediments. In Physics of Sound in Marine Sediments, Hampton, L.(ed). Plenum (New York).

Taylor Smith, D. (1983) Seismo-acoustic wave velocity and sediments engineering properties in <u>Acoustic and the sea-bed</u>, ed. Pace N.G. Institute of Acoustics conference proceedings, Bath, Bath Univ. Press. p.9-17.

Taylor Smith, D. (1986) Geotechnical characteristics of the sea bed related to seismo-acoustics. <u>In Ocean Seismo Acoustics</u>. Akal, T. and Berkson J.M. (eds). Plenum (New York).

Telford, W.M., Geldart, L.P., Sherriff, R.E. & Keys, D.A. (1978) <u>Applied Geophysics</u>, Cambridge University Press. p. 222-235.

Terzaghi, K. (1925) <u>Principles of soil mechanics</u>. Eng. News Record. 95, p. 265-295.

Urick, R.J. (1947) A sound velocity method for determining the compressibility of finely divided substances. J. Acoust. Soc. Am. 18,p. 983-987.

Urish, D. W. (1981) Electrical resistivity-hydraulic conductivity relationships in glacial outwash aquifers. Water Resources Res. 17(5) p. 1401-1408.

White, R.E. (1981) <u>Introduction to the Principles and Practices of Soil Science</u>. Blackwell Scientific, p. 97-117.

Williams, D.J.A & Williams, P.R. (1989a) Rheology of concentrated cohesive sediments. J. Coastal Research 5, p. 165-173.

Williams, P.R. & Williams, D.J.A. (1989b) Rheometry for concentrated cohesive suspensions. J. Coastal Research 5. p.150-164.

Winsauer, W.O., Shearin, H.M., Masson, P.H., & Williams, M. (1952)   Resistivities of brine saturated sands in relation to pore geometry, Bulletin, American Association of Petroleum Geologists, 36, p. 253.

Wright, J.E., Hull, J.H., McQuillin, R. and Arnold, S.E. (1971)   Irish Sea investigations. Report Inst. Geol. Sci. no. 71/19.

Yamamoto, T. and Turgut, A. (1988)   Acoustic wave propagation through porous media with arbitrary pore size distributions, J. Acoust. Soc. Am., 83, p. 1744-1751.

Younis, M.G.A. (1983)   Mineralogical studies on soils derived from 'Red Northern Drift' in north west Wales. Ph.D. Thesis (University of Wales)

Yuan, F. (1992)   Acoustical and geotechnical properties of Western Irish Sea sediments. Ph.D. Thesis (University of Wales) in prep.